Ruthenium Arene Azo Anticancer Complexes

A Thesis Submitted for the Degree of Doctor of Philosophy

by

Sarah J. Dougan, *MChem*

School of Chemistry
Faculty of Science and Engineering
The University of Edinburgh

November 2007

Abstract

Ruthenium(II) arene complexes of the type $[(\eta^6\text{-arene})Ru(en)Cl]PF_6$ (en = ethylenediamine) exhibit promising anticancer activity *in vitro* and *in vivo*. The complexes are thought to be activated by hydrolysis of Ru-Cl to allow for interactions with biomolecules such as DNA. Structure-activity relationships have revealed that changes to the chelating ligand and the arene can have dramatic effects on the cytotoxicity, whilst the 'leaving group' typically plays a more minor role.

This thesis is concerned with the design of ruthenium(II) arene anticancer complexes where the chelating ligand contains an azo-imine group (N=N-C=N) which binds to the ruthenium to form a five-membered chelate ring.

Several mononuclear complexes containing the chelating 2-phenylazopyridine ligand or derivatives thereof were found to be moderately cytotoxic towards A2780 human ovarian and A549 human lung cancer cells (IC_{50} 18-88 μM). These complexes were found to hydrolyse (Ru-Cl → $Ru\text{-}OH_2$) slowly in aqueous solution and arene loss was a competing reaction. X-ray crystal structures revealed that the arene ligand is not as tightly bound to the ruthenium as in the case when the chelating ligand is en.

Synthesis of the corresponding dinuclear analogues, where two 2-phenylazopyridine ligands were joined together via a linker, did not improve the cytotoxicity. Unlike their mononuclear analogues, the complexes appeared to undergo electrochemical reduction with radical formation in aqueous solution. An EPR spectrum of the mono-reduced anion revealed an entirely ligand based radical.

Surprisingly, replacement of Cl^- by I^- in the mononuclear complexes led to compounds that were highly cytotoxic towards both A2780 and A549 cancer cells (IC_{50} 1-5 μM). Interestingly these complexes were resistant to hydrolysis in aqueous solution suggesting that this class of compounds had a novel mechanism of cytotoxic action not involving activation by hydrolysis.

The redox chemistry of these complexes proved to be central to their observed cytotoxicity. The complexes were rapidly reduced by the biological reductant ascorbate, catalytically oxidised the tripeptide glutathione and generated reactive oxygen species (radicals) inside A549 cancer cells. These reactive oxygen species were shown to be involved in cell death.

These iodide complexes were also found to be cytotoxic towards non-cancerous WI38 human lung cells (IC_{50} 1-6 μM) and attempts were made to target one complex specifically to cancer cells, through conjugation to transferrin.

Overall this thesis demonstrates that ruthenium(II) arene anticancer complexes can be cytotoxic through mechanisms of action different from the classical mechanism involving hydrolysis and binding to biomolecules.

Declaration

I hereby declare that except where specific reference is made to other sources, the work contained in this thesis is the original work of the author. It has been composed by myself and has not been submitted, in whole or in part, for any other degree, diploma or other qualification.

Sarah Dougan

November 2007

Acknowledgements

I would like to thank Professor Peter Sadler for his supervision throughout my project. He was always very enthusiastic about the project and I learnt a lot from him.

I would also like to thank Dr Abraha Habtemariam for his help, not only with synthetic work but also help with chemistry and my PhD work in general. All his suggestions have helped this project greatly. Thanks also to Professor Fuyi Wang who taught me how to use a lot of the analytical machines and gave me advice on cell experiments. Furthermore I would like to thank Dr Arindam Mukherjee for his help with protein work and advice on my project.

I would like to thank Dr Michael Melchart for helping me at the beginning of my PhD, ensuring that the project got off to a good start. I would also like to thank Dr Anna Peacock for all her help and guidance on my project, suggesting experiments and showing me new techniques. I would also like to thank Ms Veronika Ehmke and Ms Lucy Jarvis, two undergraduate project students, whose work formed the basis of Chapter 4.

I would like to thank Mr Juraj Bella and Mr John Miller for help with NMR, and Mr Robert Smith and Mr John Dalrymple for help with mass spectrometry. I would also like to thank Ms Lucy Jarvis, Dr Paul Murray, Dr Neil Robertson and Professor Lesley Yellowlees for help with electrochemical techniques and EPR spectroscopy. Thanks also to Professor Simon Parsons and his research group for solving the crystal structures reported in this thesis. Thanks also to Dr Lorna Eades for assistance with ICP-OES, and thanks to the CHN services (University of Edinburgh and University of St Andrews) for analysing my samples.

I would like to thank Ms Emily Jones (Oncosense ltd) for teaching me how to perform the cytotoxicity tests and for advice on cell experiments, and both Ms Emily Jones and Mr Daniel Cole (Oncosense ltd) for testing the cytotoxicity of several complexes reported in this thesis. I would also like to thank my industry supervisor Mr Mark Burton (Oncosense ltd) for all his help allowing me to come to the Oncosense laboratories and perform some experiments that proved central to my

project. Thanks also to all the staff members at MMI Group plc who made me feel very welcome during my industrial placement.

I would like to thank Ms Lisa Pang, Ms Jennifer Crystal and Professor Ted Hupp (Cancer Research United Kingdom) for assistance with the immunochemical assays.

I would like to thank all members of the PJS group, both past and present for their help and support, and also friendship throughout these past three years.

For financial assistance for this project I would like to thank the BBSRC and Oncosense ltd. Furthermore I would like to acknowledge The University of Edinburgh Chemistry Department for financial assistance to present my work at the Gordon Research Conference (2006) and to Oncosense ltd for financial assistance to allow me to present my work at the American Chemical Society's National Meeting (2007).

I would like to thank my friends for being there over the past three years and special thanks to Dave for all his patience and support over the last three years. Lastly I would like to thank my parents for their support and encouragement.

Contents

Abstract ii
Declaration iv
Acknowledgements v
Contents vii

Chapter 1 1

Introduction 1

1.1 The Elements of Life 2

1.2 Therapeutic uses of inorganic compounds 2

1.3 Cancer 3

1.3.1 What is cancer? 3

1.3.2 Strategies to combat cancer 4

1.3.3 Inorganic drugs used in cancer therapy 4

1.3.3.1 Platinum 4

1.3.3.2 Ruthenium 5

1.3.3.2.1 Properties of Ruthenium 5

1.3.3.2.2 Early Work 5

1.3.3.2.3 Ruthenium(III) Complexes 6

1.3.3.2.4 Ruthenium(II) Complexes 6

1.4 Ruthenium(II) arenes as anticancer agents 6

1.4.1 Structure-Activity Relationships 8

1.4.1.1 Role of the η^6-arene 8

1.4.1.1.1 Influencing Cellular Uptake 11

1.4.1.1.2 Arene-Nucleobase Stacking and Intercalation 11

1.4.1.1.3 Rates of Hydrolysis 13

1.4.1.1.4 Rates of Reaction with cGMP 13
1.4.1.2 Role of the Leaving Group 15
1.4.1.3 Role of the Chelating Ligand 16
1.4.1.3.1 Specific Hydrogen Bonding 17
1.4.1.3.2 pKa of coordinated water 17
1.4.1.3.3 Other N,N-chelating ligands 18
1.4.1.3.4 O,O Chelating Ligands 18
1.4.2 Comparison with Cisplatin and other Platinum Complexes 19
1.4.2.1 Activity towards A2780cis (Cisplatin Resistant) Cell Line 19
1.4.2.2 Reactions with DNA 20
1.4.2.3 RNA synthesis 20
1.4.2.4 DNA Repair Synthesis 20
1.5 2-Phenylazopyridine (azpy) Chelating Ligands 21
1.5.1 The anticancer activity of ruthenium(II) azpy complexes 22
1.5.1.1 Mononuclear complexes 22
1.5.1.2 Dinuclear Complexes 24
1.6 Aims 25
1.7 References 26

Chapter 2 31

Experimental Section 31

2.1 Nuclear Magnetic Resonance (NMR) Spectroscopy 32
2.1.1 Experimental Technique Overview 32
2.1.2 Chemical Shift, Resonance Intensities and Spin-Spin Coupling 34
2.1.2.1 Chemical Shift 34

2.1.2.2 Resonance Intensities 35
2.1.2.3 Spin-Spin Coupling 35
2.1.3 Two Dimensional Techniques: COSY (COrrelation SpectroscopY) and TOCSY (TOtal Correlation Spectroscopy) 36
2.1.4 Water Suppression 36
2.1.5 Experimental Methods 36
2.2 Ultraviolet-visible (UV-VIS) Spectroscopy 37
2.2.1 Experimental Technique Overview 37
2.2.2 Allowed and Forbidden Transitions 38
2.2.3 Experimental Methods 39
2.2.3.1 Determination of Molar Extinction Coefficients 39
2.3 Electrochemistry[9, 10] 39
2.3.1 Cyclic Voltammetry 40
2.3.2 Differential Pulse Polarography (DPP) 40
2.3.3 Constant Potential Coulometry 40
2.3.4 Experimental Methods 41
2.4 Electrospray Ionisation Mass Spectrometry (ESI-MS) 41
2.4.1 Experimental Technique 41
2.4.2 Experimental Methods 43
2.5 Inductively Coupled Plasma Optical Emission Spectroscopy (ICP-OES) 43
2.5.1 Experimental Technique 43
2.5.2 Experimental Methods 43
2.6 X-ray Diffraction (XRD) 44
2.6.1 Experimental Technique 44
2.6.2 Methods Used 45

2.7 High Performance Liquid Chromatography (HPLC)[4, 11] 45
2.7.1 Experimental Technique 45
2.7.2 Experimental Methods 46
2.7.3 Fast Protein Liquid Chromatography (FPLC) 46
2.8 Cell Culture 47
2.8.1 Experimental technique 47
2.8.2 Materials and Maintenance of Cell Lines 47
2.8.3 Determination of IC_{50} values 48
2.9 pH measurements 49
2.10 CHN (Carbon-Hydrogen-Nitrogen) Elemental Analysis 49
2.10.1 Experimental Technique 49
2.10.2 Methods Used 50
2.11 Synthesis of Starting Materials 50
2.11.1 Materials 50
2.11.2 Methods 50
2.11.3 Synthesis and Characterisation 51
2.11.3.1 1,4-Dihydrobiphenyl 51
2.11.3.2 $[(\eta^6\text{-biphenyl})RuCl_2]_2$ 51
2.11.3.3 $[(\eta^6\text{-benzenel})RuCl_2]_2$ 51
2.11.3.4 $[(\eta^6\text{-}p\text{-cymene})RuCl_2]_2$ 52
2.11.3.5 $[(\eta^6\text{-hexamethylbenzene})RuCl_2]_2$ 52
2.11.3.6 $[(\eta^6\text{-biphenyl})RuI_2]_2$ 52
2.11.3.7 $[(\eta^6\text{-}p\text{-cymene})RuI_2]_2$ 53
2.12 References 53

Chapter 3 55

Mononuclear Ruthenium(II) Arene Chlorido Azo Complexes 55

3.1 Introduction 56

3.2 Experimental 58

3.2.1 Materials 58

3.2.2 Synthesis 58

3.2.2.1 2-(Phenylazopyridine) (azpy) 58

3.2.2.2 4-(2-Pyridylazo)phenol (azpy-OH) 58

3.2.2.3 3-Amino-pyrazoline hydrochloride 59

3.2.2.4 3-Amino-1-nitroso-2-pyrazoline 59

3.2.2.5 4-(1H-pyrazol-3-ylazo)-N,N dimethylaniline (azpyz-NMe_2) 60

3.2.2.6 [(η^6-*p*-cym)Ru(azpy)Cl]PF_6 (1) 60

3.2.2.7 [(η^6-thn)Ru(azpy)Cl]PF_6 (2) 60

3.2.2.8 [(η^6-bz)Ru(azpy)Cl]PF_6 (3) 61

3.2.2.9 [(η^6-bip)Ru(azpy)Cl]PF_6 (4) 61

3.2.2.10 [(η^6-*p*-cym)Ru(azpy-NMe_2)Cl]PF_6 (5) 62

3.2.2.11 [(η^6-thn)Ru(azpy-NMe_2)Cl]PF_6 (6) 62

3.2.2.12 [(η^6-bz)Ru(azpy-NMe_2)Cl]PF_6 (7) 63

3.2.2.13 [(η^6-bip)Ru(azpy-NMe_2)Cl]PF_6 (8) 63

3.2.2.14 [(η^6-*p*-cym)Ru(azpy-OH)Cl]PF_6 (9) 64

3.2.2.15 [(η^6-thn)Ru(azpy-OH)Cl]PF_6 (10) 64

3.2.2.16 [(η^6-bz)Ru(azpy-OH)Cl]PF_6 (11) 64

3.2.2.17 [(η^6-bip)Ru(azpy-OH)Cl]PF_6 (12) 65

3.2.2.18 [(η^6-*p*-cym)Ru(azpyz-NMe_2)Cl]PF_6 (13) 65

3.2.2.19 [(η^6-thn)Ru(azpyz-NMe_2)Cl]PF_6 (14) 66

3.2.2.20 [(η^6-bz)Ru(azpyz-NMe_2)Cl]PF_6 (15) 66

3.2.2.21 [(η^6-bip)Ru(azpyz-NMe_2)Cl]PF_6 (16) 67

3.2.3 Methods 67

3.2.3.1 X-Ray Crystallography 67

3.2.3.2 Determination of pK_a* Values 69

3.2.3.3 Aqueous Solution Chemistry 69

3.2.3.3.1 Speciation of the complexes 1-4 and 13-15 after 24 h 69

3.2.3.3.2 Rate of arene loss from complexes 1 - 4 70

3.2.3.3.3 Rate of decomposition of complexes 5 - 12 70

3.2.3.3.4 Rate of hydrolysis of complexes 13-16 70

3.2.3.3.5 Reactions of complex 13 with 9-EtG 71

3.3 Results 71

Synthesis and Characterisation 72

3.3.1.1 2-Phenylazopyridine (azpy) 72

3.3.1.2 2-p-Phenolazopyridine (azpy-OH) 73

3.3.1.3 3(5) – 4 dimethylphenylamino(phenylazo) pyrazole (azpyz-NMe_2) 73

3.3.1.4 Ruthenium complexes 74

3.3.2 X-ray Crystallography 75

3.3.3 UV-Vis Spectroscopy 79

3.3.3.1 Azo Ligands 79

3.3.3.2 Ruthenium Complexes 81

3.3.4 Aqueous Solution Chemistry 86

3.3.4.1 Phenylazopyridine ligands 86

3.3.4.2 Aqueous Solution Chemistry of Ruthenium complexes 87

3.3.4.2.1 Speciation after 24 h incubation at 310 K 88
3.3.4.2.2 Complexes 13-15 89
3.3.4.2.3 pKa* of aquated 13 (13A) 91
3.3.4.2.4 Reaction of 13A with 9-Ethyl guanine (9-EtG) 91
3.3.4.2.5 Complexes 1-4 92
3.3.4.2.6 Complexes 5-12 94
3.3.4.2.7 pK_a* of Phenolic group in $[(\eta^6$-p-cym)Ru(azpy-OH)Cl]PF_6 (9). 95
3.3.5 Cytotoxicity 95
3.4 Discussion 97
3.4.1 Structures of complexes. 97
3.4.2 Electronic Absorption Spectroscopy 98
3.4.3 Acidity of ligands 98
3.4.4 Aqueous Solution Chemistry. 99
3.4.4.1 Arene Loss 99
3.4.4.2 Hydrolysis and Arene Loss 100
3.4.4.3 Hydrolysis Only 100
3.4.4.4 Acidity of aquated complex 13 and 9-EtG binding 101
3.4.4.5 pKa* of Phenol group in azpy-OH and complex 9 102
3.4.5 Cytotoxicity 102
3.5 Summary 103
3.6 References 103

Chapter 4 107

Dinuclear Ruthenium(II) Arene Chlorido Azo Complexes 107

4.1 Introduction 108

4.2 Experimental 110

4.2.1 Materials 110

4.2.2 Synthesis 111

4.2.2.1 *S,S*-dimethyl-*N*-(2-pyridyl)sulfilimine 111

4.2.2.2 2-Nitrosopyridine 111

4.2.2.3 2,2'-[methylenebis(4,1-phenyleneazo)]bis-pyridine (CH_2-(azpy)$_2$) 112

4.2.2.4 2,2'-[oxybis(4,1-phenyleneazo)]bis-pyridine (O-(azpy)$_2$) 112

4.2.2.5 2,2'-[carbonylbis(4,1-phenyleneazo)]bis-pyridine (CO-(azpy)$_2$) . 112

4.2.2.6 [(η^6-*p*-cym)$_2$ Ru_2(CH_2-(azpy)$_2$)Cl_2] (PF_6)$_2$ (17) 113

4.2.2.7 [(η^6-hmb)$_2$ Ru_2(CH_2-(azpy)$_2$)Cl_2] (PF_6)$_2$ (18) 113

4.2.2.8 [(η^6-*p*-cym)$_2$ Ru_2(O-(azpy))Cl_2] (PF_6)$_2$ (19) 114

4.2.2.9 [(η^6-hmb)$_2$ Ru_2(O-(azpy))Cl_2] (PF_6)$_2$ (20) 114

4.2.2.10 [(η^6-*p*-cym)$_2$ Ru_2(CO-(azpy))Cl_2] (PF_6)$_2$ (21) 115

4.2.2.11 [(η^6-*p*-hmb)$_2$ Ru_2(CO_2-(azpy))Cl_2] (PF_6)$_2$ (22) 115

4.2.3 Methods 116

4.2.3.1 Electron Paramagnetic Resonance (EPR) Spectroscopy 116

4.2.3.2 Aqueous Solution Chemistry 116

4.2.3.3 Phosphorus-31 Spin Trap Experiment 116

4.3 Results 116

4.3.1 Synthesis and Characterisation 117

4.3.1.1 Chelating bis-phenylazopyridine ligands 117

4.3.1.1.1 Nitrosopyridine 118

4.3.1.1.2 Chelating Bis-Phenylazopyridine Ligands 119

4.3.2 Dinuclear Ru^{II} arene chloride bis-complexes 120
4.3.3 Characterisation by ^{1}H NMR 120
4.3.4 Aqueous Solution Chemistry 123
4.3.5 Cyclic Voltammetry 127
4.3.5.1 First Electrochemical Reduction 127
4.3.5.2 Second Electrochemical Reduction 130
4.3.6 EPR Spectroscopy 131
4.3.7 ^{31}P Spin Trap Experiment 131
4.3.8 Cytotoxicity 134
4.4 Discussion 135
4.4.1 Synthesis of Nitrosopyridine 135
4.4.2 Dinuclear complexes 137
4.4.3 Aqueous Solution Chemistry and ^{31}P Spin Trap Experiment 137
4.4.4 Electrochemistry and EPR Spectroscopy 138
4.4.5 Cytotoxicity 138
4.5 Summary 139
4.6 References 139

Chapter 5 142

Ruthenium(II) Arene Iodido Azo Complexes 142

5.1 Introduction 143
5.2 Experimental 144
5.2.1 Materials 144
5.2.2 Synthesis 144
5.2.2.1 $[(\eta^6$-*p*-cymene)Ru(azpy-NMe_2)I]PF_6 (23) 144

5.2.2.2 [(η^6-biphenyl)Ru(azpy-NMe_2)I]PF_6, (24) 144

5.2.2.3 [(η^6-p-cymene)Ru(azpy-OH)I]PF_6 (25) 145

5.2.2.4 [(η^6-biphenyl)Ru(azpy-OH)I]PF_6 (26) 145

5.2.2.5 [(η^6-*p*-cymene)Ru(azpy)I]PF_6 (27) 146

5.2.2.6 [(η^6-biphenyl)Ru(azpy)I]PF_6 (28) 146

5.2.3 Methods 147

5.2.3.1 Unbuffered Aqueous Solution Behaviour of Complexes 23-28 .. 147

5.2.3.2 Buffered Aqueous Solution Behaviour of Complexes 23-28 147

5.2.3.3 Investigating Substitution of Iodide by Chloride in Complex 24 147

5.2.3.4 Determination of the Rates of Reduction of complexes 23, 24, 25 and 26 by ascorbic acid 148

5.2.3.5 Reduction of complexes 23, 24, 25 and 26 by ascorbic acid followed by ^{1}H NMR 148

5.2.3.6 Reactions of Ru-X with Glutathione (GSH) for complexes 8 and 24 by UV-Vis Spectroscopy, HPLC and ^{1}H NMR 148

5.2.3.7 Detection of Oxidation of GSH to GSSG 149

5.2.3.8 Detection of Reactive Oxygen Species 150

5.2.3.9 Increasing Intracellular Thiol Levels 150

5.2.3.10 Qualification of Cell Survival in HCT-116 (p53 +/-) Colon Cancer Cells 150

5.2.3.11 p53 Immunochemical Assays 151

5.3 Results 152

5.3.1 Synthesis and Characterisation 154

5.3.2 Aqueous Solution Chemistry 154

5.3.2.1 Buffered Solutions 154

5.3.2.2 Unbuffered Solutions 156

5.3.2.3 Reaction of complex 24 with excess NaCl 157

5.3.2.4 pKa of Phenolic group in [(η^6-p-cym)Ru(azpy-OH)I]PF_6 (25).... 157

5.3.3 Electrochemistry 157

5.3.3.1.1 First Electrochemical Reduction 158

5.3.3.1.2 Second Electrochemical Reduction..... 161

5.3.4 Reactions with Ascorbate..... 161

5.3.4.1 Phenylazopyridine Ligands..... 161

5.3.4.2 Ruthenium Complexes..... 162

5.3.5 Reactions with Glutathione (GSH) 166

5.3.5.1 Ru-X (X = Cl^-, I^-) Substitution..... 166

5.3.5.2 GSH oxidation..... 168

5.3.6 Cytotoxicity..... 172

5.3.6.1 A2780, A549 and WI38 Cell Lines 172

5.3.6.2 HCT-116 (Wild Type) and HCT116 (p53 Null) Cell Lines 173

5.3.7 Measurement of Oxidative Stress 174

5.3.7.1 Detection of Reactive Oxygen species (ROS) 174

5.3.7.2 Effect of Increasing Intracellular Thiol Levels 175

5.3.8 p53 and p21 Status 176

5.3.8.1 p53 levels and phosphorylation of p53 at Ser-15 and Ser-392 176

5.3.8.2 p21 Levels 177

5.4 Discussion 178

5.4.1 Complexes 23-26 are cytotoxic, despite the lack of hydrolysis..... 178

5.4.2 Substitution of iodide for chloride dramatically increases the cytotoxicity of the [(η^6-arene)Ru(azpy-R)X]$^+$ complexes and this may be due to the extra stability of Ru-I vs. Ru-Cl..... 179

5.4.3 The coordination of the phenylazopyridine ligands to the arene-ruthenium iodido centre generates a redox active site biologically accessible to ascorbate 180

5.4.4 Ruthenium Complexes 24 and 26 catalytically oxidise GSH to GSSG unlike the free ligands Azpy-NMe_2 and Azpy-OH 181

5.4.5 A build up of Reactive Oxygen Species occurs inside A549 cancer cells 183

5.4.6 Oxidative Stress is an important factor contributing to cell death ... 184

5.4.7 Precedence for anticancer drugs that cause an increase in ROS 185

5.4.8 The role of p53 and p21/Waf1 proteins 186

5.5 Summary 187

5.6 References 188

Chapter 6 194

Targeting Ruthenium(II) Arene Iodido Azo Complexes to Cancer Cells 194

6.1 Introduction 195

6.2 Experimental 197

6.2.1 Materials 197

6.2.2 Synthesis 198

6.2.2.1 Azpy-$O_2CCH_2CH_2$-maleimide 198

6.2.2.2 [(η^6-*p*-cym)Ru(azpy-$O_2CCH_2CH_2$-maleimide)I]PF_6 (29) 198

6.2.2.3 [(η^6-p-cymene)Ru(azpy-OH)I]$^+$-Holo-Transferrin (HTf-25) 199

6.2.2.4 [(η^6-p-cymene)Ru(azpy-OH)I]$^+$-Ferric-Binding-Protein (Fbp-25) 199

6.2.3 Methods 200

6.2.3.1 FTICR-MS (Fourier Transform Ion Cyclotron Resonance-Mass Spectrometry 200

6.2.3.2 ICP-MS (Inductively Coupled Plasma Mass Spectrometry) 200

6.3 Results 201

6.3.1 Ester-Maleimide Linker (29) 201

6.3.1.1 Synthesis and Characterisation of [(η^6-*p*-cym)Ru(azpy-$O_2CCH_2CH_2$-maleimide)I]PF_6 (29) 201

6.3.1.2 Stability in Water 202

6.3.2 Ru-Transferrin-Conjugate (HTf-25) 204

6.3.2.1 Synthesis 204

6.3.2.2 Purification by FPLC 204

6.3.2.3 Characterisation by ICP-OES 204

6.3.2.4 Characterisation by UV-Vis Spectroscopy 206

6.3.2.5 Stability in Aqueous Solution 207

6.3.2.6 Stability in the presence of Bicarbonate Anion 208

6.3.2.7 Characterisation of FbP-25 complex by FTICR-MS 208

6.4 Discussion 209

6.4.1 Ester-Maleimide Linker (29) 209

6.4.2 Ru-Transferrin (HTf-25) 210

6.5 Summary 211

6.6 References 212

Chapter 7 214

Conclusions and Future Work 214

7.1 Conclusions 215

7.2 Future Work 217

7.2.1 Determination of mechanism of catalytic oxidation of GSH 217

7.2.2 Measurement of intracellular thiol levels 217

7.2.3 Role of iodide in the cytotoxicity 218

7.2.4 Determination of cytotoxicity under hypoxic conditions 219

7.2.5 Ruthenium distribution in the cytoplasm / nucleus and on DNA / RNA / protein 220

7.3 References 221

Chapter 1

Introduction

This thesis is concerned with the synthesis and characterisation of ruthenium complexes and their use as anticancer agents. In this Chapter an introduction to inorganic biochemistry and inorganic drugs is given, followed by an introduction to cancer and the inorganic anticancer drugs that are used for its treatment. Then previous work on the potential use of ruthenium(II) arene complexes as anticancer agents will be reported followed by cytotoxic ruthenium complexes containing chelating azo ligands. The aims of this thesis are also described in this Chapter.

1.1 The Elements of Life

The elements carbon, hydrogen, nitrogen, oxygen, phosphorus and sulfur provide the building blocks for major cellular components including proteins, nucleic acids, lipids-membranes, polysaccharides and metabolites. However, life cannot survive with these elements alone and it is now clear that >20 elements are thought to be essential for most species to function. Inorganic elements are involved in all of life's processes e.g. charge balance and electrolytic conductivity (Na, K), signalling (Ca), Lewis acid-base catalysis (Zn, Fe, Ni, Mn), redox catalysis (V, Mn, Fe, Co, Ni, Cu, W) and electron transfer (Fe, Cu, Mo).[1] For example, catalytic activities for *ca.* 12% of all enzymes can be attributed to metal centres.[2]

1.2 Therapeutic uses of inorganic compounds

Metal compounds have been used in medicine since the 16th century. Currently a range of metal containing drugs are used therapeutically to treat a wide range of diseases including silver[3] (antibacterial), gold[4] (antiarthritic), bismuth[5] (antiulcer), vanadium[6] (antidiabetic), iron[7] (antimalarial) and platinum[8, 9] (anticancer).

Metal ions are electron deficient whereas most biological targets e.g. proteins, DNA, are electron rich so consequently there is a general tendency for metal ions to bind to and interact with many important biological molecules.[2] Furthermore metal ions have a high affinity for many small molecules e.g. O_2 that are crucial for life.[2]

Whilst metal-based drugs are often more active in vitro at lower concentrations than organic drugs, several problems need to be overcome in order for an inorganic

compound to be successful:[2] metals are often toxic at higher concentrations and so a balance between therapeutic and toxic effect needs to be reached. Often metal complexes have poor aqueous solubility, hydrolytic instability and the tendency to rapidly decompose when exposed to solvents, humidity, light or air. Interestingly, however, the statistical success of metal-based compounds reaching the clinic through the NIH anticancer screening program is about the same as for carbon-based compounds (1 in 6000 tested).[10]

1.3 Cancer

This thesis is concerned with the design of anticancer drugs and so an introduction to cancer is first given.

1.3.1 What is cancer?

Cancer is the name given to any illness resulting from one of our body's own cells growing out of control. It is caused in almost all instances by mutation or abnormal activation of cellular genes that control cell growth and cell mitosis.[11, 12] Only a fraction of the cells that mutate in the body ever lead to cancer since (a) most mutated cells have less survival capacity than normal cells and simply die, (b) only a few of the mutated cells that do survive lose the normal feedback controls that prevent excessive growth, and (c) those cells that are potentially cancerous are usually destroyed by the body's immune system before they grow into a cancer.[11]
The three main differences between cancerous and normal cells are as follows:[11]

- The cancer cell does not respect normal cellular growth limits. The reason for this is that the cells presumably do not require the growth factors that are necessary to cause growth of normal cells.
- Cancer cells are much less adhesive to each other than are normal cells. They can thus enter the bloodstream and be transported all throughout the body and form new cancerous growths.
- Some cancers produce angiogenic factors that cause new blood vessels to grow into the cancer, thus supplying the nutrients required for cancer growth.

Cancer kills because cancer tissue competes with normal tissue for nutrients. Because cancer cells continue to proliferate indefinitely, they eventually demand all the nutrients available to the body and as a result normal tissue gradually develops nutritive death.

1.3.2 Strategies to combat cancer

There are several treatments available to try to combat cancer [13] and two of the most common are as follows; chemotherapy which involves treating the patient with cytotoxic (cell killing) drugs whereas radiotherapy involves the use of radiation to destroy the cells in the treated area. This can be achieved by using X-rays (external radiotherapy) or by a radioactive material (internal radiotherapy). In both these treatments healthy cells are affected but normal cells tend to be better at repairing themselves than the cancer cells.

1.3.3 Inorganic drugs used in cancer therapy

1.3.3.1 Platinum

The anti-tumour activity of platinum was discovered in 1969 by accident in the study of the inhibition of cell division in *Escherichia coli* by electrolysis.[14] It was found that trace amounts of platinum from the electrode caused inhibition of cell division and filamentous growth. Several platinum complexes were subsequently tested for anti-tumour activity[15] and it was found that cisplatin, *cis*-$[PtCl_2(NH_3)_2]$, was a potent anticancer agent. Cisplatin is currently used clinically to treat a wide range of cancers including testicular tumours (where there is *ca* 90% cure rate), ovarian carcinomas, as well as head and neck cancers.[16] The mode of action of cisplatin is well understood and its anticancer activity is thought to be due to its interaction with cellular DNA.[17] When administered to the blood stream the cisplatin encounters relatively high chloride ion concentrations (~100 mM), which suppresses its hydrolysis. Upon entering the cells, the reduced chloride concentration (~20 mM) facilitates hydrolysis. The aquated form, $[PtCl(NH_3)_2(OH_2)]^+$ can react more readily with cellular targets. This aquated *cisplatin* binds preferentially to the N^7 atom of a guanine base of DNA since this is the most electron rich site of DNA, with displacement of the water molecule, to form a mono-functional adduct. The bi-

functional adduct is then formed by hydrolysis of the second Cl^- ligand. The major product is a 1,2-intrastrand adduct with binding at two neighbouring G-N^7 bases. By binding to DNA, *cisplatin* is thought to inhibit replication or transcription (and hence inhibit unregulated cell division). The ultimate result is apoptosis (programmed death) of the cancer cell.

This drug, however, has several major drawbacks including toxicity and tumour resistance.[17] These drawbacks, and the fact that the drug is ineffective to some cancers, have led to the development of several other potential platinum containing drugs. In general, however, the spectrum of activity for the active analogues is similar to and not broader than that of *cisplatin* itself. Thus whilst to date there have been thousands of platinum analogues synthesised and tested for anti-cancer activity,[18] only five other platinum drugs have been approved for clinical use (in at least one country).[19]

1.3.3.2 Ruthenium

1.3.3.2.1 Properties of Ruthenium

Ruthenium is a group 8 transition metal and displays many characteristic properties of the platinum group metals. It has the ability to exist in a wide range of oxidation states (Ru^0 to Ru^{VIII})[20] with the most common oxidation states in aqueous solution being Ru^{II} and Ru^{III}. Perhaps the most interesting feature of substitution at ruthenium(II) and ruthenium(III) is that both oxidation states are inert, thought the former much less so. This double inertness is an enormous advantage for studies of electron transfer and ruthenium is the only element in the periodic table with two substitution inert oxidation states.[21] The inertness is an advantage that is exploited in the design of ruthenium complexes as anticancer agents since the success of platinum compounds is mainly due to their lack of reactivity.

1.3.3.2.2 Early Work

Due to both the success and drawbacks of cisplatin and related platinum drugs the search of inorganic anticancer agents has been extended to other metals. In 1978 Clarke postulated that by using other metal ions and paying a careful attention to

their chemical properties, more selective and less toxic drugs could be developed.[22] Around this time the anticancer properties of ruthenium was reported when the Ru^{III} compound *fac*-$[RuCl_3(NH_3)_3]$ was found to induce filamentous growth of *E. Coli* at a concentration comparable to the concentration required for cisplatin to produce similar effects.[23] This compound, and analogues such as *cis*-$[RuCl_2(NH_3)_4]$ demonstrated the potential anticancer activity of ruthenium complexes. However, they were too insoluble for pharmacological use.[24]

1.3.3.2.3 Ruthenium(III) Complexes

Since this discovery, there have several other reports of ruthenium complexes which exhibit anticancer activity, most of which contain Ru^{III}. Perhaps two of the most exciting Ru^{III} anticancer compounds are imidazolium trans-tetrachlorodimethylsulfoxideimidazoleruthenate(III) complex or NAMI-A and indazolium trans-tetrachlorobis(1H-indazole)ruthenate(III) complex or KP-1019 since both compounds have entered clinical trials[25, 26] as anticancer drugs.

It has been suggested that Ru^{III} complexes are "activated by reduction" *in vivo* to Ru^{II} to coordinate more rapidly to biomolecules[10] due to the increased lability of Ru^{II}-Cl bonds.[25] There is a lower oxygen content and more acidic pH in tumours than in normal tissue and so the production of Ru^{II} relative to Ru^{III} should be favoured in tumours.[10]

1.3.3.2.4 Ruthenium(II) Complexes

Because Ru^{II} may be an active form of ruthenium, there is now an increased effort into research on the anticancer activity of Ru^{II} complexes. Early work on ruthenium(II) complexes, for example *cis*-$[RuCl_2(DMSO)_4]$ and trans-$[RuCl_2(DMSO)_4]$[27-29] showed that Ru^{II} complexes are potentially interesting in the design of new drugs.

1.4 Ruthenium(II) arenes as anticancer agents

This thesis is concerned with the use of Ru^{II} arene complexes as anticancer agents. Their general structure is shown in **Figure 1.1**. All complexes contain an η^6 arene occupying three coordination sites, a chelating ligand occupying two and a mono-

dentate ligand occupying the final site. The η^6-arene stabilizes the ruthenium in the +2 oxidation state so that oxidation to ruthenium(III) becomes unfavourable.[30] Depending on the nature of the chelated ligand, these complexes are either neutral or positively charged (and isolated as salts). Variations to all three ligand types can be achieved, so there is a great scope for the synthesis of a vast library of potential anticancer complexes. There are several synthetic routes to the complexes and these have recently been summarized.[31]

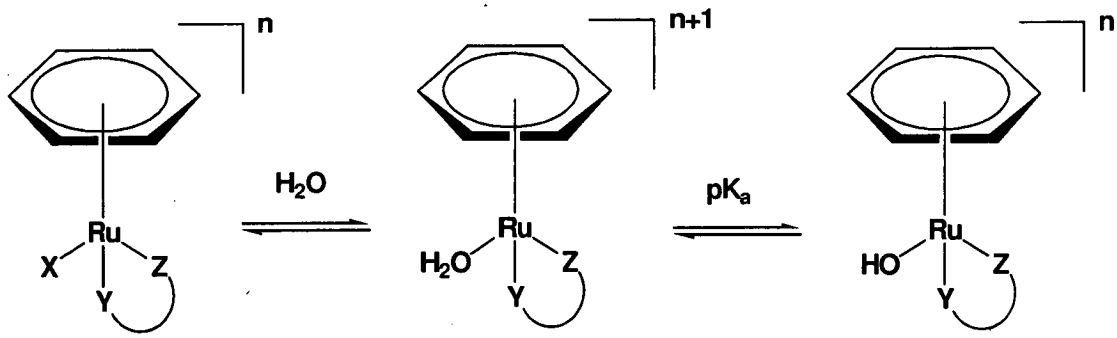

Figure 1.1. General structure of Ru^{II} arene anticancer complexes containing an η^6-arene, a chelating ligand YZ and a monodentate labile ligand X that provides a reactive site for the molecule. In water, the Ru-X bond is subject to hydrolysis to generate the corresponding aqua adduct which can be deprotonated (depending on the pH) to give the hydroxo form.

The mechanism of cytotoxic action of Ru^{II} arenes is generally thought to involve initial activation of the Ru-X bond by hydrolysis generating an active Ru-OH_2 species. This species will exist over a range of pH values, but above pH = pK_a value (the pH at which 50% of the species exists as Ru-OH_2 and Ru-OH through deprotonation of the H_2O ligand), the hydroxo Ru-OH species will predominate, and this complex is usually considered to be a less reactive species (**Figure 1.1**). Hydroxide is a less labile ligand than water and hence will not be as easily displaced by biomolecule targets. Thus ideally pK_a values of *ca.* pH >7 for aqua adducts should ensure that the active species predominates at physiological pH (7.2-7.4). Furthermore the rate of hydrolysis is important; if the complexes hydrolyse too fast they may not reach the target site.

Hydrolysis can be suppressed extracellularly due to high [Cl^-] (*ca.* 0.1 M) but becomes possible after the complex enters the cells due a lower [Cl^-] (*ca.* 4-25 mM)

found intracellularly. We thus obtain selective activation inside the cell. The primary cellular target for Ru^{II} arenes, as for many metal-based drugs is thought to be DNA[32] and so factors affecting DNA binding such as rate and extent of binding and non-covalent interactions such as hydrogen bonding and DNA intercalation become important.

1.4.1 Structure-Activity Relationships

Structure–activity relationships between the molecular structure and the cytotoxicity displayed reveal that the choice of arene, chelating ligand and even leaving group can all have an effect on the cytotoxicity.

1.4.1.1 Role of the η^6-arene

The arene is considered as a π-acid / π-acceptor ligand towards ruthenium. Evidence for this comes from (a) arene ^1H proton resonances which, upon coordination to Ru^{II} shift to a lower frequency due to increased electron density[33] and (b) from UV-Vis spectroscopic observations.[34] Ru-arene bonds are generally stable towards hydrolysis, although it has recently been reported that the photochemical displacement of the arene can occur in aqueous solution for dinuclear complexes such as $[\{(\eta^6\text{-indan})RuCl\}_2(\mu\text{-2,3-dpp})](PF_6)_2$, (2,3-dpp = 2,3-bis(2-pyridyl)pyrazine).[35] The structural and electronic features (especially with respect to Molecular Orbital Diagrams) of metal-arene bonding have been thoroughly reviewed.[36]

Initial results demonstrated that complexes containing more hydrophobic extended arenes were more cytotoxic.[37, 38] **Table 1.1** shows the IC_{50} values against the A2780 human ovarian cancer cell line for Ru^{II} arene complexes containing ethylenediamine (en) as the chelating ligand, chloride as the leaving group and a variety of η^6-arenes (**Figure 1.2**). Thus derivatives such as $[(\eta^6\text{-}p\text{-cym})Ru(en)Cl]^+$ and $[(\eta^6\text{-bip})Ru(en)Cl]^+$ (*p*-cym = *p*-cymene, bip = biphenyl) inhibited the growth of the A2780 cancer cells with IC_{50} values of between 6-10 μM, comparable to the clinically-used anticancer drug carboplatin (6 μM). When the arene is benzene (bz) the cytotoxicity decreased approximately two-fold. However, the complex $[(\eta^6$-

tetrahydronapthalene)Ru(en)Cl]$^{+}$ containing a fused three ring tetrahydroanthracene (tha) arene was equipotent with cisplatin (0.6 μM).

Table 1.1. IC_{50} values against the A2780 cancer cell line for Ru^{II} arene complexes containing different arenes. The results for the platinum controls are also included. Data from references [37, 38].

Arene / Pt control	IC_{50} (μM)
bz	17
p-cym	10
bip	5
tha	0.5
cisplatin	0.6
carboplatin	6

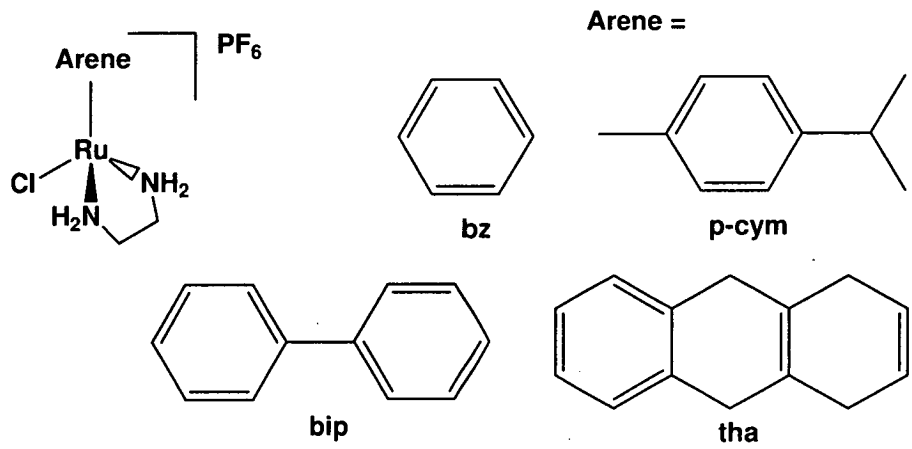

Figure 1.2. Molecular structure of $[(\eta^6\text{-arene})Ru(en)Cl]PF_6$ complexes containing different arenes.

Further studies showed that introduction of polar substituents into the coordinated benzene ring in $[(\eta^6\text{-arene})Ru(en)Cl]PF_6$ complexes lowers their cytotoxicity towards A2780 human ovarian cancer cells.[31] On the other hand, benzene arenes substituted with relatively non-polar sterically-demanding alkyl, phenyl or benzyl groups are much more potent with IC_{50} values as low as 3 μM. The activity against the A2780 cancer cell line for analogous complexes in which the arene is a fused system has

also been evaluated.[31] In general the trend is that cytotoxicity increases with arene ring size in these cases, as described earlier.

1.4.1.1.1 Influencing Cellular Uptake

A major role of the arene is thought to be to provide a hydrophobic face to the molecule and this may help in crossing cell membranes and allow for greater accumulation inside cells. More hydrophobic arenes can thus allow for a greater uptake into the cell. For example, analysis of total ruthenium taken up into A2780 cancer cells after 24 h exposure to 2.7 μM Ru was measured for [(η^6-tha)Ru(en)Cl]PF_6 and [(η^6-bip)Ru(en)Cl]PF_6.[39] The former compound, containing the more hydrophobic anthracene type arene was taken up into cells at a concentration of *ca.* 37 pmol/10^6 cells, whereas the latter, containing the less hydrophobic biphenyl arene was taken up at a concentration of *ca.* 5 pmol/10^6 cells.

1.4.1.1.2 Arene-Nucleobase Stacking and Intercalation

The choice of arene can dramatically influence the interactions of the complex with DNA. The interaction of [(η^6-arene)Ru(en)Cl]$^+$ complexes (arene = tetrahydronapthalene (tha), dihydronapthalene (dha)) and guanine DNA derivatives 9-ethylguanine (9EtG) has been studied extensively, in both the solid (X-ray crystal structures) and solution (NMR) state.[40] Although there is strong bonding between the DNA nucleobase and Ru^{II}, other non-covalent interactions including intercalation and hydrogen-bonding become important for DNA recognition. The X-ray crystal structures of [(η^6-tha)Ru(en)9Et-G (N7)]$^+$ and [(η^6-dha)Ru(en)9Et-G (N7)]$^+$ show the presence of strong intramolecular π-π arene-nucleobase stacking. The outer ring of tha/dha lies directly over the purine base and the centroid-centroid separation between the outer ring of the arene and the purine ring is 3.45 Å for [(η^6-tha)Ru(en)9Et-G (N7)]$^+$, and 3.31 Å for [(η^6-dha)Ru(en)9Et-G(N7)]$^+$, with dihedral angles of 3.3° and 3.1° respectively. This strong stacking is essentially optimum; the outer arene ring is parallel to and fully overlaps the purine ring (see **Figure 1.3**).

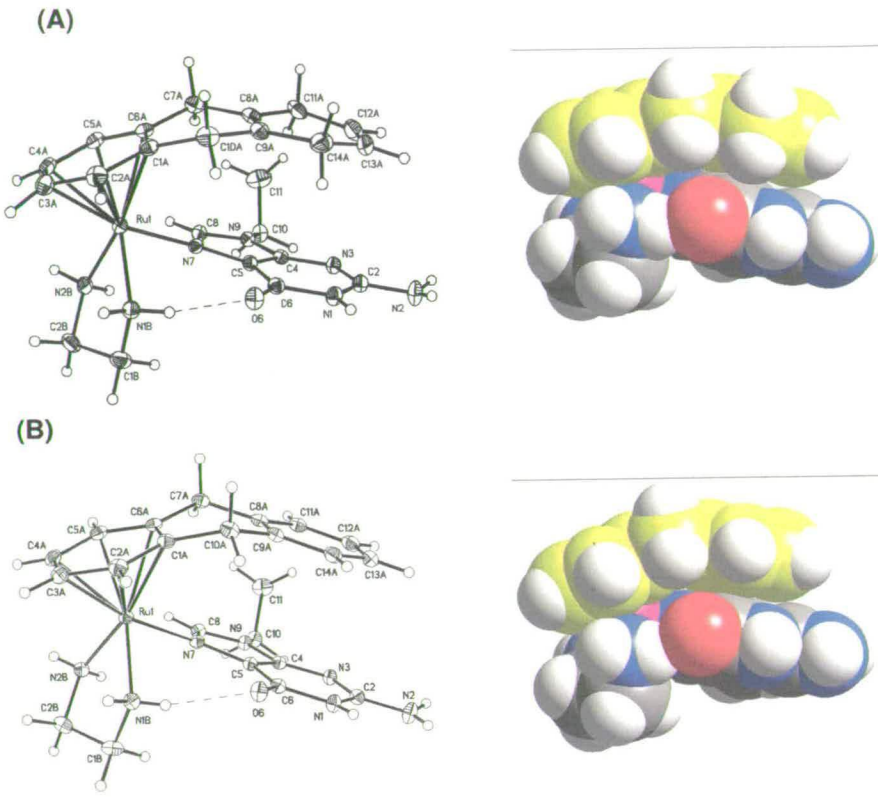

Figure 1.3. X-ray structures (at 30% probability thermal ellipsoids) and atom numbering schemes for (A) [(η6-$C_{14}H_{14}$)Ru(en)(9EtG-*N7*)]$^{2+}$, and (B) [(η^6-$C_{14}H_{12}$)Ru(en)(9EtG-*N7*)]$^{2+}$. The space-filling models show the intramolecular arene-guanine base stacking and H-bonding interactions between en NH and G O6. Color code: C of $C_{14}H_{14}$ and $C_{14}H_{12}$ yellow, C of 9EtG and en gray, Ru purple, O red, N blue, and H white. Reproduced from reference [40].

The intercalation of the arene ligands into double helical DNA has been confirmed by ethidium bromide (EtBr) fluorescence experiments.[41] EtBr is a probe which is fluorescent when bound to DNA and can be used to distinguish intercalating and non-intercalating ligands on DNA by competition.[42] Complexes (η^6-bip)Ru(en)Cl]$^+$), ([(η^6-tha)Ru(en)Cl]$^+$) and ([(η^6-dha)Ru(en)Cl]$^+$ can intercalate into the double helix of DNA, whereas (η^6-*p*-cym)Ru(en)Cl]$^+$) does not.

Further evidence for intercalation comes from DNA unwinding experiments. Complexes (η^6-bip)Ru(en)Cl]$^+$), ([(η^6-tha)Ru(en)Cl]$^+$) and ([(η^6-dha)Ru(en)Cl]$^+$ unwind negatively supercoiled pSP73KB plasmid DNA by 14 ± 1° per bound ruthenium and (η^6-*p*-cym)Ru(en)Cl]$^+$) by only 7 ± 0.5°.[41] These results suggest

that the extra unwinding is a result of the intercalation of the extended arene or another non-covalent interaction of these complexes with DNA upon mono-functional binding. Large unwinding angles of 15 or 19 ° produced for the platinum compounds *cis*-[Pt-$(NH_3)_2$(N8-ethidium)Cl]$^{2+}$ and *cis*-[Pt-$(NH_3)_2$(N3-ethidium)Cl]$^{2+}$ which contain the known intercalator ethidium and can form only mono-functional adducts of DNA, have also been explained this way.[43]

1.4.1.1.3 Rates of Hydrolysis

The rates of hydrolysis of [(η^6-bip)Ru(en)Cl]$^+$, [(η^6-tha)Ru(en)Cl]$^+$ and [(η^6-dha)Ru(en)Cl]$^+$ (bip = biphenyl, tha = tetrahydroanthracene, dha = dihydroanthracene) are essentially independent of ionic strength and increase with the size of the arene: 3.95 x 10^{-3} s^{-1}, $t_{1/2}$ = 2.92 min for arene = bip, 6.84 x 10^{-3} s^{-1}, $t_{1/2}$ = 1.69 min for arene = tha and 6.49 x 10^{-3} s^{-1} $t_{1/2}$ = 1.78 min for arene = dha (310 K, 0.1M $NaClO_4$, 0.3 mM bip, 0.5 mM tha and dha complexes)).[44] The rates of the corresponding anation reactions (replacement of H_2O by Cl^-) were also studied and decrease by about two-fold on increasing the ionic strength from 0.015 to 0.5 M $NaClO_4$. This decrease is expected on the basis of the Brønsted equation, i.e. that the rate constant is expected to be independent of the ionic strength when one of the reactants remains uncharged, whereas the rate constant decreases with ionic strength if the charges on the two ions are of opposite sign. The anation reactions were rapid, reaching equilibrium within *ca.* 100-1600 s. Generally the anation reactions of the [(η^6-tha)Ru(en)Cl]$^+$ and [(η^6-dha)Ru(en)Cl]$^+$ complexes were about 2.5-fold faster than [(η^6-bip)Ru(en)Cl]$^+$. These results demonstrate that the arene influence the rates of hydrolysis, and this is obviously important in the design of Ru^{II} arene anticancer complexes.

1.4.1.1.4 Rates of Reaction with cGMP

The half-lives for reaction of five ruthenium(II) arene en chloride complexes (arene = bip, tha, dha, bz and cym) and the corresponding aqua adducts with c-GMP are summarized in **Table 1.2**.[40] The rates of reaction of c-GMP with [(η^6-tha)Ru(en)OH_2]$^{2+}$ [(η^6-dha)Ru(en)OH_2]$^{2+}$ and [(η^6-bip)Ru(en)OH_2]$^{2+}$ complexes are more than three times faster than those for the [(η^6-*p*-cym)Ru(en)OH_2]$^{2+}$ and [(η^6-

bz)Ru(en)OH_2]$^{2+}$ complexes. The rates of reaction of the chloride complexes are slower due to the two-step process of reaction: hydrolysis followed by Ru-N7 binding. The same trend in reactivity was observed for the chlorido and aqua complexes. For the complexes [(η^6-tha)Ru(en)Cl]$^+$, [(η^6-dha)Ru(en)Cl]$^+$ and [(η^6-bip)Ru(en)Cl]$^+$, 100% of the N7-bound product was observed after 2 d whereas only *ca.* 80% of the N7 bound product formed for the p-cym and bz complexes after 4 d. Thus the rate of reaction of the Ru aqua complexes (and chloro complexes) with c-GMP depends markedly on the nature of the arene decreasing by over an order of magnitude as the arene is changed from tha > bip > dha >> *p*-cym > bz.

Table 1.2. Half lives ($t_{1/2}$) for reactions of Ru^{II} arene complexes [(η^6-arene)Ru(en)Cl]$^+$ and the corresponding aqua complexes [(η^6-arene)Ru(en)OH_2]$^{2+}$ with cGMP[a].

[(η^6-arene)Ru(en)Cl]$^+$	$t_{(1/2)}$ / h	[(η^6-arene)Ru(en)OH_2]$^{2+}$	$t_{(1/2)}$ / h
tha	1.1	tha	0.38
bip	2.0	bip	0.69
dha	3.6	dha	0.78
p-cym	7.1	p-cym	2.23
bz	13	bz	4.94

[a]conditions Ru:G 1:1, 100 mM $NaClO_4$, 298 K, 5 mM for [(η^6-arene)Ru(en)OH_2]$^{2+}$, 2 mM for [(η^6-arene)Ru(en)Cl]$^+$.

Because the fastest rates are for the complexes containing the larger arene ligands, this implies lower activation energies ($\Delta G^{\ddagger}$) for formation of seven-coordinate transition states (assuming an associative mechanism). A significant contribution to $\Delta G^{\ddagger}$ may arise from $\pi - \pi$ stacking of the arene and the purine ring in the transition state (negative $\Delta H^{\ddagger}$). Such an interaction is not possible for the p-cymene and benzene complexes. Thus these hydrophobic interactions could produce a driving force for DNA binding.

1.4.1.2 Role of the Leaving Group

Hydrolysis of the Ru-X bond is thought to be central to the cytotoxicity of Ru^{II} arene complexes since it is this step that activates the complex for potential binding to DNA or other possible cellular targets.

Good correlations between hydrolysis rates, hydrolysis equilibrium and cytotoxicity has been observed for the ruthenium complexes $[(\eta^6\text{-hexamethylbenzene})Ru(en)X]^+$ (**Figure 1.4**).[45]

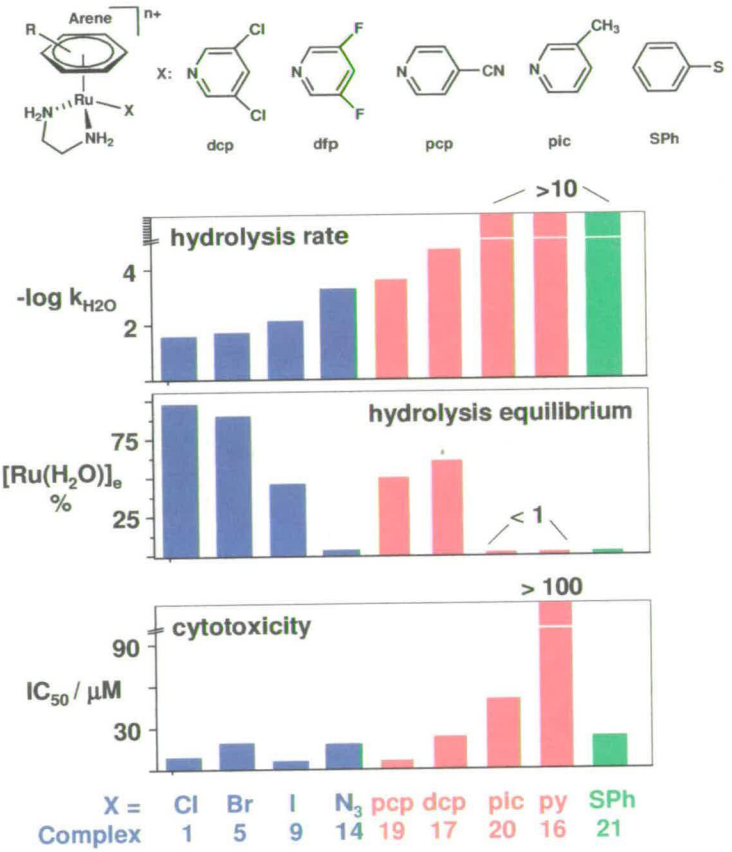

Figure 1.4. Correlation of hydrolysis with cytotoxicity. (Upper) Structures of the complexes and leaving groups. (Lower) Hydrolysis rates, equilibrium percentage of total Ru as $[(\eta^6\text{-hmb})Ru(en)(H_2O)]^{2+}$ ($[Ru(H_2O)]_e$ %) and A2780 cancer cell cytotoxicity IC_{50} values for $[(\eta^6\text{-hmb})Ru(en)X]^{n+}$ complexes with different 'leaving groups'. Reproduced from reference [45].

In general, a faster hydrolysis rate and a high percentage of aqua species at equilibrium correlated with good cytotoxicity towards the A2780 human ovarian cancer cell line. An exception is for the complex $[(\eta^6\text{-hmb})Ru(en)SPh]^+$ which hydrolyses very slowly and to a low extent. This complex may be activated by oxidation of bound SPh to the sulfenate or sulfinate by oxygen and subsequent labilisation, since reactions of Ru^{II} arenes with GSH show similar behavior.[46] Density functional theory calculations[45] for aquation of $[(\eta^6\text{-benzene})Ru(en)X]^+$, X = Cl^-, Br^-, I^-, N_3^- suggest that the aquation proceeds via a concerted interchange pathway and does not appear to be strongly associatively- or dissociatively-activated. The reaction barriers and overall reaction energies for aquation follow the order Br < Cl < I < N_3. The reactions appear to occur nearer the I_a (interchange-associative) mechanistic continuum rather than the I_d (interchange-dissociative mechanism). On the basis of electronegativity, the N_3 complex would be expected to hydrolyze at a rate between the Cl^- and Br^-, analogues but a much slower rate is observed. The lower rate is ascribed to the increased steric bulk of this polyatomic pseudohalide; an I_a substitution is more influenced by steric factors than an I_d pathway. Furthermore, the electron-accepting effect of the strong π-acid arene ligands is thought to be responsible for the shift towards a more associative I_a pathway. Ru^{III} complexes usually react via associative pathways[47] whereas Ru^{II} complexes are more suited to dissociative mechanisms.[48] The π-acid arene accepts electron density from ruthenium to produce a higher charge on the metal. Thus Ru^{II} in $\{(\eta^6\text{-arene})Ru\}^{2+}$ may behave more like a Ru^{III} centre.

1.4.1.3 Role of the Chelating Ligand

Increased cytotoxicity is associated with a chelating ligand and a single reactive site. Ruthenium complexes containing mono-dentate ligands such as $[(\eta^6\text{-p-cymene})Ru(CH_3CN)_2Cl]^+$ and $[(\eta^6\text{-}p\text{-cym})Ru(\text{isonicotinamide})_2Cl]^+$ were found to be inactive towards A2780 cancer cells (IC_{50} > 150 μM). Monodentate ligands on Ru^{II} arenes are more labile than bidentate ligands[49] and can readily exchange with solvent whereas the chelating ligand is more resistant to hydrolysis/solvent exchange. Most of the work to date on Ru^{II} arene anticancer complexes involves the chelating ligand ethylenediamine (en).

1.4.1.3.1 Specific Hydrogen Bonding

In all three crystal structures of $[(\eta^6\text{-biphenyl})Ru(en)9Et\text{-}G(N7)]^+$, $[(\eta^6\text{-tha})Ru(en)9Et\text{-}G(N7)]^+$ and $[(\eta^6\text{-dha})Ru(en)9Et\text{-}G(N7)]^+$, strong stereospecific hydrogen-bonding occurs between an en NH proton oriented away from the arene, pointing towards the DNA base (so called NH_{down} protons) and the C6 cabonyl oxygen of the guanine (average distances 2.8 Å N···O, N-H···O 163°) (see **Figure 1.3**).[40] Such stereospecific hydrogen-bonding between the en ligand and the exocyclic oxygen atom of guanine, may play an important role in both the stability and conformation of this adduct.

Structure-activity relationships have revealed that replacement of the ethylenediamine chelating ligand with the N,N-dimethyl-ethylenediamine derivative results in a dramatic loss of cytotoxicity (e.g. $[(\eta^6\text{-}p\text{-cym})Ru(en)Cl]^+$, IC_{50} = 10 μM, $[(\eta^6\text{-bip})Ru(N,N\text{-dimethyl-en})Cl]^+$, IC_{50} >100 μM).[31] This may be related to the inability of the complex to form strong stereospecific C6O···HN hydrogen bonds with guanine bases, an interaction thought to stabilize and enhance the recognition.[40] The reaction of $[(\eta^6\text{-bip})Ru(N,N\text{-dimethyl-en})Cl]^+$ with 9-EtG was followed by ^1H NMR spectroscopy and no binding was observed. Thus steric effects of the methyl groups (preventing approach by 9-EtG) as well as a lack of potential hydrogen bonding towards DNA bases may contribute to the loss of activity.

1.4.1.3.2 pKa of coordinated water

The pK_a values of the aqua complexes $[(\eta^6\text{-bip})Ru(en)H_2O]^{2+}$, $[(\eta^6\text{-dha})Ru(en)H_2O]^{2+}$ and $[(\eta^6\text{-tha})Ru(en)H_2O]^{2+}$ are 7.71, 7.89 and 8.01, respectively.[44] Thus in the blood plasma, where the chloride concentration is high (*ca.* 0.14 M) all three complexes exist largely (>89%) in this inactive chlorido form. Upon entering the cytoplasm and nucleus, the chloride concentrations drop to *ca.* 23 and 4 mM, respectively. Hence the extent of aquation is predicted to increase from about 30% in the cytoplasm to about 70% in the nucleus. This would represent an activation mechanism for these chloro complexes inside the cytoplasm/nucleus. Interestingly, only a small amount of Ru-OH hydroxo adducts (average <10% of total ruthenium) is predicted to exist inside cells due to the high pK_a value of the aqua adducts This becomes important for DNA binding, since the Ru-OH bond is

found to be less reactive towards DNA nucleobases compared to Ru-OH_2 (*vide supra*).

1.4.1.3.3 Other N,N-chelating ligands

Changing the chelating ligand from ethylenediamine to propylene-diamine (prop) (i.e. changing the chelate ring size from five to six membered) did not affect the cancer cell cytotoxicity $[(\eta^6\text{-p-cym})Ru(en)Cl]^+$ IC_{50} = 10 μM, $[(\eta^6\text{-p-cym})Ru(prop)Cl]^+$ IC_{50} = 10 μM.[31] However, addition of a polar OH substituent on the propylenediamine backbone decreased the activity. Further derivatisation of en ligands has varying effects on the cytotoxicity;[31] mono-methylation of en does not affect IC_{50} values, whereas dialkylation via ring formation lowers the activity three fold and cyclisation of en to give homopiperazine results in an inactive compound (IC_{50} >50 μM).

Good cytotoxicity is retained when ethylenediamine ligands are replaced with chelating 1,2-diaminobenzene ligands.[31] A slightly different trend was observed with cytotoxicity on changing the arene in 1,2-diaminobenzene complexes; the IC_{50} value increased in the order biphenyl (5 μM), dha (7 μM) < p-cymene (11 μM), tetralin (13 μM) <tha (23 μM). Interestingly these complexes are able to overcome cross-resistance to the 2780^{AD} cell line, in contrast to en complexes.[38]

1.4.1.3.4 O,O Chelating Ligands

A σ-donor π-donor oxygen-chelating ligand dramatically changes the reactivity of the ruthenium arene with respect to hydrolysis, cytotoxicity and DNA base specificity. The chemistry of ruthenium(II) arenes containing the anionic O,O-chelating ligand acetylacetonate (acac) has been reported.[50] Complexes such as $[(\eta^6\text{-}p\text{-cym})Ru(acac)Cl]$ hydrolyze rapidly in water and equilibrium is reached in less than 5 minutes (298 K). The pK_a of the coordinated water molecule in the aqua adduct $[(\eta^6\text{-}p\text{-cym})Ru(acac)OH_2]^+$ is 9.41, which means that at physiological pH (pH 7.4) the complex exists almost exclusively in the reactive aqua form. The increased pKa value is due to the acac ligands being strong σ-donor and π-donors towards the Ru^{II} centre, increasing the electron density and hence decreasing the acidity of the ruthenium centre.[51] In the reaction of $[(\eta^6\text{-p-cym})Ru(acac)Cl]$ with guanosine (2

mM 1:1) at equilibrium *ca.* 80% of the guanosine is bound. A similar result is obtained for adenosine (*ca.* 80% is bound ratio of adoN7:adoN1 4:1). This selectivity is in stark contrast to the corresponding ethylenediamine analogues for which negligible binding to adenosine is observed and a strong preference for guanosine is observed.[52]

The complexes [(η^6-arene)Ru(acac)Cl] (arene = *p*-cym, bip, bz, indan and dha) exhibit moderate activity towards A2780 ovarian cancer cells (IC_{50} 19-70 μM).[31] In general the acac complexes hydrolyze rapidly and have poor aqueous solubility. The reason for the reduced cytotoxicity compared to the en analogues may in part be due to the protonation and irreversible displacement of the chelated acac derivative under some conditions; the aqueous solution chemistry of the osmium analogue [(η^6-p-cym)Os(acac)Cl] was studied using conditions mimicking the cytotoxicity testing[53] and this revealed that only one species was present, assignable to the hydroxo-bridged dimer [(η^6-p-cym)Os(μ_2-OD)$_3$Os(η^6-p-cym)]$^+$, i.e. acac is readily lost from the complex. This complex is inactive towards the A2780 cancer cell line (IC_{50} > 50 μM).

1.4.2 Comparison with Cisplatin and other Platinum Complexes

Because Ru^{II} arene complexes are mono-functional (as opposed to cisplatin which is bifunctional) they are expected to differ in their mechanism of action. This is desirable since most platinum analogues of cisplatin are cross resistant with cisplatin and this severely limits their therapeutic application.[18]

1.4.2.1 Activity towards A2780cis (Cisplatin Resistant) Cell Line

Firstly Ru^{II} arene complexes are completely non-cross resistant with cisplatin towards the A2780cis cell line.[38] This is interesting as it suggests that the mechanism of action differs from that of cisplatin. Furthermore the *in vivo* antitumour activity in human ovarian A2780, and A2780cis xenografts for the complex [(η^6-bip)Ru(en)Cl]$^+$ showed that it produced a significant growth delay in A2780 cells and maintained the growth inhibitory activity in the A2780cis xenograft. Thus, encouragingly, the patterns established *in vitro* was mirrored to a large degree *in vivo*.

1.4.2.2 Reactions with DNA

The interaction of several ruthenium arene complexes with DNA in a cell-free medium have been compared to cisplatin.[41] The extent of ruthenation of double helical CT-DNA (0.1 mg/mL) (CT = Calf Thymus) by the arene complexes at an r_i value of 0.1 (molar ratio of free ruthenium complex to nucleotide phosphates at the onset of incubation with DNA) in 10 mM $NaClO_4$ at 310 K was followed. The amount of ruthenium bound per DNA nucleotide phosphate increased with time and the time at which binding reaches 50% ($t_{50\%}$) was markedly dependent on the arene: 10 min ($[(\eta^6\text{-bip})Ru(en)Cl]^+$) and ($[(\eta^6\text{-tha})Ru(en)Cl]^+$), 15 min ($[(\eta^6\text{-dha})Ru(en)Cl]^+$) and 3.5 h ($[(\eta^6\text{-p-cym})Ru(en)Cl]^+$). Under the same conditions $t_{50\%}$ for cisplatin binding is *ca.* 2 h. Thus for ($[(\eta^6\text{-bip})Ru(en)Cl]^+$), ($[(\eta^6\text{-tha})Ru(en)Cl]^+$) and ($[(\eta^6\text{-tha})Ru(en)Cl]^+$), reactions are an order of magnitude faster than for cisplatin.

1.4.2.3 RNA synthesis

The *in-vitro* RNA synthesis by RNA polymerases on DNA templates has been studied using a linear DNA fragment modified by these ruthenium arene complexes, cisplatin and monofunctional [PtCl(dien)]Cl.[41] RNA synthesis on these modified plasmid fragments yielded fragments of defined size, which indicates that RNA synthesis on these templates was prematurely terminated. For cisplatin, the termination sites are similar as for the Ru^{II} arenes (i.e. mainly at G) but the efficiency of the ruthenium-adducts to terminate RNA synthesis in vitro is reduced relative to that of cisplatin. Furthermore the efficiency of the ($[(\eta^6\text{-}p\text{-cym})Ru(en)Cl]^+$) adducts was noticeably lower than for the other three Ru^{II} arenes. Interestingly, no termination of RNA synthesis by the mono-functional [Pt(dien)Cl]Cl was observed, and this inability has been observed for several mono-functional platinum adducts.[54-56] This suggests that the ruthenium complexes bind and distort DNA in a somewhat different fashion to the mononuclear Pt complex [Pt(dien)Cl]Cl.

1.4.2.4 DNA Repair Synthesis

Considerably different levels of damage-induced DNA repair synthesis were detected in plasmids modified by $[(\eta^6\text{-tha})Ru(en)Cl]^+$, $[(\eta^6\text{-}p\text{-cym})Ru(en)Cl]^+$ and cisplatin.[57]

DNA repair synthesis can occur by various repair mechanisms including the nucleotide excision repair (NER) mechanism (which is the usual repair mechanism for cisplatin). Compared to cisplatin the monofunctional adducts of $[(\eta^6\text{-tha})Ru(en)Cl]^+$ and $[(\eta^6\text{-}p\text{-cym})Ru(en)Cl]^+$ are excised with a significantly lower efficiency than the major intrastrand crosslink of cisplatin, and $[(\eta^6\text{-}p\text{-cym})Ru(en)Cl]^+$ adducts are excised slightly more than those of $[(\eta^6\text{-tha})Ru(en)Cl]^+$. The HMG (High Mobility Group) protein plays a role in sensitizing the cells to cisplatin. For example it has been shown that the HMG domain proteins recognize and bind to DNA adducts formed by cisplatin.[17] An important structural motif recognized by HMG domain proteins on DNA modified by cisplatin is a directional bend of the helix axis towards the major groove. No recognition of the DNA monofunctional adducts of $[(\eta^6\text{-tha})Ru(en)Cl]^+$ or $[(\eta^6\text{-}p\text{-cym})Ru(en)Cl]^+$ by HMGB1 has been observed, suggesting that these adducts do not afford structural motifs recognized by HMG domain proteins. Thus the mechanism of antitumour activity of Ru^{II} arenes does not involve recognition of its DNA adducts by HMG domain proteins as a crucial step, in direct contrast to cisplatin.

1.5 2-Phenylazopyridine (azpy) Chelating Ligands

Ruthenium(II) is well recognized as a metal ion capable of entering into $d\pi$-$p\pi$ back bonding with π-acceptor ligands[58] and to date the most common π-acceptor ligand studied with ruthenium is bipyridine.[59] The chelation of less common π-acceptor ligands such as 2-phenylazopyridine to ruthenium was first investigated in 1980[60] with the view that these complexes may exhibit interesting chemical properties similar to bipy, since most of the novelty of Ru-bipy complexes arises from the π-interactions between the metal and ligand. 2-Phenylazopyridine (azpy), in complexes such as $[RuCl_2(azpy)_2]$ was found to be a much better ligand for stabilization of Ru^{II} than bipy ($E_{1/2}$ $Ru^{II} \rightarrow Ru^{III}$ 1.00-1.21 V (azpy), 0.30 V (bipy)) showing greater difficulty in oxidation of Ru-azpy complexes to Ru^{III}.[60]

The pK_a values of the corresponding aquo complexes $[Ru(azpy)_2(H_2O)_2]^{2+}$ (pK_{a1} = 6.80 ± 0.05) and pK_{a2} = 8.66 ± 0.05) and $[Ru(azpy)_2(py)(OH_2)]^{2+}$ (pK_a = 6.80 ± 0.05) are much lower than the corresponding bipy complexes (for example

$[Ru(bipy)_2(py)(OH_2)]^{2+}$ (pK_a = 10.26 ± 0.05),[61] again attributed to the much stronger π-acceptor character of azpy compared with bipy; the Ru-OH_2 σ-bond is correspondingly stronger in the azpy case resulting in easier deprotonation.

The azo N=N infrared stretch for ruthenium-2-phenylazopyridine complexes of the type $[Ru(azpy)_2(AB)]^{n+}$ is sensitive to the π-accepting nature of the coligand (AB) with a better π-acceptor ligand giving a higher υ(N=N), and can thus be used as a π-bonding probe.[62] Other applications of Ru-phenylazopyridine complexes include as catalysts for the oxidation of alcohols to acids by $NaBrO_3$[63] and of glucose.[64]

1.5.1 The anticancer activity of ruthenium(II) azpy complexes

Previous work has shown that the ruthenium(II) complexes containing the chelating azo ligand azpy display interesting anticancer activity.

1.5.1.1 Mononuclear complexes

Because the chelating ligand azpy lacks a two-fold symmetry axis, ruthenium complexes of the type $[Ru(azpy)_2Cl_2]$ can theoretically exist as 5 isomers, but early work reported only three α-$[Ru(azpy)_2Cl_2]$, β-$[Ru(azpy)_2Cl_2]$ and γ-$[Ru(azpy)_2Cl_2]$ (**Figure 1.5**).[65]

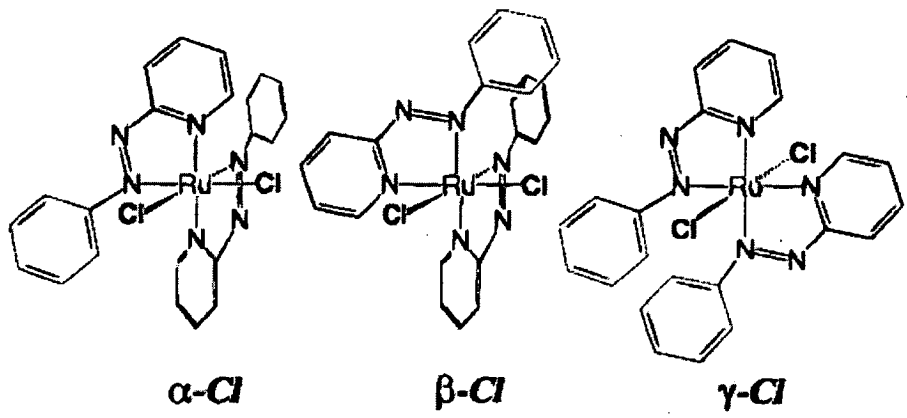

Figure 1.5. Structural representations of α-[Ru(azpy)$_2$Cl$_2$] (α-Cl), β-[Ru(azpy)$_2$Cl$_2$] (β-Cl) and γ-[Ru(azpy)$_2$Cl$_2$] (γ-Cl). Reproduced from Reference [65].

More recently the structure of a fourth isomer (δ-[Ru(azpy)$_2$Cl$_2$]) has been reported.[66] The cytotoxicity of these three isomers against a series of human tumour cell lines was determined[65] and whilst β-Cl and γ-Cl showed low to moderate cytotoxicity[67], the α-Cl isomer was roughly an order of magnitude more cytotoxic with IC_{50} values comparable to cisplatin in some cell lines, and even more active than cisplatin in some of the faster growing cell lines. Furthermore, no cross-resistance was observed in the A2780cis resistant cell line suggesting that this compound may be able to avoid the DNA repair mechanisms that are present in cisplatin-resistant cells, or be unaffected by the elevated GSH levels.[68] Cellular uptake studies showed that after one hour exposure to TS/A murine adenocarcinoma cells, the ruthenium concentration for the α-Cl isomer was approximately six fold higher than the β-Cl isomer (0.0160 μg vs 0.0028 μg / 1 x 10^6 cells).

Several azpy derivatives have subsequently been synthesized including methylated phenylazopyridine derivatives (o-tolylazopyridine (tazpy) and 4-methyl-2-phenylazopyridine (mazpy)) where α-[Ru(tazpy)$_2$Cl$_2$] was found to be more cytotoxic than α-Cl whereas α-[Ru(mazpy)$_2$Cl$_2$] slightly less active.[69] The α-Cl analogue was poorly soluble in water and so the nitrate analogue α-[Ru(azpy)$_2$(NO$_3$)$_2$] was developed[70] in order to study the interaction of this compound with DNA bases, since DNA is considered the target for this type of complexes.[71] In the reactions of this complex with DNA model bases (9-EtG, Guo)

no bifunctional adducts were obtained and the orientation of the 9-EtG in the monofunctional adduct α-[$Ru(azpy)_2$(9-EtG)X] varied depending on X (X = Cl, H_2O), with two rotamers being observed in solution.[70] This was in contrast to the structurally similar yet non-cytotoxic *cis*-[$Ru(bipy)_2Cl_2$] which, upon reaction with 9-EtG, gave only one 9-EtG orientation.[72] Thus the larger, more flexible azpy ligand allowed for more orientations with guanine derivatives. Interestingly, upon reaction of α-[$Ru(azpy)_2(NO_3)_2$] with 9-MeA, a rare neutral imine tautomer of 9-MeA is observed whereby one nucleobase mimic coordinated to the ruthenium in a bidentate fashion via its N7 and exocyclic N6 atoms to form α-[$Ru(azpy)_2$9-MeA]$^{2+}$.[73] The nitrate derivatives, although showing an increased aqueous solubility, were about a factor of ten less cytotoxic then the less soluble chloride analogues.[68]

It was thus hypothesized that Structure-Activity Relationships must specify two labile *cis* chloride ligands (which can hydrolyse enabling DNA binding). In order to test this hypothesis a series of tris-chelating ligand complexes [RuL_3]$(PF_6)_2$ (mer-[$Ru(azpy)_3$]$(PF_6)_2$, α-[$Ru(azpy)_2$(bipy)]$(PF_6)_2$ and β-[$Ru(azpy)_2$(bipy)]$(PF_6)_2$, and [Ru(azpy)$(bipy)_2$]$(PF_6)_2$) all incapable of hydrolysis were tested for cytotoxicity.[74] These complexes were predicted not to display cytotoxicity but surprisingly, when evaluated against a series of human tumour cell lines significant cytotoxicity was demonstrated in one or more line. This result may mean that the cytotoxicity of these complexes is by a different mechanism of action to α-[$Ru(azpy)_2Cl_2$] and may be caused by an intercalative interaction with DNA as opposed to direct coordination by Ru..

1.5.1.2 Dinuclear Complexes

There is a growing interest in the design of anticancer complexes which impart cytotoxicity in a different way to cisplatin (i.e. not through coordinative DNA binding),[75, 76] and the cytotoxicity of two isomeric dinuclear unsaturated ruthenium(II) complexes linked via the dinuclear chelating ligand 2,2'-[methylenebis(4,1-phenyleneazo)]bis-pyridine (L) to form [$Ru_2Cl_4L_2$] has recently been reported.[77] The complexes exist as three different double-stranded architectures: the *trans-trans* (γγ) isomer (in which the chlorine ligands at both ruthenium centres are in a trans configuration), the *trans-cis* isomer (γα) and the *cis-*

cis (αα) isomer. The *trans-trans* isomer and the *trans-cis* isomer were tested for cytotoxicity towards two human breast tumors cell lines HBL100 and T47D. Both complexes were very active in these cell lines with the *trans-cis* having similar activity to cisplatin in the HBL100 cell line (5.1 vs. 4.9 μM) and better activity in the TD47D cell line (IC50 6.7 vs. 28.3 μM) whereas the *trans-trans* isomer was approximately 30 times more potent than cisplatin in the HBL100 cell line (0.16 μM) and 100 times more in the T47D line (0.16 μM). Interestingly thus the same trend in cytotoxicity was observed as seen for the mononuclear species in that the highest activity is observed for the γ-isomer than the α-isomer.[66, 69]

1.6 Aims

The overall aim of this thesis is to investigate the anticancer activity of ruthenium(II) arene complexes containing a 2-phenylazopyridine as the N,N-chelating ligand. Much of the work to date had focused on the use of N,N-chelating ligands that bind to ruthenium in a σ-donor-only fashion and so the effect of changing the type of bonding of the ligand to ruthenium (i.e. the incorporation of a π-acceptor ligand) can be investigated. More specific aims are as follows.

1. To synthesise and characterise ruthenium arene complexes containing 2-phenylazopyridine ligands with variations to the arene, leaving group and the azo ligand.
2. To study the aqueous solution chemistry of these complexes and compare the behaviour to that reported for en and acac derivatives.
3. To investigate the reactivity of the complexes towards nucleobases, potential cellular targets.
4. To investigate the cancer cell cytotoxicity of the complexes.
5. To elucidate the mechanism of cancer cell cytotoxicity

Thus essentially the overall aim of the work is to assess the potential of using ruthenium(II) arene complexes containing chelating azo ligands as anticancer agents by gaining knowledge of their chemical and biological properties.

1.7 References

[1] I. Bertini, H. B. Gray, E. I. Stiefel, J. S. Valentine, *Biological Inorganic Chemistry Structure and Reactivity*, University Science Books, Sausalito, CA, **2007**.

[2] R. Huang, A. Wallqvist, D. G. Covell, *Biochem. Pharmacol.* **2005**, *69*, 1009-1039.

[3] J. L. Clement, P. S. Jarret, *Metal-Based Drugs* **1994**, *1*, 467-482.

[4] L. Messori, G. Marcon, *Met. Ions Biol. Syst.* **2004**, *41*, 279-304.

[5] H. Sun, L. Zhang, K.-Y. Szeto, *Met. Ions Biol. Syst.* **2004**, *41*, 333-378.

[6] K. H. Thompson, C. Orvig, *J. Inorg. Biochem.* **2006**, *100*, 1925-1935.

[7] V. R. Gordeuk, M. Loyevsky, *Adv. Exp. Med. Biol.* **2002**, *509*, 251-272.

[8] A. S. Abu-Surrah, *Mini-Rev. Med. Chem.* **2007**, *7*, 203-211.

[9] Z. Guo, P. J. Sadler, *Adv. Inorg. Chem.* **2000**, *49*, 183-306.

[10] M. J. Clarke, *Coord. Chem. Rev.* **2003**, *236*, 209-233.

[11] A. C. Guyton, *Textbook of Medical Physiology, Vol. Eighth Edition*, W. B. Saunders Company, Philadelphia, USA, **1991**.

[12] H. Lodish, A. Berk, P. Matsudaira, C. A. Kaiser, M. Krieger, M. P. Scott, S. L. Zipursky, J. Darnell, *Molecular Cell Biology*, Fifth Edition ed., W. H. Freedman and Company, New York, USA, **2004**.

[13] www.cancerresearchuk.org

[14] B. Rosenberg, L. Van Camp, T. Krigas, *Nature* **1965**, *205*, 698-699.

[15] B. Rosenberg, L. VanCamp, J. E. Trosko, V. H. Mansour, *Nature* **1969**, *222*, 385-386.

[16] C. F. J. Barnard, *Platinum Metals Rev.* **1989**, *33*, 162-167.

[17] E. R. Jamieson, S. J. Lippard, *Chem. Rev.* **1999**, *99*, 2467-2498.

[18] R. B. Weiss, M. C. Christian, *Drugs* **1993**, *46*, 360-377.

[19] M. Galanski, M. A. Jakupec, B. K. Keppler, *Curr. Med. Chem.* **2005**, *12*, 2075-2094.

[20] E. A. Seddon, K. R. Seddon, *Topics in Inorganic and General Chemistry, Vol. 19: The Chemistry of Ruthenium*, **1984**.

[21] M. L. Tobe, J. Burgess, *Inorganic Reaction Mechanisms*, Addison Wesley Longman Inc, Essex, **1999**.

[22] M. J. Clarke, *J. Am. Chem. Soc.* **1978**, *100*, 5068-5075.

[23] J. R. Durig, J. Danneman, W. D. Behnke, E. E. Mercer, *Chem.-Biol. Interact.* **1976**, *13*, 287-294.

[24] M. J. Clarke, *Met. Ions Biol. Syst.* **1980**, *11*, 231-283.

[25] C. G. Hartinger, S. Zorbas-Seifried, M. A. Jakupec, B. Kynast, H. Zorbas, B. K. Keppler, *J. Inorg. Biochem.* **2006**, *100*, 891-904.

[26] J. M. Rademaker-Lakhai, D. Van Den Bongard, D. Pluim, J. H. Beijnen, J. H. M. Schellens, *Clin. Cancer Res.* **2004**, *10*, 3717-3727.

[27] G. Sava, S. Zorzet, T. Giraldi, G. Mestroni, G. Zassinovich, *Eur. J. Cancer Clin. Oncol.* **1984**, *20*, 841-847.

[28] G. Sava, S. Pacor, S. Zorzet, E. Alessio, G. Mestroni, *Pharmacol. Res.* **1989**, *21*, 617-628.

[29] G. Mestroni, E. Alessio, M. Calligaris, W. M. Attia, F. Quadrifoglio, S. Cauci, G. Sava, S. Zorzet, S. Pacor, et al., *Prog. Clin. Biochem. Med.* **1989**, *10*, 71-87.

[30] M. A. Bennett, M. J. Byrnes, I. Kovacik, *J. Organomet. Chem.* **2004**, *689*, 4463-4474.

[31] A. Habtemariam, M. Melchart, R. Fernandez, S. Parsons, I. D. H. Oswald, A. Parkin, F. P. A. Fabbiani, J. E. Davidson, A. Dawson, R. E. Aird, D. I. Jodrell, P. J. Sadler, *J. Med. Chem.* **2006**, *49*, 6858-6868.

[32] C. X. Zhang, S. J. Lippard, *Curr. Opin. Chem. Biol.* **2003**, *7*, 481-489.

[33] M. Stebler-Roethlisberger, W. Hummel, P. A. Pittet, H. B. Buergi, A. Ludi, A. E. Merbach, *Inorg. Chem.* **1988**, *27*, 1358-1363.

[34] Y. Hung, W.-J. Kung, H. Taube, *Inorg. Chem.* **1981**, *20*, 457-463.

[35] S. W. Magennis, A. Habtemariam, O. Novakova, J. B. Henry, S. Meier, S. Parsons, I. D. H. Oswald, V. Brabec, P. J. Sadler, *Inorg. Chem.* **2007**, *46*, 5059-5068.

[36] E. L. Muetterties, J. R. Bleeke, E. J. Wucherer, T. Albright, *Chem. Rev.* **1982**, *82*, 499-525.

[37] R. E. Morris, R. E. Aird, P. d. S. Murdoch, H. Chen, J. Cummings, N. D. Hughes, S. Parsons, A. Parkin, G. Boyd, D. I. Jodrell, P. J. Sadler, *J. Med. Chem.* **2001**, *44*, 3616-3621.

[38] R. E. Aird, J. Cummings, A. A. Ritchie, M. Muir, R. E. Morris, H. Chen, P. J. Sadler, D. I. Jodrell, *Br. J. Cancer* **2002**, *86*, 1652-1657.

[39] F. Wang, S. Guichard, R. Aird, B. Zeitlin, L. Eades, A. Habtemariam, H. Chen, D. Jodrell, P.J. Sadler, Unpublished results.

[40] H. Chen, J. A. Parkinson, S. Parsons, R. A. Coxall, R. O. Gould, P. J. Sadler, *J. Am. Chem. Soc.* **2002**, *124*, 3064-3082.

[41] O. Novakova, H. Chen, O. Vrana, A. Rodger, P. J. Sadler, V. Brabec, *Biochemistry* **2003**, *42*, 11544-11554.

[42] T. C. Jenkins., *Drug-DNA Interaction Protocols*, Humana Press Inc., Totowa, NJ. 195-218, **1997**.

[43] M. V. Keck, S. J. Lippard, *J. Am. Chem. Soc.* **1992**, *114*, 3386-3390.

[44] F. Wang, H. Chen, S. Parsons, I. D. H. Oswald, J. E. Davidson, P. J. Sadler, *Chem. Eur. J.* **2003**, *9*, 5810-5820.

[45] F. Wang, A. Habtemariam, E. P. L. van der Geer, R. Fernandez, M. Melchart, R. J. Deeth, R. Aird, S. Guichard, F. P. A. Fabbiani, P. Lozano-Casal, I. D. H. Oswald, D. I. Jodrell, S. Parsons, P. J. Sadler, *Proc. Natl. Acad. Sci. U. S. A.* **2005**, *102*, 18269-18274.

[46] F. Wang, J. Xu, A. Habtemariam, J. Bella, P. J. Sadler, *J. Am. Chem. Soc.* **2005**, *127*, 17734-17743.

[47] M. T. Fairhurst, T. W. Swaddle, *Inorg. Chem.* **1979**, *18*, 3241-3244.

[48] I. Rapaport, L. Helm, A. E. Merbach, P. Bernhard, A. Ludi, *Inorg. Chem.* **1988**, *27*, 873-879.

[49] W. S. Sheldrick, S. Heeb, *Inorg. Chim. Acta* **1990**, *168*, 93-100.

[50] R. Fernandez, M. Melchart, A. Habtemariam, S. Parsons, P. J. Sadler, *Chem. Eur. J.* **2004**, *10*, 5173-5179.

[51] T. Hasegawa, T. C. Lau, H. Taube, W. P. Schaefer, *Inorg. Chem.* **1991**, *30*, 2921-2928.

[52] H. Chen, J. A. Parkinson, R. E. Morris, P. J. Sadler, *J. Am. Chem. Soc.* **2003**, *125*, 173-186.

[53] A. F. A. Peacock, A. Habtemariam, R. Fernandez, V. Walland, F. P. A. Fabbiani, S. Parsons, R. E. Aird, D. I. Jodrell, P. J. Sadler, *J. Am. Chem. Soc.* **2006**, *128*, 1739-1748.

[54] V. Brabec, M. Leng, *Proc. Natl. Acad. Sci. U. S. A.* **1993**, *90*, 5345-5349.

[55] V. Brabec, V. Boudny, Z. Balcarova, *Biochemistry* **1994**, *33*, 1316-1322.

[56] M. A. Lemaire, A. Schwartz, A. R. Rahmouni, M. Leng, *Proc. Natl. Acad. Sci. U. S. A.* **1991**, *88*, 1982-1985.

[57] O. Novakova, J. Kasparkova, V. Bursova, C. Hofr, M. Vojtiskova, H. Chen, P. J. Sadler, V. Brabec, *Chem. Biol.* **2005**, *12*, 121-129.

[58] H. Taube, *Survey Progr. Chem.* **1973**, *6*, 1-46.

[59] V. Balzani, G. Bergamini, F. Marchioni, P. Ceroni, *Coord. Chem. Rev.* **2006**, *250*, 1254-1266.

[60] R. A. Krause, K. Krause, *Inorg. Chem.* **1980**, *19*, 2600-2603.

[61] S. Goswami, A. R. Chakravarty, A. Chakravorty, *Inorg. Chem.* **1983**, *22*, 602-609.

[62] R. A. Krause, K. Krause, *Inorg. Chem.* **1982**, *21*, 1714-1720.

[63] A. E. M. Boelrijk, A. M. J. Jorna, J. Reedijk, *J. Mol. Catal. A: Chem.* **1995**, *103*, 73-85.

[64] K. Bamba, J. M. Leger, E. Garnier, C. Bachmann, K. Servat, K. B. Kokoh, *Electrochim. Acta* **2005**, *50*, 3341-3346.

[65] A. H. Velders, H. Kooijman, A. L. Spek, J. G. Haasnoot, D. De Vos, J. Reedijk, *Inorg. Chem.* **2000**, *39*, 2966-2967.

[66] A. H. Velders, K. van der Schilden, A. C. G. Hotze, J. Reedijk, H. Kooijman, A. L. Spek, *Dalton Trans.* **2004**, 448-455.

[67] Later reports suggested that the isomer actually tested for cytotoxicity was the β-isomer in both cases and that the γ-isomer showed good cytotoxicity

[68] A. C. G. Hotze, M. Bacac, A. H. Velders, B. A. J. Jansen, H. Kooijman, A. L. Spek, J. G. Haasnoot, J. Reedijk, *J. Med. Chem.* **2003**, *46*, 1743-1750.

[69] C. G. Hotze Anna, E. Caspers Sabrine, D. de Vos, H. Kooijman, L. Spek Anthony, A. Flamigni, M. Bacac, G. Sava, G. Haasnoot Jaap, J. Reedijk, *J. Biol. Inorg. Chem.* **2004**, *9*, 354-364.

[70] A. C. G. Hotze, A. H. Velders, F. Ugozzoli, M. Biagini-Cingi, A. M. Manotti-Lanfredi, J. G. Haasnoot, J. Reedijk, *Inorg. Chem.* **2000**, *39*, 3838-3844.

[71] M. J. Clarke, F. Zhu, D. R. Frasca, *Chem. Rev.* **1999**, *99*, 2511-2533.

[72] O. Novakova, J. Kasparkova, O. Vrana, P. M. van Vliet, J. Reedijk, V. Brabec, *Biochemistry* **1995**, *34*, 12369-12378.

[73] A. C. G. Hotze, M. E. T. Broekhuisen, A. H. Velders, K. Van der Schilden, J. G. Haasnoot, J. Reedijk, *Eur. J. Inorg. Chem.* **2002**, 369-376.

[74] A. C. G. Hotze, E. P. L. van der Geer, H. Kooijman, A. L. Spek, J. G. Haasnoot, J. Reedijk, *Eur. J. Inorg. Chem* **2005**, 2648-2657.

[75] K. K. Patel, E. A. Plummer, M. Darwish, A. Rodger, M. J. Hannon, *J. Inorg. Biochem.* **2002**, *91*, 220-229.

[76] G. I. Pascu, A. C. G. Hotze, C. Sanchez-Cano, B. M. Kariuki, M. J. Hannon, *Angew. Chem. Int. Ed.* **2007**, *46*, 4374-4378.

[77] C. G. Hotze Anna, M. Kariuki Benson, J. Hannon Michael, *Angew. Chem. Int. Ed.* **2006**, *45*, 4839-4842.

Chapter 2

Experimental Section

This Chapter details the major experimental techniques used in this work. An overview of the technique is given, followed by the methods used. Some more specific techniques are outlined in individual chapters. The synthesis of the starting materials that are used in subsequent chapters for the synthesis of the ruthenium complexes is also described here.

2.1 Nuclear Magnetic Resonance (NMR) Spectroscopy[1-5]

Nuclear magnetic resonance spectroscopy is one of the most powerful tools available to chemists for elucidating the structure of both organic and inorganic species. In this thesis the main nucleus studied is ^{1}H, although a small number of experiments was performed on ^{31}P. ^{1}H NMR spectroscopy was used to characterise synthesised complexes as well as to follow the reaction of complexes in aqueous solutions.

2.1.1 Experimental Technique Overview

Nuclear magnetic resonance spectroscopy involves the study of transitions that are induced between nuclear spin energy levels, whose degeneracy has been lifted by the presence of a magnetic field.

For every nucleus, the spin properties of the protons and neutrons present combine to define the overall spin of the nucleus, termed the nuclear spin quantum number (I). When both the number of protons and neutrons are even and paired there is a net spin angular momentum of zero (I=0). When both the number of protons and neutrons are odd generally the nucleus has an integral non-zero quantum number because the total number of unpaired nucleons is even and each contributes ½ to the quantum number. When there is either an odd number of protons or an odd number of neutrons, the nuclear spin quantum number adopts a ½ integral quantum number. Some properties of common nuclides are listed in **Table 2.1.**

Table 2.1 NMR properties of some common nuclides

Nucleus	Natural Abundance (%)	γ / ($10^7 T^{-1}s^{-1}$)	υ at 9.4 T	I
^1H	99.985	26.75	400.0	½
^2H	0.02	4.11	61.4	1
^{13}C	1.108	6.73	100.6	½
^{14}N	99.63.	1.93	28.9	1
^{15}N	0.37	-2.71	40.5	½
^{31}P	100	10.84	162.1	½

For a spinning nucleus, the magnitude of the magnetic moment (μ) produced by a nucleus varies from atom to atom as defined by the equation:

$$\mu = \gamma \hbar I$$

where γ is the gyromagnetic ratio, which is a characteristic of each nucleus and $\hbar$ is Planks constant h divided by 2π. In the absence of a magnetic field the spin angular momentum has no preferred direction. In the presence of a magnetic field the orientation of the magnetic moment μ to the field direction (z-axis) is quantised and depends on I:

$$\mu_z = \gamma \hbar m_I$$

where m_I is the magnetic quantum number which has 2I +1 values in integral steps between +I and –I.

Thus to study nuclear magnetic properties, nuclei are subjected to a strong magnetic field (B_0 / Tesla) along the z-axis and this affects the energies of the nuclei. There is a slight preference for alignment in the general direction of B_0 (+z) over the opposite direction (-z). The nuclear magnetic moments are not lined up fully in the +z/-z direction; instead the force of B_0 causes the magnetic moment to move in a circular

fashion about the +z / -z direction, see **Figure 2.1.** This rotating particle moves in a circular path (precesses) around the magnetic field and the frequency of precession (υ_0), called the Larmor Frequency is defined as $\upsilon_0 = \gamma B_0 / 2\pi$.

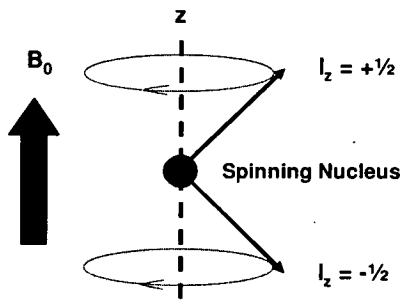

Figure 2.1. The alignment of nuclear magnetic moments in the presence of the magnetic field B_0 for a nucleus with I = ½. The population difference between +z/-z is given by Boltzmann's Law: n(+ ½)/n(- ½) = exp ($\Delta E/kT$)

In NMR experiments these two states (+z/-z) are made to interconvert by applying a second magnetic frequency, B_1, whose frequency corresponds to the Larmor Frequency. Because there is an excess of alignment at +z, there is a net absorption of energy. This process is called resonance and the absorption may be detected electronically and displayed as a plot of frequency vs. amount of energy absorbed. Modern NMR experiments used a pulsed (Fourier transform) technique where the nuclei in a magnetic field are subjected periodically to brief pulses of intense radiofrequency radiation (length ~ < 10 μs) and in the interval between pulses (T, several seconds) a time domain radio-frequency signal is emitted as nuclei return to their original state.

2.1.2 Chemical Shift, Resonance Intensities and Spin-Spin Coupling

2.1.2.1 Chemical Shift

NMR is such a powerful structural tool because the observed resonance frequency (υ_0) depends on the molecular environment as well as on γ and B_0, since the electron cloud that surrounds the nucleus also has a charge, motion and hence a magnetic moment. This electronic modulation of B_0 is termed (de)shielding and variation of the resonance frequency with (de)shielding is termed the *chemical shift.* As an

example, an electron-withdrawing group attached to a proton will reduce the electron density around the proton resulting in less shielding and a higher resonance frequency than in the case of a molecule that lacks the electron-withdrawing group. Similarly an electron donating group attached to a proton will increase the electron density around the proton resulting in more shielding and a lower resonance frequency. Several effects including inductive effects, resonance effects and hydrogen bonding will all modify the magnetic environment of the proton.

2.1.2.2 Resonance Intensities

The intensity of a resonance (the area under the peak; the integral) is proportional to the number of nuclei giving rise to it. However, it is important to remember that the values obtained may be in error by as much as *ca.* 10% lower than their true values. For integration to be reliable, it is essential that all the nuclei relax to their equilibrium values between successive pulses and this is governed by the longitudinal relaxation time T_1.

In order to determine if the resonance is equivalent to e.g. one, two or three protons, the level of accuracy is usually enough to determine this unambiguously.

2.1.2.3 Spin-Spin Coupling

If a nearby nucleus has a spin, then that spin affects the magnetic environment of the nucleus and the signal detected is not a singlet but a multiplet, the complexity of which is dependent upon the nature and number of nearby atoms. This phenomenon is called spin-spin coupling. This spin-spin coupling is measured by the *coupling constant, J* (Hz). For first order proton spectra, in which the chemical shift is large compared to the coupling constant, the following characteristics are exhibited. Firstly, multiplicities resulting from coupling reflect the 2nI+1 rule. Thus, as an example, two neighbouring nuclei of I = ½ will split the resonating nucleus into three peaks. Secondly, the intensities of the spin-spin multiplets correspond to the coefficients of the binomial expansion given by Pascal's triangle for spin ½ nuclei. Thirdly, spacings between adjacent components of a spin-spin multiplet are equal to J. Furthermore, protons that are equivalent show no coupling towards each other. Thus splitting patterns can be used to aid the assignment of proton peaks.

2.1.3 Two Dimensional Techniques: COSY (COrrelation SpectroscopY) and TOCSY (TOtal Correlation Spectroscopy)

In these 2D-NMR techniques a second frequency dimension is introduced into the experiment in which the magnetic interactions between nuclei through structural connectivity are further considered. In both cases two identical chemical shift axes are plotted orthogonally, with the one-dimensional spectrum appearing on the diagonal of the plot. In COSY experiments, the peaks that are mutually spin-spin coupled are shown by cross-peaks which are symmetrically placed about this diagonal. The cross-peaks usually include geminally (two-bond) or vicinally (three-bond) coupled protons but longer range coupling is not usually observed. In TOCSY experiments the connectivity within an entire spin system is mapped out by bringing all protons in the same spin system into equivalence.

2.1.4 Water Suppression

Proton NMR experiments performed in aqueous medium (100% D_2O or 90% H_2O / 10% D_2O) have a large residual solvent peak (H_2O, HOD) which can be suppressed using 1D Double Pulse Field Gradient Spin Echo (DPFGSE) experiments or by pre-saturation methods. Pre-saturation involves saturating the water signal by irradiating the frequency of the water signal in between pulse sequences whereas in DPFGSE experiments pulsed field gradient spin echoes are used in which the refocusing pulse is the sequence soft $\pi(x)$-hard $\pi(x)$.[6]

2.1.5 Experimental Methods

NMR spectra were recorded on either a Bruker Avance 600 MHz equipped with a TXI [^{1}H, ^{13}C, ^{15}N] *x,y,z*-gradient probe or a TXI [^{1}H, ^{13}C, ^{15}N] *z*-gradient cryoprobe, a Bruker Avance 800 MHz equipped with a TCI [^{1}H, ^{13}C, ^{15}N] *z*-gradient cryoprobe or a TXI [^{1}H, ^{13}C, ^{15}N] *x,y,z*-gradient probe, a Bruker DMX 500 MHz equipped with a TBI [^{1}H, ^{13}C, ^{15}N] *z*-gradient probe, or a Bruker DPX 360 MHz spectrometer equipped with a QNP [^{1}H, ^{13}C, ^{15}N] probe. ^{1}H NMR signals were referenced against the residual solvent peak, δ 7.27 (chloroform), 2.52 (DMSO), 2.07 (acetone) 3.32 (methanol) and for aqueous solutions (containing D_2O) dioxan was added as an internal reference (δ 3.75). All spectra were recorded in 5 mm quartz NMR tubes at

298 K unless otherwise stated using standard pulse sequences modified by Mr Juraj Bella or Dr Dusan Uhrin (The University of Edinburgh) and data were processed using Xwin-NMR (Version 2.0 or 3.6 Bruker UK Ltd).

2.2 Ultraviolet-visible (UV-VIS) Spectroscopy[1, 5, 7]

UV-VIS spectroscopy is one of the oldest methods of molecular spectroscopy and the introduction of UV spectroscopic analysis in the 1930s was an important milestone in analytical chemistry. UV-VIS spectroscopy can give useful information about the electronic structure of the complex studied. In this work, UV-VIS spectroscopy was routinely used as a means of characterising the complexes synthesised.

2.2.1 Experimental Technique Overview

In UV-VIS spectroscopy absorption of electromagnetic radiation in the UV-VIS region (200-800 nm) causes transitions between the electronic energy levels of the bonds of a molecule. Electrons are thus excited from their ground electronic state to an excited electronic state, see **Figure 2.2.**

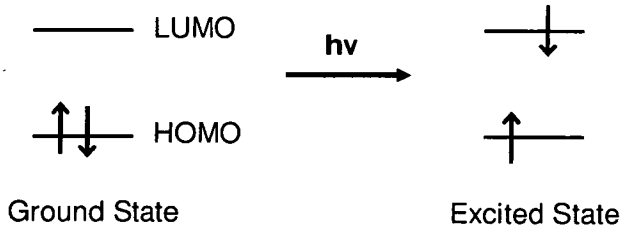

Figure 2.2. After absorbing a photon with the same energy as the HOMO-LUMO gap, the electronic configuration of the corresponding excited state that arises is due to the promotion of an electron from the HOMO to the LUMO.

Although electronic transitions arise between ground and excited states of the entire molecule, the transition can usually be assigned to parts of the molecule (called chromophores) where valence electrons are found (e.g. non-bonding n-electrons or π-electrons).

Absorption of UV-VIS light is typically seen as broad absorption maxima and not as sharp lines corresponding representing the absorption in an extremely narrow range. This is because there are vibrational levels associated with each electronic level. Thus excitation can occur to any of the vibrational levels of the excited electronic states, leading to a large number of lines for each transition. In practice, however, the lines overlap so that a continuous band is observed.

2.2.2 Allowed and Forbidden Transitions

In UV-VIS spectroscopy we not only measure the energy of exciting a molecule from its ground electronic state to its electronically excited state but also the probability of this transition. This is represented by the *molar extinction coefficient* (ε) which is a measure of the ease of the transition caused by the absorption of the radiation.[8]

The molar extinction coefficient can be determined by the Beer-Bouger-Lambert Law, which states that the proportion of light absorbed by a transparent medium is independent of the intensity of the incident light and proportional to the number of absorbing molecules through which the light passes:

$$\log (I_0/I) = \varepsilon cl$$

where I_0 is the intensity of incident light, I is the intensity of transmitted light, ε is the molar extinction coefficient, c is the concentration and l is the path length (cm). Since $\log (I_0/I)$ is defined as absorbance (A) the equation simplifies to $A = \varepsilon cl$. Thus by measuring the absorbance at a known concentration, the extinction coefficient can be determined.

Electronic transitions are classed as allowed (intense) or forbidden (weak) according to their extinction coefficient. There are three rules that govern allowed or forbidden transitions.

(1) The *spin selection rule*, which states that transitions between states of different spin multiplicity are forbidden since electrons cannot undergo spin inversion during the change of the electronic state i.e $\Delta S=0$.

(2) The change in angular momentum must be 0, or ± 1

(3) The *symmetry selection rule*, or the *Laporte selection rule*, which states that in a centrosymmetric molecule or ion, the only allowed transitions are those accompanied by a change in parity.

Whilst coupling of spin and angular momenta can relax the spin selection rule, the transitions are much weaker than the spin allowed transitions. The Laporte selection rule is much easier to relax since a complex may depart from perfect centrosymmetry or may undergo an asymmetrical vibration, both resulting in destroying the center of inversion. Thus Laporte-forbidden transitions tend to be more intense than spin-forbidden transitions.

2.2.3 Experimental Methods

A Perkin-Elmer Lambda-16 UV/Vis spectrophotometer was used with 1 cm path length quartz cuvettes (0.5 mL volume) and a PTP1 Peltier temperature controller. Spectra were recorded at 298 K (unless otherwise stated) from 800-200 nm at a scan rate of 420 nm / min and at 1 nm intervals. In all cases, the solvent used was double distilled water, unless otherwise stated. Spectra were processed using UV-Winlab software for Windows' 95.

2.2.3.1 Determination of Molar Extinction Coefficients

Molar extinction coefficients (ε) were calculated using the Beer-Bouger-Lambert Law (*vide supra*) where a plot of absorbance versus concentration for a single wavelength should be linear and pass through the origin and the gradient of this line gives, ε. Thus for each UV-VIS band, a plot of absorbance measured at λ_{max} vs. concentration for five separate concentrations of sample, gave as the gradient, ε.

2.3 Electrochemistry[9, 10]

Electrochemistry involves the study of electron transfer reactions between electrodes and reactant molecules in a solution phase. Three electrochemical techniques were used to help to characterise several of the complexes studied in this thesis.

2.3.1 Cyclic Voltammetry

In cyclic voltammetry, the current is measured as the electrode potential is swept from a potential E_1 to a potential E_2 then back to E_1. A reduction causes a decrease in the measured current (electrons going into the electroactive species), and an oxidation causes an increase in the measured current (release of electrons to surroundings). Redox reactions can be classed as reversible, quasi-reversible or irreversible, and there are diagnostic tests that can be used to distinguish between all three cases. Furthermore, chemical reactions can follow reductions/oxidations and these can similarly be assigned on the basis of diagnostic tests.

A three-electrode configuration was used whereby current is passed through the working/counter electrode circuit whilst the potential of the working electrode is measured relative to the reference electrode. This results in little/no current being passed through the working electrode/reference electrode loop giving a more accurate potential.

2.3.2 Differential Pulse Polarography (DPP)

Differential pulse polarography provides an enhanced sensitivity compared to cyclic voltammetry and was used in this thesis to confirm the number of redox processes occurring in a system. The same three-electrode configuration is used, but in DPP, the pulse height is kept constant (50 mV) and the base potential is swept slowly with time. The current shortly before the pulse is applied, and that at the end of the pulse are measured and the difference between these values as a function of the potential is recorded.

2.3.3 Constant Potential Coulometry

This technique is used to determine the overall number of electrons involved in an electrode process. In the experimental set up, a divided cell is used in which the working electrode compartment is separated from the secondary electrode by a glass frit. The working electrode compartment is fitted with a magnetic stirrer and filled with a known number of moles of electro-active species. The potential of the working electrode is fixed (usually just past the redox potential in question) and the current is monitored as a function of time until the current falls to *ca.* 1% of its initial

value. The total charge consumed at the end of the experiment, q(∞) can be extrapolated to i(t) = 0 and this is related to the number of electrons involved in the process by:

$$q(\infty) = nFm$$

Where F is Faraday's constant and m is the number of moles added.

2.3.4 Experimental Methods

Electrochemical studies were performed with General Purpose Electrochemical System (GPES) Version 4.5 software connected to an Autolab system containing a PSTAT20 potentiostat. All of the electrochemical techniques used a three-electrode configuration. The reference electrode used was Ag/AgCl in a solution of 0.1 M [TBA][BF_4] in DMF against which $E_{1/2}$ for the ferrocinium/ferrocene couple was measured to be +0.55 V. The working and counter electrodes were a platinum microdisc (0.5 mm diameter) and a large surface area platinum wire respectively. Coulometric experiments were performed in a conventional H-type cell using large surface-area Pt working and counter electrodes. All solutions were purged with dry nitrogen prior to electrochemical study.

2.4 Electrospray Ionisation Mass Spectrometry (ESI-MS)[1, 4]

ESI-MS is a solution-based mass spectrometrric technique, so compounds can be studied directly in aqueous solutions. ESI-MS was used routinely in this work to characterise complexes synthesised and also to assign products of reactions.

2.4.1 Experimental Technique

The sample must be present as an ion in solution and this can be achieved (if species is not already charged) by adding a small amount of acid to protonate (ESI positive) or base to deprotonate (ESI negative). Molecules are taken directly from the solution to the gas phase ionised state by passing the solution through the exit of a fine needle held at a potential of around 4 kV. The solution disperses into a fine mist of ionised droplets which quickly lose their solvent leaving behind an aerosol of (de)protonated sample which is then desorbed into the gas phase and interfaced with the vacuum for

mass spectrometric analysis. Ion analysis was performed using a quadrupole mass spectrometer.

In a quadrupole mass filter, ions drift through an assembly of four cylindrical metal parallel rods in which DC voltages of opposite sign are applied to opposite rods. An oscillating (AC) radiofrequency field is also applied to opposite rods, which successively reinforces and then overwhelms the DC field. The effects of AC and DC potentials on the trajectory of ions as they pass through the channel between the rods explain the filtering capability of the quadrupole:

(1). The pair of positive rods act as a *high pass mass filter.* In the absence of a DC potential, ions in the channel will converge in the centre of the channel during the positive half of the AC cycle and diverge during the negative half (where, if it strikes the rod the charge is neutralised and the resulting charge carried away). Whether or not an ion strikes the rod will depend on the rate of movement of the ion along the motion direction, its mass-to-charge ratio and the frequency and magnitude of the AC signal. In the presence of the DC signal, because of $E_K = ½ mv^2$, it becomes more difficult to deflect a heavier ion than deflect a lighter one. Thus if an ion in the channel is heavy and/or the frequency of the AC potential is large, the ion will not respond significantly to the alternating potential and will be influenced largely by the dc potential. Under these circumstances the ion will tend to remain in the space between the rods. In contrast, if the ion is light and/or the frequency is low, the ion may collide with the rod and be eliminated during the negative cycle of the ac signal.

(2). The pair of negative rods (orthogonal to positive rods) act as a *low pass mass filter.* In the absence of the AC potential, all positive ions are drawn to the rods where they are annihilated and neutralised. However, for lighter ions, this may be offset by the positive excursion of the AC potential.

Thus in order for an ion to travel through the quadrupole it must have a stable trajectory in both planes (i.e. not be too heavy that it will be eliminated by high pass, nor too light so that it is not eliminated from the low pass filter). Varying the electrical signals to the quadropole varies the range of m/z values transmitted, thus spectral scanning becomes possible.

2.4.2 Experimental Methods

ESI-MS were obtained on a Micromass Platform II Mass Spectrometer or a Micromass ZMD Mass Spectrometer (Micromass, Manchester, UK). Solutions were infused directly at a rate of 3-30 μL/min. The capillary voltage was 3.5 kV and the cone voltage was either varied between 15 to 40 V, depending on the solution. The source temperature was dependent on the solvent used, and different mass ranges were scanned, again depending on the solution.

2.5 Inductively Coupled Plasma Optical Emission Spectroscopy (ICP-OES)[4, 11, 12]

ICP-OES is a very sensitive technique that can be used to determine concentrations of elements in both aqueous and organic solutions. Here, it was used to determine the ruthenium, sulfur, iron and iodide concentrations in aqueous solutions.

2.5.1 Experimental Technique

ICP-OES uses inductively coupled argon plasma to dissociate a sample into its constituent atoms or ions, and then thermally excite them to a level where they emit visible or UV light of a characteristic wavelength. Atomic emission occurs when a valence electron in a higher-energy atomic orbital returns to a lower-energy atomic orbital. The intensity of the emission line is proportional to the number of atoms populating the excited state.

In an argon plasma (containing argon ions and electrons), once formed, the argon ions absorb sufficient power from an external radiofrequency source so that the temperature is maintained at a level at which further ionisation sustains the plasma indefinitely. The sample is introduced into the hot plasma causing atomisation and emission can then be monitored.

2.5.2 Experimental Methods

A Perkin Elmer Optima 5300 DV ICP-OES machine was used. Standard solutions (0.1-100 ppm) were prepared from stock 1000 ppm solutions (ruthenium, iron, sulfur, Sigma Aldrich, iodide prepared by dissolving KI to 1000 ppm) and run to give a calibration curve from which unknown concentrations of the element could be

determined. Ruthenium emissions were followed at 240.272 and 349.849 nm and the average concentration determined from these two emissions was used. For iron the emissions were averaged from 238.204 and 239.562 nm, for sulfur 181.975 and 180.699 nm and for iodide 206.188 and 182.976 nm

2.6 X-ray Diffraction (XRD)[13, 14]

X-ray diffraction is the most widely used and least ambiguous method for the precise determination of the position of atoms in molecules in the crystalline solid state. XRD was used in this thesis to characterise the crystal structure of several synthesised compounds.

2.6.1 Experimental Technique

X-rays are electromagnetic radiation with wavelengths of the order 10^{-10} m. In 1912, Max von Laue suggested that x-rays might be diffracted when passed through a crystal since their wavelength was comparable to the separation of lattice planes. In a crystal there are a large number of identical molecules that are held together in a regular arrangement and together this gives significant x-ray scattering, and it is the electrons in the atoms that cause x-ray scattering.

The x-ray diffraction data pattern contains important information. Firstly the pattern has a particular geometry which is related to the lattice and unit cell geometry of the crystal and so can give information about repeat distances between molecules. Secondly the pattern has symmetry which is closely related to the unit cell of the crystal structure (i.e. crystal system and space group). Thirdly the intensities of the pattern holds all the information about the positions of atoms in the unit cell of the crystal structure since it is the relative atomic positions which, through the combination of their individual interactions with the x-rays, generate different amplitudes for different directions of scattering. The structure is solved using Patterson/Direct methods to determine approximate positions of all / most non-hydrogen atoms. This approximate structure is then refined by varying numerical parameters describing the structure to produce the 'best' agreement between the

diffraction pattern calculated from it by a Fourier transform and the observed diffraction pattern.

2.6.2 Methods Used

All diffraction data were collected by Professor Simon Parsons and colleagues at The University of Edinburgh on a Bruker Smart Apex CCD Diffractometer using Mo Kα radiation (λ = 0.71073Å) equipped with an Oxford Cryosystems device operating at 150 K. Structures were solved by Professor Simon Parsons and colleagues using either Patterson (dirdif) or direct (SHELXS-97) methods, as indicated in the text. Structures were refined against F^2 using either SHELXL-97 or CRYSTALS, as indicated in the text.

2.7 High Performance Liquid Chromatography (HPLC)[4, 11]

HPLC is the most widely used of all the analytical separation techniques. In this thesis HPLC was used to separate reaction mixtures of ruthenium complexes for subsequent analysis.

2.7.1 Experimental Technique

The technique used in this thesis was Reverse Phase-HPLC (RP-HPLC). Compounds bind to RP-HPLC columns from high aqueous mobile phases and are eluted with a high organic mobile phases.

The column used was a Polymer-Reverse Phased PLRP-S column which comprises a rigid non-polar macroporous styrene/divinylbenzene polymer as the stationary phase, where an analyte is retained on the surface by physical adsorption. The use of a polar eluent (e.g. water) favours the migration of a polar compound over a non-polar one through the column and under these conditions non-polar substances will be retained. By decreasing the polarity of the mobile phase (by increasing the percentage of organic phase) less polar substances are eluted.

The separation of easily-ionised compounds can be improved by adding trifluoroacetic acid (TFAH) to the mobile phase. This induces the formation of dipole-dipole interactions between the compounds rendering them less polar and relatively stable and hence their retention on the reversed phase column is increased.

2.7.2 Experimental Methods

A Hewlett-Packard series 1100 quaternary pump and a Rheodyne sample injector with a 0.1 mL (analytical) or 1.0-mL (semi-preparative) loop, a HP 1100 series UV-vis detector and HP 1100 series Chemstation was used. Analytical separations were carried out on PLRP-S reversed-phase column (250 mm x 4.6 mm, 100 Å, 5 μm, Polymer Labs) and semi-preparative separations on a PLRP-S reversed-phase column (250 mm x 7.5 mm, 100 Å, 8 μm, Polymer Labs) with detection at 286 nm. The mobile phases were mobile phase A: water (for HPLC application, Fisher Chemicals) containing 0.1% TFAH; mobile phase B: acetonitrile (for HPLC application, Fisher Chemicals) containing 0.1% TFAH. The flow rate was either 1.0 mL min^{-1} (analytical) or 3.5 mL min^{-1} (semi-preparative). Gradients were dependent on the analysis mixture and are reported in the subsequent chapters.

2.7.3 Fast Protein Liquid Chromatography (FPLC)[15]

FPLC is a form of column chromatography used to separate or purify proteins from a complex of mixtures. In this thesis, an anion exchange resin was used whereby the resin is positively-charged and attracts negatively-charged molecules. As the protein is introduced to the column, it diffuses to the stationary phase surface, displacing the counter anion. The binding of the protein to the resin is based upon the competition between the charged groups on the surface of the protein and the charge on the counter anions, and the bound protein will be displaced when the counter anion is concentrated enough to overcome the attraction between the protein and the ion exchange resin. The concentration of the counter anion can thus be increased gradually using a salt gradient. It is important to note that the protein will bind to an anion exchange resin only when there is sufficient charge on the protein, i.e. above its pI value.

FPLC was performed on an AKTA FPLC system (Amersham Biosciences) using a 5 mL Hi-Trap Capto Q column (GE healthcare) with help from Dr Arindam Mukherjee (The University of Warwick). The samples were first concentrated to 1 mL in Tris – HCl buffer (pH 8) and injected into the loop (1 mL). The solvents were thoroughly degassed before use and were A: 5 mM Tris-HCl (pH 8) and B: 50 mM Tris-HCl pH

8, 5 mM $NaHCO_3$, 800 mM NaCl. The flow rate used was 5 mL/min and the gradient used was 0% B to 100% B over 60 minutes.

2.8 Cell Culture[16]

The following section outlines some more general cell experiment procedures used in this thesis although individual chapters contain details about more specific experiments.

2.8.1 Experimental technique

The major purpose of cell culture is to allow cells to be removed from their complex interactions in the organism and hence attempt to reproduce *in vitro* the environmental conditions that the cells experience *in vivo.* Cells are attached to a substratum and are covered with a thin layer of cell medium which approximates the extracellular fluid of the organism. The cells are kept at physiological pH using a bicarbonate (HCO_3^-) buffering system because this is the closest to the physiological medium that surrounds cells in an organism. The bicarbonate is in equilibrium with the CO_2 in the air and so to maintain the correct concentration of bicarbonate that provides the appropriate pH, the concentration of CO_2 in the environment must be kept higher than its concentration in air. Cells are thus grown by incubation at 310 K, 5% CO_2 and at a high humidity (to prevent any evaporation).

2.8.2 Materials and Maintenance of Cell Lines

All cell lines were obtained from the ECACC (European Collection of Cell Cultures). DMEM, RPMI and MEM media, L-glutamine, penicillin/streptomycin and foetal bovine serum were obtained from Sigma Aldrich. McCoys 5A medium and 0.25% trypsin/EDTA were obtained from Invitrogen. The A549 human lung cancer cell line was grown in DMEM medium supplemented with 10% foetal bovine serum, 1% penicillin/ streptomycin and 2mM L-glutamine. The A2780 human ovarian cancer cell line was grown in RPMI medium supplemented with 5% foetal bovine serum, 1% penicillin/ streptomycin and 2mM L-glutamine. The HCT116 (WT) human colon cancer cell line (wild type) was grown in McCoys 5A medium supplemented with 10% foetal bovine serum. The HCT116 ($p53^-$) human colon

cancer cell line (p53 null) was grown in McCoys 5A medium supplemented with 10% foetal bovine serum. The WI38 human lung fibroblast cell line was grown in MEM medium supplemented with 10 % fetal bovine serum, 1% penicillin/ streptomycin and 2mM L-glutamine.

All cells were split twice weekly before 100% confluence was reached using 0.25% trypsin/EDTA. All cells were kept incubated at 310 K, 5% CO_2, high humidity.

2.8.3 Determination of IC_{50} values

All IC_{50} values against the WI38 non-cancerous cell line, and IC_{50} values against the A2780 and A549 cell line for compounds **1**, **4**, **5**, **8**, **9**, **10**, **11**, **13** and **16** and ligand azpy-OH were determined as part of this thesis work. All other IC_{50} data were determined by Ms Emily Jones or Mr Daniel Cole (Oncosense Ltd). The concentration of complex added to the cells which causes 50% inhibition of cell growth is termed IC_{50}. These experiments were performed in 96-well plates.

A2780 cancer cells were plated out at 5 x 10^4 cells/well (3.33 x 10^6 cells/mL) (±10%) and incubated for 48 h before compound addition. A549 cancer cells and WI38 normal cells were plated out at 2x 10^4 cells/well (1.33 x 10^6 cells/mL) (±10%) and incubated for 24 h before drug addition.

The test compounds were dissolved in DMSO to give a stock solution of 20 mM and serial dilutions were carried out in DMSO to give concentrations of drug in DMSO of 10, 2, 1, 0.2 and 0.02 mM. These were added to the wells to give the six testing concentrations (100, 50, 10, 5, 1 and 0.1 μM) and a final concentration of DMSO of 0.5% (v/v) with a total volume of drugs and media to be 200 μl. Each concentration was tested in triplicate and a cisplatin control was added to the plate, since cisplatin gave reproducible values in the cell lines used. The cells were exposed to the drug for 24 hours then, after drug removal and washing the wells twice with PBS, fresh medium was given and the cells were incubated for 96 hours recovery time.

The remaining biomass after this time was determined using the Sulforhodamine-B (SRB) assay.[17] SRB is a bright pink aminoxanthene dye with two sulfonic acid groups. Under mildly acidic conditions it binds to proteins basic amino acid residues in proteins and under more basic conditions the dye is liberated and can be quantitatively extracted for measurement of optical density (λ_{max} = 568 nm).

Briefly to each well 50μL 50% (w/v) TCA was added and the wells were incubated at 277 K for one hour to fix the remaining biomass. This was stained with 100 μL 0.4% (w/v) sulforhodamine B in 1% acetic acid. This dye was solubilised with Tris Buffer and the absorbance was read using a BMG Fluostar microplate reader at 595 nm. A baseline correction at 690nm was subtracted from the absorbance values. The absorbance value taken as 100% cell survival was the averaged triplicate absorbance for the 0.1 μM dosed wells. The percentage cell survival relative to this control could then be determined. IC_{50} values were calculated using XL-Fit version 4.0 (IDBS, Surrey, UK) by plotting percentage cell survival against compound concentration and noting the concentration that leads to 50% cell survival.

2.9 pH measurements

The pH meter used was a Corning pH meter 145 calibrated with pH 4, pH 7 and pH 10 buffer solutions (Sigma Aldrich) equipped with a Therom microcombination KCl (chloride) / KNO_3 (chloride free) electrode. The pH values were recorded at room temperature. The pH meter readings for D_2O solutions were recorded without the correction for the effect of deuterium on the glass electrode, and are termed pH*.

2.10 CHN (Carbon-Hydrogen-Nitrogen) Elemental Analysis[4]

CHN elemental analysis provides a means for assessing the purity of a sample, by determining the percentage of carbon, nitrogen and hydrogen and comparing to the theoretical value.

2.10.1 Experimental Technique

Pre-weighed samples are combusted in an oxidising atomosphere (at high temperatures, *ca.* 1170 K) and this produces a gaseous mixture of CO, CO_2, H_2O, N_2 and N-oxides. The gaseous mixture is swept with a stream of helium to a reduction reactor which reduces N-oxides to elemental N_2 , CO to CO_2 and removes the extra oxygen. The products move to a mixing chamber, where they are brought to a constant temperature and analysed by passing through three thermal conductivity detectors, which generate electrical signals proportional to the concentrations.

Hydrogen (H) is analysed from the water content by passing the mixture through a magnesium perchlorate absorption trap. Carbon (C) is analysed from the CO_2 and N_2 is analysed from the elemental N_2 present.

2.10.2 Methods Used

CHN analyses were carried out either by The University of Edinurgh using an Exeter Analytical Elemental Analyser (CE440), or at the The Univeristy of St. Andrews using a Carlo-Erba CHNS Analyser.

2.11 Synthesis of Starting Materials

The ruthenium dimers $[(\eta^6\text{-arene})RuCl_2]_2$ and $[(\eta^6\text{-arene})RuI_2]_2$ are used as starting materials for the synthesis of ruthenium complexes studied in this thesis.

2.11.1 Materials

$RuCl_3.xH_2O$ was purchased from Precious Metals Online, 1,4-cyclohexadiene, α-terpenine, hexamethylbenzene, biphenyl and ammonium hexafluorophosphate (NH_4PF_6) were purchased from Sigma Aldrich and all other reagents were obtained from commercial suppliers. Ethanol was dried by distilling over Mg/I_2 and tetrahydrofuran was dried by distilling over Na.

2.11.2 Methods

The precursors $[(\eta^6\text{-biphenyl})RuCl_2]_2$, $[(\eta^6\text{-benzene})RuCl_2]_2$ and $[(\eta^6\text{-}p\text{-cymene})RuCl_2]_2$ can be conveniently prepared from the reaction of $Ru^{III}Cl_3$ and the 1,3- or 1,4-cyclohexadiene by refluxing in ethanol [18, 19]. Whilst 1,4-cyclohexadiene (to form $[(\eta^6\text{-benzene})RuCl_2]_2$, and α-terpenine (to form $[(\eta^6\text{-}p\text{-cymene})RuCl_2]_2$) are commercially available, the Birch reduction of biphenyl [20] afforded 1-phenyl-2,5-cyclohexadiene which could then be used to form the corresponding dimer. Arene exchange of *p*-cymene for hexamethylbenzene in $[(\eta^6\text{-}p\text{-cymene})RuCl_2]_2$ afforded $[(\eta^6\text{-hexamethylbenzene})RuCl_2]_2$[19] and $[(\eta^6\text{-thn})RuCl_2]_2$ (thn = tetrahydronaphthalene) was prepared previously.[21] The corresponding iodide dimers $[(\eta^6\text{-arene})RuI_2]_2$ were synthesised easily from $[(\eta^6\text{-arene})RuCl_2]_2$ and excess KI.

2.11.3 Synthesis and Characterisation

2.11.3.1 1,4-Dihydrobiphenyl

Ammonia gas (1 L) was condensed into a flask cooled with dry ice/acetone to 197 K under an argon atmosphere. Biphenyl (17.50 g, 0.114 mol) was dissolved in distilled and dried tetrahydrofuran (250 mL) and added to the ammonia via canulla. Lithium metal (1.99 g, 0.287 mol) was cut into small pieces and added. The reaction mixture was stirred for 30 min and the solution turned green then red. NH_4Cl (22 g, 0.411 mol) was added to quench the reaction and the colour turned to white. The vessel was left overnight to allow excess ammonia to evaporate. Water (300 mL) was added and the solution was extracted with diethyl ether (3 x 200 mL). The combined organic fractions were re-extracted from water (500 mL) saturated with NaCl. The organic layer was dried over magnesium sulphate and the solvent was removed to leave a yellow oily crude product. This was distilled at 10^{-1} mbar, 371 K to give colourless oil. Yield 14.40 g (81.3%). ^{1}H NMR ($CDCl_3$): δ 7.28 (m, 5H), 5.79 (m, 4H), 3.98 (t, 1H), 2.77 (m, 2H).

2.11.3.2 $[(\eta^6\text{-biphenyl})RuCl_2]_2$

$RuCl_3.xH_2O$ (5 g, 0.024 mol) was dissolved in distilled and dried ethanol (85 mL) and l-phenyl-2,5-cyclohexadiene (4.3 g, 0.028 mol) was added drop-wise. The resulting mixture was heated to reflux for 48 h during which time a brown precipitate had formed. The solution was cooled to room temperature, filtered and the brown precipitate was washed with ethanol and dried overnight *in vacuo*. Yield 6.43g (82.2%). (Found C, 43.40; H, 2.85. Calcd for $Ru_2C_{24}H_{20}Cl_4$ C, 44.19; H, 3.09 %). ^{1}H NMR (DMSO-d_6): δ 7.86 (d, 2H), 7.54 (m, 3H), 6.47 (d, 2H), 6.11 (m, 3H)

2.11.3.3 $[(\eta^6\text{-benzenel})RuCl_2]_2$

$RuCl_3.xH_2O$ (3 g, 0.015 mol) was dissolved in distilled and dried ethanol (80 mL) and 1,4-cyclohexadiene (11.6 g, 0.145 moles) was added drop-wise. The resulting mixture was heated to reflux for 4 h during which time an orange/brown precipitate had formed. The solution was cooled to room temperature, filtered and the resulting precipitate was washed with cold ethanol and then diethyl ether and dried overnight

in vacuo. Yield 1.98 g (27.3%). (Found C, 27.84; H, 2.09. Calcd for $Ru_2C_{12}H_{12}Cl_4$ C, 28.82; H, 2.42 %). ^1H NMR (DMSO-d_6): δ 5.99 (s, 6H)

2.11.3.4 [(η^6-*p*-cymene)$RuCl_2]_2$.

$RuCl_3.xH_2O$ (3.54 g, 0.017 mol) was dissolved in distilled and dried ethanol (100 mL). To this solution α-terpinene (25.11g, 0.202 mol) was added drop-wise and the solution was heated to reflux for 24 h. During this time the solution changed from brown to red. After cooling to room temperature the solution was filtered to give a red/orange precipitate which was washed with diethyl ether until the filtrate was clear and dried overnight *in vacuo*. Yield 3.51 g (67.4%). (Found C, 39.37; H, 4.21. Calcd for $Ru_2C_{20}H_{28}Cl_4$ C, 39.23; H, 4.61 %). ^1H NMR ($CDCl_3$): δ 5.50 (d, 4H), 5.35 (d, 4H), 2.95 (septet, 1H), 2.15 (s, 6H), 1.30 (d, 12H)

2.11.3.5 [(η^6-hexamethylbenzene)$RuCl_2]_2$

The dimer [(η^6-*p*-cymene) $RuCl_2]_2$ (1.98 g, 3.23 mmol) and hexamethylbenzene (20 g, 123 mmol) were placed in a flask and heated to 456 K for 3 hours where the solution gradually turned from orange-red to orange-brown. During heating hexamethylbenzene solidified around the top of the flask and this was continually scraped back down into the solution. The reaction mixture was cooled, filtered and washed with hexane (200 mL) and diethyl ether (200 mL) to give a dull brown solid. Excess hexamethylbenzene can be removed by sublimation, although in this instance instead the solid was repeatedly dissolved in hexane and filtered until there was no hexamethylbenzene present in the filtrate. The brown solid left was filtered through celite and washed with chloroform (400 mL) until the filtrate turned clear. The solvent from the filtrate was removed on a rotary evaporator to leave a reddish brown solid. Yield 1.37 g (63.5%). (Found C. 45.22; H, 5.52. Calcd for $Ru_2C_{24}H_{36}Cl_4$ C, 43.12; H, 5.43 %). ^1H NMR ($CDCl_3$): δ 2.03 (s, 6H)

2.11.3.6 [(η^6-biphenyl)$RuI_2]_2$

The dimer [(η^6- biphenyl)$RuCl_2]_2$ (0.3 g, 0.40 mmol) was stirred at ambient temperature in water (250 mL) for 30 minutes. The solution was filtered and KI (2.12 g, 0.013 mol) was added to the filtrate. A brown/red precipitate immediately formed. This was filtered off and washed with cold ethanol and diethyl ether. Yield:

388 mg (38.8%). (Found C, 28.38; H, 1.98. Calcd for $Ru_2C_{24}H_{20}I_4$ C, 28.31; H, 1.61 %). ^{1}H NMR (DMSO-d_6): δ 7.84 (d, 2H), 7.54-7.46 (m, 3H), 6.66 (d, 2H), 6.38 (t, 1H), 6.12 (d, 2H)

2.11.3.7 [(η^6-*p*-cymene)RuI_2]$_2$

The dimer [(η^6-*p*-cymene) $RuCl_2$]$_2$ (0.65 g, 1.06 mmol) was refluxed in water (200 mL) for 1 h. The solution was hot filtered and KI (4.45 g, 0.027 mol) was added to the filtrate. A brown/red precipitate immediately formed. This was filtered off and washed with cold ethanol and diethyl ether. Yield: 841 mg (81.1%). (Found C, 24.70; H, 2.50. Calcd for $Ru_2C_{20}H_{28}I_4$ C, 24.56; H, 2.59 %). ^{1}H NMR (DMSO-d_6): δ 5.87 (d of d, 4H), 3.16 (septet, 1H), 2.40 (s, 3H), 1.22 (d, 6H).

2.12 References

[1] J. B. Lambert, H. F, Shurvell, D. A Lightner, R. G Cooks,., *Organic Structural Spectroscopy*, Prentice-Hall, Inc, New Jersey, **1998**.

[2] L. M. Harwood, Claridge, T. D. W., *Introduction to Organic Spectroscopy*, Oxford University Press Inc, New York, **1997**.

[3] P. J. Hore, *Nuclear Magnetic Resonance*, Oxford University Press Inc, New York, **2001**.

[4] D. A. Skoog, J. J Leary, *Principles of Instrumental Analysis*, Fourth ed., Saunders College Publishing, Florida, **1992**.

[5] D. H. Williams, I. Fleming, *Spectroscopic Methods in Organic Chemistry*, Fifth ed., McGraw-Hill Book Company Europe, Berkshire, **1996**.

[6] T.-L. Hwang, A. J. Shaka, *J. Mag. Res.* **1995**, *112*, 275-279.

[7] D. F. Shriver, P. W. Atkins, *Inorganic Chemistry*, Third ed., Oxford University Press, Belgium, **1999**.

[8] To get the probability of the transition the area of the peak should also be taken into account.

[9] R. Greef, R. Peat, L. M. Peter, D. Pletcher, J. Robinson, *Instrumental Methods in Electrochemistry*, Ellis Horwood Limited, West Sussex, **1985**.

[10] A. C. Fisher, *Electrode Dynamics*, Oxford University Press Inc, New York, **1998**.

[11] F. Rouessac, *Chemical Analysis - Modern Instrumental Methods and Techniques*, English Ed ed., New York : Wiley, Chichester, **2000**.

[12] D. Harvey, *Modern Analytical Chemistry*, London : McGraw-Hill, Boston, **2000**.

[13] W. Clegg, *Crystal Structure Determination*, Oxford University Press Inc, New York, **2003**.

[14] P. W. Atkins, *Physical Chemistry*, Sixth ed., Oxford University Press, **2000**.

[15] P. L. R. Bonner, *Protein Purification*, Taylor & Francis Group, Abingdon, UK, **2007**.

[16] *Essential Cell Biology (International Edition)*, Williams and Wilkins Baltimore, USA, **1990**.

[17] P. Skehan, R. Storeng, D. Scudiero, A. Monks, J. McMahon, D. Vistica, J. T. Warren, H. Bokesch, S. Kenney, M. R. Boyd, *J. Natl. Cancer Inst.* **1990**, *82*, 1107-1112.

[18] M. A. Bennett, A. K. Smith, *J. Chem. Soc.; Dalton Trans.* **1974**, 233-241.

[19] M. A. Bennett, T. N. Huang, T. W. Matheson, A. K. Smith, *Inorg. Synth.* **1982**, *21*, 74-78.

[20] A. J. Birch, G. Nadamuni, *J. Chem. Soc'; Perkin Trans.* **1974**, 545-552.

[21] A. Habtemariam, M. Melchart, R. Fernandez, S. Parsons, I. D. H. Oswald, A. Parkin, F. P. A. Fabbiani, J. E. Davidson, A. Dawson, R. E. Aird, D. I. Jodrell, P. J. Sadler, *J. Med. Chem.* **2006**, *49*, 6858-6868.

Chapter 3

Mononuclear Ruthenium(II) Arene Chlorido Azo Complexes

3.1 Introduction

Ruthenium complexes have potential as anticancer drugs.[1] Previous work has shown that ruthenium(II) arene complexes of the type $[(\eta^6\text{-arene})Ru^{II}(XY)Z]^+$, where XY is a chelating diamine and Z is a leaving group exhibit cytotoxicity against several cancer cell lines including cisplatin-resistant cells.[2, 3] Increased hydrophobicity of the arene increases cytotoxicity and complexes containing chelating di-amines were more active than complexes containing only monodentate ligands. It has been proposed that hydrolysis of the reactive ruthenium-chloride bond may activate the complex for DNA binding,[4] and that distortions of DNA may contribute to the mechanism of action.[5] In these types of complexes, ruthenium is stabilized in the +2 oxidation state by the π-acidic η^6-arene and in the case of ethylenediamine (en), the chelating diamine N ligands are σ donors.

Azo ligands such as 2-phenylazopyridine (azpy), which contain the -N=N-C=N- linkage have unusual properties.[6] The pyridine ring is an intermediate π-acceptor and its nitrogen is a weak σ-donor. The azo group has low σ-donor ability to the metal, but possesses enhanced π-accepting ability through the azo π* orbital. Consequently chelating ligands of this type are able to stabilise metals in their lower oxidation states. Several ruthenium(II) compounds containing such ligands have been reported previously.[7, 8] For example, the cytotoxic properties of isomers and derivatives of $[Ru(azpy)_2Cl_2]$ have been investigated in several cancer cell lines.[9-12] In particular, α-$[Ru(azpy)_2Cl_2]$ (α = *trans* pyridines, *cis* azo nitrogens and *cis* chlorides) was found to be highly active against a broad range of cancer cell lines, with cytotoxicities comparable to cisplatin and 5-fluorouracil, and superior activity in faster-growing cell lines.

In this Chapter the effects of changing the nature of the bonding by the N,N-chelating ligand (from a σ donor to a π-acceptor) on the properties of Ru^{II} arene complexes is studied. Thus the synthesis, characterization, aqueous solution chemistry and cytotoxicity of a series of novel ruthenium(II) complexes containing both an η^6-coordinated arene and a chelated 2-phenylazopyridine or phenylazopyrazole derivative are reported. The molecular structures of the complexes studied in this Chapter are shown in **Figure 3.1.**

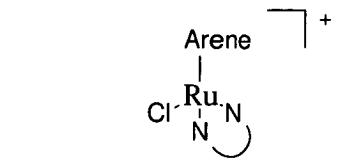

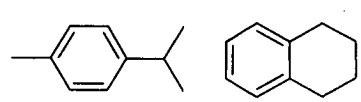

p-cym thn

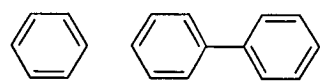

bz bip

Compound	Arene	N-N
1	*p*-cym	azpy
2	thn	azpy
3	bz	azpy
4	bip	azpy
5	*p*-cym	azpy-NMe_2
6	thn	azpy-NMe_2
7	bz	azpy-NMe_2
8	bip	azpy-NMe_2
9	*p*-cym	azpy-OH
10	thn	azpy-OH
11	bz	azpy-OH
12	bip	azpy-OH
13	*p*-cym	azpyz-NMe_2
14	thn	azpyz-NMe_2
15	bz	azpyz-NMe_2
16	bip	azpyz-NMe_2

Figure 3.1. General structure of the complexes synthesized in this work as PF_6 salts.

3.2 Experimental

3.2.1 Materials

The preparations of the starting materials $[(\eta 6\text{-arene})RuCl_2]_2$ (arene = p-cymene, tetrahydranapthalene, benzene, biphenyl) is reported in Chapter 2. 4-(2-Pyridylazo)-N, N-dimethylaniline (azpy-NMe_2), aniline, $NaNO_2$, 2-cyanoethylhydrazine, N, N-dimethylaniline, ortho-phosphoric acid, benzoquinone, 2-hydrazinopyridine and nitrosyl sulfuric acid were purchased from Sigma-Aldrich. Ethanol and methanol were dried over Mg/I_2 or anhydrous quality was used (Sigma-Aldrich). The ruthenium ICP-OES standard (1000 ppm) was purchased from Sigma Aldrich. All other reagents used were obtained from commercial suppliers and used as received.

3.2.2 Synthesis

3.2.2.1 2-(Phenylazopyridine) (azpy)

The solid 2-aminopyridine (5.49 g, 0.0583 mol) was added to NaOH (27.06 g, 0.677 mol) in 30 mL water containing 5 mL benzene. Over a 15 min period, nitrosobenzene (6.08 g, 0.0567 mol) was added whilst the mixture was warmed on an oil bath. The mixture was heated under reflux for a further 10 min and was then extracted 3 x with 100 mL portions of toluene. The organic layer was dried with magnesium sulfate and treated with decolourising charcoal. The toluene was removed on a rotary evaporator, the solid residue dried *in vacuo* under argon, and recrystallisation from petroleum ether was attempted. The solid was dissolved in 500 mL of hot petroleum ether (313-323 K), leaving a brown residue which was decanted off. The solution was cooled in a container of dry ice overnight in an attempt for solid to precipitate out. Recrystallisation from petroleum ether (313-323 K) was repeated twice and the red solid product was used for further synthesis without further purification. Yield: 3.773 g (36.3%). ^{1}H NMR ($CDCl_3$): δ8.76 (d, 1H), 8.08-8.05 (m, 2H), 7.93 (t, 1H), 7.85 (d,1H), 7.57-7.53 (m, 3H), 7.42 (t, 1H) ESI-MS: Calcd for $C_{11}H_9N_3$ [M^+] m/z 184.1, found 184.2.

3.2.2.2 4-(2-Pyridylazo)phenol (azpy-OH)

Benzoquinone (0.493 g, 4.56 mmol) was dissolved in 50 mL water and 3.6 mL 60%

perchloric acid. Hydrazinopyridine (0.504 g, 4.62 mmol), dissolved in 8 mL water was added dropwise and the solution gradually turned brown/orange. The solution was stirred at ambient temperature for 1 h and filtered to leave an orange crystalline precipitate, which was dissolved in 25 mL methanol and 1.5 mL formic acid and ammonia gas was bubbled through the mixture until re-precipitaion occurred. The product was filtered and left to dry overnight in vacuo. A second crop was obtained by reducing the volume of the solvent of the filtrate. Yield 213 mg (23.4%) ^{1}H NMR ($(CD_3)_2SO$): δ 8.73 (d, 1H), 8.13 (t, 1H), 7.91 (d, 2H), 7.75 (d, 1H), 7.61 (t, 1H), 7.01 (d, 2H). ESI-MS: Calcd for $C_{11}H_9N_3O$ [M^+] m/z 200.1, found 200.2.

3.2.2.3 3-Amino-pyrazoline hydrochloride

Sodium metal (0.096 g, 4.17 mmol) was added to 15 mL dry ethanol. 2-Cyanoethylhydrazine (2.5 g, 29.4 mmol) was added dropwise and the mixture was heated under reflux for 4 h. The reaction mixture was left to cool and 50 mL 37% HCl was added dropwise. The reaction mixture turned green/yellow and a white precipitate formed at the bottom of the flask. The flask was kept cool by surrounding in ice and the solution was filtered through a frit under suction. The crude product was dissolved in acidified water where NaCl impurities precipitated out. These salts were removed by filtration, water was removed on the rotary evaporator and the white solid product was dried overnight *in vacuo*. Yield: 2.48 g (68%). ^{1}H NMR ($(CD_3)_2SO$): δ7.09 (br s, 1H), 3.42 (t, 2H), 2.85 (t, 2H)

3.2.2.4 3-Amino-1-nitroso-2-pyrazoline

The solid 3-amino-pyrazoline hydrochloride (1 g, 8.23 mmol) was suspended in 8 mL acetic acid and the flask was cooled by surrounding in ice. $NaNO_2$ (0.57 g, 8.23 mmol) was dissolved in 1 mL water and added dropwise to the cooled solution over 70 min. The solution was stirred at 273 K for 4 h. The solvent was removed and the orange solid was re-dissolved in 3 mL water. The flask was kept cold by surrounding in ice and the mixture was filtered under suction. The orange powder obtained was dried overnight *in vacuo*. Yield: 204 mg (22%). ESI-MS: Calcd for $C_3H_6N_4O$ [M] m/z 114.1, $C_3H_6N_3$ [M-NO] 84.1, found 114.6, 84.6.

3.2.2.5 4-(1H-pyrazol-3-ylazo)-N,N dimethylaniline (azpyz-NMe_2)

3-Amino-1-nitroso-2-pyrazoline (353 mg, 3.07 mmol) was dissolved in 3 mL o-phosphoric acid and stirred at 298 K. H_2SO_4 (2.4 mL of 18 M) was added slowly to this mixture so that the temperature did not exceed *ca.* 313 K. Once the mixture has stopped bubbling a solution of $NOHSO_4$ (0.98 g of 40% wt) in H_2SO_4 (0.98 g) was added over 1 h. The reaction was subsequently stirred at 321-323 K for 1.5 h then poured onto 35 g ice. N,N-dimethylaniline (0.361 g, 3 mmol) was dissolved in 20 mL water. To this solution the diazotised mixture was added dropwise and the pH was kept between 4 and 5 by addition of sodium carbonate (saturated solution). The yellow solution was filtered and the precipitate was washed with water. The yellow solid was dried overnight *in vacuo*. Yield: 375 mg (57%). ^{1}H NMR (D_2O) δ8.05 (d, 2H), 7.84 (d, 1H), 7.75 (d, 2H), 6.76 (d, 1H), 3.37 (s, 6H) ESI-MS: Calcd for C11H13N5 [M^+] m/z 216.1, found 215.5.

3.2.2.6 [(η^6-*p*-cym)Ru(azpy)Cl]PF_6 (1)

The dimer [(η^6-p-cym)$RuCl_2$]$_2$ (257.6 mg, 0.421 mmol) was dissolved in 25 mL methanol and left to stir at room temperature until the solution turned clear. Azpy (155.7 mg, 0.850 mmol) dissolved in 10 mL methanol was added drop-wise and the solution gradually turned from brown to deep red. The solution was stirred at room temperature for one hour. The volume of solvent was reduced to about 10mL by removal of methanol on a rotary evaporator. NH_4PF_6 (417 mg, 2.773 mmol) was then added and the solution was placed in the freezer for one hour. A black powder precipitated out and this was filtered off and washed with ether. Yield: 408 mg (80.9%) (Found: C, 42.09; H, 4.02; N, 7.03. Calc for $RuC_{21}H_{23}N_3ClPF_6$: C, 42.07; H, 3.87; N, 7.01). ^{1}H NMR ($CDCl_3$): δ 9.45 (d, 1H), 8.58 (d, 1H), 8.27 (t, 1H), 8.09 (m, 2H), 7.90 (t, 1H), 7.77 (t, 1 H), 7.67 (t, 2H) 6.24 (d, 1H), 5.90 (d, 1H), 5.77(d of d, 2H), 2.53, (m, 1H), 2.23 (s, 3H), 1.06 (d of d, 6H).

3.2.2.7 [(η^6-thn)Ru(azpy)Cl]PF_6 (2)

The dimer [(η^6-thn)$RuCl_2$]$_2$ (99.8 mg, 0.164 mmol) was dissolved in 20 mL methanol and left to stir at room temperature until the solution turned clear. Azpy (60.09 mg, 0.332 mmol) dissolved in 10 mL methanol was added drop-wise and the solution

gradually turned from orange to dark brown. The solution was stirred at room temperature for one hour. The volume of solvent was reduced to about half by removal of methanol on a rotary evaporator. NH_4PF_6 (166 mg, 1.020 mmol) was then added and the solution was left at room temperature for one hour. A black shiny powder precipitated out and this was filtered off and washed with ether. Yield: 166 mg (86.7%) (Found: C, 41.35; H, 3.67; N, 6.98. Calc for $RuC_{20}H_{21}N_3ClPF_6$: C, 41.02; H, 3.62; N, 7.18). ^1H NMR ($CDCl_3$): δ 9.14 (d, 1H), 8.63 (d, 1H), 8.27 (t, 1H), 8.07 (m, 2H), 7.83 (t, 1H), 7.72 (t, 1H), 7.66 (t, 2H), 6.01 (d, 1H), 5.84 (t, 1H), 5.56 (d, 1H), 5.34 (t, 1H), 2.92-2.64 (m, 4H), 2.03-1.76 (m, 4H).

3.2.2.8 [(η^6-bz)Ru(azpy)Cl]PF_6 (3)

The dimer [(η^6-bz)$RuCl_2$]$_2$ (51.1 mg, 0.102 mmol) was dissolved in 25 mL methanol and left to stir at room temperature until the solution turned clear. Azpy (37.74 mg, 0.206 mmol) dissolved in 10 mL methanol was added drop-wise and the solution gradually turned from light to dark brown. The solution was stirred at room temperature for one hour. The volume of solvent was reduced to about 15 mL by removal of methanol on a rotary evaporator. NH_4PF_6 (112 mg, 0.690 mmol) was then added and the solution was left in the freezer overnight. The volume was then reduced to around 10 mL and a dark brown powder precipitated out. This was filtered off and washed with ether. Yield: 81.6 mg (73.7%) (Found: C, 37.82; H, 2.73; N, 7.63. Calc for $RuC_{17}H_{15}N_3ClPF_6$: C, 37.57; H, 2.78; N, 7.74). ^1H NMR ($(CD_3)_2CO$): δ 9.80 (d, 1H), 8.90 (d, 1H), 8.61 (t, 1H), 8.31 (m, 2H), 8.03 (t, 1H), 7.82-7.79 (m, 3H), 6.43 (s, 6H).

3.2.2.9 [(η^6-bip)Ru(azpy)Cl]PF_6 (4)

The dimer [(η^6-bip)$RuCl_2$]$_2$ (101.6 mg, 0.156 mmol) was dissolved in a solution of 40 mL methanol and 10 mL water. The solution was refluxed under argon for 2 hours and was hot-filtered to remove a black residue. Azpy (62.75 mg, 0.343 mmol) dissolved in 5 mL methanol was added drop-wise and the solution almost immediately turned from orange to deep red. The solution was stirred and left to cool to room temperature for one hour. The volume of solvent was reduced to about 25 mL by removal of methanol on a rotary evaporator. NH_4PF_6 (189 mg, 1.16 mmol)

was then added and the solution was left in the fridge overnight during which time a light brown powder precipitated out. This was filtered off and washed with ether. Yield: 130 mg (68.3%) (Found: C, 44.11; H, 2.92; N, 6.85. Calc for $RuC_{23}H_{19}N_3ClPF_6$: C, 44.59; H, 3.09; N, 6.79) ^{1}H NMR ($(CD_3)_2CO$): δ 9.55 (d, 1H), 8.88 (d, 1H), 8.57 (t, 1H), 8.10 (d, 2H), 7.95 (t, 1H), 7.80 (t, 1H), 7.76 (d, 2H), 7.67-7.59 (m, 3H), 7.53 (t, 2H), 6.82-6.77 (m, 2H) 6.69 (d of t, 2H), 6.45 (t, 1H).

3.2.2.10 [(η^6-*p*-cym)Ru(azpy-NMe$_2$)Cl]PF$_6$ (5)

The dimer [(η^6-*p*-cym)$RuCl_2]_2$ (255.8 mg, 0.418 mmol) was dissolved in 25 mL methanol and left to stir at room temperature until the solution turned clear. Azpy-NMe_2 (184.7 mg, 0.816 mmol) dissolved in 15 mL methanol was added drop-wise and the solution immediately turned from brown to dark blue. The solution was stirred at room temperature for one hour. The volume of solvent was reduced to about 10 mL by removal of methanol on a rotary evaporator. NH_4PF_6 (470 mg, 2.883 mmol) was then added and the solution was placed in the freezer overnight. A black microcrystalline product precipitated out and this was filtered off and washed with ether. Yield: 480 mg (91.8%) (Found: C, 43.19; H, 4.52; N, 8.62. Calc for $RuC_{23}H_{27}N_4ClPF_6$: C, 43.05; H, 4.24; N, 8.62). ^{1}H NMR ($CDCl_3$): δ 9.22 (d, 1H), 8.2-8.15 (m, 3H), 8.07 (t, 1H), 7.62 (t, 1H) 6.82 (d, 2H), 6.03 (d, 1H), 5.85 (d, 1H), 5.76 (d of d, 2H), 3.31 (s, 6H), 2.48 (m, 1H), 2.27 (s, 3H), 1.43 (d, 3H), 0.61 (d, 3H).

3.2.2.11 [(η^6-thn)Ru(azpy-NMe$_2$)Cl]PF$_6$ (6)

The dimer [(η^6-thn)$RuCl_2]_2$ (104.9 mg, 0.173 mmol) was dissolved in 25 mL methanol and left to stir at room temperature until the solution turned clear. Azpy-NMe_2 (74.94 mg, 0.331 mmol) dissolved in 10 mL methanol was added drop-wise and the solution immediately turned from orange to dark blue. The solution was stirred at room temperature for one and a half hours. The volume of solvent was reduced to about half by removal of methanol on a rotary evaporator. NH_4PF_6 (172 mg, 1.056 mmol) was then added and the solution was left at room temperature for one hour. A green powder precipitated out and this was filtered off and washed with ether. Yield: 188 mg (90.6%) (Found: C, 42.40; H, 4.22; N, 8.81. Calc for $RuC_{22}H_{26}N_3ClPF_6$: C, 42.03; H, 4.17; N, 8.92). ^{1}H NMR ($CDCl_3$): δ 9.03 (d, 1H),

8.21 (m, 3H), 8.09 (t, 1H), 7.61 (t, 1H), 6.83 (d, 2H), 5.89 (t, 1H), 5.83 (t, 1H), 5.79 (m, 2H), 3.31 (s, 6H), 2.74-2.39 (m, 4H), 1.79-1.58 (m, 4H).

3.2.2.12 $[(\eta^6\text{-bz})Ru(azpy\text{-}NMe_2)Cl]PF_6$ (7)

The dimer $[(\eta^6\text{-bz})RuCl_2]_2$ (51.1 mg, 0.102 mmol) was dissolved in 25 mL methanol and left to stir at room temperature until the solution turned clear. Azpy-NMe_2 (45.65 mg, 0.200 mmol) dissolved in 10 mL methanol was added drop-wise and the solution immediately turned from orange to dark blue/purple. The solution was stirred at room temperature for one hour. The volume of solvent was reduced to about half by removal of methanol on a rotary evaporator. NH_4PF_6 (106 mg, .650 mmol) was then added and the solution was left in the freezer overnight. A dark brown powder precipitated out and this was filtered off and washed with ether. Yield: 86 mg (73.4%) (Found: C, 39.05; H, 3.29; N, 9.48. Calc for $RuC_{19}H_{20}N_4ClPF_6$: C, 38.91; H, 3.44; N, 9.56). ^{1}H NMR ($(CD_3)_2CO$): δ 9.56 (d, 1H), 8.43-8.33 (m, 4H), 7.72 (t, 1H), 7.05 (d, 2H), 6.35 (s, 6H), 3.39 (s, 6H).

3.2.2.13 $[(\eta^6\text{-bip})Ru(azpy\text{-}NMe_2)Cl]PF_6$ (8)

The dimer $[(\eta^6\text{-bip})RuCl_2]_2$ (105.1 mg, 0.161 mmol) was dissolved in a solution of 40 mL methanol and 10 mL water. The solution was refluxed under argon for 2 hours. Azpy-NMe_2 (78.15 mg, 0.345 mmol) dissolved in 5 mL methanol was added drop-wise and the solution immediately turned from brown to very dark blue. The mixture was hot filtered and left to cool to room temperature whilst stirring. After thirty minutes, the volume of solvent was reduced to about 15 mL by removal of methanol on a rotary evaporator. NH_4PF_6 (187 mg, 1.14 mmol) was then added and the solution was left in the fridge overnight. The black crystalline powder precipitated out and was filtered off and washed with methanol until the filtrate turned blue. Yield: 130 mg (61.1%) (Found: C, 45.31; H, 3.56; N, 8.44. Calc for $RuC_{25}H_{24}N_4ClPF_6$: C, 45.31; H, 3.61; N, 8.46) ^{1}H NMR ($(CD_3)_2CO$): δ 9.25 (d, 1H), 8.36 (d, 1H), 8.29 (t, 1H), 8.22 (d, 2H), 7.75-7.71 (m, 2H), 7.60-755 (m, 2H), 7.54-7.48 (t, 2H), 6.91 (d, 2H), 6.75 (d, 1H), 6.65 (d, 1H), 6.57 (d of d, 2H), 6.38 (t, 1H), 3.36 (s, 6H,).

3.2.2.14 [(η^6-*p*-cym)Ru(azpy-OH)Cl]PF_6 (9)

The dimer [(η^6-*p*-cym)$RuCl_2$]$_2$ (40 mg, 0.048 mmol) was dissolved in methanol (15 mL) and left to stir at room temperature until the solution turned clear. Azpy-OH (21 mg, 0.096 mmol) dissolved in methanol (10 mL) was added drop-wise and the solution gradually turned from brown to deep brown/red with a yellow tinge. The solution was stirred at room temperature for 3 h. The volume of solvent was reduced to about 10 mL and NH_4PF_6 (80 mg, 0.49 mmol) was added and the solution was placed in the freezer overnight. A black powder precipitated out and this was filtered off and washed with diethyl ether. The product was dried overnight *in vacuo*. Yield: 50 mg (84.7%) ^{1}H NMR ($(CD_3)_2SO$): δ 9.49 (d, 1H), 8.55 (d, 1H), 8.37, (t, 1H), 8.12 (d, 2H), 7.80 (t, 1H), 6.99 (d, 2H), 6.40 (d, 1H), 6.16 (t, 2H), 6.06 (d, 1H), 2.37 (septet, 1H), 2.23 (s, 3H), 0.88 (dd, 6H). ESI-MS: calcd for $RuC_{21}H_{23}N_3O^+$ [M^+] m/z 470.1, found 469.9.

3.2.2.15 [(η^6-thn)Ru(azpy-OH)Cl]PF_6 (10)

The dimer [(η^6-thn)$RuCl_2$]$_2$ (30 mg, 0.049 mmol) was dissolved in methanol (15 mL) and left to stir at room temperature until the solution turned clear. Azpy-OH (21 mg, 0.098 mmol) dissolved in methanol (5 mL) was added drop-wise and the solution immediately turned from orange to deep purple. The solution was stirred at room temperature for 1 h. The volume of solvent was reduced to about half by removal of methanol on a rotary evaporator. NH_4PF_6 (166 mg, 1.020 mmol) was then added and the solution was placed in the freezer overnight. A black powder precipitated out and this was filtered off and washed with diethyl ether. The product was dried overnight *in vacuo*. Yield: 45 mg (73.4%) (Found: C, 40.79; H, 3.19; N, 6.78. Calcd for $RuC_{21}H_{21}N_3ClOPF_6$: C, 41.15; H, 3.45; N, 6.86).^{1}H NMR (DMSO-d_6) δ 9.49 (d, 1H), 8.71 (d, 1H), 8.45 (t, 1H), 8.16 (d, 2H), 7.94 (t, 1H), 7.08 (d, 2H), 6.39 (d, 1H), 6.25 (t, 1H), 6.095 (t, 1H), 6.06 (d, 1H), 2.71-2.62 (m, 1H), 2.62-2.5 (m, 1H), 2.34-2.25 (m, 1H), 2.15-2.06(m, 1H), 1.62-1.49 (m, 2H), 1.33-1.11 (m, 2H).

3.2.2.16 [(η^6-bz)Ru(azpy-OH)Cl]PF_6 (11)

The dimer [(η^6-bz)$RuCl_2$]$_2$ (25 mg, 0.05 mmol) was dissolved in methanol (20 mL) and warmed to *ca.* 323 K until the solution turned clear. Azpy-OH (20 mg, 0.1

mmol) dissolved in methanol (10 mL) was added drop-wise and the solution turned from brown to deep brown/red with a yellow tinge. The solution was cooled to room temperature and stirred for 4 h. The volume of solvent was reduced to about 10 mL by removal of methanol on a rotary evaporator. NH_4PF_6 (80 mg, 0.5 mmol) was then added and the solution was left in the freezer overnight. Diethyl ether was added drop-wise to the flask to precipitate out the product as a black solid. This was filtered off and washed with diethyl ether. The product was dried overnight *in vacuo*. Yield: 35 mg (62.6%) (Found: C, 36.65; H, 2.50; N, 7.60. Calcd for $RuC_{17}H_{15}N_3ClOPF_6$: C, 36.54; H, 2.71; N, 7.52) ^{1}H NMR ($(CD_3)_2SO$): δ 9.66 (d, 1H), 8.71 (d, 1H), 8.44 (t, 1H), 8.19 (d, 2H), 7.89 (t, 1H), 7.05 (d, 2H), 6.29 (s, 6H).

3.2.2.17 [(η^6-bip)Ru(azpy-OH)Cl]PF$_6$ (12)

The dimer $[(\eta^6\text{-bip})RuCl_2]_2$ (33 mg, 0.05 mmol) was dissolved in methanol (40 mL) and water (10 mL) and heated to reflux for 2 h. Azpy-OH (20 mg, 0.1 mmol) dissolved in methanol (5 mL) is added and the solution was refluxed for a further 1 h. The solution was hot-filtered, the solvent was removed and the solid was re-dissolved in methanol (*ca.* 20 mL). NH_4PF_6 (84 mg, 0.5 mmol) was added and the solution was placed in the freezer overnight. A brown solid precipitated out and this was filtered and washed with diethyl ether. The product was dried overnight *in vacuo* Yield: 45 mg (46.0%) ^{1}H NMR ($(CD_3)_2SO$): δ 9.41 (d, 1H), 8.63 (d, 1H), 8.36 (t, 1H), 7.99 (d, 2H), 7.74 (t, 1H), 7.63 (d, 2H), 7.54 (t, 1H), 7.46 (t, 2H), 6.90 (d, 2H), 6.79 (d, 2H), 6.78 (d, 2H), 6.57 (t, 1H), 6.49 (t, 1H), 6.30 (t, 1H). ESI MS: Calcd for $RuC_{23}H_{19}N_3O^+$ [M^+] m/z 491.0, found 489.75.

3.2.2.18 [(η^6-*p*-cym)Ru(azpyz-NMe$_2$)Cl]PF$_6$ (13)

The dimer $[(\eta^6\text{-}p\text{-cym})RuCl_2]_2$ (103 mg, 0.17 mmol) was dissolved in methanol (30 mL) and left to stir at room temperature until the solution turned clear. Azpyz-NMe_2 (69 mg, 0.32 mmol) dissolved in methanol (10 mL) was added drop-wise and the solution immediately turned from brown to deep purple. The solution was stirred at room temperature for 1 h. The volume of solvent was reduced to about 10 mL and NH_4PF_6 (103 mg, 0.63 mmol) was then added and the solution was placed in the freezer overnight. A black powder precipitated out and this was filtered off and

washed with diethyl ether. The product was dried overnight *in vacuo*. Yield: 126 mg (62.4%) (Found: C, 40.35; H, 4.06; N, 10.56. Calcd for $RuC_{21}H_{27}N_5ClPF_6$: C, 39.98; H, 4.31; N, 11.10). ^1H NMR ($CDCl_3$) δ 8.02 (d, 2H), 7.95 (d, 1H), 7.07 (d, 1H), 6.77 (d, 2H), 6.34 (dd, 2H), 5.68 (dd, 2H), 3.22 (s, 6H), 2.4-2.33 (m, 4H), 0.92 (dd, 6H).

3.2.2.19 $[(\eta^6\text{-thn})Ru(azpyz\text{-}NMe_2)Cl]PF_6$ (14)

The dimer $[(\eta^6\text{-thn})RuCl_2]_2$ (30 mg, 0.049 mmol) was dissolved in methanol (15 mL) and left to stir at room temperature until the solution turned clear. Azpyz-NMe_2 (21 mg, 0.098 mmol) dissolved in methanol (5 mL) was added drop-wise and the solution immediately turned from orange to deep purple. The solution was stirred at room temperature for 1 h. The volume of solvent was reduced to about 10 mL and NH_4PF_6 (166 mg, 1.020 mmol) was then added and the solution was placed in the freezer overnight. A black powder precipitated out and this was filtered off and washed with diethyl ether. The product was dried overnight *in vacuo*. Yield: 46 mg (74.6%) ^1H NMR ($CDCl_3$) δ 8.15 (m, 3H), 7.21 (d, 1H), 6.93 (d, 2H), 6.35 (d, 1H), 6.0-5.8 (m, 3H), 3.24 (s, 6H), 3.0-1.5 (m, 8H). ESI MS: calcd for $RuC_{21}H_{25}N_5Cl^+$ [M^+] m/z 484.1, found 483.9

3.2.2.20 $[(\eta^6\text{-bz})Ru(azpyz\text{-}NMe_2)Cl]PF_6$ (15)

The dimer $[(\eta^6\text{-bz})RuCl_2]_2$ (50mg, 0.1 mmol) was dissolved in methanol (30 mL) and left to stir at room temperature until the solution turned clear. Azpyz-NMe_2 (42.3 mg, 0.2 mmol) dissolved in methanol (15 mL) was added drop-wise and the solution immediately turned from brown to deep purple. The solution was stirred at room temperature 2 h. The volume of solvent was reduced to about 10 mL and NH_4PF_6 (117 mg, 0.7 mmol) was then added and the solution was left in the freezer overnight. The volume of solvent was further reduced and a black powder precipitated out. This was filtered off and washed with diethyl ether. The product was dried overnight *in vacuo*. Yield: 92 mg (80.0%) (Found: C, 34.89; H, 2.68; N, 12.18. Calcd for $RuC_{17}H_{19}N_5ClPF_6$: C, 35.52; H, 3.33; N, 12.18). ^1H NMR ($(CD_3)_2CO$): δ 8.31 (d, 1H), 8.21 (d, 2H), 7.31 (d, 1H), 6.96 (d, 2H), 6.29 (s, 6H), 3.28 (s, 6H).

3.2.2.21 [(η^6-bip)Ru(azpyz-NMe$_2$)Cl]PF$_6$ (16)

The dimer [(η^6-bip)RuCl$_2$]$_2$ (100 mg, 0.17 mmol) was dissolved in a solution of methanol (40 mL) and water (10 mL). The solution was refluxed under argon for 2 h and was hot-filtered to remove a small amount of black residue. Azpyz-NMe$_2$ (74 mg, 0.35 mmol) dissolved in methanol (10 mL) was added dropwise and the solution immediately turned from orange/brown to deep purple. The solution was stirred and left to cool to room temperature for 3 h. The volume of solvent was reduced to about 20 mL and NH_4PF_6 (134 mg, 82 mmol) was then added and the solution was left in the fridge overnight, during which time a dark powder precipitated out. This product was filtered off and washed with diethyl ether. The product was dried overnight *in vacuo*. Yield: 153 mg (67.2%) (Found: C, 42.97; H, 3.50; N, 11.70. Calcd for $RuC_{23}H_{23}N_5ClPF_6$: C, 42.44; H, 3.56; N, 10.76) ^{1}H NMR ($(CD_3)_2CO$): δ 8.21 (d, 1H), 8.04 (d, 2H), 7.71-7.34 (m, 5H), 7.29 (d, 1H), 6.81 (d, 2H), 6.71 (d, 1H), 6.66-6.55 (m, 2H), 6.52 (t, 1H), 6.31 (t, 1H), 3.25 (s, 6H).

3.2.3 Methods

3.2.3.1 X-Ray Crystallography

The crystal structure of **1** was solved using direct methods (SHELXS)[13] and was refined against F^2 using SHELXL.[14] The crystal structures of **4** and **5** were solved using Patterson methods (DIRDIF)[15] and were refined against F^2 using SHELXL or CRYSTALS.[16] In all cases the hydrogen atoms were placed in calculated positions and non-H atoms were refined with anisotropic displacement parameters. Crystals of **4** formed in clump-like aggregates. The diffraction pattern from the sample selected for data collection was indexed on the basis of two orientation matrices. The relationship between these matrices (the 'twin law') could be expressed with the matrix

$$\begin{pmatrix} -0.955 & -0.011 & -0.111 \\ -0.428 & -0.482 & 0.574 \\ -0.404 & 1.282 & 0.456 \end{pmatrix}$$

The data set used for structure elucidation was taken from the more strongly diffracting of the two domains. X-rat crystallographic data for complexes 1, 4 and 5 can be found on the enclosed cd. In addition, The crystal structures of **1**, **4**, and **5** have been deposited in the Cambridge Crystallographic Data Centre under the accession numbers CCDC 616620, 616621, and 616622, respectively

Crystal Data for Complex 1. Crystals suitable for X-ray diffraction were obtained by diffusion of diethyl ether into an acetone solution at ambient temperature. The sample was dark brown of dimensions 0.23 x 0.22 x 0.18 mm^3: triclinic, space group P-1; *a* = 9.1789(10), *b* = 9.7628 (11), *c* = 13.0987(14) Å; α = 84.6880(10), β = 72.951(2), γ = 89.7950(10) °; V = 1117.1(2) $Å^3$; Z = 1; D_{calc} = 1.781 Mg m^{-3}; μ = 0.958 mm^{-1}; F(000) = 600. The final conventional R factor [R1, based on |F| and 3651 data with F > 4σ(F)] was 0.0350, and weighted R2 (based on F2 and all 5695 unique data from θ = 1.63 – 25.00°) was 0.0872. The final ΔF synthesis extremes were +0.84 and -0.54 e $Å^{-3}$.

Crystal Data for Complex 4. Crystals suitable for X-ray diffraction were obtained by slow evaporation of an acetone/toluene solution at ambient temperature. The sample was red of dimensions 0.66 x 0.43 x 0.20 mm^3: orthorhombic, space group Pbca; *a* = 10.0146(4), *b* = 17.6860(7), *c* = 25.9129(10) Å; α = 90, β = 90, γ = 90 °; V = 4589.6(3) $Å^3$; Z = 8; D_{calc} = 1.791 Mg m^{-3}; μ = 0.936 mm^{-1}; F(000) = 2464. The final conventional R factor [R1, based on |F| and 5751 data with F > 4σ(F)] was 0.0646, and weighted R2 (based on F2 and all 36328 unique data from θ = 1.572 – 28.970°) was 0.1534. The final ΔF synthesis extremes were +3.32 and -0.78 e $Å^{-3}$.

Crystal Data for Complex 5. Crystals suitable for X-ray diffraction were obtained by slow evaporation of an acetone/toluene solution at ambient temperature. The sample was dark green of dimensions 0.76 x 0.46 x 0.16 mm^3: triclinic, space group P-1; *a* = 8.2676(2), *b* = 12.2633(4), *c* = 12.8805(4) Å; α = 84.8160(10), β = 83.1510(10), γ = 80.5010(10) °; V = 1275.50.(7) $Å^3$; Z = 2; D_{calc} = 1.672 Mg m^{-3}; μ = 0.846 mm^{-1}; F(000) = 648. The final conventional R factor [R1, based on |F| and 5879 data with F > 4σ(F)] was 0.0484, and weighted R2 (based on F2 and all 12210 unique data from θ = 1.60 – 28.89°) was 0.1300. The final ΔF synthesis extremes were +2.00 and -1.70 e $Å^{-3}$.

3.2.3.2 Determination of pK_a* Values

The pH* values of NMR samples in D_2O were measured at 298 K directly in the NMR tube before and after recording NMR data to give an average pH* value. The pH* values were adjusted with NaOD and DCl or $HClO_4$. pK_a* values were determined by plotting the change in chemical shift against pH* and fitting the curve to the to the Henderson-Hasselbalch equation (equation 1) using the program KALEIDOGRAPH (version 3.09., Synergy Software: Reading, PA, 1997) with the assumption that the observed chemical shifts are weighted averages of the populations of the protonated and deprotonated forms.

$$\delta_{obs} = \delta_{XH}[XH] + \delta_X[X] / [XH] + [X] \qquad (1)$$

where δ_{obs} is the observed chemical shift, δ_{XH} is the limiting chemical shift of the fully protonated form and δ_X is the limiting chemical shift of the deprotonated form. The errors are estimated as ±0.05 pK units. pKa* values were determined using the titration curves for a minimum of two ^1H resonances for each complex and the mean value was taken. The proton resonances followed (see **Figure 3.2** for labels) were Ha and Hc for azpy, Hf and Hg for azpy-NMe_2, Hb and Hf for azpy-OH, Ha and Hc for $[(\eta^6$-*p*-cym)Ru(azpy-OH)Cl]PF_6 **9**, and Hg and CH_3 proton in *p*-cym arene for $[(\eta^6$-*p*-cym)Ru(azpyz-NMe_2)$OH_2]^{2+}$, **13A**.

For determination of the pK_a^* value of aquated complex **13A**, complex **13** was dissolved in D_2O and 0.98 mol equiv of $AgPF_6$ was added. The solution was stirred for 24 h at 298 K and AgCl was removed by filtration.

3.2.3.3 Aqueous Solution Chemistry

3.2.3.3.1 Speciation of the complexes 1-4 and 13-15 after 24 h

Samples were dissolved in 90% H_2O/ 10% D_2O (pre-warmed to 310 K), filtered, the pH was recorded (pH_i), the NMR spectra were recorded initially and after 24 h and then the pH was re-measured (pH_f). Between acquisitions, they were kept in the water bath at 310 K. The pH values measured were **1**: pH_i 6.40 pH_f 6.51, **2**: pH_i 7.25

pH_f 6.49, **3**: pH_i 6.29 pH_f 6.11, **4**: pH_i 6.30 pH_f 6.03, **13**: pH_i 5.12 pH_f 4.84, **14**: pH_i 4.80 pH_f 5.05 and **15**: pH_i 4.75 pH_f 4.94.

3.2.3.3.2 Rate of arene loss from complexes 1 - 4

Complexes were dissolved in methanol and diluted with water to give *ca.* 100 μM solutions (95% H_2O, 5% MeOH). The absorbance was recorded at 3 min / 5 min intervals at 375 nm over 24 h at 310 K. The pH values of the solutions were 6.03 (**1**), 6.27 (**2**), 6.58 (**3**) and 6.30 (**4**). Plots of the change in absorbance with time were fitted to the appropriate equation for pseudo-first order kinetics using Origin version 7.5 (Origin Lab Corporation) to give the half-life and rate constant for arene loss.

3.2.3.3.3 Rate of decomposition of complexes 5 - 12

The complexes were dissolved in 90% H_2O/ 10% D_2O (or 100% D_2O, complex **6**) to give concentrations of *ca.* 100 μM. The solutions were sonicated for *ca.* 10 min to ensure complete dissolution, and then filtered. The pH was recorded (pH_i) and ^1H NMR spectra were recorded over 24 h at selected time intervals. The samples were kept at 310 K in a water bath between NMR data acquisitions. After 24 h the pH was re-recorded. The pH values were: (**5:** pH_i 7.34 pH_f 6.61, **6:** pH* 7.38, **7:** pH_i 7.17 pH_f 6.05, **8:** pH_i 6.42 pH_f 5.61, **9:** pH_i 5.14 pH_f 5.65, **10:** pH_i 6.34 pH_f 6.15, **11:** pH_i 6.29 pH_f 6.16 and **12:** pH_i 6.22 pH_f 5.46). The percentages of species present in solution were determined by integration of the azo ligand Ha proton resonance (see **Figure 3.2**) for the ligand present in the chloride, aqua and arene loss complexes. The decay of percentage of chloride species present over time was plotted and data were fitted to the appropriate equation for pseudo-first order kinetics using Origin version 7.5 (Origin Lab Corporation) or version 6.1 (Microcal Software Ltd) to give an approximate half-life and rate constant.

3.2.3.3.4 Rate of hydrolysis of complexes 13-16

Complexes were dissolved in methanol and diluted in acidified H_2O (pH adjusted to 2.27 by addition of $HClO_4$) to give a ca. 50 μM solution (95% H_2O, 5% MeOH). The absorbance was recorded at 1 min intervals at 620 nm over 24 h at 310 K. The measured pH values of the solutions were 2.21-2.25. Plots of the change in absorbance with time were fitted to the appropriate equation for pseudo-first order

kinetics using Origin version 7.5 (Origin Lab Corporation) to give the half-life and rate constant.

3.2.3.3.5 Reactions of complex 13 with 9-EtG

The aqua adduct 13A was prepared by dissolving 13 in methanol-d_4 and diluting with D_2O to give a *ca.* 100 μM solution (95% D_2O, 5% MeOD), adding $AgPF_6$ (0.98 mol equiv), stirring the solution for 24 h at ambient temperature and then filtering to remove AgCl. The pH* of the solution was adjusted to 7.42 by addition of $NaOH/HClO_4$ and then incubated at 310 K. To this solution 9-ethylguanine (*ca.* 100 μM, 95% D_2O, 5% MeOD, at 310 K) was added to give a 1:1 molar ratio of 13A and 9-ethylguanine (50 μM) with a pH* of 7.46. The reaction of the two species was followed by ^1H NMR over 24 h with readings taken every hour. The extent of reaction of 13A with 9EtG was determined by integration azpyzNMe_2 Hb (see **Figure 3.2**) ^1H NMR peaks for 13A and the 9-EtG adduct.

3.3 Results

Sixteen chlorido Ru^{II} arene complexes containing the chelated phenylazopyridine or phenylazopyrazole ligands azpy, azpy-OH, azpy-NMe_2 and azpyz-NMe_2 were synthesized and the structures of complexes **1**, **4** and **5** were determined by X-ray crystallography. Electronic absorption spectra of the complexes in aqueous solution are compared to those of the free azo ligands. The pKa* values of the pyridine conjugate acids of azpy, azpy-NMe_2 and azpy-OH have been determined. The aqueous solution chemistry of the complexes was investigated, mainly with respect to hydrolysis and arene loss, but also in relation to acidity of coordinated water (complex **13A**) and the phenolic OH (complex **9**). Finally the cytotoxicity of these complexes towards the A2780 human ovarian and A549 human lung cancer cells was investigated.

Synthesis and Characterisation

The chelating ligands used and their hydrogen numbering schemes are shown in **Figure 3.2.**

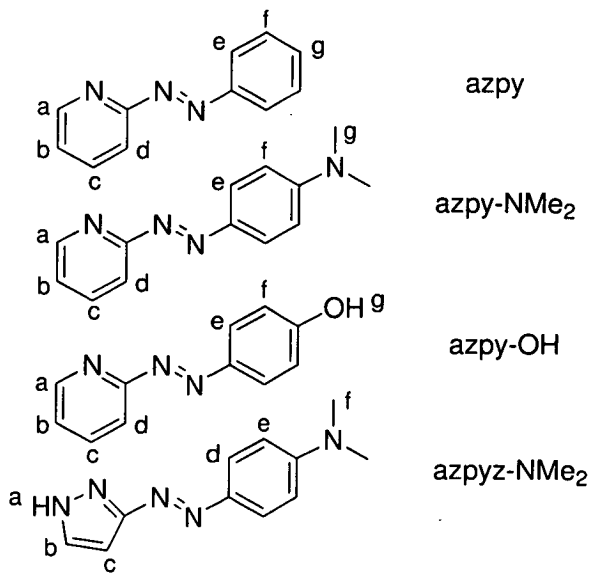

Figure 3.2. Molecular structures of chelating azo ligands, ligand abbreviations and hydrogen atom numbering schemes.

3.3.1.1 2-Phenylazopyridine (azpy)

This ligand was synthesised in moderate yields using a literature procedure[17] in a base-induced condensation reaction between 2-aminopyridine and nitrosobenzene (**Figure 3.3**).

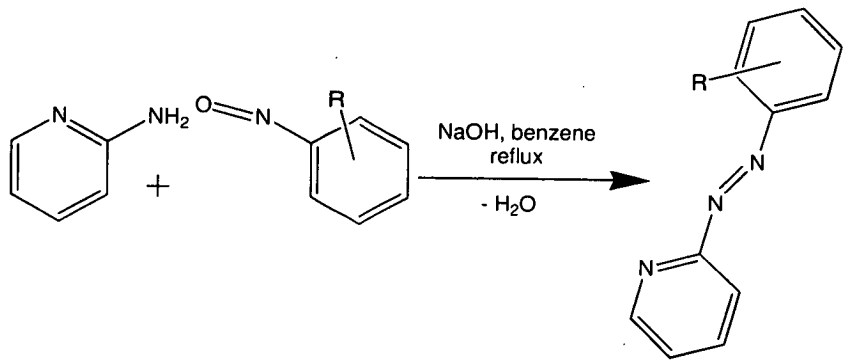

Figure 3.3 The reaction scheme for the formation of azpy.

The ligand was characterised by ^{1}H NMR and ESI-MS.

3.3.1.2 2-p-Phenolazopyridine (azpy-OH)

This ligand was synthesised in good yields using a literature procedure.[18] The reaction scheme is shown in **Figure 3.4.**

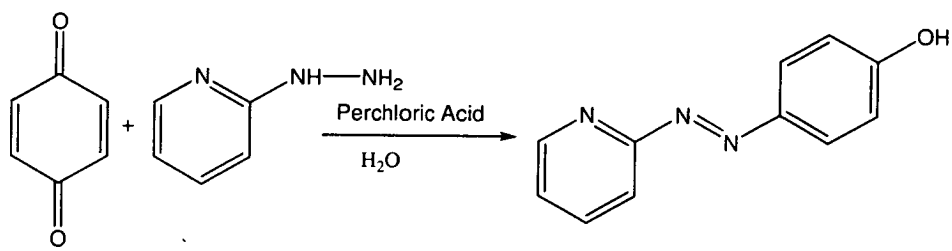

Figure 3.4. The reaction scheme for the formation of azpy-OH

In this reaction, the first step is attack on a δ^+ ipso carbon of the benzoquinone by the nucleophilic NH_2 group of hydrazinoquinone. Protonation of the oxygen causes OH_2^+ to be lost from the benzene ring with simultaneous aromatization. The remaining (now) phenolic oxygen is then protonated under the acidic conditions of the reaction. The product formed was characterised by NMR and ESI-MS.

3.3.1.3 3(5) – 4 dimethylphenylamino(phenylazo) pyrazole (azpyz-NMe_2)

This ligand was synthesised in a moderate yield from literature procedures[19, 20]. The reaction scheme is shown in **Figure 3.5**.

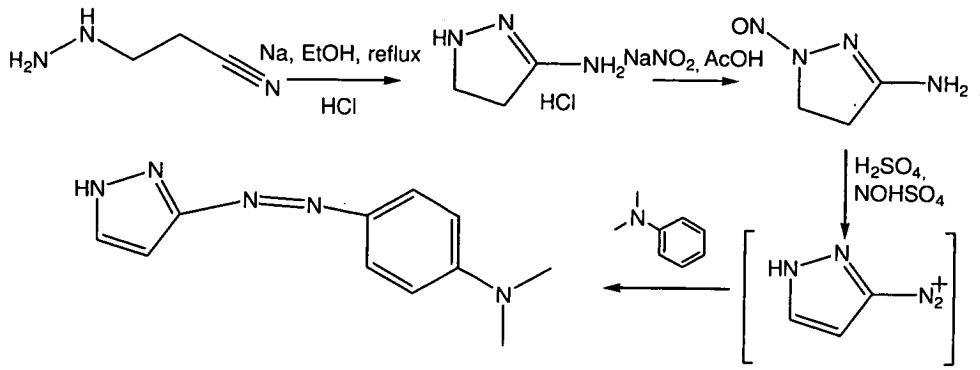

Figure 3.5. The reaction scheme for the formation of azpyz-NMe_2

The first step of this reaction is a base-induced intramolecular cyclisation of 2-cyanoethylhydrazine. In the second step the endocyclic nitrogen is attacked to form the nitrosopyrazoline using sodium nitrite. The third step uses acidic conditions to de-nitrosate with simultaneous aromatisation and azo formation to generate the diazo intermediate. The final step is the azo coupling reaction with dimethylaniline to form the product. The product was characterised by NMR and ESI-MS.

3.3.1.4 Ruthenium complexes

The complexes were typically synthesised by direct reaction of the ruthenium arene dimer and the azo ligand (**Figure 3.6**). The dimer was first dissolved in methanol causing the weak dichloro bridges to break. The ligand was then added drop-wise and the complexes were isolated as their PF_6 salts.

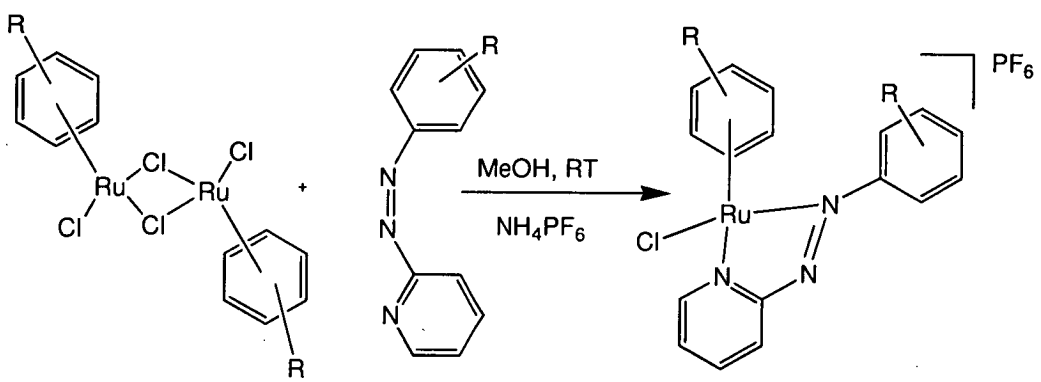

Figure 3.6. Reaction scheme for the formation of complexes of the type [(η^6-arene-R)Ru(azpy-R)Cl]PF_6

All compounds were synthesised in high yields and were characterised by ^{1}H NMR and CHN; where CHN was not available ESI-MS was carried out. In general the ^{1}H NMR resonances for the arene protons of Ru^{II} arene complexes are shifted downfield compared to the corresponding starting ruthenium dimers. For example for complexes containing the chelating azo ligand azpy-OH, the *p*-cym proton resonances for $[(\eta^6\text{-}p\text{-cym})Ru(azpy\text{-}OH)Cl]PF_6$ (**9**) are shifted downfield by *ca.* 0.6 ppm, thn resonances for complex **10** by *ca.* 0.5 ppm, biphenyl resonances for complex **11** by *ca.* 0.2 ppm, and benzene resonance for complex **12** by *ca.* 0.2 ppm. **Figure 3.1** (p 59) shows the complexes studied in this Chapter.

3.3.2 X-ray Crystallography

The molecular structures of the ruthenium complexes **1** and **5** were determined by single crystal X-ray diffraction. The crystal structure of **4** was determined from a twinned crystal, which accounts for the slightly higher conventional R value of 6.46%. Selected bond lengths and angles are listed in **Table 3.1** and the structures along with their atom numbering schemes are shown in **Figure 3.7.**

Table 3.1. Selected bond lengths (Å) and angles (deg) for $[(\eta^6\text{-}p\text{-cym})Ru(azpy)]ClPF_6$ (1), $[(\eta^6\text{-bip})Ru(azpy)Cl]PF_6$ (4) and, $[(\eta^6\text{-}p\text{-cym})Ru(azpy\text{-}NMe_2)Cl]PF_6$ (5). [a]Cent = centroid of η^6-arene.

Bond length / Angle	1	4	5
Ru(1)–N(28)	2.026(3)	2.046(5)	2.040(3)
Ru(1)–N(25)	2.052(3)	2.067(5)	2.053(3)
Ru(1)–Cl(1)	2.3704(9)	2.3830(15)	2.3705(9)
Ru(1)–C(11)	2.256(4)	2.236(5)	2.263(3)
Ru(1)–C(12)	2.226(4)	2.238(6)	2.217(3)
Ru(1)–C(13)	2.220(4)	2.192(5)	2.221(3)
Ru(1)–C(14)	2.241(4)	2.170(6)	2.213(3)
Ru(1)–C(15)	2.181(4)	2.208(6)	2.176(4)
Ru(1)–C(16)	2.230(4)	2.254(6)	2.224(3)
Ru(1)– cent[a]	1.7203(16)	1.707(2)	1.7107(15)
N(27)–N(28)	1.280(4)	1.271(6)	1.290(4)
N(28)–Ru(1)– N(25)	75.41(12)	75.27(19)	75.61(11)

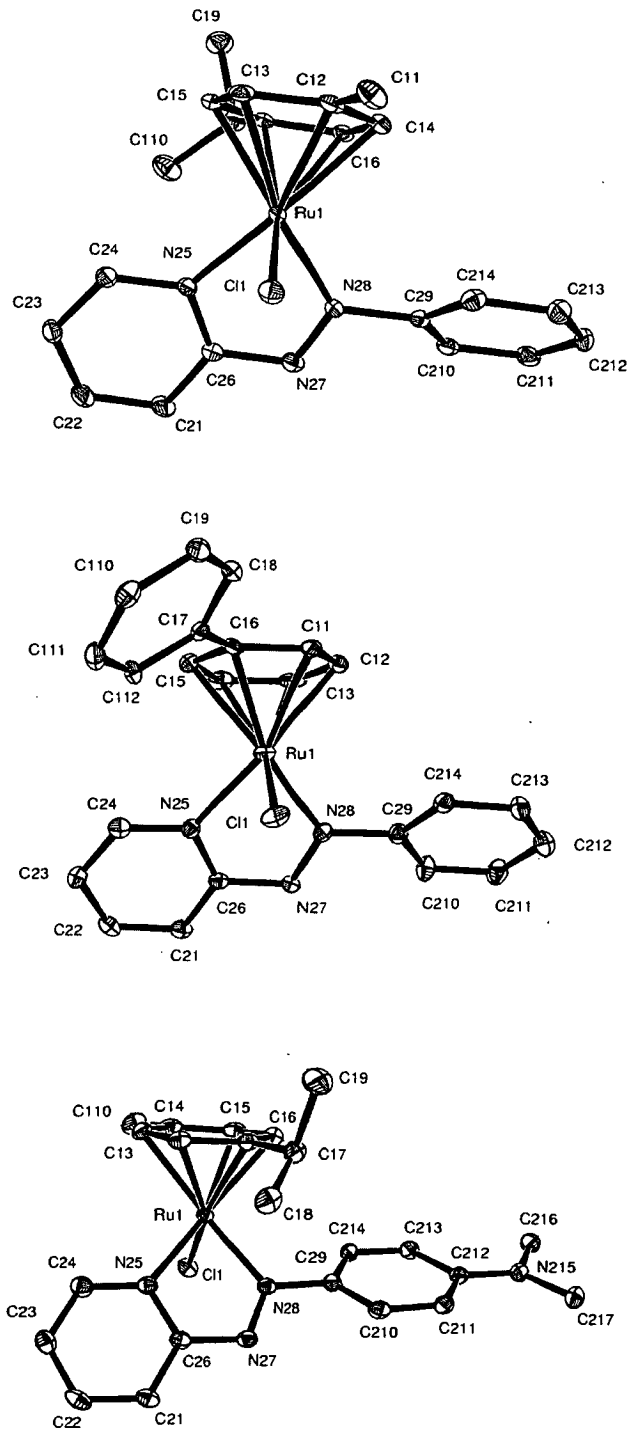

Figure 3.7. X-ray structures of the cations of (A) $[(\eta^6\text{-}p\text{-cym})Ru(azpy)Cl]PF_6$ (1), (B) $[(\eta^6\text{-bip})Ru(azpy)Cl]PF_6$ (4) and (C) $[(\eta^6\text{-}p\text{-cym})Ru(azpy\text{-}NMe_2)Cl]PF_6$ (5). Thermal ellipsoids show 30% probability. The hydrogen atoms have been omitted for clarity.

The structures are similar and complexes adopt the 'piano stool' type geometry common to several other ruthenium(II) arene structures.[2, 21] The ruthenium – arene centroid ring distances (1 1.7203(16) Å, 4 1.707(2) Å and 5 1.7107(15) Å) are longer than for analogous ruthenium(II) arene complexes containing chelated ethylenediamine ligands (e.g. $[(\eta^6\text{-}p\text{-cym})Ru(en)Cl]PF_6$ 1.6692(14) Å, $[(\eta^6\text{-bip})Ru(en)Cl]PF_6$ 1.662(3) Å).[21]

Furthermore, the five-membered ring formed by the chelating phenylazopyridine ligand and ruthenium is quite strained (N (28) –Ru (1) – N (25) angle *ca.* 75.5°) in all cases. In analogous ruthenium(II) arenes containing ethylenediamine as the chelating ligand, the angle was 78.2-79.2°.[21]

It is interesting to note that the Ru(1) – N(28) azo bonds in these arene complexes, which range from 2.026(3) Å– 2.046(5) Å, are longer than in the crystal structures of Ru^{II} phenylazopyridine structures α-$[Ru(azpy)_2Cl_2]$, (1.977(4)-2.0084(4) Å), β-$[Ru(azpy)_2Cl_2]$ (1.958(9)-2.003(9) Å) and γ-$[Ru(azpy)_2Cl_2]$ (1.986(5)-1.988(5) Å).[6, 22] Ru (1) – N (25) pyridine bond lengths, however, are within the same range as the $[Ru(azpy)_2Cl_2]$ complexes. In all three structures, the Ru (1) – Cl (1) bond lengths (2.37041(9) Å – 2.3830(15) Å) are comparable to other ruthenium(II) phenylazopyridine complexes, but shorter than analogous ruthenium arene complexes containing the chelating ligand en, for which distances are in the range *ca.* 2.39-2.45 Å.[2, 21]

Intermolecular π-π stacking interactions are present in crystals of **1** between phenyl rings of the azo ligand, with arene centroid-centroid intermolecular distances of 3.732(2) Å and an angle of 12.35° between the centroid-centroid vector and the vector normal to the plane of one of the rings. For complex **4**, all four aromatic rings are involved in stacking interactions with neighbouring molecules (see **Figure 3.8**) with parameters listed in **Table 3.2.**

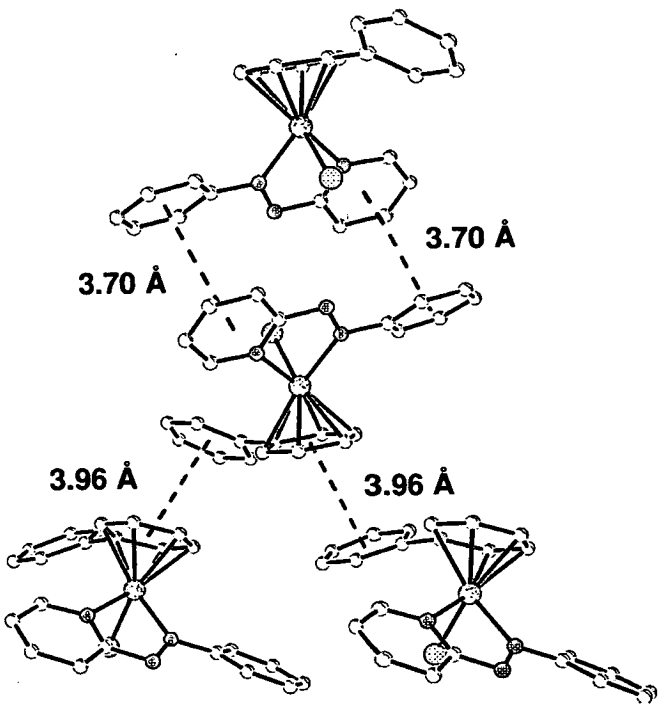

Figure 3.8. π-π stacking interactions in crystals of $[(\eta^6\text{-bip})Ru(azpy)Cl]PF_6$ (**4**) (distances are centroid-to-centroid).

Table 3.2. Intermolecular π-π stacking interaction parameters for complex **4**

Ring(1)[a]	Ring(2)[a]	Distance[b] (Å)	Angle[b] (deg)
N_{25}-C_{24}-C_{23}-C_{22}-C_{21}-C_{26}	C_{29}-C_{210}-C_{211}-C_{212}-C_{213}-C_{214}	3.958(3)	40.5
C_{11}-C_{12}-C_{13}-C_{14}-C_{15}-C_{16}	C_{17}-C_{18}-C_{19}-C_{110}-C_{111}-C_{112}	3.700(3)	20.18
C_{17}-C_{18}-C_{19}-C_{110}-C_{111}-C_{112}	C_{11}-C_{12}-C_{13}-C_{14}-C_{15}-C_{16}	3.701(3)	12.51
C_{29}-C_{210}-C_{211}-C_{212}-C_{213}-C_{214}	N_{25}-C_{24}-C_{23}-C_{22}-C_{21}-C_{26}	3.959(3)	17.08

[a] For atom numbering see Figure 3.7 (B). [b] Centroid-to-centroid. [c] Between normal to the plane of ring(1) and ring(1)-ring(2) centroid-to-centroid vector.

3.3.3 UV-Vis Spectroscopy

3.3.3.1 Azo Ligands

The wavelengths and intensities of the bands in the electronic absorption spectra of the free azo ligands in methanol are summarized in **Table 3.3**. Each free ligand exhibits a $\pi \rightarrow \pi^*$ transition above 300 nm centred primarily on the azo group. The assignment this transition (as $\pi \rightarrow \pi^*$, opposed to $n \rightarrow \pi^*$) was confirmed by solvent effects. Upon changing solvent from methanol to 90% water / 10% methanol (i.e. to a more polar solvent) the transition shifted to a longer wavelength. This trend is characteristic for $\pi \rightarrow \pi^*$ transitions[23] and is caused by attractive polarization forces between the solvent and the absorber, which lowers the energy levels of both the excited and unexcited states. The effect is greater for the excited state and so the energy difference between the excited and unexcited states is slightly reduced – resulting in a small red shift. In contrast, $n \rightarrow \pi^*$ transitions are characteristically shifted to shorter wavelengths with increasing solvent polarity.[23] This is due to increased solvation of the lone pair, which lowers the energy of the n orbital.

The λ_{max} of this band shifts to longer wavelengths with increasing σ-donating ability of the para substituent on the benzene ring (NMe_2 > OH > H), and on changing the heterocycle from pyrazole to pyridine, i.e. λ_{max} azpy-NMe_2 432 nm, azpyz-NMe_2 402 nm, azpy-OH 358 nm, and azpy 318 nm. The peaks below 300 nm are also tentatively assigned to $\pi \rightarrow \pi^*$ transitions. Azpy displays a weak $n \rightarrow \pi^*$ (forbidden) transition at 445 nm.

Table 3.3. Wavelengths of maximum absorbances, extinction coefficients and assignments for azo ligands in methanol ((asym) = asymmetric peak)

Ligand	λ_{max} /nm	ε /$M^{-1}cm^{-1}$	Assignment
Azpy	218	10600	$\pi \rightarrow \pi^*$
	318	18400	$\pi \rightarrow \pi^*$
	445	420	$n \rightarrow \pi^*$
Azpy-NMe_2	272	10700	$\pi \rightarrow \pi^*$
	432	35900(asym)[a]	$\pi \rightarrow \pi^*$
Azpyz-NMe_2	267	12200	$\pi \rightarrow \pi^*$
	402	33000(asym)[a]	$\pi \rightarrow \pi^*$
Azpy-OH	246	10000	$\pi \rightarrow \pi^*$
	358	25200	$\pi \rightarrow \pi^*$

The effect of deprotonation of the OH group in azpy-OH on the UV-Vis spectrum was investigated. **Figure 3.9** compares the UV-Vis spectrum of azpy-OH in water at *ca.* pH 7 and *ca.* pH 13. Upon deprotonation of azpy-OH the $\pi \rightarrow \pi^*$ transitions shift from 246 and 358 nm to 268 and 435 nm. This shift to longer wavelength correlates with the increased σ-donation from O^- vs. OH into the benzene ring of the ligand.

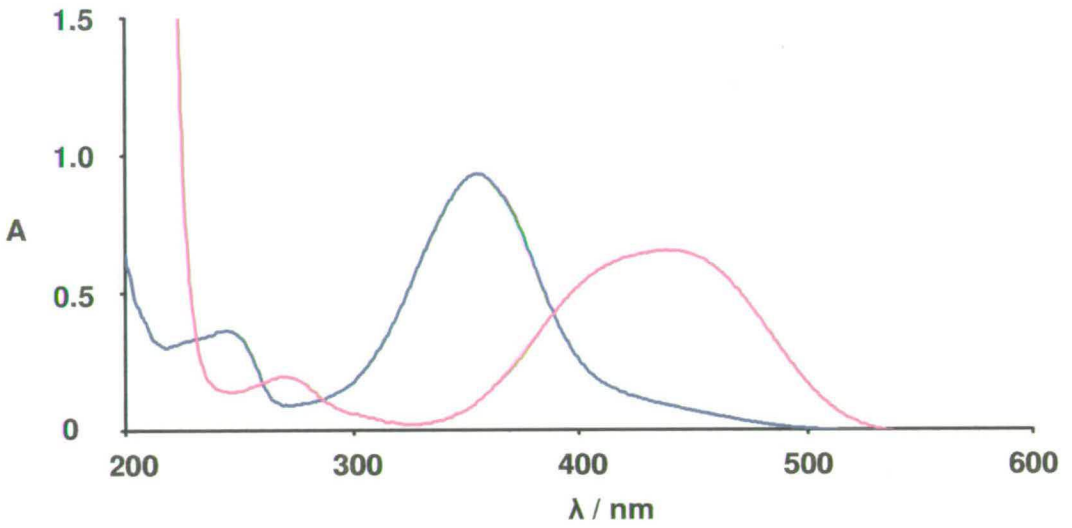

Figure 3.9. UV-Vis spectra for aqueous solutions of azpy-OH at pH *ca.* 7 (——) and *ca.* 13 (——) showing the dependence of π→π* transitions on pH.

3.3.3.2 Ruthenium Complexes

The wavelengths and intensities of the bands in the electronic absorption spectra of fresh aqueous solutions of the ruthenium complexes containing azpy, azpy-NMe_2 and azpyz-NMe_2 are summarised in **Table 3.4**, and those for azpy-OH and its corresponding deprotonated form in **Table 3.5**. All complexes display intense transitions in the visible region assignable to MLCT (Metal-to-Ligand-Charge-Transfer) from the filled 4d-orbitals of Ru^{II} to the empty π* ligand orbitals ($4d^6$ Ru→ π*). Both the position and the intensity of these transitions are highly dependent on the chelating ligand. For example, the effect on the UV-Vis spectrum of changing the chelating ligand in ruthenium *p*-cym complexes is shown in **Figure 3.10**. The wavelength of the MLCT increases from azpy-OH (469 nm) ~ azpy (471 nm) < azpyz-NMe_2 (577 nm) < azpy-NMe_2 (626 nm). This increase in wavelength is also accompanied by an increase in the molar extinction coefficient, i.e. **1** (ε = 6000 $M^{-1}cm^{-1}$ < **9** (7000 $M^{-1}cm^{-1}$) < **13** (22100 $M^{-1}cm^{-1}$) < **5** (42700 $M^{-1}cm^{-1}$). There are also small differences in both the position and the intensity of the MLCT bands when the arene is changed, for a given series with the same chelating ligand. There appears, however, to be no simple correlation between the position and intensity of the MLCT band and the arene. The UV-Vis spectra of these ruthenium complexes also display similar intraligand π→π* transitions to those in the free ligands, but shifted to longer

wavelengths for the complexes. Specific features of the spectra of the various classes of complexes are described below.

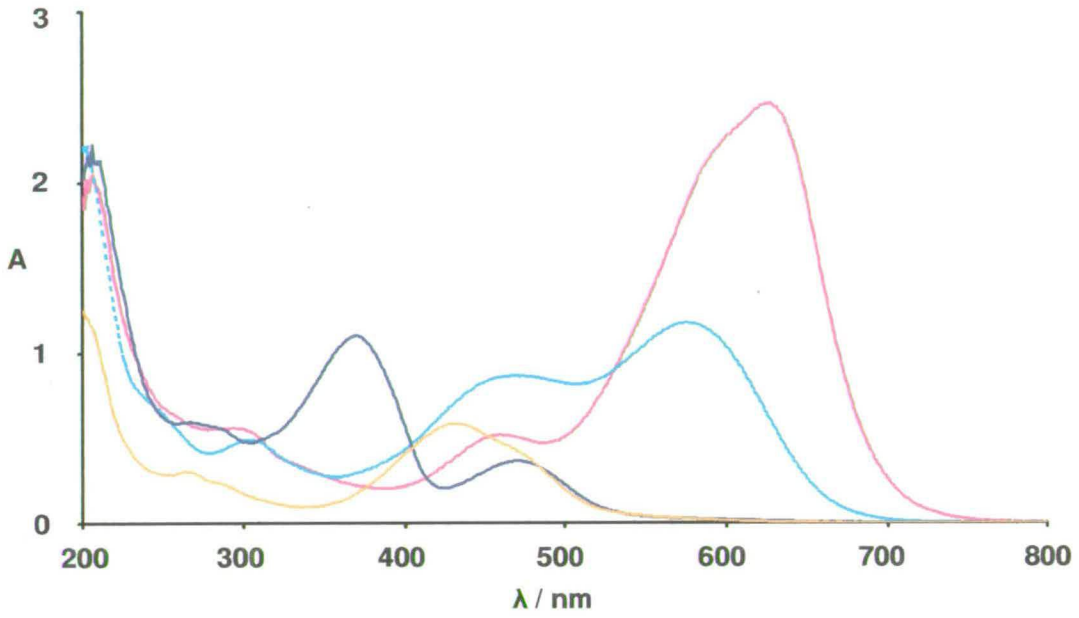

Figure 3.10. UV-Vis spectra for fresh aqueous solutions of [(η^6-*p*-cym)Ru(azpy)Cl]PF_6 (**1**, 58 μM, ——), [(η^6-*p*-cym)Ru(azpy-NMe_2)Cl]PF_6 (**5**, 54 μM, ——), [(η^6-*p*-cym)Ru(azpy-OH)Cl]PF_6 (**9**, 49 μM , ——), and [(η^6-*p*-cym)Ru(azpyz-NMe_2)Cl]PF_6 (**13**, 56 μM, ——) showing the effect of variations in the azo ligand on the absorption spectrum.

Table 3.4. Wavelengths of maximum absorbance, extinction coefficients and assignments for Ru^{II} arene complexes containing ligands azpy, azpy-NMe_2 and azpyz-NMe_2 in Water (sh = shoulder. IL = Intraligand).

Compound	λ_{max} /nm	ε / M^{-1} cm^{-1}	Assignment
1	262	9500	IL $\pi \rightarrow \pi^*$
	370	18000	IL $\pi \rightarrow \pi^*$
	471	6000	Ru ($4d^6$) $\rightarrow \pi^*$
2	268	9500	IL $\pi \rightarrow \pi^*$
	368	17100	IL $\pi \rightarrow \pi^*$
	471	5900	Ru ($4d^6$) $\rightarrow \pi^*$
3	359	12200	IL $\pi \rightarrow \pi^*$
	465	4000	Ru ($4d^6$) $\rightarrow \pi^*$
4	269	14100	IL $\pi \rightarrow \pi^*$
	364	14000	IL $\pi \rightarrow \pi^*$
	470	5000	Ru ($4d^6$) $\rightarrow \pi^*$
5	294	10000	IL $\pi \rightarrow \pi^*$
	457	9100	IL $\pi \rightarrow \pi^*$
	584	36000(sh)	Ru ($4d^6$) $\rightarrow \pi^*$
	626	42700	Ru ($4d^6$) $\rightarrow \pi^*$
6	296	15300	IL $\pi \rightarrow \pi^*$
	458	13400	IL $\pi \rightarrow \pi^*$
	584	39400(sh)	Ru ($4d^6$) $\rightarrow \pi^*$
	627	46700	Ru ($4d^6$) $\rightarrow \pi^*$
7	295	10000	IL $\pi \rightarrow \pi^*$
	452	8200	IL $\pi \rightarrow \pi^*$
	584	38700(sh)	Ru ($4d^6$) $\rightarrow \pi^*$
	620	44200	Ru ($4d^6$) $\rightarrow \pi^*$
8	295	13100	IL $\pi \rightarrow \pi^*$
	452	11000	IL $\pi \rightarrow \pi^*$
	584	53700(sh)	Ru ($4d^6$) $\rightarrow \pi^*$
	621	63700	Ru ($4d^6$) $\rightarrow \pi^*$
13	302	8900	IL $\pi \rightarrow \pi^*$
	469	14300	IL $\pi \rightarrow \pi^*$
	577	22100	Ru ($4d^6$) $\rightarrow \pi^*$
14	303	7800	IL $\pi \rightarrow \pi^*$
	481	11900	IL $\pi \rightarrow \pi^*$
	581	22500	Ru ($4d^6$) $\rightarrow \pi^*$
15	303	8000	IL $\pi \rightarrow \pi^*$
	469	13200	IL $\pi \rightarrow \pi^*$
	573	20600	Ru ($4d^6$) $\rightarrow \pi^*$
16	295	12800	IL $\pi \rightarrow \pi^*$
	481	13000	IL $\pi \rightarrow \pi^*$
	592	25700	Ru ($4d^6$) $\rightarrow \pi^*$

Table 3.5. Wavelengths of maximum absorbance, extinction coefficients and assignments for Ru^{II} arene complexes containing protonated azpy-OH or deprotonated azpy-O^- in Water ((sh) = shoulder, IL = intraligand)

Compound	λ_{max} /nm	ε / M^{-1} cm^{-1}	Assignment
9 (OH)	264	5100	IL $\pi \rightarrow \pi^*$
	432	9500	IL $\pi \rightarrow \pi^*$
	469	7000(sh)	Ru ($4d^6$) $\rightarrow \pi^*$
9 (O^-)	280	4600	IL $\pi \rightarrow \pi^*$
	457	4900(sh)	IL $\pi \rightarrow \pi^*$
	560	15100	Ru ($4d^6$) $\rightarrow \pi^*$
	588	15600	Ru ($4d^6$) $\rightarrow \pi^*$
10 (OH)	267	5600	IL $\pi \rightarrow \pi^*$
	430	10200	IL $\pi \rightarrow \pi^*$
	469	7600(sh)	Ru ($4d^6$) $\rightarrow \pi^*$
10 (O^-)	280	4800	IL $\pi \rightarrow \pi^*$
	460	5100(sh)	IL $\pi \rightarrow \pi^*$
	563	16700	Ru ($4d^6$) $\rightarrow \pi^*$
	587	16500	Ru ($4d^6$) $\rightarrow \pi^*$
11 (OH)	260	5800	IL $\pi \rightarrow \pi^*$
	429	11100	IL $\pi \rightarrow \pi^*$
	469	8000(sh)	Ru ($4d^6$) $\rightarrow \pi^*$
11 (O^-)	278	5700	IL $\pi \rightarrow \pi^*$
	454	5600(sh)	IL $\pi \rightarrow \pi^*$
	557	18900	Ru ($4d^6$) $\rightarrow \pi^*$
	587	19900	Ru ($4d^6$) $\rightarrow \pi^*$
12 (OH)	267	9900	IL $\pi \rightarrow \pi^*$
	430	10800	IL $\pi \rightarrow \pi^*$
	469	8600(sh)	Ru ($4d^6$) $\rightarrow \pi^*$
12 (O^-)	269	9100	IL $\pi \rightarrow \pi^*$
	457	5500(sh)	IL $\pi \rightarrow \pi^*$
	561	17400	Ru ($4d^6$) $\rightarrow \pi^{**}$
	591	19000	Ru ($4d^6$) $\rightarrow \pi^*$

Azpy Complexes (**1-4**). The UV-Vis spectra display a symmetrical MLCT band at *ca.* 470 nm and the extinction coefficient varies slightly (between 4000 M^{-1} cm^{-1} and 6000 M^{-1} cm^{-1}) when the arene is changed from bz, to bip, to *p*-cym and thn. The $\pi \rightarrow \pi^*$ intraligand transitions shift from 218 nm and 318 nm for the free ligand to *ca.* 266 nm and 365 nm for the complex.

Azpy-NMe$_2$ Complexes (**5-8**). The UV-Vis spectra display an intense unsymmetrical MLCT band at *ca.* 624 nm with a shoulder at 584 nm. The extinction coefficient of this band varies significantly with the arene; **5**/*p*-cym (ε 42700 M^{-1} cm^{-1}), **7**/bz (ε 44200 M^{-1} cm^{-1}), **6**/thn (ε 46700 M^{-1} cm^{-1}) and **8**/bip (ε 63700 M^{-1} cm^{-1}). The $\pi \rightarrow \pi^*$ intraligand transitions shift by *ca.* 20 nm to longer wavelengths compared to the free azpy-NMe$_2$ ligand.

Azpy-OH Complexes (**9-12**). The complexes containing the azpy-OH ligand display interesting pH dependent spectra. The UV-Vis spectra for all complexes at pH 2.5, where the ligand is fully protonated, display a MLCT band at *ca.* 469 nm with an extinction coefficient which varies between 7000 M^{-1} cm^{-1} and 8600 M^{-1} cm^{-1} as the arene is changed from *p*-cym, to thn and bz, to bip. This transition is partially obscured by the intraligand $\pi \rightarrow \pi^*$ transitions, which have shifted from 246 nm and 358 nm for the free ligand to *ca.* 265 nm and 430 nm for the complex. Raising the pH of the aqueous solutions to *ca.* 10.5 led to deprotonation of the azpy-OH ligand, and dramatically changed the UV-Vis spectrum. For example, the MLCT band of **12** shifts from 469 nm to *ca.* 588 nm with a shoulder at *ca.* 560 nm (**Figure 3.11**). For these deprotonated forms, the extinction coefficient increases from 15100 M^{-1} cm^{-1} to 18900 M^{-1} cm^{-1} as the arene is changed from *p*-cym, to thn, to bip, to bz. The intense intraligand $\pi \rightarrow \pi^*$ transitions also shift to longer wavelengths (to *ca.* 277 nm and 457 nm).

Azpyz-NMe$_2$ Complexes (**13-16**). The UV-Vis spectra display an intense symmetrical MLCT band at *ca.* 581 nm. The extinction coefficient of this band increases from 20600 M^{-1} cm^{-1} to 25700 M^{-1} cm^{-1} on changing the arene from bz, to *p*-cym, to thn, to bip and the intense $\pi \rightarrow \pi^*$ intraligand transitions shift to longer wavelengths by *ca.* 30 nm.

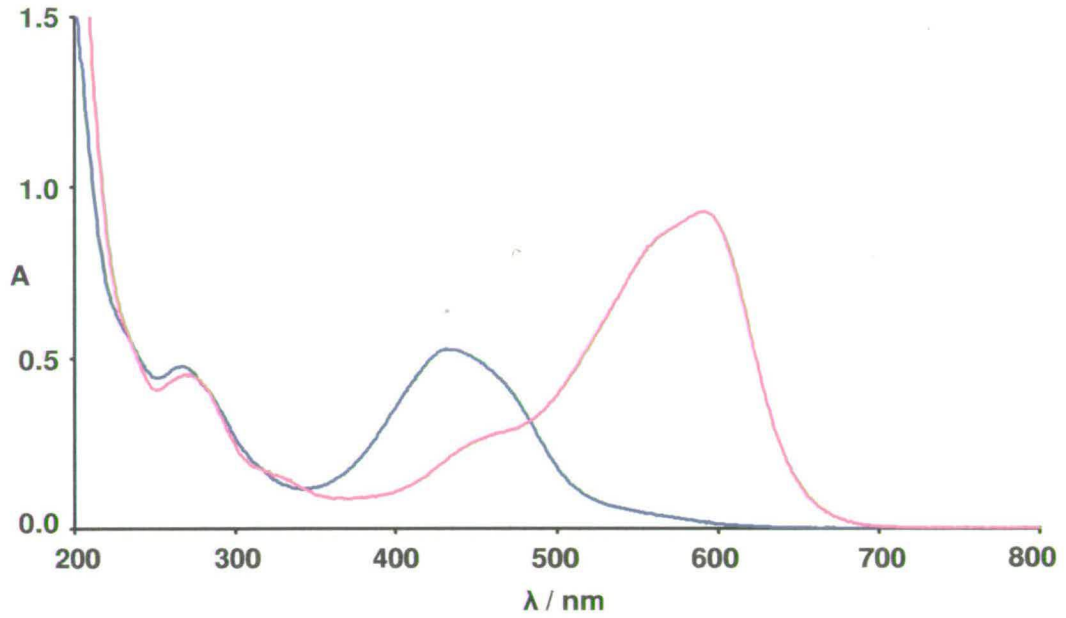

Figure 3.11. UV-Vis spectra for aqueous solutions of $[(\eta^6\text{-bip})Ru(azpy\text{-}OH)Cl]PF_6$ (12, 42 μM) at pH *ca.* 2.5 (——) and *ca.* 10.5 (——), showing the dependence of $\pi \rightarrow \pi^*$ and MLCT transitions on pH.

3.3.4 Aqueous Solution Chemistry

3.3.4.1 Phenylazopyridine ligands

The variation in 1H NMR chemical shifts with pH* allowed for determination of the pKa* values for the ionisable groups of the chelating phenylazopyridine ligands in an aqueous solution. Thus the pKa* values for the conjugate acids of the pyridine nitrogens of the free ligands were determined as 2.47 for azpy, 3.06 for azpy-OH, 4.60 for azpy-NMe_2 and for the OH of azpy-OH 8.08 and $NHMe_2^+$ in azpy-NMe_2 2.11 (**Figure 3.12**).

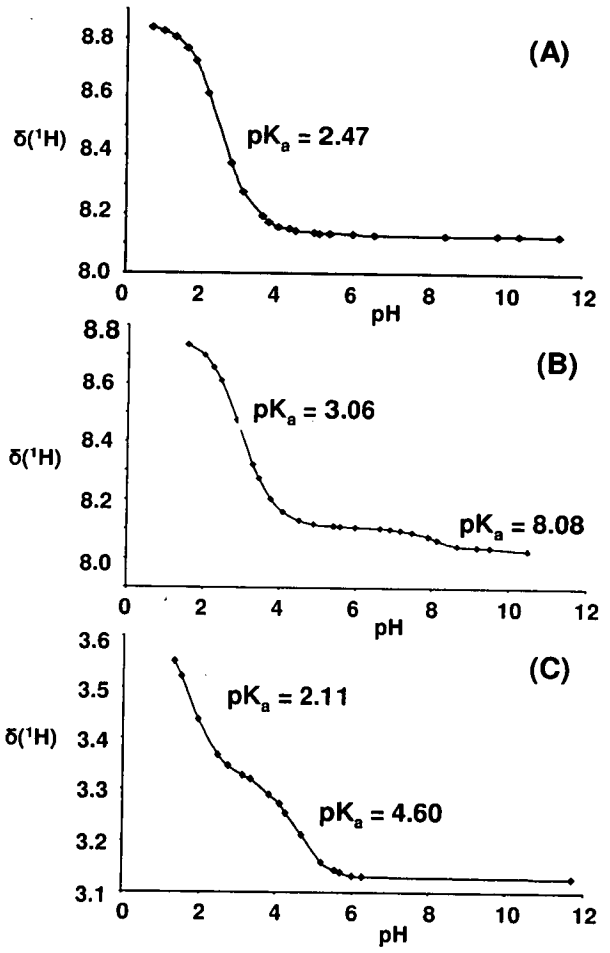

Figure 3.12. Dependence of the ^{1}H NMR chemical shifts on pH for (**A**) azpy, (**B**) azpy-NMe_2, and (**C**) azpy-OH. The curves represent best fits to the Henderson-Hasselbalch equation giving pK_a^* values of 2.47 for azpy, 3.06 for azpy-OH and 4.60 for azpy-NMe_2.

3.3.4.2 Aqueous Solution Chemistry of Ruthenium complexes

The aqueous solution chemistry (with respect to hydrolysis and arene loss) of complexes **1-16** was studied at 310 K, typically over 24 h. In general, the complexes were found to undergo a mixture of slow hydrolysis and arene loss (to give products in which the three coordination sites originally occupied by the arene are now occupied by solvent). Exchange between species present in solution was slow on the NMR timescale; separate sets of peaks were observed for the chlorido, aqua and arene-loss species. For example, **Figure 3.13** shows the ^{1}H NMR spectrum recorded for complex 5 *ca.* 30 minutes after dissolution and after *ca.* 24 h at 310 K where

distinct peaks corresponding to the intact cation (A), the ruthenium complex after arene loss (C) and the hydrolysed product (D) are observed.

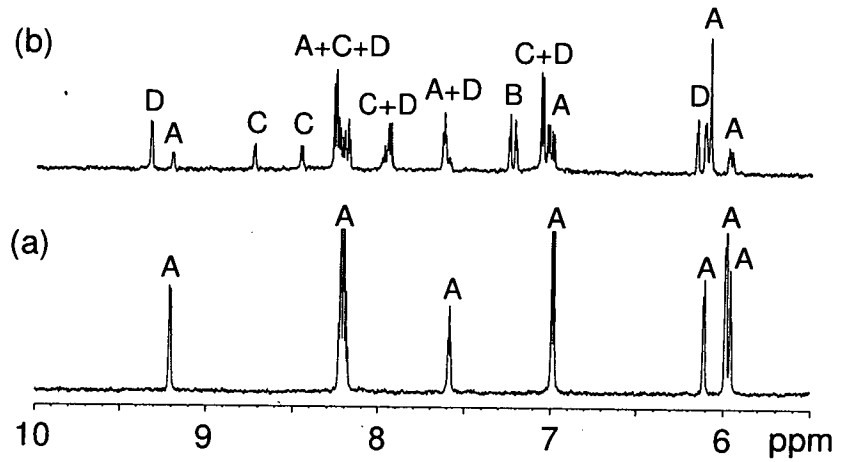

Figure 3.13. ^{1}H NMR spectrum of complex **5** in 90%H_2O/10%D_2O. (a) at 310 K 35 min after dissolution, (b) at 310 K 24 h after dissolution. Peak assignments: A intact chloride complex 1, B free p-cymene, C a ruthenium phenylazopyridine complex after arene loss, and D aquated 5. Assignment was aided by 2D-^{1}H TOCSY NMR techniques.

Hydrolysis was confirmed by adding excess NaCl (100 mM) and noting the decrease in the intensity of the aqua peaks as the water is replaced by chloride. Arene loss was inferred by the presence of resonances for free *p*-cym (*ca.* δ 7.23 (d of d)), free biphenyl (*ca.* δ 7.9 (d), 7.70 (t), 7.45 (t)), free benzene (*ca.* δ 7.27 (s)) or free tetrahydronapthalene (δ 7.15 (s)) in the aromatic region of the ^{1}H NMR spectra.

3.3.4.2.1 Speciation after 24 h incubation at 310 K

Initially the speciation after 24 h incubation at 310 K of an aqueous solution (90% H_2O/ 10 % D_2O) containing 100 μM ruthenium was determined (*vide infra,* summarised in **Figure 3.14**). The aqueous solution chemistry of the complexes was found to be dependent on the chelating azo ligand and more detailed solution chemistry of each set of complexes is given below.

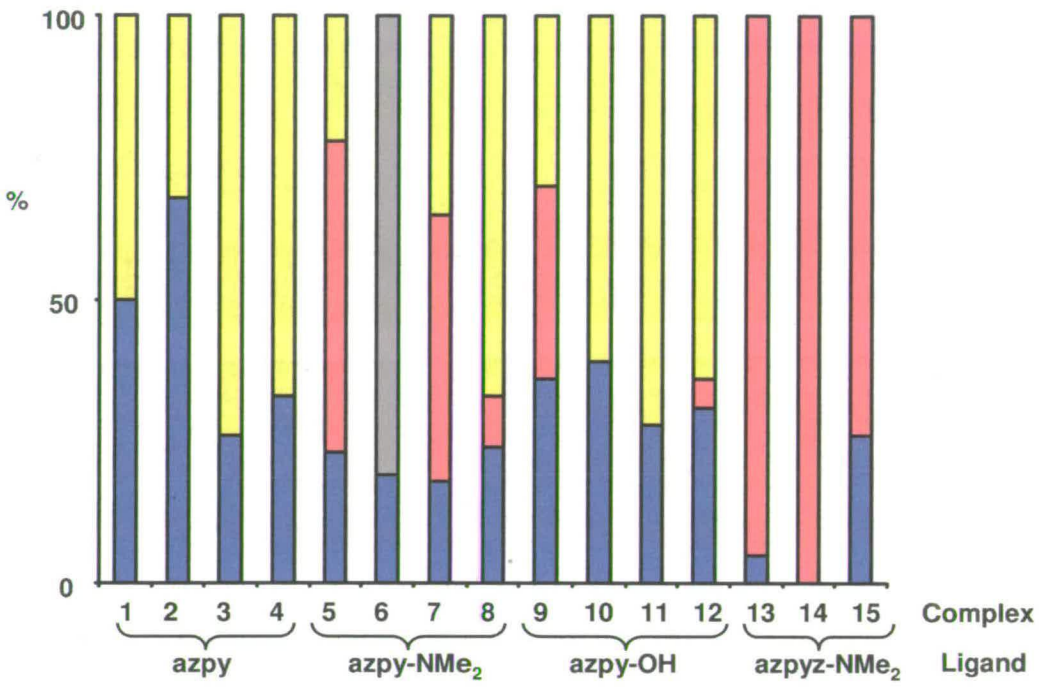

Figure 3.14. Speciation of ruthenium complexes **1-15** (100 μM) after 24 h incubation at 310 K in an aqueous solution. Complex **16** was too insoluble for this study. Key: Blue intact cation, Yellow arene loss species, Red hydrolysed species, Grey Undefined.

3.3.4.2.2 Complexes 13-15

Complexes **13-15**, containing the phenylazopyrazole ligand azpyz-NMe_2 were all found to only undergo hydrolysis of Ru-Cl in an aqueous solution (100 μM Ru, 310 K). The rates of hydrolysis were determined by UV-Vis spectroscopy (50 μM Ru, pH 2.3 95% H_2O, 5% MeOH) by first plotting a difference spectrum to find an optimum wavelength to use then following that optimum wavelength with time to derive kinetic data (see **Figure 3.15** for **13** as an example).

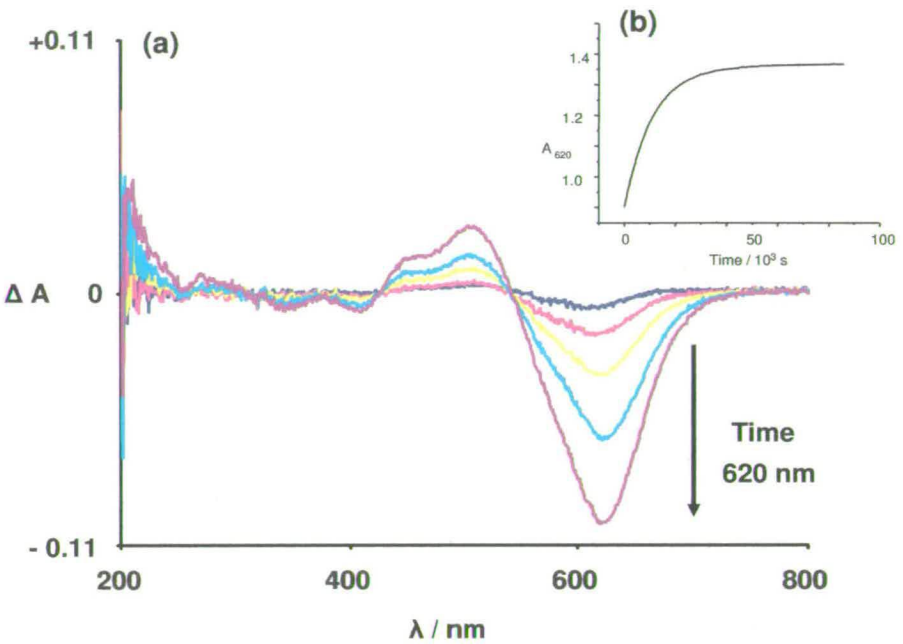

Figure 3.15. Hydrolysis studies of $[(\eta^6\text{-}p\text{-cym})Ru(azpyz\text{-}NMe_2)Cl]PF_6$, **13**: (a) the UV-Vis difference spectrum shows the biggest change in absorbance occurs at *ca.* 620 nm, and inset (b) the change in absorbance at 620 nm with time from which kinetic data were derived. $\Delta A = A_t - A_o$ where A_t = absorbance at time t and A_o = absorbance at t = *ca.* 20 s i.e. after dilution of methanol solutions in water.

The rates of hydrolysis, corresponding half lives and speciation after 24 h are shown in **Table 3.6.** A half-life for hydrolysis for **16** could also be determined although the shape of the curve suggested a second process occurring after hydrolysis, thought to be arene loss (observed in ^{1}H NMR, data not shown).

Table 3.6. Observed rate constants (k_{obs}), half lives of hydrolysis ($t_{1/2}$) (50 μM, 310 K) and speciation after 24 h dissolution (% intact, % hydrolysed) for complexes **13-16** (100 μM, 310 K). nd = not determined due to poor aqueous solubility

Complex	k_{obs} / h^{-1}	$t_{1/2}$ / h	% intact	% hydrolysed
13	0.3233 (± 0.0004)	2.14	5	95
14	0.3310 (± 0.0026)	2.09	0	100
15	0.2617 (± 0.0007)	2.67	26	74
16	0.2866 (± 0.0012)	2.42	nd	nd

Thus all four complexes appear to hydrolyse at similar rates with the half lives for hydrolysis rates in the following order thn < *p*-cym < bip < bz.

3.3.4.2.3 pKa* of aquated 13 (13A)

The pK_a* value for the aqua adduct of **13** was determined as 4.60, see **Figure 3.16**. This would mean at physiological pH (close to 7) the complex exists almost exclusively as the de-protonated form.

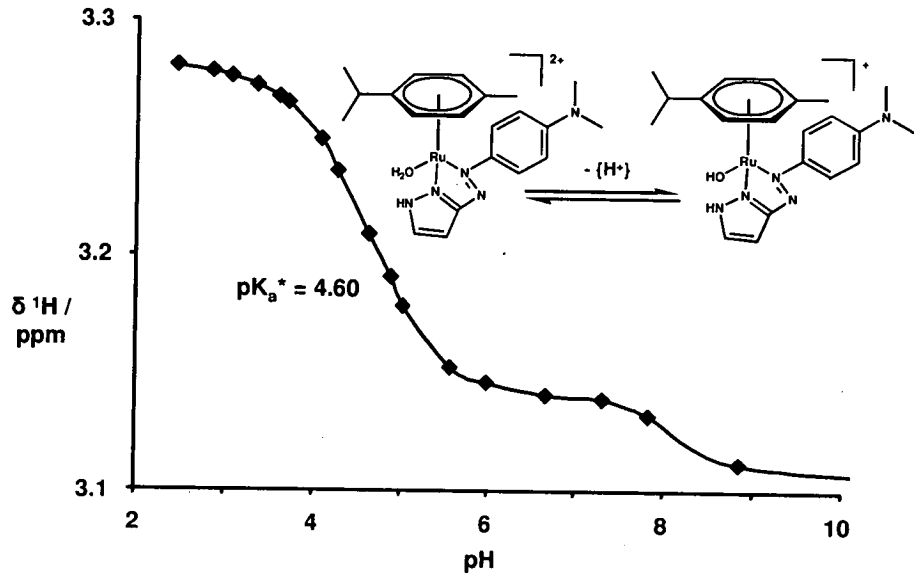

Figure 3.16. pH* titration showing the change in chemical shift for the H7 (NMe_2) protons with pH* for ruthenium complex $[(\eta^6\text{-}p\text{-cym})Ru(azpyz\text{-}NMe_2)OH_2/OH]^{2+/+}$ which gave a pK_a* value of the coordinated water as 4.60. The decrease in chemical shift at *ca.* pH 8 is thought to correspond to deprotonation of the pyrazole NH proton.

3.3.4.2.4 Reaction of 13A with 9-Ethyl guanine (9-EtG)

The reaction between **13A** and 1 mol equiv of 9-ethylguanine (9EtG) at pH* 7.46 (where the aqua adduct is predominantly in the hydroxo form (pK_a*=4.60 *vide supra*)) was followed by ^{1}H NMR spectroscopy. The coordination of 9-EtG to the ruthenium complex gave rise to new peaks in the ^{1}H NMR spectrum corresponding to the ruthenium-9-EtG complex. The reaction reached equilibrium after *ca.* 10 h when *ca.* 28% of the ruthenium was bound to 9-ethylguanine. **Figure 3.17** shows the variation in time in the amount of **13A** which reacted with 9-EtG.

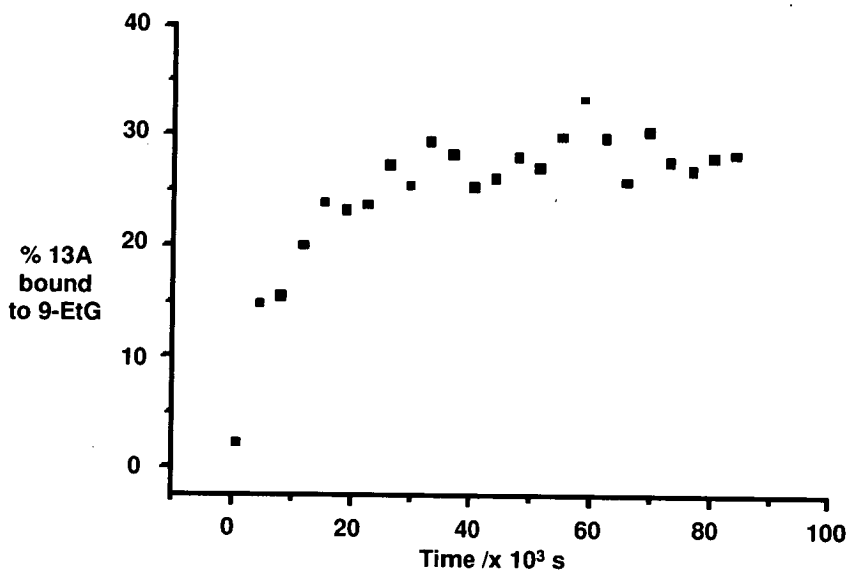

Figure 3.17. Variation in the percentage of $[(\eta^6\text{-}p\text{-cym})Ru(azpyz\text{-}NMe_2)(OH)]^+$ (**13A**) bound to 9-ethylguanine with time (as determined by integration of the Hb peak of the azpyz-NMe_2 ligand (see **Figure 3.2**)) during a 1 : 1 mol ratio (50 μM) reaction at pH* 7.46 , at 310 K followed over 24 h.

3.3.4.2.5 Complexes 1-4

Complexes **1-4**, all containing the phenylazopyridine ligand azpy, form one new species in aqueous solution which involves arene loss from the complex (hydrolysis of η^6 arene – ruthenium bonds). No species corresponding to simple hydrolysis of Ru-Cl was observed.

Figure 3.18 shows the HPLC chromatogram of a solution of complex $[(\eta^6\text{-}p\text{-cym})Ru(azpy)Cl]PF_6$, 1 (100 μM, 100% H_2O) after 24 h incubation at 310K. Two main peaks are present ((a) and b)) and these were thought to correspond to the arene loss species and the intact cation. Subsequent analysis of each fraction by ESI-MS revealed that peak (a) corresponds to the cation $[Ru(azpy)(MeCN)_3(TFA)]^+$ (TFA = trifluoroacetic acid) , ESI-MS: calcd for $RuC_{19}H_{18}N_6O_2F_3^+$ $[M^+]$ m/z 521.05, found 521.1 and peak (b) to $[(\eta^6\text{-}p\text{-cym})Ru(azpy)Cl]PF_6$, ESI-MS: calcd for $RuC_{21}H_{23}N_3Cl+$ $[M^+]$ m/z 454.07, found 456.2. Thus the ruthenium-bound arene and chloride are both lost from the phenylazopyridine complex.

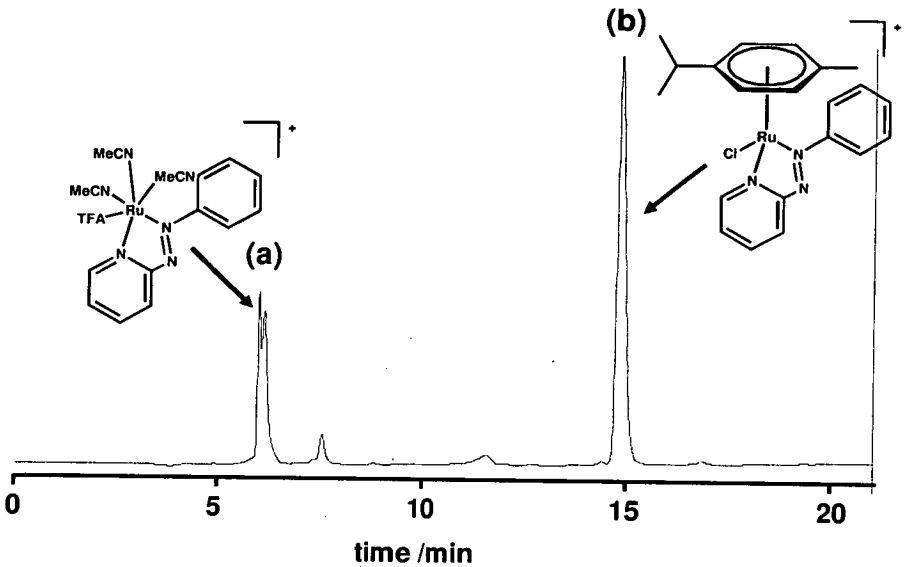

Figure 3.18. HPLC chromatogram (λ = 254 nm) for an aqueous solution of **1** after 24 incubation at 310 K. Gradient: 30% B (MeCN, 0.1% TFAH) to 90% over 30 minutes. Fractions were collected, freeze dried then re-dissolved in MeCN for ESI-MS analysis. Molecular structures show the assignment of the peaks based on ESI-MS analysis.

The rates and half-lives of arene loss, determined by UV-Vis spectroscopy, are listed in **Table 3.7** along with the speciation results after 24 h incubation at 310 K.

Table 3.7. Observed rate constants (k_{obs}), half lives of arene loss ($t_{1/2}$) and speciation after 24 h dissolution for complexes **1-4** (100 μM, 310 K).

Complex	k_{obs} (h^{-1})	$t_{1/2}$ (h)	% intact	% arene loss
1	0.0601 (±0.0004)	11.6	50	50
2	0.0576 (±0.001)	12.0	68	32
3	0.0381 (±0.004)	18.2	26	74
4	0.0782 (±0.007)	8.9	33	67

Thus the data show that arene lability follows the order bz > bip > *p*-cym > thn.

3.3.4.2.6 Complexes 5-12

These complexes, containing the phenylazopyridine ligands azpy-OH and azpy-NMe_2, were generally found to undergo a mixture of hydrolysis of both Ru-Cl and Ru-η^6-arene bonds. Approximate rate constants and half-lives were determined by plotting the decrease in the percentage of intact chloride complex with time. **Figure 3.19** shows the speciation over 24 h for complex $[(\eta^6\text{-}p\text{-cym})Ru(azpy\text{-}OH)Cl]PF_6$ (**9**) and the corresponding pseudo first order plot from which the rate constant and the half life was determined. The rates and half-lives of decomposition of the cation are listed in **Table 3.8** along with the speciation results after 24 h incubation (100 μM, 90% H_2O /10% D_2O, 310 K).

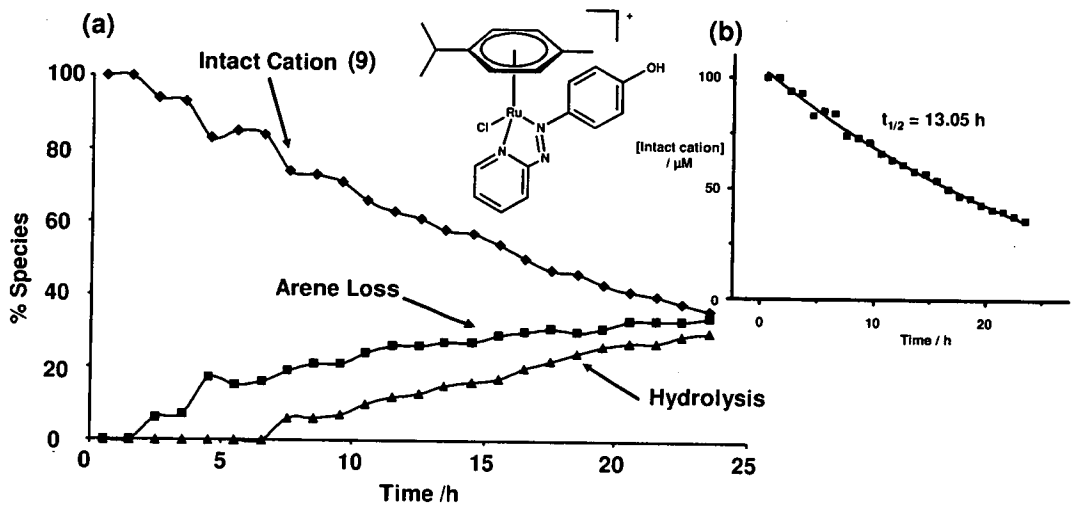

Figure 3.19. (a) Speciation distribution over 24 h for 100 μM solution of **9** as determined by the ratio of the integrals of the Ha proton resonance (see **Figure 3.2**) of the phenylazopyridine ligand in the different environments and (b) decay of the intact cation fitted to a first-order rate equation, giving a half-life of 13.05 h.

Table 3.8. Observed rate constants (k_{obs}), half-lives for decomposition of the intact cation ($t_{1/2}$) and speciation after 24 h dissolution (% intact, % hydrolysed, % arene loss) for complexes **5-12** (100 μM, 310 K). (nd = not determined).

Compound	k_{obs} / h^{-1}	$t_{1/2}$ / h	% intact	% hydrolysed	% arene loss
5	0.078 (± 0.014)	8.90	23	55	22
6	nd[a]	nd[a]	18	-	-
7	0.113 (± 0.009)	6.16	18	47	35
8	0.034 (± 0.007)	20.27	24	9	67
9	0.033 (± 0.006)	21.03	36	34	30
10	0.068 (± 0.003)	10.19	39	0	61
11	0.094 (± 0.004)	7.39	28	0	72
12	0.053 (± 0.007)	13.05	31	5	64

[a] the products of the reaction of complex **6** in were not observable by ^{1}H NMR.

3.3.4.2.7 pK_a* of Phenolic group in [(η^6-p-cym)Ru(azpy-OH)Cl]PF_6 (9).

A pK_a* value of 6.48 was determined for deprotonation of the phenol group of azpy-OH in complex **9** (**Figure 3.20**)

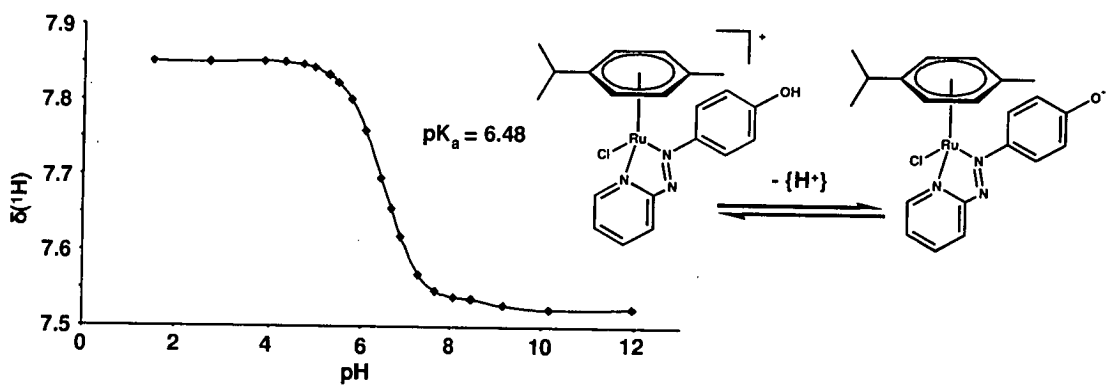

Figure 3.20. Variation of the ^{1}H NMR chemical shifts with pH* for complex **9**. The pK_a^* value was determined by fitting the data points to the Henderson-Hasselbalch equation, corresponding to a pK_a*of 6.48.

3.3.5 Cytotoxicity

The IC_{50} values for complexes **1-16** against the A2780 human ovarian and A549 human lung cancer cell lines are given in **Table 3.9**. All complexes appeared to be

soluble at the testing concentrations with the exception of complex **16** at 100 μM. However, none of the cells survived even at 50 μM of **16**.

Table 3.9. IC_{50} values for Ru^{II} arene complexes against the A2780 human ovarian and A549 human lung cancer cell lines and comparison with cisplatin

Complex	IC_{50} (μM)	
	A2780	**A549**
1	>100	>100
2	>100	>100
3	>100	>100
4	>100	>100
5	>100	>100
6	>100	>100
7	>100	>100
8	44	49
9	58	>100
10	34	63
11	>100	>100
12	18	56
13	18	41
14	57	>100
15	88	>100
16	24	32
cisplatin	5	5

None of the Ru^{II} arene complexes with the chelating azo ligand azpy (**1-4**) were cytotoxic to either cell line, and of the complexes containing azpy-NMe_2 (**5-8**), the bip complex **8** was cytotoxic in both the A2780 and A549 cell lines with IC_{50} values of *ca.* 45 μM. All the complexes containing the azpyz-NMe_2 (**13-16**) ligand exhibit cytotoxicity against the A2780 cancer cell line, the most potent being the *p*-cym and bip complexes, which also displayed good cytotoxicity in the A549 cell line. With the exception of the benzene complex **11**, all Ru complexes containing azpy-OH exhibited activity against the A2780 cancer cell line, with **10** and **12** also displaying moderate cytotoxicity against A549 cancer cells.

3.4 Discussion

The introduction of chelating azopyridine and azopyrazole ligands into chlorido Ru^{II} arene complexes has given rise to highly coloured complexes, which exhibit new properties in comparison with complexes containing diamines such as en as chelating ligands. In the literature there are several examples of ruthenium azpy complexes (*vide supra*), but there appear to be no reports of ruthenium complexes containing the chelated ligands azpy-NMe_2, azpy-OH or azpyz-NMe_2. Furthermore, to the best of my knowledge, this is the first example of azpyz-NMe_2 being used as a chelating ligand for any metal.

3.4.1 Structures of complexes.

The relatively long Ru –N(28) azo bonds in the X-ray crystal structures of azopyridine complexes **1**, **4**, and **5** can be ascribed to back-bonding competition for the ruthenium $4d^6$ electron density by the azopyridine and arene π-acceptor ligands. Such an effect has also been observed in the crystal structure of $[Ru(azpy)_3](PF_6)_2$.[12] Further evidence for such competition in complexes **1**, **4** and **5**, is the lengthening of the Ru-arene centroid distances by *ca.* 0.04Å compared to analogous ruthenium(II) arenes with ethylenediamine as the chelating ligand (a non-π acceptor) is also observed.

The phenyl-phenyl and phenyl-pyridyl π-π intermolecular interactions all fall within the commonly observed range for stacks of aromatic groups, with approximately parallel planes, separation distances of 3.3-3.8 Å and angles between the normal to one ring and the centroid vector of *ca.* 16-40°.[24] Polarisation of the phenyl ring of the ligand in **1** and **4** by the electron-withdrawing azo group is likely to enhance its ability to stack. Similarly, the π-electron deficiency of the pyridine ring in **4** is also likely to favour stacking.

The ability of the η^6-arene to stabilise Ru^{II} by π-acceptor interactions[25] is evident from the ^1H NMR resonances of the metal-coordinated η^6-arenes. These are shifted to a lower frequency due to increased electron density on the ring, compared with the uncoordinated arene.[26] It is noteworthy that the protons of the η^6-arenes in the azo compounds studied in this work are deshielded (resonance moved by between 0.2 - 0.6 ppm to a higher frequency) compared to the corresponding starting dimers [(η^6-

arene)$RuCl_2]_2$, i.e. are shifted to a higher frequency (deshielded). This is consistent with a reduced electron density at the ring upon chelation indicating that the π-accepting arene and π-accepting azo ligand are competing for Ru electron density.

3.4.2 Electronic Absorption Spectroscopy

The major differences in the UV-Vis spectra occur with changing the chelating ligand and these changes can be rationalised as follows. For the complexes containing phenylazopyridine, the introduction of electron-donating groups on to the phenyl ring (O^- in azpy-O^- and NMe_2 in azpy-NMe_2) decreases the π-acidity of the azo group[27] which causes an increase in the energy of the Ru^{II} $4d^6$ orbitals and results in a smaller energy gap between the Ru $4d^6$ bonding and azo π* orbitals. This is manifested in the spectrum as a progressive shift of the MLCT band to longer wavelengths with increased σ-donor strengths of the phenyl substituents on the ligand. The replacement of pyridine by pyrazole as a substituent results in a decrease in the wavelength of the MLCT, presumably the azopyrazole π* orbital must be at a higher energy.

3.4.3 Acidity of ligands

The pK_a* values of the (conjugate acids) of the pyridine nitrogens for the free azo ligands are 2.77 (azpy), 2.18 (azpy-OH) and 0.64 (azpy-NMe_2) pK_a units lower than for pyridine itself (5.24).[28] This is attributed to the electron-withdrawing effects of the azo group, which serves to reduce their basicity.[29] The presence of the NMe_2 and, to a lesser extent the OH substituent, on the phenyl ring increases the basicity of the pyridine nitrogen relative to azpy (H), due to electron donation by the dimethylamino/hydroxyl groups, which opposes the electron-withdrawing effect of the azo group on the pyridyl ring.[30] The relatively low pK_a* values for the pyridyl ligands suggests that they are poor σ-donors, compared with, for example ethylenediamine, pK_{a1} = 7.08 and pK_{a2} = 9.89.[28] Pyridine is a six-membered π-electron deficient ligand and, besides being a σ-donor, can also act as a π-acceptor towards Ru^{II}. The pyridine ring in azpy is expected to be a better π-acceptor than the pyridine ring in azpy-NMe_2 since it is more electron deficient. Thus overall, azpy would be expected to give rise to a higher positive charge on Ru^{II} / lower electron

density on Ru^{II}, compared to azpy-OH and azpy-NMe_2 since it is a weaker σ-donor and a stronger π-acceptor. Correlations between the substituents on pyridine rings and metal pyridine π-bonding have been discussed previously in the literature.[31, 32]

3.4.4 Aqueous Solution Chemistry.

The complexes studied undergo a combination of hydrolysis and arene loss in water. Reactions are slow, with half-lives of the order of hours at 310 K (body temperature). The rates of ligand substitution in hexa-coordinated Ru^{II} complexes are known to span about ten orders of magnitude.[33] The trend in rates correlates with the extent of back bonding[34] from moderately fast exchange for non π-acceptor ligands (e.g. $[Ru(H_2O)_6]^{2+}$) to very inert behaviour with π-acceptor ligands (e.g. $[Ru(MeCN)_6]^{2+}$). The inertness results from the high thermodynamic stability of the starting complex due to π back-bonding from Ru^{II} $4d^6$ to the π^* orbital of MeCN. Therefore the presence of both the arene and the azo ligand in the complexes studied here would be expected to give rise to more slowly reacting compounds.

3.4.4.1 Arene Loss

For complexes **1-4** (which undergo only arene loss) arene lability follows the order bz > bip > p-cym > thn. The presence of electron-donating alkyl groups on the bound arene strengthens the ruthenium-arene bond[35] and therefore thn and p-cym are expected to be less labile arenes than bz. For example, the amount of arene loss from $[(\eta^6\text{-bz})Ru(azpy)Cl]PF_6$ (**1**) is 74% after 24 h compared with 32% for $[(\eta^6\text{-thn})Ru(azpy)Cl]PF_6$ (**4**).Whilst the pendant phenyl ring in bip is electron withdrawing by inductive effects it is electron donating by resonance and this should make it a more labile arene (c.f. *p*-cym, thn).

In the literature, there are several examples of the photochemical displacement of an η^6 arene from Ru,[36, 37] but thermal displacement, especially under such mild conditions (low temperatures, aqueous solution), is uncommon, and most displacements occur in the presence of strong nucleophiles, these reactions still being relatively rare.[38] The observed loss of arene in aqueous solution can be rationalized by considering the nature of the bonding of an η^6 arene to Ru^{II}, which is strengthened by π-back donation from the ruthenium centre. In the azopyridine complexes, the

arene is less tightly bound to ruthenium due to competition with the azo ligand for π-electron density.

3.4.4.2 Hydrolysis and Arene Loss

The chloride complexes **5-8** and **9-12** containing the chelating azo ligands azpy-NMe_2 and azpy-OH tend to undergo a mixture of both hydrolysis and arene loss. There appears to be no correlation between the arene and the preference for arene loss vs. hydrolysis. However, complexes containing azpy-NMe_2 tend have a higher percentage of hydrolysed species compared with their azpy-OH analogues (for example compare $[(\eta^6\text{-}p\text{-cym})Ru(azpy\text{-}NMe_2)Cl]PF_6$ (**5**) 55% hydrolysis and $[(\eta^6\text{-}p\text{-cym})Ru(azpy\text{-}OH)Cl]PF_6$ 34% hydrolysis). The conjugate acid of the pyridine ring in the azpy-NMe_2 ligand has a higher pKa* than in the azpy-OH ligand and this should result in increased electron density at the ruthenium facilitating the substitution of chloride by water and disfavouring arene loss.

3.4.4.3 Hydrolysis Only

Complexes **13-16** all underwent hydrolysis, with no arene loss observed for **13-15**. The rates of hydrolysis followed the order thn ~ p-cym < bip < bz which is in line with the notion that alkyl substituents on the arene increase electron density at Ru and this make the Ru-Cl bond weaker (*vide supra*).

Thus there is a marked difference in aqueous solution chemistry between e.g. $[(\eta^6\text{-}p\text{-cym})Ru(azpy\text{-}NMe_2)Cl]PF_6$ (**5**) and $[(\eta^6\text{-}p\text{-cym})Ru(azpzy\text{-}NMe_2)Cl]PF_6$ (**13**) i.e. changing the chelating ligand from a phenylazopyridine to a phenylazopyrazole. Complex **13** undergoes more extensive and more rapid hydrolysis than **5** with no arene loss (**Table 3.7, Table 3.8**). Pyridine is a π-electron-deficient heterocycle, functioning as a σ-donor / π-acceptor ligand, whereas pyrazole is formally classed as a five membered π-electron rich heterocycle[39] and binds to metals primarily in a σ-donor fashion. The lack of π-back-bonding ability of pyrazole has been noted in the literature.[40] Thus phenylazopyrazole is a less efficient π-acceptor ligand, resulting in a subsequent increase in chloride lability and a decrease in arene lability.

The half-lives for aquation of the chlorido ethylenediamine ruthenium(II) arene complexes, $[(\eta^6\text{-dha})Ru(en)Cl]^+$, $[(\eta^6\text{-tha})Ru(en)Cl]^+$ and $[(\eta^6\text{-bip})Ru(en)Cl]^+$, (dha =

dihydroanthracene, tha = tetrahydroanthracene) have been reported to be 1.7-2.9 min at 310 K.[41] The hydrolysis of **13-16** under comparable conditions is more than two orders of magnitude slower, with half lives of 2.08-2.67 h.

It is well documented that the coordination of an η^6-arene to Ru^{II} increases the lability of the coordinated water in $[(\eta^6\text{-arene})Ru(OH_2)_3]^{2+}$ compared with $[Ru(OH_2)_6]^{2+}$ (by three orders of magnitude), and this phenomenon is ascribed to the differences in transition state properties and the strong trans-labilising effect of the aromatic ligand on the coordinated water.[26] The rate of aquation for these types of complexes, however, decreases by two orders of magnitude when two of the aqua ligands are replaced by the π-acceptor chelating ligand bipy, attributable to a smaller trans effect due to competition between the arene and bipy for Ru $4d^6$ electron density.[35] The presence of the π-acceptor azo ligand in **13** decreases the rate of hydrolysis compared with the ethylenediamine analogues.

3.4.4.4 Acidity of aquated complex 13 and 9-EtG binding

The interaction of Ru(II) arene complexes with DNA is thought to be important with respect to their observed cytotoxicity.[2, 5, 42] In aqueous solution, for example, $[(\eta^6\text{-bip})Ru(en)Cl]^+$ binds specifically to guanosine[4] and this reaction proceeds through the initial aquation of the chloride complex. The pK_a of the coordinated water of the aqua adduct $[(\eta^6\text{-bip})Ru(en)Cl]^+$ is 7.71,[41] which means that at physiological pH (close to 7) the complex exists mainly in the aqua form. The increased reactivity of $Ru\text{-}OH_2$ versus Ru-OH towards guanine bases has been reported previously for other Ru(II) arene complexes.[4]

In contrast, the pK_a* of the aqua adduct **13A** (4.60) is considerably lower. The high acidity of the coordinated water in **13A** is indicative of a low electron density at ruthenium since the acidity of a coordinated water molecule increases with decreasing charge density on the metal.[35] At physiological pH (*ca.* 7) the complex would exist predominantly in the more inert hydroxo form. Hence it is perhaps not surprising that it has a lowered affinity for DNA bases. After 24 h, only *ca.* 28% of 13A reacted with 9EtG to form $[(\eta^6\text{-}p\text{-cym})Ru(azpzy\text{-}NMe_2)(9EtG)]^+$.

3.4.4.5 pKa* of Phenol group in azpy-OH and complex 9

The pK_a* of the phenol group of azpy-OH in complex **9** (6.48) is 1.6 pK_a units lower than that in the free ligand. This suggests that electron density from the phenolate group is more readily delocalised when azpy-O^- is coordinated to Ru. At physiological pH (close to 7), the compound exists predominantly in the deprotonated form and so will bear no overall charge.

3.4.5 Cytotoxicity

None of the compounds containing the phenylazopyridine ligand azpy exhibited cytotoxicity against either A2780 human ovarian or A549 human lung cancer cells. With the ligands azpy-NMe_2 and azpy-OH, complexes **8**, **10** and **12** show cytotoxicity in both cell lines, as do complexes **13** and **16** containing the azpyz-NMe_2 ligand. The species responsible for the cytotoxicity could be the intact cation, the corresponding aqua/hydroxo complex or the Ru^{II} phenylazopyridine complex produced after arene loss, since the speciation over 24 h suggests that all three species could be present in varying amounts.

Intact cations might exert a cytotoxic effect by mechanisms which include modification of mitochondrial membrane permeability (as observed, for example, with lipophilic cations of Au(I) carbene complexes[43]) or DNA intercalation by the arene (when extended) or the azopyridine ligand. Recently the cytotoxicity of several isomers of $[Ru(azpy)_2(bipy)]^{2+}$ incapable of hydrolysis has been reported.[12] Anticancer activity has also recently been reported for the complex $[(\eta^6$-hmb)Ru(en)(SPh)$]^+$ (hmb = hexamethylbenzene) which does not undergo hydrolysis.[44]

Loss of the η^6-arene would create three potentially reactive sites on Ru^{II} for interaction with DNA or other bio-molecules. Arene loss followed by binding to a 14-mer oligonucleotide has been reported for the Ru^{II} arenes $[(\eta^6$-p-cym)Ru(pta)$Cl_2]$ and [(p-cym)Ru(pta-Me)Cl_2]Cl[45] (pta is 1,3,5-triaza-7-phosphatricyclo [3.3.1.1] decane).

The aquated phenylazopyridine complexes may bind to DNA bases by a mechanism similar to that proposed for analogous Ru^{II} arene complexes.[4] However, the pK_a value of the coordinated water in azo arene complexes is predicted to be low as the

metal is more electropositive. This might give rise to a lowered affinity for DNA. Whilst the phenylazopyrazole complexes **13-16** undergo hydrolysis (and no arene loss) **13** binds to 9EtG to a limited extent only.

3.5 Summary

A series of intensely coloured Ru^{II} arene complexes containing the chelating azo ligands azpy, azpy-NMe_2, azpyz-NMe_2 and azpy-OH has been synthesized and characterized by X-ray crystallography, ^1H NMR and UV-Vis spectroscopy. The η^6-arene in the pyridine complexes appears to be more labile than in Ru^{II} arene complexes containing chelated ligands such as ethylenediamine. Arene loss is attributable to the strong π-acceptor character of phenylazopyridine ligands, which effectively compete with the arene for π-back donation from the metal. There is evidence for this competition in the crystal structures, where Ru to arene-centroid distances are longer than in the corresponding en complexes, and in NMR spectra where ^1H NMR arene resonances are shifted to a higher frequency (lower field) upon chelation of phenylazo pyridine, compared with the corresponding starting dimers. For the *p*-cym complexes, hydrolysis was detected for **5** (azpy-NMe_2) and **9** (azpy-OH) but not for **1** (azpy). Thus hydrolysis is favoured by an increase in the electron density on ruthenium (increase in the pK_a of the pyridine, increase in electron density on Ru), but arene loss is still competitive. Complexes **13-15**, containing the azopyrazole ligand, hydrolyze fully and this can be rationalized by the inability of pyrazole compared to pyridine to act as a π-acceptor, so increasing the electron density on Ru further. This may also explain why no arene loss was detected for **13-15**: the arene experiences less competition for π-back donation. Several of these compounds exhibit cytotoxicity against both A2780 and A549 cancer cell lines and may have a novel mechanism of action compared to en Ru^{II} arenes.

3.6 References

[1] M. J. Clarke, *Coord. Chem. Rev.* **2003**, *236*, 209-233.

[2] R. E. Morris, R. E. Aird, P. d. S. Murdoch, H. Chen, J. Cummings, N. D. Hughes, S. Parsons, A. Parkin, G. Boyd, D. I. Jodrell, P. J. Sadler, *J. Med. Chem.* **2001**, *44*, 3616-3621.

[3] R. E. Aird, J. Cummings, A. A. Ritchie, M. Muir, R. E. Morris, H. Chen, P. J. Sadler, D. I. Jodrell, *Br. J. Cancer* **2002**, *86*, 1652-1657.

[4] H. Chen, J. A. Parkinson, R. E. Morris, P. J. Sadler, *J. Am. Chem. Soc.* **2003**, *125*, 173-186.

[5] O. Novakova, H. Chen, O. Vrana, A. Rodger, P. J. Sadler, V. Brabec, *Biochemistry* **2003**, *42*, 11544-11554.

[6] A. H. Velders, K. van der Schilden, A. C. G. Hotze, J. Reedijk, H. Kooijman, A. L. Spek, *Dalton Trans.* **2004**, 448-455.

[7] G. K. Lahiri, S. Bhattacharya, S. Goswami, A. Chakravorty, *J. Chem. Soc.; Dalton Trans.* **1990**, 561-565.

[8] R. A. Krause, K. Krause, *Inorg. Chem.* **1982**, *21*, 1714-1720.

[9] A. H. Velders, H. Kooijman, A. L. Spek, J. G. Haasnoot, D. De Vos, J. Reedijk, *Inorg. Chem.* **2000**, *39*, 2966-2967.

[10] C. G. Hotze Anna, M. Bacac, H. Velders Aldrik, A. J. Jansen Bart, H. Kooijman, L. Spek Anthony, G. Haasnoot Jaap, J. Reedijk, *J. Med. Chem.* **2003**, *46*, 1743-1750.

[11] C. G. Hotze Anna, E. Caspers Sabrine, D. de Vos, H. Kooijman, L. Spek Anthony, A. Flamigni, M. Bacac, G. Sava, G. Haasnoot Jaap, J. Reedijk, *J. Biol. Inorg. Chem.* **2004**, *9*, 354-364.

[12] A. C. G. Hotze, E. P. L. van der Geer, H. Kooijman, A. L. Spek, J. G. Haasnoot, J. Reedijk, *Eur. J. Inorg. Chem.* **2005**, 2648-2657.

[13] G. M. Sheldrick, SHELXS, University of Göttingen, Göttingen, Germany, **1997**.

[14] G. M. Sheldrick, SHELXL, University of Göttingen, Göttingen, Germany, **1997**.

[15] P. T. Beurskens, G. Beurskens, R. D. Gelder, S. Garcia-Granda, R. O. Gould, R. Israel, J. M. M. Smits, Cyrstallography Laboratory, University of Nijmegen, Nijmegen, The Netherlands, **1999**.

[16] P. W. Betteridge, J. R. Carruthers, R. I. Cooper, K. Prout, D. J. Watkin, *J. Appl. Crystallogr.* **2003**, *36*, 1487.

[17] R. A. Krause, K. Krause, *Inorg. Chem.* **1980**, *19*, 2600-2603.

[18] D. Betteridge, D. John, *Analyst* **1973**, *98*, 377-389.

[19] S. I. Suminov, *Zh. Org. Khim.* **1968**, *4*, 1864-1865.

[20] M. V. Gorelik, V. I. Lomzakova, *Zh. Org. Khim.* **1986**, *22*, 1054-1061.

[21] H. Chen, J. A. Parkinson, S. Parsons, R. A. Coxall, R. O. Gould, P. J. Sadler, *J. Am. Chem. Soc.* **2002**, *124*, 3064-3082.

[22] A. Seal, S. Ray, *Acta Crystallogr., Sect. C: Cryst. Struct. Commun.* **1984**, *C40*, 929-932.

[23] J. B. Lambert, H. F Shurvell, D. A Lightner, R. G Cooks, *Organic Structural Spectroscopy*, Prentice-Hall, Inc, New Jersey, **1998**.

[24] C. Janiak, *Dalton* **2000**, 3885-3896.

[25] M. A. Bennett, M. J. Byrnes, I. Kovacik, *J. Organomet. Chem.* **2004**, *689*, 4463-4474.

[26] M. Stebler-Roethlisberger, W. Hummel, P. A. Pittet, H. B. Buergi, A. Ludi, A. E. Merbach, *Inorg. Chem.* **1988**, *27*, 1358-1363.

[27] R. A. Krause, K. Krause, *Inorg. Chem.* **1984**, *23*, 2195-2198.

[28] L. S. S. Kotrly, *Handbook of Chemical Equilibria in Analytical Chemistry*, Ellis Horwood Ltd, Chicester, **1985**.

[29] M. N. Ackermann, W. G. Fairbrother, N. S. Amin, C. J. Deodene, C. M. Lamborg, P. T. Martin, *J. Organomet. Chem.* **1996**, *523*, 145-151.

[30] L. Pentimalli, *Tetrahedron* **1960**, *9*, 194-201.

[31] A. B. P. Lever, S. M. Nelson, T. M. Shepherd, *Inorg. Chem.* **1965**, *4*, 810-813.

[32] J. d. O. Cabral, H. C. A. King, S. M. Nelson, T. M. Shepherd, E. Koros, *J. Chem. Soc.* **1966**, 1348-1353.

[33] W. Luginbuehl, P. Zbinden, P. A. Pittet, T. Armbruster, H. B. Buergi, A. E. Merbach, A. Ludi, *Inorg. Chem.* **1991**, *30*, 2350-2355.

[34] I. Rapaport, L. Helm, A. E. Merbach, P. Bernhard, A. Ludi, *Inorg. Chem.* **1988**, *27*, 873-879.

[35] L. Dadci, H. Elias, U. Frey, A. Hoernig, U. Koelle, A. E. Merbach, H. Paulus, J. S. Schneider, *Inorg. Chem.* **1995**, *34*, 306-315.

[36] T. Karlen, A. Hauser, A. Ludi, *Inorg. Chem.* **1994**, *33*, 2213-2218.

[37] S. W. Magennis, A. Habtemariam, O. Novakova, J. B. Henry, S. Meier, S. Parsons, I. D. H. Oswald, V. Brabec, P. J. Sadler, *Inorg. Chem.* **2007**, *46*, 5059-5068.

[38] D. A. Freedman, D. E. Janzen, K. R. Mann, *Inorg. Chem.* **2001**, *40*, 6009-6016.

[39] A. P. Sadimenko, S. S. Basson, *Coord. Chem. Rev.* **1996**, *147*, 247-297.

[40] B. P. Sullivan, D. J. Salmon, T. J. Meyer, J. Peedin, *Inorg. Chem.* **1979**, *18*, 3369-3374.

[41] F. Wang, H. Chen, S. Parsons, I. D. H. Oswald, J. E. Davidson, P. J. Sadler, *Chem. Eur. J.* **2003**, *9*, 5810-5820.

[42] O. Novakova, J. Kasparkova, V. Bursova, C. Hofr, M. Vojtiskova, H. Chen, P. J. Sadler, V. Brabec, *Chem. Biol.* **2005**, *12*, 121-129.

[43] P. J. Barnard, M. V. Baker, S. J. Berners-Price, D. A. Day, *J. Inorg. Biochem.* **2004**, *98*, 1642-1647.

[44] F. Wang, A. Habtemariam, E. P. L. van der Geer, R. Fernandez, M. Melchart, R. J. Deeth, R. Aird, S. Guichard, F. P. A. Fabbiani, P. Lozano-Casal, I. D. H. Oswald, D. I. Jodrell, S. Parsons, P. J. Sadler, *Proc. Natl. Acad. Sci. U. S. A.* **2005**, *102*, 18269-18274.

[45] A. Dorcier, P. J. Dyson, C. Gossens, U. Rothlisberger, R. Scopelliti, I. Tavernelli, *Organometallics* **2005**, *24*, 2114-2123.

Chapter 4

Dinuclear Ruthenium(II) Arene Chlorido Azo Complexes

4.1 Introduction

There is currently an increased interest in the design of dinuclear metal based complexes as anticancer agents since these complexes can exhibit different properties to their mononuclear analogues. For example the dinuclear platinum complex [{*trans*-$PtCl(NH_3)_2$}$_2${μ-($NH_2(CH_2)_6NH_2$)}]$(NO_3)_2$ (BBR3005), which contains two mono-functional platinum centres with a hexane-1,6-diamine linker was found to be active against cisplatin – resistant cell lines.[1, 2] This work led to the synthesis of the trinuclear complex [{*trans*-$PtCl(NH_3)_2$}$_2$ μ-(trans-$Pt(NH_3)_2(H_2N(CH_2)_6$-$NH_2)_2$)]$_4^+$ (BBR3464).[3] The third (central) platinum unit is unreactive, but it improves the solubility and the electrostatic interactions of the drug with DNA. This complex forms intrastrand adducts with DNA but, unlike cisplatin, it does not bend the DNA and the Pt-DNA adducts are not recognised by High Mobility Group (HMG) Proteins, again different to cisplatin.[4] This could be the reason for the ability of the complexes to overcome cisplatin resistance. BBR3464 has undergone phase two clinical trials as an anticancer drug.[5, 6]

Dinuclear ruthenium arene complexes have also been synthesised in our laboratory and their DNA interactions compared with the mononuclear analogues. For example consider the dinuclear ruthenium arene complex [($(\eta^6$-bip)RuCl(en))$_2$-$(CH_2)_6]^{2+}$ (**Figure 4.1**), in which two Ru^{II} arene centres are linked with a flexible chain contains four stereogenic centres (Ru, N, N, Ru) which gives rise to ten potential configurations.[7]

Interestingly, in aqueous solution the complex exists as a diastereomeric mixture of AA/AB/BB (A = ($R^*_{Ru}R^*_N$), B = ($S^*_{Ru}R^*_N$)) as 67.7:24.0:8.3 %. Analysis of the complex after reaction with 9-EtG (to give [($(\eta^6$-bip)Ru (N7-9-EtG)(en))$_2$-$(CH_2)_6]^{2+}$) showed that the B ($S^*_{Ru}R^*_N$) configuration is highly favoured (*ca.* 95%) due to steric interactions Thus upon reacting with 9-EtG, a facile epimerization at Ru / N centres occurs to allow dynamic switching between these configurations leading to a high selectivity in the formation of G adducts.[7]

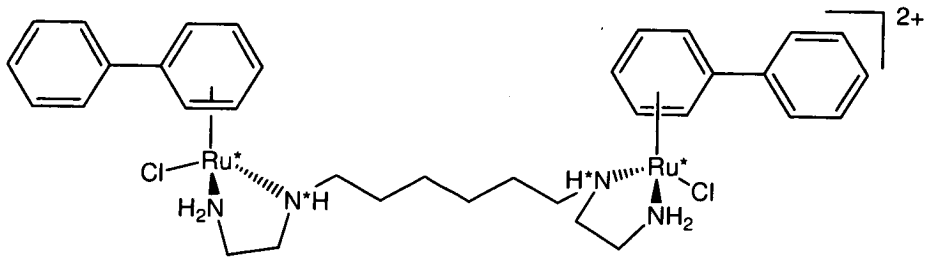

Figure 4.1. Dinuclear complex $[((\eta^6\text{-bip})\text{Ru Cl (en)})_2\text{-}(CH_2)_6](PF_6)_2$. The four chiral centres are marked *.

This dinuclear complex inhibits RNA synthesis more effectively[7] than the mononuclear complex $[(\eta^6\text{-bip})\text{Ru(en)Cl}]^+$.[8] Binding to CT-DNA induced a positive CD band centered at 370-380 nm suggesting intercalation of the extended phenyl ring into DNA (as observed previously for the mononuclear complexes).[8] The dinuclear complex was able to unwind pSp73KB DNA with an angle of 31° which was over double than that of $[(\eta^6\text{-bip})\text{Ru(en)Cl}]^+$ (14°) suggesting that cross-linking of DNA and perturbation of DNA structure by the two pendant phenyl rings is important. Evidence of cross-linking came from the observations (a) that the efficiency of the interstrand cross-linking on a 213-bp EcoRI fragment of pSP73 randomly modified by the dinuclear complex was similar to that of the known DNA cross-linker cisplatin, and (b) a site-specifically ruthenated 20-mer formed a 1,3-GG interstrand cross-link (20% frequency) and 1,2-GG and 1,2-GTG cross-links were also detected.

In this Chapter, two $\{(\eta^6\text{-arene})\text{RuCl}\}^+$sub units are linked together via dinuclear bis-phenylazopyridine chelating ligands to create potentially bifunctional ruthenium-arene complexes. The molecular structures of the complexes studied in this chapter are shown in **Figure 4.2.** In the examples discussed above, the linkers were flexible alkyl chains but here the ligands have a higher degree of rigidity due to the linker consisting of aryl residues. The cytotoxicity, solution chemistry and electrochemistry are investigated and compared to the corresponding mono-nuclear analogues.

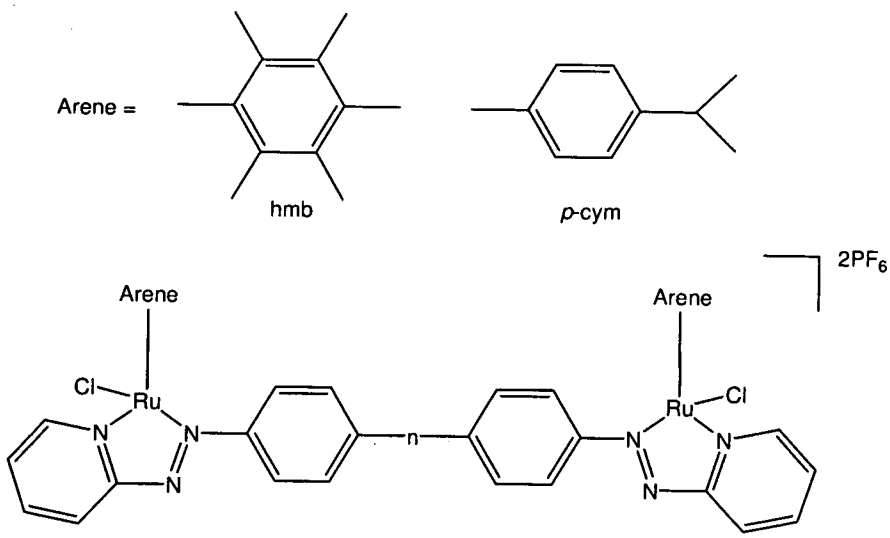

Compound	Arene	n
17	*p*-cym	CH_2
18	hmb	CH_2
19	*p*-cym	O
20	hmb	O
21	*p*-cym	CO
22	hmb	CO

Figure 4.2 Structure of the dinuclear ruthenium(II) arene complexes synthesised and studied in this Chapter.

4.2 Experimental

4.2.1 Materials

2-Aminopyridine, N-chlorosuccinimide, dimethylsulfide, m-chloroperbenzoic acid, ammonium hexafluorophosphate (NH_4PF_6), 4,4'-methylenedianiline, 5-(diethoxyphosphoryl)-5-methyl-1-pyrroline-N-oxide (DEPMPO) and glacial acetic acid were purchased from Sigma-Aldrich and used as received. Ethanol and methanol were dried over Mg/I_2 or anhydrous quality was used (Sigma-Aldrich) and methylene chloride was either dried over P_2O_5 (1 % w/v) or anhydrous quality was

used (Fisher). All other organic solvents and reagents were obtained from commercial suppliers and used as received.

4.2.2 Synthesis

4.2.2.1 *S,S*-dimethyl-*N*-(2-pyridyl)sulfilimine

To a solution of 2-aminopyridine (9.4 g, 0.1 mol) and dimethyl sulfide (6.8 g, 0.11 mol) in dry methylene chloride (100 mL), a solution of *N*-chlorosuccinimide (13.4 g, 0.1 mol) in dry methylene chloride (250 mL) was added dropwise over a period of 1 h, while the temperature was maintained at 253 K (dry ice / ethanol). After the addition was complete, the reaction mixture was stirred at 253 K for 1 h and then for an additional hour at room temperature. A solution of sodium methoxide (9.5 g, 0.17 mol) in methanol (75 mL) was added and the mixture is stirred for 10 min. Subsequently, water (150 mL) was added and stirring continued for 4 h. The layers were separated and the aqueous layer was extracted three times with dry methylene chloride (50 mL). The combined organic extracts were washed with water, dried over $MgSO_4$ and evaporated to give thick yellow-brown oil which solidified upon being cooled. The product was purified by re-crystallisation from diethyl ether giving a cream-coloured solid. Yield: 3.95 g (25% after re-crystallisation) ^{1}H NMR ($CDCl_3$): δ 7.95 (d, 1H), 7.30 (m, 1H), 6.65 (d, 1H), 6.45 (t, 1H), 2.75 (s, 6H). ESI MS: Calcd for $C_7H_{10}N_2S^+$ [M^+] m/z 154.1, found 155.1.

4.2.2.2 2-Nitrosopyridine

To a solution of *m*-chlorobenzoic acid (3.5 g, 0.023 mol) in dry methylene chloride (100 mL), cooled to 273 K, a solution of *S,S*-dimethyl-*N*-(2-pyridyl)sulfilimine (1.95 g, 0.013 mol) in dry methylene chloride (20 mL) was added at once. The mixture was stirred at 273 K for 90 min, dimethyl sulfide (0.6 g, 9.6 mmol) was added, and stirring continued for additional 30 min. A saturated aqueous solution of sodium carbonate (100 mL) was added to the reaction mixture, the layers were separated, and the green organic layer was washed with water and dried over $MgSO_4$. Evaporation of the dried extracts gave a light tan solid which was stored in a freezer. Yield: 0.67 g (48%) ^{1}H NMR (($CDCl_2$)$_2$, 398 K): δ 8.80 (d, 1H), 8.10 (t, 1H), 7.70 (t, 1H), 7.20 (d, 1H). ESI MS: Calcd for $C_5H_4N_2O^+$ [M^+] m/z 109.0, found 109.9.

4.2.2.3 2,2'-[methylenebis(4,1-phenyleneazo)]bis-pyridine (CH_2-(azpy)$_2$)

2-Nitrosopyridine (25 mg, 0.231 mmol) was dissolved in dry methylene chloride (10 mL). 4,4'-Methylenedianiline (23 mg, 0.012 mmol) dissolved in dry methylene chloride (2 mL) and glacial acetic acid (1 drop) were added and the orange solution was stirred at room temperature overnight, while shielded from light. The solution was evaporated to dryness to provide an orange-red coloured solid. The product was purified by column chromatography using silica and 95% methylene chloride/ 5% methanol as eluting solvent, collecting the first orange-coloured fraction. Yield: 4.0 mg (93%) (Found: C, 71.14; H, 5.28; N, 20.12. Calcd for $C_{23}H_{18}N_6$: C, 73.00; H, 4.79; N, 22.21) ^{1}H NMR ($CDCl_3$): δ 8.75 (d, 2H), 8.05 (d, 4H), 7.90 (t, 2H), 7.85 (d, 2H), 7.40 (t, 4H), 7.35 (d, 4H), 4.20 (s, 2H). ESI MS: Calcd for $C_{23}H_{18}N_6^+$ [M+H$^+$] m/z 379.4, found 379.1.

4.2.2.4 2,2'-[oxybis(4,1-phenyleneazo)]bis-pyridine (O-(azpy)$_2$)

2-Nitrosopyridine (0.40 g 3.71 mmol) was dissolved in dry methylene chloride (160 mL). 4-4'-Diaminodiphenylether (0.37 g 1.93mmol) dissolved in dry methylene chloride (30 mL) and glacial acetic acid (3 drops) were added. The orange solution was stirred at room temperature overnight shielded from the light. The solution was evaporated leaving an orange / red oil. The product was purified by column chromatography using silica and 95% methylene chloride/ 5% methanol as eluting solvent, collecting the first orange-coloured fraction as an oil. The oil was subsequently washed with ether to extract an orange solid which was dried under vacuum. Yield: 0.28 g (40%) ^{1}H NMR ($CDCl_3$): δ 8.76 (d, 2H), 8.13 (d, 4H), 7.93 (t, 2H), 7.85 (d, 2H), 7.42 (t, 2H), 7.24 (d, 4H). ESI MS: calculated for $C_{22}H_{16}N_6O^+$ [M$^+$] m/z 380.4, found 380.87

4.2.2.5 2,2'-[carbonylbis(4,1-phenyleneazo)]bis-pyridine (CO-(azpy)$_2$)

2-Nitrosopyridine (0.70 g 6.48 mmol) was dissolved in dry methylene chloride (250 mL). 4-4'-diaminobenzophenone (0.68 g 3.24 mmol) dissolved in dry methylene chloride (50 mL) and glacial acetic acid (3 drops) were added. The green solution was stirred at room temperature for 48h shielded from the light. The reaction mixture was filtered to remove any un-reacted solid and subsequently any remaining solvents

evaporated off leaving an orange / red oil. The oil was washed with a mixture of methanol and ether leaving an orange solid. The product was purified by column chromatography using silica and 95% methylene chloride/ 5% methanol as eluting solvent, collecting the first orange coloured fraction was collected as an oil. This was washed with ether leaving an orange solid. Yield: 0.11 g (9%) ^{1}H NMR (DMSO): δ 8.81 (d, 2H), 8.17 (d, 4H), 8.14 (t, 2H), 8.10 (d, 4H), 7.86 (d, 2H) 7.68 (t, 2H). ESI MS calculated for $C_{23}H_{16}N_6O^+$ [M^+] m/z 392.4, experimental value 392.82.

4.2.2.6 [(η^6-*p*-cym)$_2$ Ru_2(CH_2-(azpy)$_2$)Cl_2] (PF_6)$_2$ (17)

The ligand (CH_2-(azpy)$_2$) (25 mg, 0.065 mmol) dissolved in methanol (10 mL) was added dropwise to a solution of the ruthenium dimer [(η^6-*p*-cymene)$RuCl_2$]$_2$ (40 mg, 0.065 mmol) in methanol (15 mL). The solution immediately changed colour from orange to brown while stirring at room temperature. After stirring for 2 h, the volume of solvent was reduced and NH_4PF_6 (107 mg, 0.65 mol) was added. The brown precipitate, obtained after storage in a freezer for 1 h, was filtered off, washed with diethyl ether, and dried overnight *in vacuo*. The brown solid was recrystallised from methanol. Yield: 68 mg (87% before recrystallisation). (Found: C, 42.11; H, 3.88; N, 7.11. Calcd for $Ru_2Cl_2C_{43}H_{46}N_6P_2F_{12}$: C, 42.69; H, 3.83; N, 6.95). ^{1}H NMR (CD_3OD): δ 9.45 (d, 2H), 8.75 (d, 2H), 8.40 (t, 2H), 8.15 (d, 4H), 7.85 (t, 2H), 7.65 (d, 4H), 6.30 (d, 4H), 6.00 (m, 2H), 5.95 (s, 2H), 4.40 (s, 2H), 2.45 (sept, 2H), 2.25 (s, 6H), 0.95 (m, 12H). ESI MS: Calcd for $Ru_2C_{43}H_{46}N_6Cl_2$ [M^{2+}] m/z 461.1, found 460.0.*

4.2.2.7 [(η^6-hmb)$_2$ Ru_2(CH_2-(azpy)$_2$)Cl_2] (PF_6)$_2$ (18)

The ligand (CH_2-(azpy)$_2$) (27 mg, 0.070 mmol) dissolved in methanol (10 mL) was added drop-wise to a solution of the ruthenium dimer [(η^6-hmb)$RuCl_2$]$_2$ (47 mg, 0.070 mmol) in methanol (15 mL). The solution immediately changed colour from orange to red/brown while stirring at room temperature. After stirring for 2 h, NH_4PF_6 (115 mg, 0.70 mol) was added. The brown precipitate, obtained after storage

* The determined masses are ca. one Dalton short of the theoretical mass. The reason for this anomaly is currently unknown. However, this mass spectrometric technique has been shown to produce artefacts in Ruthenium(II) arene complexes by modification of the structure and hence mass, see for example W. H. Ang, E. Daldini, C. Scolaro, R. Scopelliti, L. Juillerat-Jeannerat, P. J. Dyson, Inorg. Chem, 2006, 45, 9006-9013.

in a freezer for 1 h, was filtered off, washed with diethyl ether, and dried overnight *in vacuo*. Attempt to recrystallise from methanol resulted in decomposition of the complex and so the product was purified by passing through a Sephadex LH-20 column (Amersham Biosciences) with methanol as the elutent. Yield: 29 mg (87% before recrystallisation). (Found: C,44.56; H, 4.42; N, 6.46. Calcd for $Ru_2Cl_2C_{47}H_{54}N_6P_2F_{12}$: C, 44.59; H, 4.30; N, 6.64 %). ^{1}H NMR ($(CD_3)_2CO$): δ 9.12 (d, 2H), 8.80 (d, 2H), 8.50 (t, 2H), 8.08-8.02 (m, 5H), 7.82 (d, 4H), 4.52 (s, 2H), 2.11 (s, 36H). ESI MS: Calcd for $Ru_2C_{47}H_{54}N_6Cl_2$ [M^{2+}] m/z 489.1, found. 487.5.*

4.2.2.8 [(η^6-*p*-cym)$_2$ Ru$_2$(O-(azpy))Cl$_2$] (PF$_6$)$_2$ (19)

The ligand (O-(azpy)$_2$) (40 mg 0.105 mmol) dissolved in dry methanol (10 mL) was added drop-wise to a solution of the ruthenium dimer [(η^6-*p*-cym)$RuCl_2$]$_2$ (63 mg 0.105 mmol in dry methanol (20 mL). The solution immediately changed colour from orange to red / brown. The mixture was left to stir at room temperature for 2 h and was shielded from light. After this, the volume of solvent was reduced and ten equivalents of NH_4PF_6 (171 mg 1.05 mmol) was added. The solution was left in a freezer overnight after which a red / brown precipitate was collected. This was washed with methanol and then ether and allowed to dry in air. Yield: 35.9 mg (28%). (Found: C, 41.75; H, 3.67; N, 6.83. Calcd for $Ru_2Cl_2C_{42}H_{44}N_6OP_2F_{12}$: C, 41.63; H, 3.66; N, 6.94 %). ^{1}H NMR ($(CD_3)_2SO$): δ 9.67 (d, 2H), 8.92 (d, 2H), 8.55 (t, 2H), 8.32 (d, 4H), 8.04 (t, 2H), 7.61 (d, 4H), 6.58 (d, 4H), 6.29 (d, 4H), 2.48 (m, 2H), 2.26 (s, 6H), 0.94 (d, 12H). ESI MS calculated for $Ru_2C_{42}H_{44}N_6Cl_2O$ [M^{2+}] m/z 462.1, found 460.7.*

4.2.2.9 [(η^6-hmb)$_2$ Ru$_2$(O-(azpy))Cl$_2$] (PF$_6$)$_2$ (20)

The ligand O-(azpy)$_2$ (40 mg 0.105 mmol) dissolved in dry methanol (10 mL) was added dropwise to a solution of the ruthenium dimer [(η^6-hmb)$RuCl_2$]$_2$ (70 mg 0.105 mmol in dry methanol (20 mL). The solution immediately changed colour from orange to red / brown. The mixture was left to stir at room temperature for 2 h and was shielded from light. After this, the volume of solvent was reduced and ten equivalents of NH_4PF_6 (171 mg 1.05 mmol) was added. The solution was left in a freezer overnight after which a red / brown precipitate was collected. This was

washed with ether and allowed to dry in air. The red / brown solid was then recrystallised from methanol. Yield: 93 mg (77% before recrystallisation). ^{1}H NMR ($(CD_3)_2SO$): δ 9.02 (d, 2H), 8.89 (d, 2H), 8.49 (t, 2H), 8.07 (d, 4H), 8.02 (t, 2H), 7.62 (d, 4H), 2.018 (s, 36H). ESI MS calculated for $Ru_2C_{46}H_{52}N_6OCl_2$ [M^{2+}] m/z 490.1, found 489.8.

4.2.2.10 [(η^6-*p*-cym)$_2$ Ru$_2$(CO-(azpy))Cl$_2$] (PF$_6$)$_2$ (21)

The ligand CO-(azpy)$_2$ (59 mg 0.151 mmol),dissolved in dry methanol (10 mL) was added drop-wise to a solution of the ruthenium dimer [(η^6-*p*-cym)$RuCl_2$]$_2$ (88 mg 0.151 mmol) in dry methanol (20 mL). The solution immediately changed colour from orange to deep red/orange. The mixture was left to stir at room temperature for 2 h and was shielded from light. After this, the volume of solvent was reduced and ten equivalents of NH_4PF_6 (246 mg 1.50 mmol) was added. The solution was left in a freezer overnight after which a deep red was collected. This was washed with ether and allowed to dry in air. Yield: 73 mg (40.4%). (Found: C, 42.94; H, 3.12; N, 6.77. Calcd for $Ru_2Cl_2C_{43}H_{44}N_6OP_2F_{12}$: C, 42.20; H, 3.62; N, 6.87 %). ^{1}H NMR ($(CD_3)_2SO$): δ 9.73 (d, 2H), 9.03 (d, 2H), 8.59 (t, 2H), 8.37 (d, 4H), 8.26 (d, 4H), 8.10 (t, 2H), 6.63 (d, 4H), 6.31 (d, 4H), 2.27 (s, 6H), 1.22 (m, 2H), 0.98 (d, 12H). ESI MS calculated for $Ru_2C_{43}H_{44}N_6OCl_2$ [M^{2+}] m/z 468.1, found 466.8.*

4.2.2.11 [(η^6-*p*-hmb)$_2$ Ru$_2$(CO$_2$-(azpy))Cl$_2$] (PF$_6$)$_2$ (22)

The ligand CO-(azpy)$_2$ (59 mg 0.151 mmol), dissolved in dry methanol (10 mL) was added drop-wise to a solution of the ruthenium dimer [(η^6-hmb)$RuCl_2$]$_2$ (101 mg 0.151 mmol in dry methanol (20 mL). The solution immediately changed colour from orange to deep purple/red. The mixture was left to stir at room temperature for 2 h and was shielded from light. After this, the volume of solvent was reduced and ten equivalents of NH_4PF_6 (166 mg 1.02 mmol) was added. The solution was left in a freezer overnight after which a red was collected. This was washed with ether and allowed to dry in air. Yield: 78 mg (41.1%). (Found: C, 44.00; H, 3.99; N, 5.73. Calcd for $Ru_2Cl_2C_{47}H_{52}N_6OP_2F_{12}$: C, 44.10; H, 4.09; N, 6.57) ^{1}H NMR ($(CD_3)_2SO$): δ 9.07 (d, 2H), 8.98 (t, 2H), 8.53 (t, 2H), 8.28 (d, 4H), 8.11 (d, 4H), 8.07 (d, 2H), 1.98 (s, 36H). ESI MS calculated for $RuC_{47}H_{52}N_6OCl_2$ [M^{2+}] m/z 496.1, found 495.9.

4.2.3 Methods

4.2.3.1 Electron Paramagnetic Resonance (EPR) Spectroscopy

An EPR spectrum of complex **22** was obtained with the help of Dr Paul Murray (The University of Edinburgh). The spectrum was acquired using a Bruker ER200D spectrometer at 233 K in DMF by electrochemical reduction of the sample at *ca.* -0.5 V (vs Ag/AgCl electrode).

4.2.3.2 Aqueous Solution Chemistry

Complexes were dissolved in $(CD_3)_2CO$ and diluted with D_2O (pre-warmed to 310 K) to give a final concentration of 100 μM ruthenium complex (95% D_2O, 5% acetone-d_6). The pH* of the samples were measured and the ^1H NMR spectra were recorded at selected time intervals over a 24 h time period. The measured pH* values were 6.90 (**17**), 7.70 (**18**), 7.16 (**19**), 6.43 (**20**), 6.77 (**21**) and 5.88 (**22**).

4.2.3.3 Phosphorus-31 Spin Trap Experiment

DEPMPO (0.01M) was dissolved in degassed 90% H_2O/ 10% D_2O containing 0.2 M phosphate buffer pH 6.99 (filtered through Chelex 100 to remove iron) and 2 mM DTPA. Care was taken to ensure minimum light exposure. Complex **21** (0.3 M in $(CD_3)_2CO$) was added to give 0.075 M DEPMPO: 0.075 M **21** (25% $(CD_3)_2CO$), and in the positive control (0.075 M $H_2O_2/FeSO_4$) and the blank control $(CD_3)_2CO$ was added to the same volume. ^{31}P NMR spectra were recorded at 310 K.

4.3 Results

Six dinuclear Ru^{II} arene complexes containing bis-phenylazopyridine ligands have been synthesised and their cytotoxicity towards the A2780 human ovarian and A549 human lung cancer lines has been evaluated. Their aqueous solution chemistry has been investigated at low (μM) concentrations and two of the complexes have been further characterised by cyclic voltammetry and one complex also by EPR spectroscopy.

4.3.1 Synthesis and Characterisation

4.3.1.1 Chelating bis-phenylazopyridine ligands

The chelating ligands used and their hydrogen labelling schemes are shown in **Figure 4.3.**

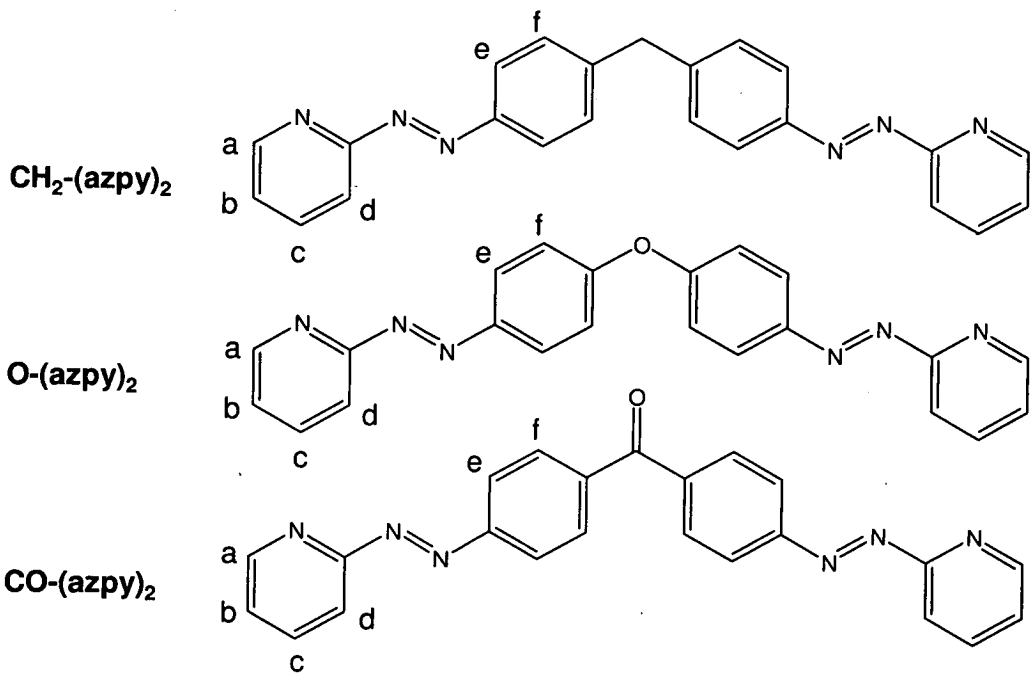

Figure 4.3. Chelating bis-phenylazopyridine ligands synthesised in this work along with their hydrogen numbering schemes.

The synthesis of these ligands firstly involved the synthesis of the nitrosopyridine precursor.

4.3.1.1.1 Nitrosopyridine

The reaction scheme for the synthesis of 2-nitrosopyridine is shown in **Figure 4.4.**

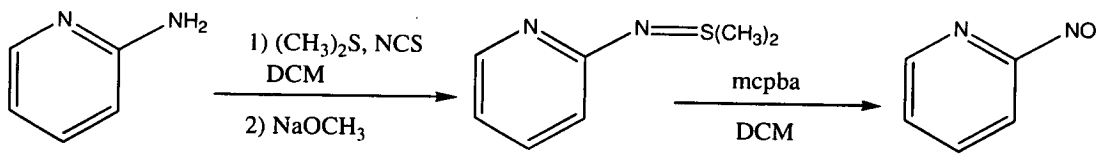

Figure 4.4. Reaction scheme for the formation of 2-nitrosopyridine

The first step involves conversion to *S,S*-dimethyl-*N*-(2-pyridyl)sulfilimine with dimethylsulfide and NCS and this sulfimine derivative is converted to the corresponding heterocyclic nitroso compound by oxidation with a slight excess of *m*-chloroperbenzoic acid in a second step. The 2-nitrosopyridine was obtained in a moderate yield and appeared to be light green in solution and tan-coloured in the solid state when stored at lower temperatures in a freezer.

Previous reports suggested that 2-nitrosopyridine exists as a temperature dependent monomer-dimer equilibrium in solution (**Figure 4.5**).[9]

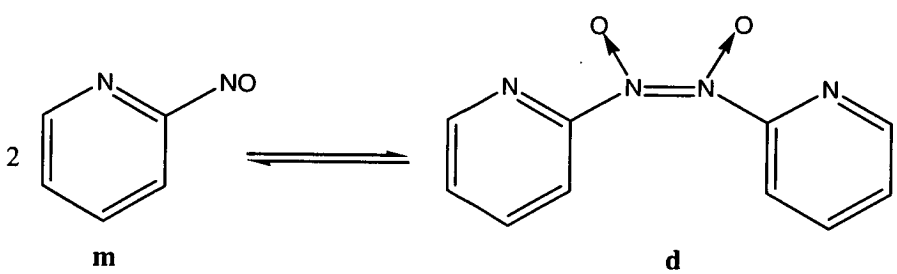

Figure 4.5. Temperature-dependent solution state equilibrium of 2-nitrosopyridine; m = monomer, d = dimer.

^{1}H NMR studies on 2-nitrosopyridine at different temperatures confirmed the presence of this monomer-dimer equilibrium (**Figure 4.6**); the room temperature ^{1}H NMR spectrum (298 K) of 2-nitrosopyridine in $(CD_2Cl_2)_2$ comprised eight signals of approximately equal intensity. Heating the solution increased the amount of monomer present since the solution equilibria of aromatic *C*-nitroso compounds

favours monomeric species on heating,[10] hence the major set of signals in the spectra at higher temperatures was attributed to the monomeric species.

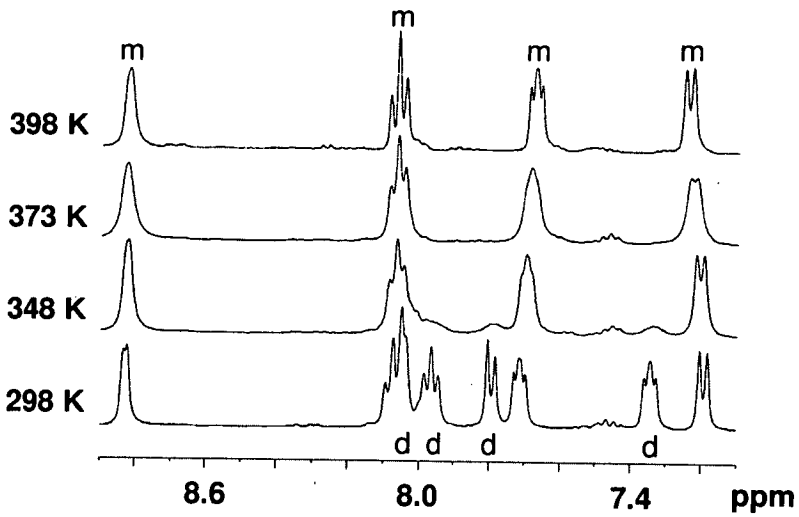

Figure 4.6. Variable temperature ^{1}H NMR spectra of 2-nitrosopyridine in $(CDCl_2)_2$ solution, showing the effect of temperature on the monomer-dimer equilibrium; m = monomer, d = dimer.

The nitrosopyridine was found to be unstable upon contact with water and reactions with it had to be carried out under anhydrous conditions. The reaction of nitrosopyridine in water at room temperature irreversibly forms 1-(2-pyridyl)-2(1H)-pyridone.[11]

4.3.1.1.2 Chelating Bis-Phenylazopyridine Ligands

The chelating ligands were all synthesised by the reaction of nitrosopyridine and the desired functionalised diamine in an acid-induced condensation reaction (**Figure 4.7**).

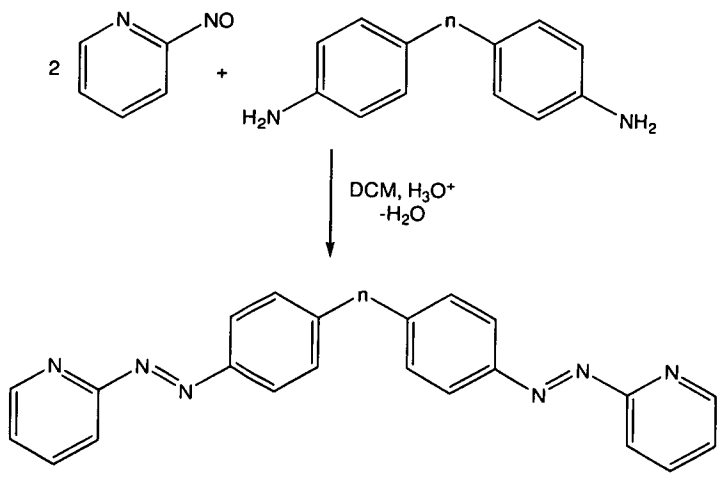

Figure 4.7. Reaction scheme for the formation of bis-azpy dinuclear chelating ligands. n = CH_2, O, CO.

All ligands were purified by column chromatography but some small impurities still remained. The ligands were subsequently used without any further purification.

4.3.2 Dinuclear Ru^{II} arene chloride bis-complexes

The complexes were synthesised by a similar route to the mononuclear analogues (**Chapter 3**) via the chloride-bridged dimers. **Figure 4.2** (p 113) shows the dinuclear complexes studied in this Chapter. All complexes were characterised by ^{1}H NMR, ESI-MS and CHN analysis.

4.3.3 Characterisation by ^{1}H NMR

Because each ruthenium centre is chiral, due to the unsymmetrical nature of the chelating phenylazopyridine ligand, there exists the possibility of two sets of diastereoisomers (RR, SS and RS, SR) which may give rise to two distinct sets of peaks in the ^{1}H NMR spectrum. Indeed it was found that the complexes existed as a mixture of diastereoisomers. For example, **Figure 4.8** shows the high frequency region of the 2D-^{1}H TOCSY NMR spectrum of complex $[(\eta^6\text{-hmb})_2\ Ru_2(CO\text{-}(azpy))Cl_2]\ (PF_6)_2$ (**22**) in $(CD_3)_2CO$.

In the first diastereoisomer (which is arbitrarily assigned A), the two phenyl rings that are linked by the carbonyl unit have equivalent proton resonances (H_e^A, H_f^A) whereas in the second diastereoisomer (assigned as B) these two rings appear separately (H_e^B, H_f^B and $H_e^{B'}$, $H_f^{B'}$) and one set ($H_e^{B'}$, $H_f^{B'}$) are shifted significantly

to a lower frequency. In both sets of diastereoisomers, the peaks corresponding to the protons on the pyridine ring have very similar chemical shifts.

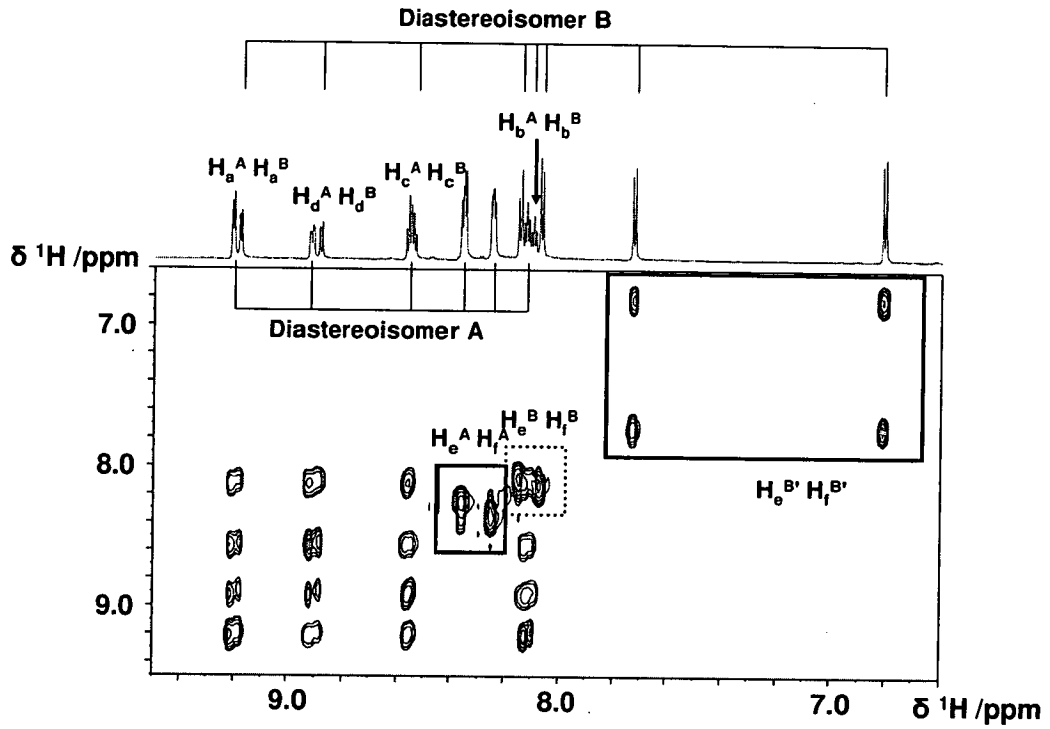

Figure 4.8. 2D-^{1}H TOCSY NMR (high frequency region, $((CD_3)_2CO)$ showing the different spin systems present in the diastereomeric mixture of complex **22**. For atom numbering system please refer to **Figure 4.3.**

Diastereoisomers usually have different chemical properties, which can allow them to be separated. For example, throughout the purification of $[(\eta^6\text{-hmb})_2\ Ru_2(O\text{-}(azpy))Cl_2](PF_6)_2$ (**20**) by recrystallisation, diastereoisomer A preferentially crystallised (**Figure 4.9**).

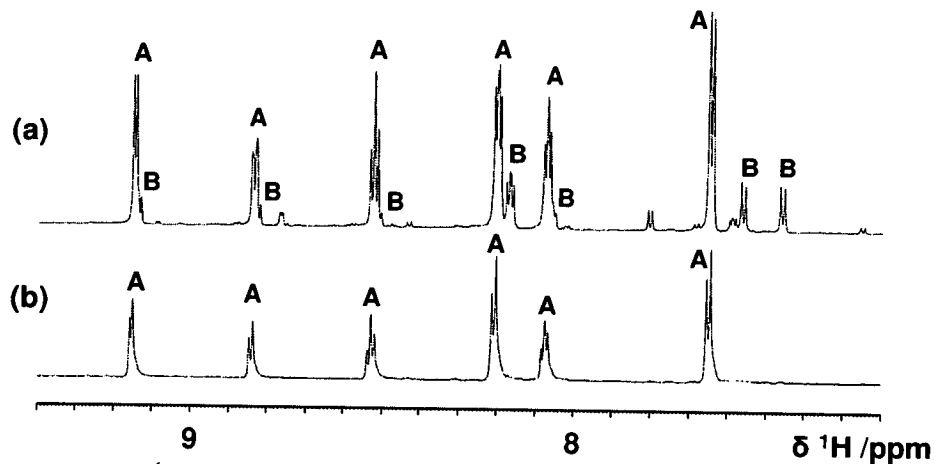

Figure 4.9. ^{1}H NMR ($(CD_3)_2CO$) showing (a) the crude product of **20** and (b) complex **20** after recrystallisation with preferential crystallisation of isomer A.

Table 4.1 shows the percentage of isomers A and B present for the six dinuclear complexes studied in this Chapter. In all cases the A isomer is preferred. However, the percentage of B isomer increases as the arene is changed from *p*-cym to hmb and as the ligand is changed from O-(azpy)$_2$, to CH_2-(azpy)$_2$ to CO-(azpy)$_2$. Interestingly, neither heating the NMR solution, diluting it, nor leaving it over time caused any change in the speciation (data not shown) suggesting that, at least in acetone, the isomers are not readily interconverted. Furthermore, immediate dissolution in 95% D_2O / 5% $(CD_3)_2CO$ showed the same percentage of isomers, indicating that the diastereomeric ratio is unaffected by solvent.

Table 4.1. Percentage of diastereoisomers A and B present in dinuclear ruthenium complexes. Brackets indicates the speciation before purification.

Complex	Diastereoisomer A (%)	Diastereoisomer B (%)
17	100 (78)	0 (12)
18	88 (57)	12 (43)
19	100	0
20	100 (70)	0 (30)
21	75	25
22	58	42

4.3.4 Aqueous Solution Chemistry

The aqueous solution chemistry was studied at 100 μM Ru-dimer, over 24 h at 310 K as these conditions mimicked the concentration, exposure time and temperature used in the cell tests. All complexes appeared to undergo decomposition in water since all ^{1}H resonances corresponding to the starting material broadened and disappeared/decreased in intensity over time. No new peaks appeared in the spectra except those corresponding to free p-cymene or hmb in aqueous solution, the intensity of which also decreased with time. Furthermore the colour of the solution changed to near colourless over the 24 h. **Figure 4.10**, **Figure 4.11** and **Figure 4.12** show the ^{1}H NMR spectra recorded initially after dissolution (after *ca.* 15 minutes) and after incubation at 310 K for *ca.* 24 h for complexes **17** and **18**, **19** and **20** and **21** and **22**, respectively.

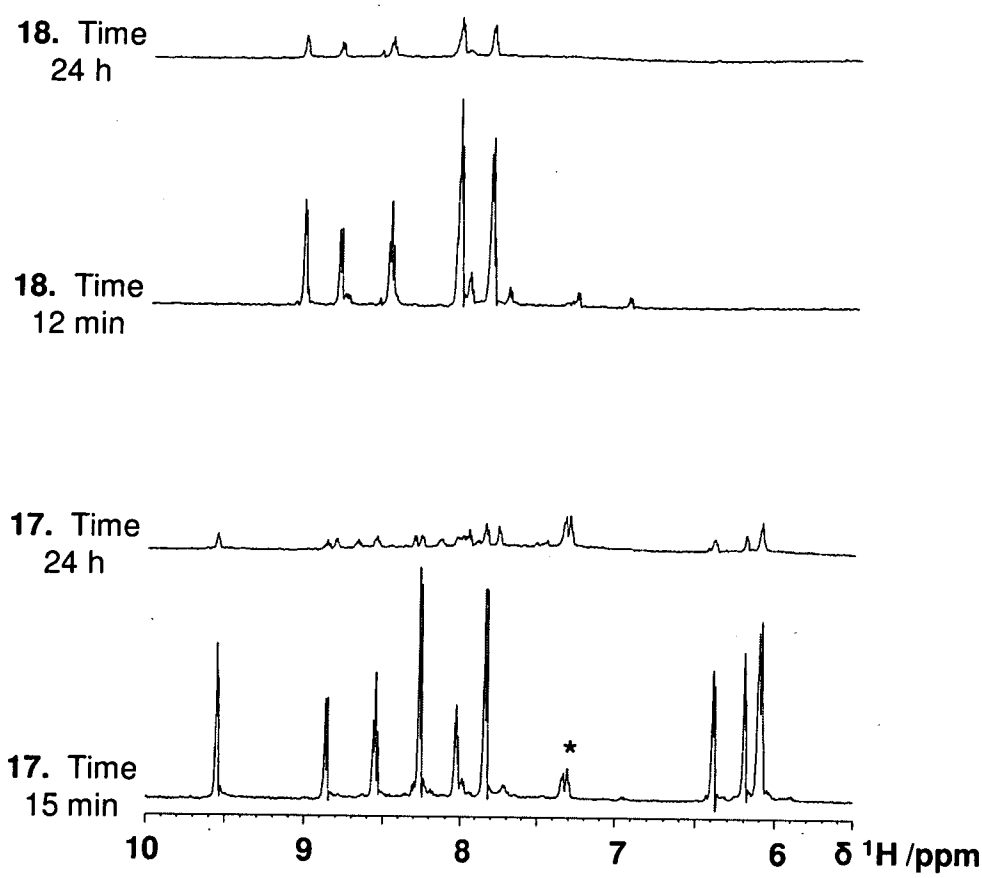

Figure 4.10. ^{1}H NMR spectra (100 μM, 95% D_2O / 5% acetone–d_6) of complexes $[(\eta^6\text{-}p\text{-cym})_2\ Ru_2(CH_2\text{-}(azpy)_2)Cl_2]\ (PF_6)_2$ (**17**) and $[(\eta^6\text{-hmb})_2\ Ru_2(CH_2\text{-}(azpy)_2)Cl_2]\ (PF_6)_2$ (**18**) recorded soon after dissolution and after 24 h at 310 K. The peaks for the starting complexes significantly decrease in intensity over time. The peak labelled with an asterisk (*) is assignable to free p-cymene in aqueous solution.

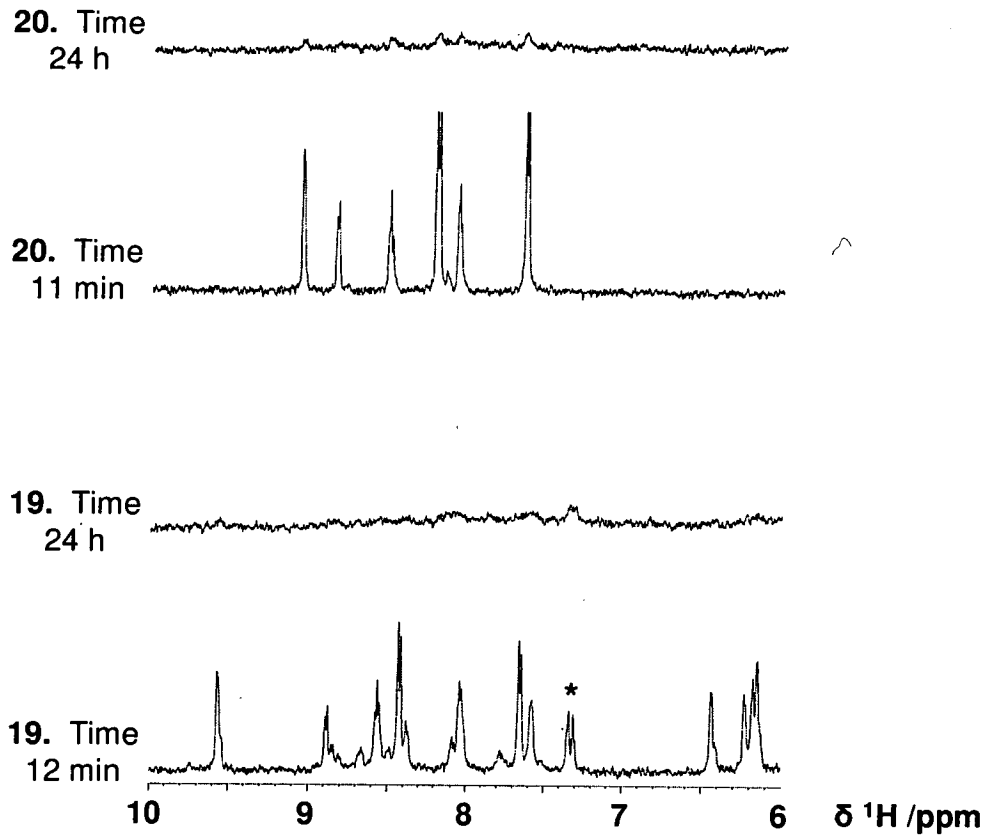

Figure 4.11. ^{1}H NMR spectra (100 μM, 95% D_2O / 5% acetone–d_6) of complexes $[(\eta^6\text{-}p\text{-cym})_2\ Ru_2(O\text{-}(azpy)_2)Cl_2]\ (PF_6)_2$ **(19)** and $[(\eta^6\text{-hmb})_2\ Ru_2(O\text{-}(azpy)_2)Cl_2]\ (PF_6)_2$ **(20)** recorded soon after dissolution and after 24 h at 310 K. The peaks for the starting complexes decrease in intensity significantly over time. The peak labelled with an asterisk (*) is assignable to free *p*-cymene in aqueous solution.

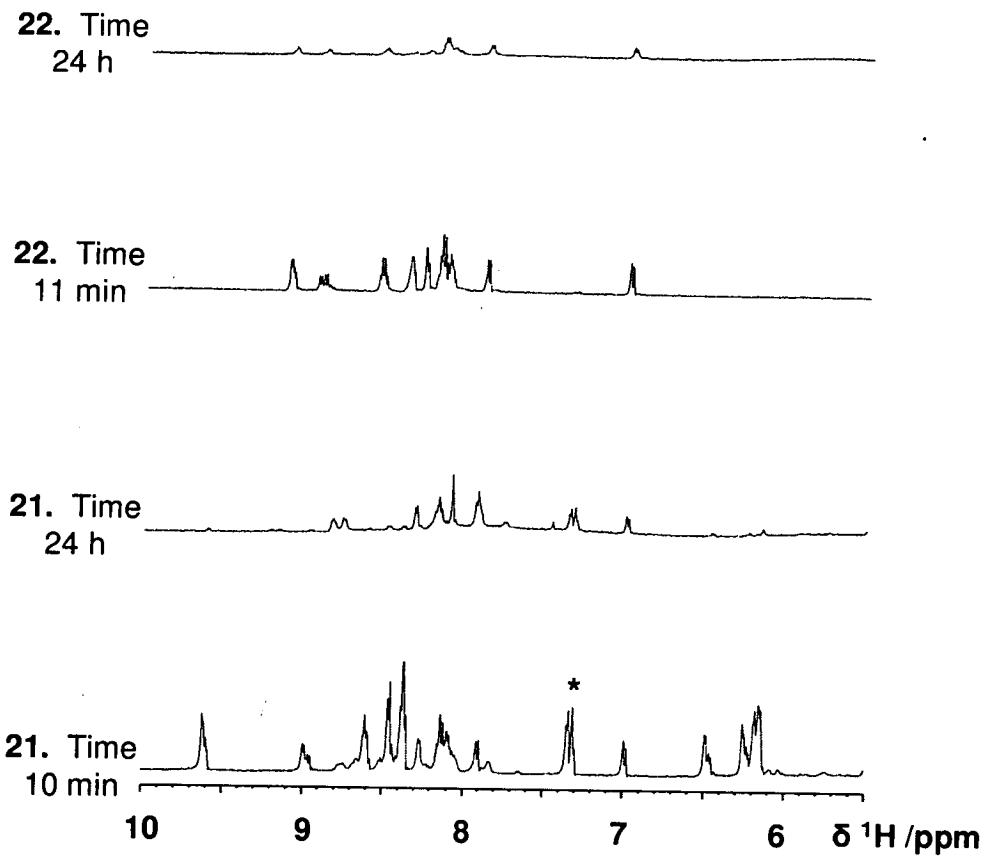

Figure 4.12. ^{1}H NMR spectra (100 μM, 95% D_2O / 5% acetone–d_6) of complexes $[(\eta^6\text{-}p\text{-cym})_2\ Ru_2(CO\text{-}(azpy)_2)Cl_2]\ (PF_6)_2$ (**21**) and $[(\eta^6\text{-hmb})_2\ Ru_2(CO\text{-}(azpy)_2)Cl_2]\ (PF_6)_2$ (**22**) recorded immediately after dissolution and after 24 h at 310 K. The peaks for the starting complexes decrease in intensity significantly over time. The peak labelled with an asterisk (*) is assignable to free *p*-cymene in aqueous solution

The absence of well defined product peaks suggested that a simple hydrolysis of Ru-Cl and /or Ru-arene bonds was not occurring since this should give rise to peaks in the ^{1}H NMR spectra, such as those observed for the corresponding mononuclear complexes (see Chapter 3). The disappearance and broadening of peaks with time, and the decrease in intensity of the peak corresponding to free *p*-cymene in aqueous solution suggested that either an insoluble product was forming (which would not be observable by ^{1}H NMR) or that radicals were forming (peaks for paramagnetic species can often be observed in NMR spectra, but the peaks are generally broader

and shifted). No observable precipitate was formed, although it must be remembered that the concentrations used were low (100 μM) and so precipitate may not be observable, even if present.

4.3.5 Cyclic Voltammetry

The electrochemical properties of complexes 21 and 22 were studied by cyclic voltammetry and differential pulse polarography. Both complexes displayed two electrochemical oxidations at *ca.* 1.08 and 1.30 V (vs. Ag/AgCl). On the reductive sweep, multiple reductions were observed up to the solvent cut off (*ca.* -2 V) and these can be seen most clearly from the differential pulse polarogram (**Figure 4.13**).

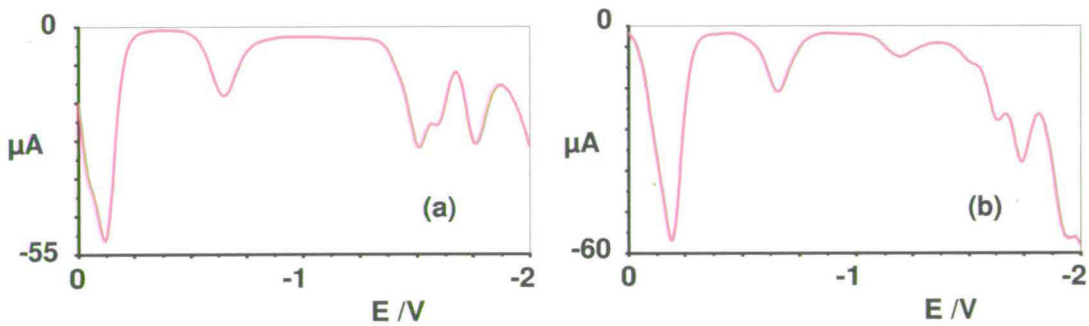

Figure 4.13. Differential pulse polarograms for (a) complex **21** and (b) complex **22** recorded in 0.1 M $TBABF_4$ in DMF from 0 to -2 V showing multiple reductions occurring.

The first two reductions were studied in more detail since these reductions occur at more biologically relevant potentials

4.3.5.1 First Electrochemical Reduction

Figure 4.14 shows the first electrochemical reduction recorded at different scan rates. The first electrochemical reduction occurs at $E_{1/2}$ = -0.06 V (complex **21**) and $E_{1/2}$ = 0.14 V (complex **22**).

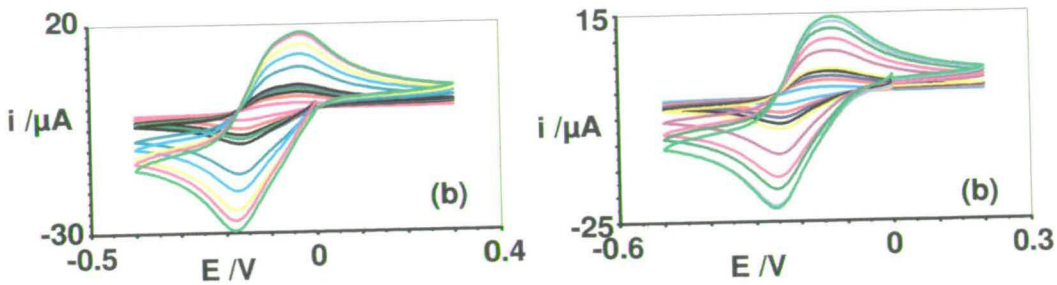

Figure 4.14. The variation of the first electrochemical reduction for (a) complex **21** (0 → -0.4 → 0.3 V) and (b) complex **22** (0 → -0.5 → 0.2 V) with scan rates (0.01-1 V/s) at ambient temperature.

For complex **21** this reduction is not fully reversible whereas for **22**, essentially it is. Diagnostic tests for a fully reversible reduction include the following.[12]

(a) A plot of the peak current density (aniodic and cathodic) versus the square root of the scan rate should give a straight line that passes through the origin whereas for a quasi-reversible system the current density increases with the square root of the scan rate but is not directly proportional to it. **Figure 4.15** shows the plots obtained for the cathodic current density and **Figure 4.16** shows the plots obtained for the aniodic current density. It can be seen that for complex **22** the goodness-of-fit (R^2 value) is much better than for **21** suggesting a higher degree of reversibility.

(b) $|I_p^A/I_p^C|=1$. For complex **22**, the average value (for all different scan rates) obtained was 1.052 whereas for complex **21** the average value was only 0.72.

(c) E_p is independent of the scan rate for a fully-reversible system. In both cases there was found to be some variation in the peak potential. However, for complex **22** this variation was much less than for complex 21; the average E_p values were **22**: 0.076 V (±0.004), **21**: 0.064 (± 0.063).

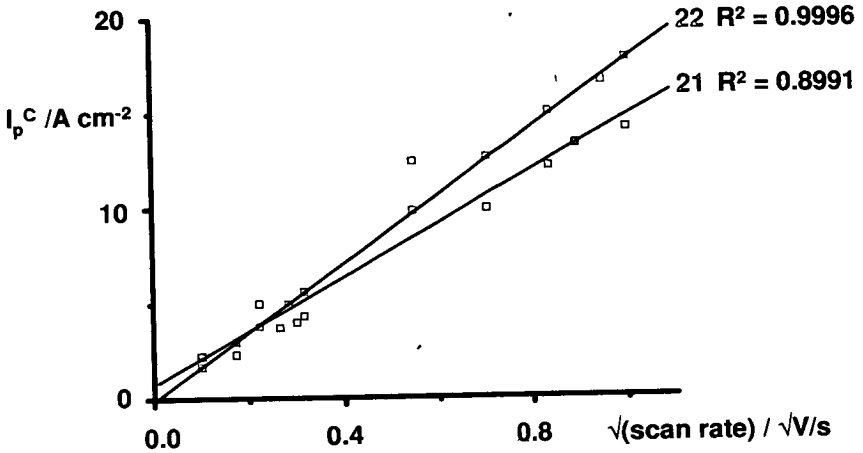

Figure 4.15. Straight line fits (though origin) for the variation of the cathodic peak current density with the square root of the scan rate for the cyclic voltammograms of complexes **21** and **22**. The goodness of fit (R^2) values are given.

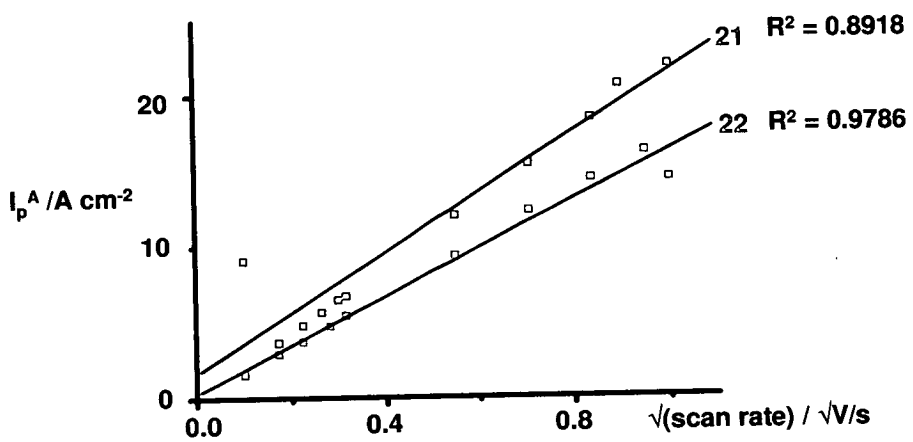

Figure 4.16. Straight line fits (through origin) for the variation of the aniodic peak current density with the square root of the scan rate for the cyclic voltammograms of complexes **21** and **22**. The goodness of fit (R^2) values are given.

The reductions are one-electron reductions, ΔE_p = 0.070 V (**22**), 0.1 Vs^{-1} (ferrocene ΔE_p = 0.067 V) and the reduction is likely to correspond to addition of an electron into the ligands' π^* antibonding orbital centred on the azo moiety, in accordance with literature assignments for other ruthenium(II) phenylazopyridine complexes.[13-16]

4.3.5.2 Second Electrochemical Reduction

Figure 4.17 shows the electrochemical response as the complexes are taken through both the first and second electrochemical reductions at varying scan rates. The second reduction occurs at E_{red} = -0.64 V (complex **21**) and E_{red} = -0.70 V (complex **22**). On the basis of similar peak heights to the first reduction, this reduction is assigned as a one-electron reduction too.

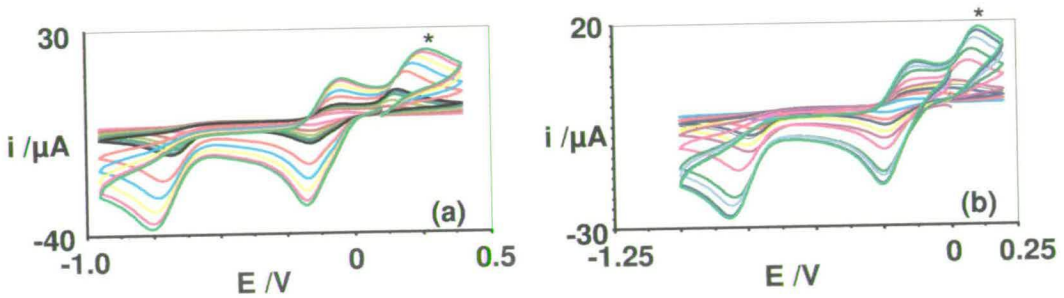

Figure 4.17. The variation of the first and second electrochemical reduction in (a) **21** (0.1 → -0.95 → 0.4 V) and (b) **22** (0 → -1 → 0.2 →) with scan rates (0.01-1 V/s).

This reduction is irreversible (no return peak observed), but on the oxidative return sweep a new peak marked * in **Figure 4.17** grows in as the scan rate is increased. The first reduction remains unaffected by this second reduction (return peaks still observed). The second reduction appears to be undergoing an EC (electrochemical-chemical) type reaction[17] whereby the species that is produced after reduction undergoes a chemical transformation which is re-oxidised at a different potential on the re-oxidation cycle. At present, this new product is unidentified.

4.3.6 EPR Spectroscopy

Figure 4.18 shows the EPR spectrum obtained for the mono-reduced cationic radical of complex **22**, $[(\eta^6\text{-hmb})_2Ru_2(CO\text{-}(azpy)_2)Cl_2]^{+\bullet}$ recorded in DMF at 233 K. The sample displayed an EPR signal centred on 3386 G at g = 1.99285 with a peak to peak linewidth of 20 G. No hyperfine coupling was observed.

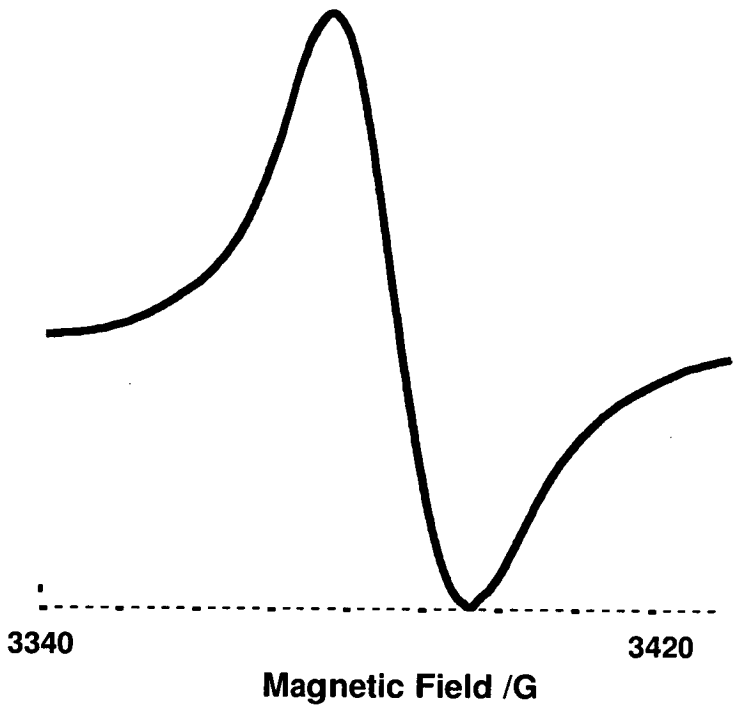

Figure 4.18. Solution EPR spectrum recorded for the mono-reduced cation of complex **22**.

4.3.7 ^{31}P Spin Trap Experiment

Spin traps are species that are highly reactive towards free radicals and normally are nitrones or nitroso species which react with unstable free radicals to form a more stable free radical (radical adduct), which can be detected by EPR spectroscopy.[18] Unfortunately, these radical adducts degrade with time becoming diamagnetic and therefore EPR-undetectable. Recently research groups have been interested in utilising the ^{31}P NMR-active phosphorus atom in the spin trap and to follow the reactions of the trap with radicals in a technique called *NMR spin trapping*.[18-21]

Figure 4.19 shows the structure of DEPMPO, a spin trapping agent, and its reactions with radical R•. The radical formed is unstable and disproportionates to the corresponding hydroxylamine and a new nitrone.

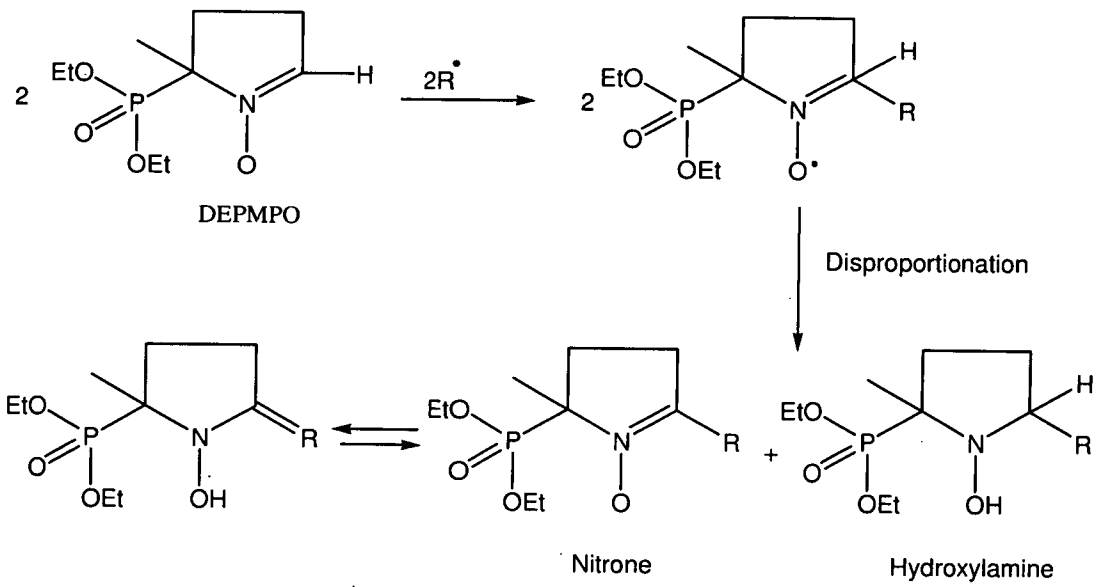

Figure 4.19. Reactions of radical spin trap DEPMPO with radical R•.

The hydroxylamine, with R=OH, can lose a molecule of H_2O to convert back to the starting material so the product observed by ^{31}P NMR is the nitrone (which can exist in two tautomeric forms).[19] **Figure 4.20** shows the ^{31}P NMR spectrum recorded for the DEPMPO solution (0.075 M) after 3 h incubation with (a) $H_2O_2/FeSO_4$ (0.075 M/0.075 M), (b) $[(\eta^6\text{-p-cym})_2\ Ru_2(CO\text{-}(azpy)_2)Cl_2]\ (PF_6)_2$ (**21**, 0.075 M) and (c) blank control in 0.15 M phosphate buffer (pH 6.99) containing 1.5 mM DTPA and 25% $(CD_3)_2CO$.

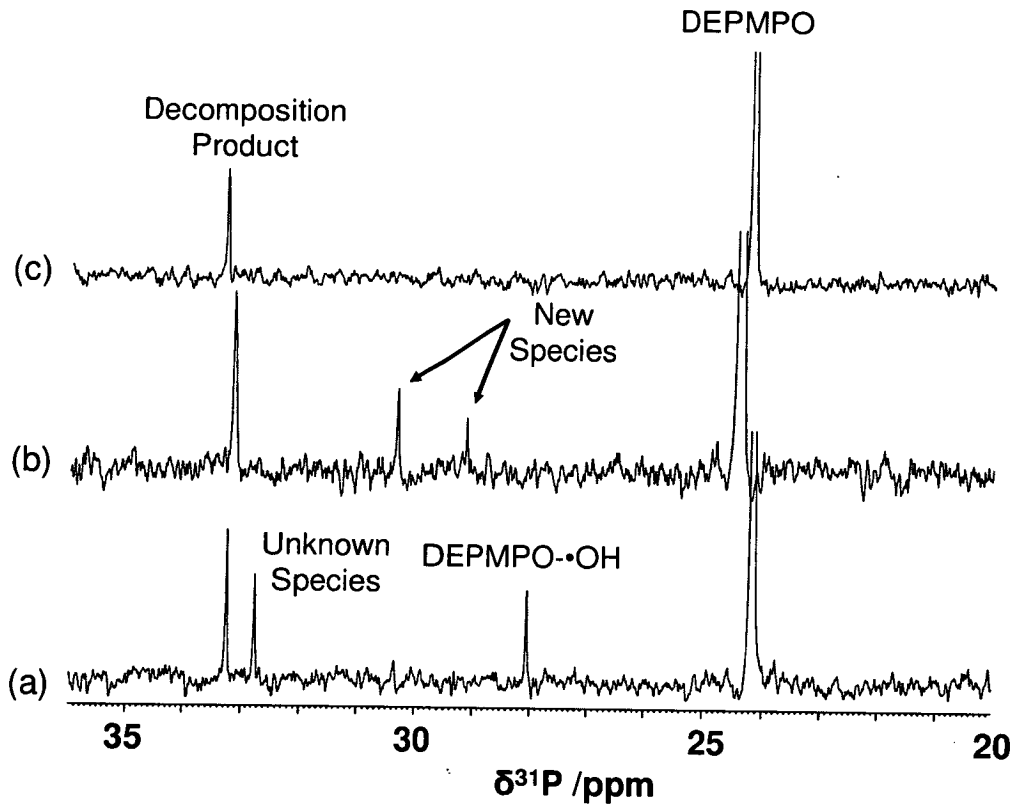

Figure 4.20. ^{31}P NMR spectra recorded after 3 h incubation at 310 K with (a) $H_2O_2/FeSO_4$ to generate •OH radicals, (b) complex **21** and (c) a blank control. All peaks were internally referenced to the phosphate buffer peak (3.80 ppm).

All spectra show the peak corresponding to DEPMPO and a decomposition peak which appears over the three hours in all three cases (blank control included). For the $H_2O_2/FeSO_4$ system (a) which uses Fenton type reactions to generate hydroxyl radicals, a new peak appears at *ca.* 28 ppm which corresponds to the product of reaction of DEPMPO with •OH.[19] An unknown species also appears at *ca.* 33 ppm. This may tentatively be assigned to the product of the reaction of the spin trap with the carbon-based -•$COCH_3$ radical formed when acetone and H_2O_2 react together.[18] For the ruthenium system two new peaks also appeared, but at *ca.* 29 and 30.5 ppm. This indicates that radicals are being formed in this system. These peaks, however, appear at a different ppm compared to the Fenton-control and it is not possible to say whether they correspond to the same paramagnetic products. It is noteworthy that the DEPMPO peak has shifted by *ca.* 0.5 ppm and the decomposition product by slightly less, in the spectrum containing the ruthenium compound, which may be a

result of paramagnetic ruthenium species being present in the solution. It is thus possible that the newly formed diamagnetic species could also be affected and appear with different chemical shifts.

4.3.8 Cytotoxicity

The cytotoxicity of complexes **17-22** against the A549 human lung and A2780 human ovarian cell line is summarised in **Table 4.2.**

Table 4.2. Cytotoxicity data for dinuclear ruthenium complexes and cisplatin against the A2780 and A549 cancer cell lines. nd = not determined

Complex	A2780 IC_{50} (μM)	A549 IC_{50} (μM)
17	>100	>100
18	nd	nd
19	nd	nd
20	nd	nd
21	>100	>100
22	38	85
Cisplatin	6	10

To date, three of these dinuclear complexes have been tested for cytotoxicity. Complexes $[(\eta^6\text{-}p\text{-cym})_2\ Ru_2(CH_2\text{-}(azpy)_2)Cl_2]\ (PF_6)_2$ **17** and $[(\eta^6\text{-}p\text{-cym})_2\ Ru_2(CO\text{-}(azpy)_2)Cl_2]\ (PF_6)_2$ **21**, which contain the *p*-cymene arene, were not cytotoxic towards both cell lines. The hmb containing complex $[(\eta^6\text{-}p\text{-cym})_2\ Ru_2(CO\text{-}(azpy)_2)Cl_2]\ (PF_6)_2$ was moderately cytotoxicity towards the A2780 cancer cell line and somewhat less so towards the A549 cell line.

4.4 Discussion

4.4.1 Synthesis of Nitrosopyridine

The synthesis of 2-nitrosopyridine is highly desirable since the major synthetic route to phenylazopyridine complexes involves an acid/base cataylsed condensation reaction between a nitroso (NO) and amino (NH_2) group; thus either an aminopyridine can be reacted with a nitrosobenzene or a nitrosopyridine with an aminobenzene. Several aminobenzene derivatives are commercially available whereas there are not many nitrosobenzene derivatives available, thus a greater variety of ligands can be potentially synthesised from 2-nitrosopyridine and an aminobenzene derivative.

Although aromatic nitroso compounds have been known since many years, only few heterocyclic nitroso compounds have been synthesised.[10] Direct nitrosation by electrophilic substitution is possible only with electron-rich systems, and heterocycles such as 2-aminopyridine are electron-poor systems that react with electrophiles at the ring nitrogen rather than on the exocyclic amino group. Electrophilic attack on the exocyclic amino group is made possible when electron density is concentrated at this position and this is achieved by first converting the amino group into a sulfilimine. The mechanism for this reaction has been debated in the literature and two reaction paths have been suggested.

The first possible mechanism (**Figure 4.21**) involves the initial conversion of the 2-aminopyridine to its mono-*N*-chlorinated derivative by using *N*-chlorosuccinimide as a chloride donor, followed by addition of dimethyl sulfide to produce the azasulfonium salt. After short treatment at low temperature with base, the sulfilimine is formed.

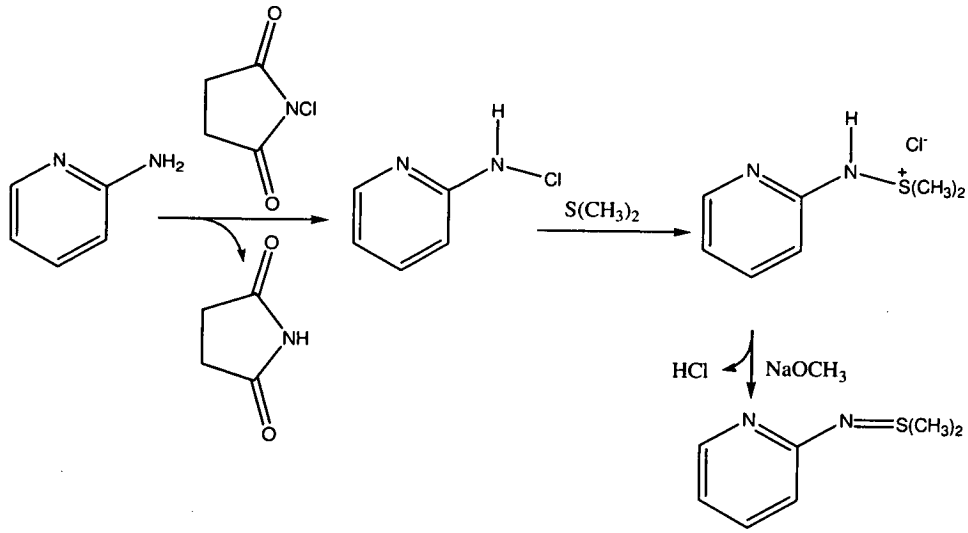

Figure 4.21. Possible reaction scheme for the formation of *S,S*-dimethyl-*N*-(2-pyridyl)sulfilimine as proposed by Gassmann et al. in 1973.[22]

The second possible mechanism (**Figure 4.22**) involves activation of dimethyl sulfide (by *N*-chlorosuccinimide to give the corresponding sulfonium compound. Nucleophilic attack by the amine gives the azasolfonium salt and treatment with base forms the sulfilimine.[23]

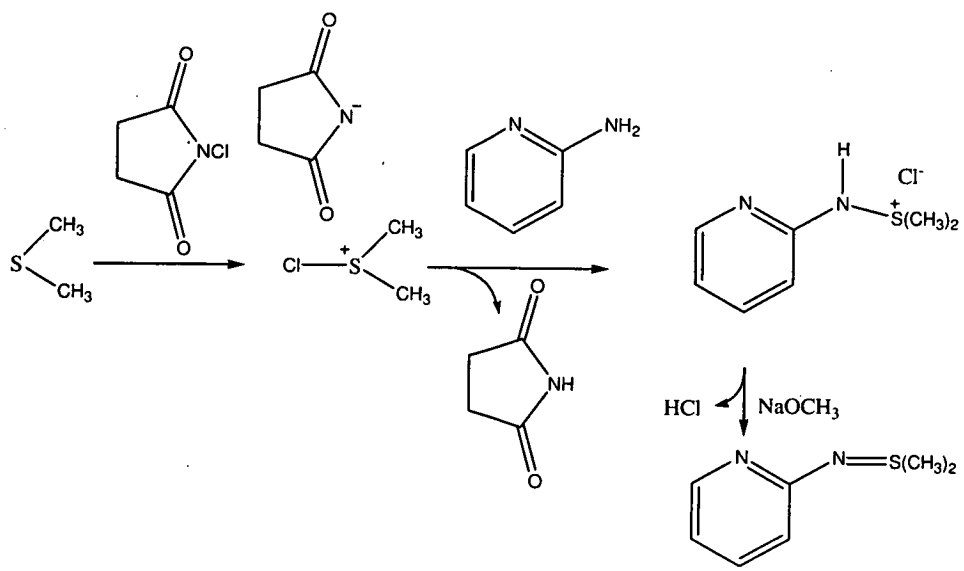

Figure 4.22. Reaction scheme for mechanism of formation of *S,S*-dimethyl-*N*-(2-pyridyl)sulfilimine proposed by Claus et al. in 1975.[23]

The successful synthesis of nitrosopyridine was an important step for future syntheses of derivatised phenylazopyridine ligands. It will allow for a much wider range of ligands to be synthesised and thus build on structure-activity-relationships.

4.4.2 Dinuclear complexes

The complexes studied in this Chapter exist as diastereomers due to the chirality imposed at the ruthenium centres, and purification of these complexes through recrystallisation led to the preferential precipitation of one isomer (called isomer A). The isomers are not readily interconverted and this is perhaps not surprising since to convert, the phenylazopyridine ligand would have to detach and reattach to a ruthenium centre. Phenylazopyridine ligands coordinate strongly to Ru^{II} centres and this bonding is strengthened by back donation from the metal to the azo π^* orbital[24] and so, the non-lability of the bis-phenylzopyridine chelating ligand may preclude any interconversion.

4.4.3 Aqueous Solution Chemistry and ^{31}P Spin Trap Experiment

These complexes are much less stable in an aqueous solution at physiologically relevant concentrations compared to similar mononuclear analogues[24] and appear to form no well defined products.

Reaction of complex $[(\eta^6\text{-}p\text{-cym})_2\ Ru_2(CO\text{-}(azpy)_2)Cl_2]\ (PF_6)_2$ (**21**) in a 75% aqueous solution containing the spin trapping agent DEPMPO showed that, through the production of new diamagnetic phosphorus species in the ^{31}P NMR, radicals were being produced in this reaction. It seems likely that a redox process is occurring in this system generating radicals. The redox process is unlikely to be an oxidation; the reactions were carried out in the absence of oxygen (thoroughly degassed), the coordination of an η^6-arene disfavours oxidation of Ru(II) to Ru(III) by stabilising the Ru(II) oxidation state[25] and oxidation of the ligands (from azo to azoxy) was found to occur only at a relatively high potential (in DMF, 1.30 V, vs.Ag/AgCl). The redox process is more likely a reduction; reduction of the azo moiety in complex **21** occurred at an easily accessible potential (in DMF, -0.06 V (vs Ag/AgCl) to form the azo anion radical) and phenylazopyridine ligands attached to ruthenium are reported to undergo electrochemical reductions (*vide supra*). The reductant,

presumably, is water. There are several examples where water takes on the role of a reductant: For example, photosynthetic organisms can use water as an electron source to reduce CO_2,[26] and water has been used as a hydrogen-atom source for radical reductions mediated by $[Cp_2TiCl]^{\bullet}$.[27] The reduction of **21** by water may be a complex reaction; simple hydrogen abstraction from water to the azo group would generate HO•, and in the ^{31}P DEPMPO spin trap experiment the same new diamagnetic species formed at 28 ppm as had formed in the positive control (generating HO• through fenton type reactions) would be expected to be present. Whilst new diamagnetic ^{31}P peaks are present, they appear at a slightly different frequency (29 and 30.5 ppm).

4.4.4 Electrochemistry and EPR Spectroscopy

Complexes **21** and **22** were studied by cyclic voltammetry and were found to undergo one electron reductions that occurred near to 0V vs. Ag/AgCl electrode (-0.06 V (**21**), -0.14 V (**22**)). The hmb complex was reduced at a slightly more negative potential and this trend, due to the increased electron donating effect of the arene substituents in hmb arene to the metal, was also observed for bis Os arene complexes containing the chelating ligand 2,2'-azobispyridine.[28] An EPR spectrum was also determined for the mono-reduced cationic radical of complex **22**. The g-value obtained for this radical is 99.8% of the free g value (2.0023) and signifies that this complex is an organic-based radical as opposed to a metal-based radical.[29] Based on the electrochemistry results, this radical is assigned as an azo-anion radical since the low-lying nature of the π^* orbital makes the azo function susceptible to one electron reduction.[14] No ^{14}N hyperfine coupling was observed; this is often the case for ligand based azo radicals on ruthenium since the ^{14}N coupling constant is small and often difficult to observe.[14-16]

4.4.5 Cytotoxicity

Three complexes were tested for cytotoxicity against both the A2780 and A549 cancer cell lines. In general the complexes displayed a low/no cytotoxicity and no improvement of cytotoxicity was gained by linking the two ruthenium units together compared to the monomer alone. The hmb complex was more cytotoxic than the

corresponding *p*-cym complexes and this may be due to its increased stability in aqueous solution, suggesting that the decomposition observed is not desirable for good cancer cell cytotoxicity.

4.5 Summary

Six dinuclear ruthenium(II) arene complexes containing bis phenylazopyridine ligands and chlorido were synthesised and characterised by ^{1}H NMR, ESI-MS and CHN analysis. Two complexes were further characterised by cyclic voltammetry and one also by EPR spectroscopy. The complexes exist as diastereomeric mixtures and intriguingly decomposed rapidly in aqueous solution forming radicals (confirmed by the presence of new DEPMPO-diamagnetic adducts in the ^{31}P NMR) and undefined products; and do not appear to display a similar type of chemistry to analogous mononuclear analogues (i.e. hydrolysis and arene loss). The complexes exhibit no/low cytotoxicity towards both A2780 and A549 cancer cells. In this Chapter this synthesis of nitrosopyridine was also reported. This is a useful precursor for the synthesis of otherwise-unattainable 2-phenylazopyridine ligands

4.6 References

[1] B. A. J. Jansen, J. Brouwer, J. Reedijk, *J. Inorg. Biochem.* **2002**, *89*, 197-202.

[2] J. D. Roberts, J. Peroutka, G. Beggiolin, C. Manzotti, L. Piazzoni, N. Farrell, *J. Inorg. Biochem.* **1999**, *77*, 47-50.

[3] V. Brabec, J. Kasparkova, O. Vrana, O. Novakova, J. W. Cox, Y. Qu, N. Farrell, *Biochemistry* **1999**, *38*, 6781-6790.

[4] J. Kasparkova, J. Zehnulova, N. Farrell, V. Brabec, *J. Biol. Chem.* **2002**, *277*, 48076-48086.

[5] C. Sessa, G. Capri, L. Gianni, F. Peccatori, G. Grasselli, J. Bauer, M. Zucchetti, L. Vigano, A. Gatti, C. Minoia, P. Liati, S. Van den Bosch, A. Bernareggi, G. Camboni, S. Marsoni, *Ann Oncol* **2000**, *11*, 977-983.

[6] T. A. Hensing, N. H. Hanna, H. H. Gillenwater, M. G. Camboni, C. Allievi, M. A. Socinski, *Anticancer. Drugs* **2006**, *17*, 697-704.

[7] H. Chen, J. A. Parkinson, O. Novakova, J. Bella, F. Wang, A. Dawson, R. Gould, S. Parsons, V. Brabec, P. J. Sadler, *Proc. Natl. Acad. Sci. U. S. A.* **2003**, *100*, 14623-14628.

[8] O. Novakova, H. Chen, O. Vrana, A. Rodger, P. J. Sadler, V. Brabec, *Biochemistry* **2003**, *42*, 11544-11554.

[9] B. G. Gowenlock, M. J. Maidment, K. G. Orrell, V. Sik, G. Mele, G. Vasapollo, M. B. Hursthouse, K. M. Abdul Malik, *Perkin 2* **2000**, 2280-2286.

[10] E. C. Taylor, C. P. Tseng, J. B. Rampal, *J. Org. Chem.* **1982**, *47*, 552-555.

[11] E. C. Taylor, K. A. Harrison, J. B. Rampal, *J. Org. Chem.* **1986**, *51*, 101-102.

[12] R. Greef, R. Peat, L. M. Peter, D. Pletcher, J. Robinson, *Instrumental Methods in Electrochemistry*, Ellis Horwood Limited, West Sussex, **1985**.

[13] K. Pramanik, M. Shivakumar, P. Ghosh, A. Chakravorty, *Inorg. Chem.* **2000**, *39*, 195-199.

[14] M. Shivakumar, K. Pramanik, I. Bhattacharyya, A. Chakravorty, *Inorg. Chem.* **2000**, *39*, 4332-4338.

[15] M. Shivakumar, K. Pramanik, P. Ghosh, A. Chakravorty, *Inorg. Chem.* **1998**, *37*, 5968-5969.

[16] M. Shivakumar, K. Pramanik, P. Ghosh, A. Chakravorty, *Chem. Commun.* **1998**, 2103-2104.

[17] *The Chemistry of Hydrazo, Azo and Azoxy Groups, Vol. Part 1*, John Wiley & Sons, Bristol, UK, **1975**.

[18] D. S. Argyropoulos, H. Li, A. R. Gaspar, K. Smith, L. A. Lucia, O. J. Rojas, *Abstracts of Papers, 231st ACS National Meeting, Atlanta, GA, United States, March 26-30, 2006* **2006**, CELL-053.

[19] V. Khramtsov, L. J. Berliner, T. L. Clanton, *Magn. Reson. Med.* **1999**, *42*, 228-234.

[20] V. V. Khramtsov, V. A. Reznikov, L. J. Berliner, A. K. Litkin, I. A. Grigor'ev, T. L. Clanton, *Free Radic. Biol. Med.* **2001**, *30*, 1099-1107.

[21] D. I. Potapenko, E. G. Bagryanskaya, Y. P. Tsentalovich, V. A. Reznikov, T. L. Clanton, V. V. Khramtsov, *J. Phys. Chem.* **2004**, *108*, 9315-9324.

[22] P. G. Gassman, C. T. Huang, *J. Am. Chem. Soc.* **1973**, *95*, 4453-4455.

[23] P. K. Claus, W. Rieder, P. Hofbauer, E. Vilsmaier, *Tetrahedron* **1975**, *31*, 505-510.

[24] S. J. Dougan, M. Melchart, A. Habtemariam, S. Parsons, P. J. Sadler, *Inorg. Chem.* **2006**, *45*, 10882-10894.

[25] M. A. Bennett, M. J. Byrnes, I. Kovacik, *J. Organomet. Chem.* **2004**, *689*, 4463-4474.

[26] C. Tommos, *Phil. Soc. Trans. Roy. Soc. B.* **2002**, *357*, 1383-1394.

[27] J. M. Cuerva, A. G. Campana, J. Justicia, A. Rosales, J. L. Oller-Lopez, R. Robles, D. J. Cardenas, E. Bunuel, J. E. Oltra, *Angew. Chem., Int. Ed.* **2006**, *45*, 5522-5526.

[28] F. Baumann, W. Kaim, G. Denninger, H.-J. Kuemmerer, J. Fiedler, *Organometallics* **2005**, *24*, 1966-1973.

[29] The orbital angular momentum of the unpaired electron gives a contribution to the total magnetic moment which produces a shift in the g-value from the free electron value. Large shifts are found for e.g. paramagnetic transition metal ions but in organic free radicals the orbital angular momentum is largely quenched so their g-values are within 1-2% of the free electron value.

Chapter 5

Ruthenium(II) Arene Iodido Azo Complexes

5.1 Introduction

Organometallic transition metal complexes have found widespread use in many areas of chemistry from materials chemistry to catalysis.[1] Research focussing on the use of organometallic complexes for medicinal purposes (bio-organometallic chemistry), and, in particular, as anticancer agents, has shown that there is great potential for these types of complexes to be used medicinally. Titanocence dichloride [Cp_2TiCl_2], for example, was the first organometallic to enter clinical trials as an anticancer drug[2, 3] and although disappointing phase II results halted its further development, several new titanocence dichloride derivatives show promising cytotoxicity and better chemical properties making them ideal candidates for further studies.[4-9] Other organometallic complexes of current interest include ferrocene derivatives of tamoxifen[10-12] which are responsive to both oestrogen receptor positive (ER+) and oestrogen receptor negative (ER-) cancer cell lines, unlike tamoxifen which is responsive to ER+ lines only.

We are investigating organometallic half-sandwich Ru^{II} arenes of the type $[(\eta^6\text{-areneRu(YZ)(X)}]^+$ where YZ is typically a chelating diammine ligand (e.g. ethylenediamine) and X is a halide (e.g. Cl). These complexes exhibit promising anti-cancer activity *in vitro* and *in vivo*.[13, 14] Examples include YZ = en, X = Cl which, for arene = biphenyl and tetrahyrdoanthracene have IC_{50} values of 5 and 0.5 μM respectively in the A2780 human ovarian cancer cell line. As with most metal-based anticancer drugs, the primary cellular target is thought to be DNA. The Ru-Cl bond is labile but hydrolysis (to form $Ru\text{-}OH_2$) is suppressed extracellularly due to the high chloride concentration (ca. 104 mM).[15] Intracellularly the chloride concentration is much lower and hydrolysis occurs generating a reactive site on the ruthenium for subsequent DNA binding. The binding of ruthenium to DNA[16-20] is thought to lead to further 'downstream' effects ultimately resulting in cell death.[21]

The following chapter reports the synthesis, characterisation and cytotoxicity of a series of novel ruthenium(II) arene complexes containing phenylazopyridine ligands. The mechanism of cytotoxicity is investigated along with some molecular signalling pathways and the results show that this class of complexes have a novel mechanism

of cytotoxicity, never before been observed for a ruthenium(II) arene anticancer complexes.

5.2 Experimental

5.2.1 Materials

Dichlorofluorescin diacetate (DCFH-DA), Glutathione (GSH) and N-acetylcysteine (NAC) were purchased from Sigma Aldrich. Ascorbic Acid was purchased from Alfa Aesar. Methanol was dried over Mg/I_2, or anhydrous quality was used (Sigma-Aldrich) all other reagents used were commercially available. The synthesis of [(η^6-bip)Ru(en)Cl]PF_6 and [(η^6-tha)Ru(en)Cl]PF_6 is reported elsewhere.[13, 22]

5.2.2 Synthesis

5.2.2.1 [(η^6-*p*-cymene)Ru(azpy-NMe_2)I]PF_6 (23)

The dimer [(η^6-*p*-cymene)RuI_2]$_2$ (54.8 mg, 0.051 mmol) was dissolved in methanol (20 ml) and heated to ca. 313 K until the solution turned clear. Azpy-NMe_2 (23 mg, 0.102 mmol) dissolved in methanol (10 ml) was added drop-wise and the solution immediately turned from brown to dark blue. The solution was stirred at room temperature for 3 h. The volume of solvent was reduced to about 10 ml by removal of methanol on a rotary evaporator. NH_4PF_6 (83 mg, 0.51 mmol) was then added and the solution was placed in the freezer overnight. A black microcrystalline product precipitated out and this was filtered off and washed with diethyl ether. The product was dried overnight *in vacuo*. Yield: 40.9 mg (68.2%) (Found: C, 37.74; H, 3.25; N, 7.40. Calc for $RuC_{23}H_{27}N_4IPF_6$: C, 37.66; H, 3.85; N, 7.64). ^{1}H NMR ($CDCl_3$) δ9.17 (d, 1H), 8.22 (d, 1H), 8.15 (d, 2H), 8.03 (t, 1H), 7.54 (t, 1H), 6.77 (d, 2H), 6.05 (d, 1H), 5.81 (t, 2H), 5.68 (d, 1H), 3.29 (s, 6H), 2.70-2.54 (m, 4H), 1.04 (d of d, 6H). ESI MS: calcd for $RuC_{23}H_{27}N_4I^+$ [M^+] m/z 589.04, found 589.2 [M^+].

5.2.2.2 [(η^6-biphenyl)Ru(azpy-NMe_2)I]PF_6, (24)

The dimer [(η^6-biphenyl)RuI_2]$_2$: (100 mg, 0.1 mmol) was dissolved in methanol (60 ml) and water (20 ml) and heated to reflux for 2 h. Azpy-NMe_2 (44.4 mg, 0.2 mmol) dissolved in methanol (20 ml) was added drop-wise and the solution

immediately turned from brown to dark blue. The solution refluxed for a further hour, hot filtered and then the volume of solvent was reduced to about 15 ml by removal of methanol on a rotary evaporator. NH_4PF_6 (160 mg, 1 mmol) was then added and the solution was placed in the fridge for 1 h. A black powder product precipitated out and this was filtered off and washed with cold ethanol then diethyl ether. The product was dried overnight *in vacuo*. Yield 121 mg (80.2%). (Found: C, 38.52; H, 2.67; N, 7.03. Calc for $RuC_{25}H_{24}N_4IPF_6$: C, 39.85; H,3.21; N,7.74 %). ^{1}H NMR (DMSO-d_6) δ9.35 (d, 1H), 8.37 (d, 1H), 8.15 (t, 1H), 8.07 (d, 2H), 7.51-7.34 (m, 5H), 6.86-6.78 (m, 3H), 6.68-6.48 (m, 4H), 3.27 (s, 6H). ESI MS: calcd for $RuC_{25}H_{24}N_4I^+$ [M^+] m/z 609.03, found 609.2 [M^+].

5.2.2.3 [(η^6-p-cymene)Ru(azpy-OH)I]PF_6 (25)

The dimer [(η^6-*p*-cymene)RuI_2]$_2$ (73 mg, 0.07 mmol) was dissolved in methanol (70 ml) was stirred until the solution turned clear. Azpy-OH (30 mg, 0.14 mmol) dissolved in methanol (10 ml) was added drop-wise and the solution immediately turned from brown to intense brown/yellow. Six drops of 1M HCl was added to the solution and the mixture was stirred for 4 h. The volume of solvent was reduced slightly and a black precipitate was filtered off. The resulting mixture was passed down a Sephadex LH20 column with methanol as the elutent. The intense brown/yellow fraction was collected and excess NH_4PF_6 (160 mg, 0.1 mmol) was added. The solvent was removed and the product was re-dissolved in dichloromethane, where a white insoluble precipitate was filtered off. The solvent was removed to give a dark brown solid. The product was dried overnight *in vacuo*. Yield 33 mg (46.6 %). (Found: C, 34.48; H, 3.24; N, 5.74. Calc for $RuC_{21}H_{23}N_3OIPF_6$: C, 35.65; H, 3.28; N, 5.94 %). ^{1}H NMR (DMSO-d_6) δ 9.87 (d, 1H), 8.92 (d, 1H), 8.78-8.65 (m, 3H), 8.07 (t, 1H), 7.37 (d, 2H), 6.83 (d, 1H), 6.64-6.51 (m, 3H), 3.18 (septet, 1H), 3.11 (s, 3H), 1.53 (dd, 6H).). ESI MS: calcd for $RuC_{21}H_{23}N_3OI^+$ [M^+] m/z 561.99, found 561.7 [M^+].

5.2.2.4 [(η^6-biphenyl)Ru(azpy-OH)I]PF_6 (26)

The dimer [(η^6-biphenyl)RuI_2]$_2$ (100 mg, 0.1 mmol) was dissolved in methanol (60 ml) and water (20 ml) and heated to reflux for 2 h. Azpy-OH (37.5 mg, 0.2 mmol)

dissolved in methanol (20 ml) was added drop-wise and the solution gradually turned from brown to intense brown/yellow. The solution refluxed for a further 2 h, hot filtered and then the volume of solvent was reduced to about 15 ml by removal of methanol on a rotary evaporator. NH_4PF_6 (160 mg, 1 mmol) was added and the solution was placed in the fridge for 2 h. A brown powder product precipitated out and this was filtered off and washed with cold ethanol then diethyl ether. T he product was dried overnight *in vacuo*. Yield 94.1 mg (66.1%). (Found: C, 38.03; H, 2.14; N, 5.35. Calc for $RuC_{23}H_{19}N_3OIPF_6$: C, 37.21; H, 2.14; N, 5.79). ^{1}H NMR (DMSO-d_6) δ 9.45 (d, 1H), 8.93 (d, 1H), 8.41 (t, 1H), 7.94 (d, 2H), 7.64-7.56 (m, 3H), 7.60-7.45 (m, 5H), 7.43-7.33 (m, 2H), 6.89 (d, 1H), 6.75 (t, 1H), 6.70-6.54 (m, 3H). ESI MS: calcd for $RuC_{23}H_{19}N_3OI^+$ [M^+] m/z 581.65, found 582.1 [M^+].

5.2.2.5 [(η^6-*p*-cymene)Ru(azpy)I]PF_6 (27)

The dimer [(η^6-*p*-cymene)RuI_2]$_2$ (100 mg, 0.1 mmol) was dissolved in methanol (50 ml) and heated to ca. 313 K until the solution turned clear. Azpy (38 mg, 0.2 mmol) dissolved in methanol (10 ml) was added drop-wise and the solution gradually turned from brown to brown/purple. The solution cooled to room temperature and stirred for 3 h. The volume of solvent was reduced to about 10 ml by removal of methanol on a rotary evaporator. NH_4PF_6 (160 mg, 1 mmol) was then added and the solution was placed in the freezer overnight. A black microcrystalline product precipitated out and this was filtered off and washed with ether. The product was dried overnight *in vacuo*. Yield 110 mg (79.6%). (Found: C, 36.90; H, 3.23; N, 5.96. Calc for $RuC_{21}H_{23}N_3IPF_6$: C, 36.54; H, 3.36; N, 6.09). ^{1}H NMR (DMSO-d_6) δ 9.67 (d, 1H), 8.93 (d, 1H), 8.52 (t, 2H), 8.28 (d, 1H), 7.95-7.86 (m, 2H), 7.77 (t, 2H), 6.55 (d, 1H), 6.23 (t, 2H), 6.15 (d, 1H), 2.76 (septet, 1H), 2.62 (s, 3H), 1.08 (dd, 6H). ESI MS: calcd for $RuC_{21}H_{23}N_3I^+$ [M^+] m/z 545.98, found 546.1 [M^+].

5.2.2.6 [(η^6-biphenyl)Ru(azpy)I]PF_6 (28)

The dimer [(η^6-biphenyl)RuI_2]$_2$ (100 mg, 0.1 mmol) was dissolved in methanol (60 ml)\and water (20 ml) and heated to reflux for 2 h. Azpy (37.5 mg, 0.2 mmol) dissolved in methanol (20 ml) was added drop-wise and the solution graduallyturned from brown to brown/purple. The solution refluxed for a further 2 h, hot filtered and

then the volume of solvent was reduced to about 15 ml by removal of methanol on a rotary evaporator. NH_4PF_6 (160 mg, 1 mmol) was then added and the solution was placed in the fridge for 2h. A black powder product precipitated out and this was filtered off and washed with cold ethanol then diethyl ether. The product was dried overnight *in vacuo*. Yield 94.1 mg (66.1%). ^{1}H NMR (DMSO-d_6) δ 9.45 (d, 1H), 8.93 (d, 1H), 8.41 (t, 1H), 7.94 (d, 2H), 7.64-7.56 (m, 3H), 7.60-7.45 (m, 5H), 7.43-7.33 (m, 2H), 6.89 (d, 1H), 6.75 (t, 1H), 6.70-6.54 (m, 3H). ESI MS: calcd for $RuC_{23}H_{19}N_3I^+$ [M^+] m/z 565.66, found 566.1 [M^+].

5.2.3 Methods

5.2.3.1 Unbuffered Aqueous Solution Behaviour of Complexes 23-28

Solutions of ruthenium complexes were prepared in 90% H_2O / 10% D_2O (**23** pH 6.19, **26** pH 6.25, **25** pH 5.64, **24** pH 6.29) or 95% D_2O, 5% MeOD (used to aid solubilisation) (**28** pH*7.09, **27** pH*6.51) at 100 μM ruthenium. ^{1}H NMR spectra were recorded at 310 K initially (time ca. 15 minutes) and after 24 h. The samples were kept in the water bath at 310 K between acquisitions.

5.2.3.2 Buffered Aqueous Solution Behaviour of Complexes 23-28

Solutions of ruthenium complexes in MeOD were diluted down in 10 mM phosphate buffer / D_2O to give a final concentration of 100 μM ruthenium (95%D_2O, 5% MeOD). ^{1}H NMR spectra were recorded at 310 K initially (time ca. 15 minutes) and after 24 h. The pH* of the samples was 7.35 (**23**), 7.38 (**24**), 7.38 (**25**), 7.40 (**26**), 7.31 (**27**) and 7.32 (**28**). The samples were kept in the water bath at 310 K between acquisitions. After 24 h, ESI-MS was performed on samples **23**, **24**, **25** and **26**.

5.2.3.3 Investigating Substitution of Iodide by Chloride in Complex 24

Complex **24** was dissolved in water, sonicated for 15 min to fully dissolve, filtered and then diluted down to ca. 30 μM. Sodium chloride was added from a concentrated stock solution to give 100 mM NaCl and the corresponding absorbance spectrum was recorded at hourly intervals over 24 h at 310 K.

5.2.3.4 Determination of the Rates of Reduction of complexes 23, 24, 25 and 26 by ascorbic acid

Ruthenium complexes were dissolved in MeOH and diluted with water to give a 50 μM solution (95% H_2O/ 5% MeOH). Phosphate buffer (final conc. 10 mM, gave pH 7.2-7.4) was added along with ascorbic acid (at four different excess concentrations, 5-20 equivalents) and the change in absorbance was followed at selected wavelengths (568 nm for **25** and **26**, 597 nm for **23** and **24**) over a time period. A plot of the change in absorbance with time was fitted to the appropriate equation for pseudo-first order kinetics using Origin version 7.5 (OriginLab Corporation) to give the observed rate constant (k_{obs}) for each concentration of ascorbate. A plot of k_{obs} against concentration of ascorbate gave a straight line, the gradient of which was the second order rate constant k', for the compounds showing behaviour dependent on the concentration of ascorbate.

5.2.3.5 Reduction of complexes 23, 24, 25 and 26 by ascorbic acid followed by ^{1}H NMR

The complexes were dissolved in MeOD and diluted in D_2O / 10 mM phosphate buffer (pH 7.3) to give 50 μM Ru (5% MeOD). The ^{1}H NMR spectra were recorded, 5 equivalents of ascorbic acid was added and the spectra were re-recorded at the half life (at 22 min (**26**), 20 min (**24**), and 88 min (**23** and **25**)) and after the reaction had finished (after 3 h (**24** and **26**) and after 7 h (**23** and **25**). Each acquisition took 7 min 43 s to acquire and so the spectra recorded represent an average speciation over this time.

5.2.3.6 Reactions of Ru-X with Glutathione (GSH) for complexes 8 and 24 by UV-Vis Spectroscopy, HPLC and ^{1}H NMR

Aqueous Solutions / buffers used were filtered through Chelex-100 to remove iron and degassed using N_2/Ar prior to dissolving GSH. After dissolution the pH of the GSH solution was adjusted to ca.7 by addition of dilute NaOH / HCl and solutions were degassed again. Solutions of GSH were made fresh for each experiment. [(η^6-biphenyl)Ru(azpy-NMe_2)I]PF_6 (**24**), and [(η^6-biphenyl)Ru(azpy-NMe_2)Cl]PF_6 (**8**), diluted in MeOH were added to GSH (final concentrations 50 μM Ru, 5 mM GSH,

10 mM phosphate buffer; 95% H_2O, 5% MeOH), the pH was 7.06 (**24**) and 7.03 (**8**) for UV-Vis experiments and 7.88 (**24**) and 7.89 (**8**) for HPLC separations.

The rate of substitution of Ru-X by GS^- was determined by UV-Vis spectroscopy, following the change in wavelength at 597 nm (298 K) with time and fitting the change in absorbance with time to the appropriate equation for pseudo-first order kinetics using Origin version 7.5 (OriginLab Corporation) to give the observed rate constant (k_{obs}) and the corresponding half life ($t_{1/2}$).

The extent of substitution of X^- in Ru-X by GS^- was followed by HPLC using the gradient 10-50% B to 30 min, 50-90% B to 40 min using semi-preparative conditions. The new fraction appearing over time was collected and analysed by ESI-MS.

Isolation of the corresponding GS^- adduct of [(η^6-biphenyl)Ru(azpy-NMe_2)I]PF_6 was from collecting the HPLC fraction of an unbuffered solution (50 μM complex **24**, 4.75 mM GSH (pH adjusted to 7.4); 95% H_2O, 5% MeOH). The GS^- adduct fraction was collected, the pH adjusted to 7.0, lyophilized, re-dissolved in 95% D_2O, 5% acetone-d_6 (pH recorded as 8.1) and the ^1H NMR spectra were subsequently recorded over 24 h.

5.2.3.7 Detection of Oxidation of GSH to GSSG

Aqueous solutions / buffers used were filtered through Chelex-100 to remove iron and degassed using N_2/Ar prior to dissolving GSH. After dissolution the pH of the GSH solution was adjusted to ca. 7 by addition of dilute NaOH / HCl and solutions were degassed again. Solutions of GSH were made fresh for each experiment. [(η^6-biphenyl)Ru(azpy-NMe_2)I]PF_6 (**24**), [(η^6-biphenyl)Ru(azpyOH)I]PF_6 (**26**), Azpy-NMe_2 and Azpy-OH dissolved in acetone-d_6 were added to GSH (final concentrations 100 μM Ru / ligand, GSH 10 mM (when ruthenium) / 9.5 mM (when ligand), 30 mM phosphate buffer; 10% D_2O, 85% H_2O, 5% acetone-d_6), the measured pH was 7.62 (**24**), 7.57 (**26**), 7.55 (Azpy-NMe_2) and 7.59 (Azpy-OH). Solutions of GSH alone (10 / 9.5 mM, 10% D_2O, 85% H_2O, 5% acetone-d_6) were also made up at the same time (measured pH 7.40 (control for **24** and **26**) and 7.60 (control for Azpy-NMe_2 or Azpy-OH) to check the amount of auto-oxidation of

GSH, and these samples were kept in the water bath at 310 K for 24 h then the ^1H NMR was run.

5.2.3.8 Detection of Reactive Oxygen Species

The experiment was based on earlier experimental protocols by Wang *et. al*[23] with some modifications. Dichlorofluorescein diacetate (DCFH-DA) was opened under a blanket of argon, aliquoted in DMSO and kept frozen. When used, care was taken to ensure minimum exposure to light. A549 cancer cells were plated out at a density of 20x 10^3 cells per well into black 96 well plates and were incubated at 310 K, 5% CO_2, high humidity for 24 h. Cells were loaded with DCFH-DA (10 μM, 0.5% DMSO (v/v)) and were incubated at 310 K, 5% CO_2, high humidity for 30 min. The probe was removed and the cells were washed twice with PBS (200 μL). The cells were then kept in Hanks Balanced Salt Solution (HBSS) and the ruthenium compounds were diluted with HBSS and added to the wells (25 μM, 0.5% DMSO (v/v)). Hydrogen peroxide (25, μM) was added as a positive control and the fluorescence was read every 200 s over a period of 6 h at 310 K by excitation at 480 ±10 nm and emission at 538 ±15 nm on a BMG Fluostar plate reader.

5.2.3.9 Increasing Intracellular Thiol Levels

For IC_{50} determinations for A549 cells with increased thiol levels, A549 cells were pre-incubated with 5 mM N-acetyl-L-cysteine for two hours, a concentration and time that had previously been reported not to be non-toxic for this cell line,[24, 25] and this was confirmed by controls throughout the experiment. The NAC was removed, cells were washed twice in PBS, fresh cell medium was added and IC_{50} determination was subsequently determined as normal (see Chapter 2).

5.2.3.10 Qualification of Cell Survival in HCT-116 (p53 +/-) Colon Cancer Cells

HCT 116 (WT) and HCT116 (p53-) were plated out at 120 x 10^4 cells/well (40 x 10^4 cells/mL) and 93 x 10^4 cells/well (31 x 10^4 cells/mL) respectively and incubated for 24 h before drug addition. The ruthenium compound was dissolved in DMSO to give a stock solution of 5 mM and serial dilutions were carried out in DMSO to give concentrations of drug in DMSO of 2, 1, 0.4, 0.2, 0.1 and 0.02 mM. These were added to the wells to give the six testing concentrations (25, 10, 5, 2, 1, 0.5 and 0.1

μM) and a final concentration of DMSO of 0.5% (v/v) with a total volume of drugs and media to be 3.015 mL. The cells were exposed to the drug for 24h, then, after drug removal, the cells were washed twice with PBS (3 mL) and the remaining biomass was fixed by adding cold MeOH (5 mL) and incubating at room temperature for five minutes. The methanol was removed and the plates were air-dried. The remaining biomass was visualised by adding Giemsa stain (diluted 1:20 with distilled water, 5 mL) to each well and incubating at room temperature for 20 minutes. The plates were washed with tap water (3 x 5 mL), left to dry then photographed for a visual indication of remaining biomass.

5.2.3.11 p53 Immunochemical Assays

All experiments were performed within ten passages of each other. Typically HCT-116 cancer cells were plated out at a density of 15 x 10^4 cells / dish (15 x 10^3 cells/mL) and the cells were incubated at 310 K, 5% CO_2, high humidity for 48 h. Ruthenium complex **24** was dissolved in DMSO, serially diluted and added to a dish at concentrations of 5, 2, 1, 0.5 and 0.1 μM (0.05% DMSO). DMSO only, a blank (no drug or DMSO) and a positive (7 Gy X-ray exposure, cells harvested 4 h after exposure) controls were also included. The cells were exposed to the complex/control for 24 h then the complex was removed, the cells were washed with PBS (10 mL) then harvested into ice-cold PBS (1 mL), centrifuged at 3000 rpm at 277 K for 4 min, the PBS removed and the pellet stored in liquid N_2. The cell lysate was collected by adding ca. 70 μL urea lysis buffer (7 M Urea, 0.1 M DTT, 25 mM NaCl, 20 mM Hepes buffer (pH 7.6), 0.05% Triton X-100), pipetting to mix, incubating on ice for 30 min, centrifuging at 13000 rpm at 277 K for 10 minutes and removing the lysate. The protein concentration of the lysate was determined by the Bradford Assay and the proteins in the lysate were separated using SDS-PAGE. Briefly 20 μg of protein was dissolved in 10 μL SDS sample buffer (4% SDS, 200 mM Tris (pH 6.8), 10 mM EDTA, 20% glycerol, 60 μL/ml 1% bromophenol blue 0.2 M DTT) and a low range loading marker was similarly prepared. The samples were heated for 5 min at 368 K and were separated using a 10% resolving gel (H_2O (1.9 mL), 1.5 M Tris pH 8.8 (1.3 mL), 10% SDS (0.05 mL), 10% ammonium persulfate (0.05 mL) and TEMED (0.002 mL) with loading on a 5% stacking gel

(H2O (3.4 mL), 1 M Tris (pH 6.8) (0.63 mL), 30% acrylamide mix (0.83 mL), 10% SDS (0.05 mL), 10% ammonium persulfate (0.05 mL) and TEMED (0.005 mL) with SDS PAGE running buffer. The gel was run at a constant voltage (180 V) for 50 minutes or until the bromophenol blue had reached the bottom of the gel. The gel was transferred to a nitrocellulose membrane at 300 mA over 1 h using tris-glycine methanol transfer buffer. The unreacted sites on the membrane were blocked using 5% Marvel Milk in PBS-Tween (100 mL) with 1 mL 1 M β-glycerol phosphate by incubating for 1 h at room temperature with gentle shaking. The primary anti bodies were used were the p-53-specific Do-1 Mouse mAB (Novocastra, Newcastle upon Tyne, UK, 1:1000, 5% Milk – PBS-T), the p53 C-terminal phosphorylation site serine 392-specific FP-3 Mouse mAB (1:500 5% Milk-PBS-T) and the p53 N-terminal phosphorylation site serine 15 Mouse mAB (1:1000 5% Milk-PBS-T) (both New England Biolabs, Hitchin, UK) and the p21 WAF1 (Dako, 1:500, 5% Milk-PBS-T) Primary antibodies were added and incubated at 277 K overnight then at room temperature for a further 15 min. The membrane was washed (3 x 5 min in PBS-T) then the horse radish peroxidase (HRP) conjugated secondary antibody was added (polyclonal rabbit-anti-mouse RAM, 1:1000 5% Milk-PBS-T) for 1 h at RT, the membrane was washed (3 x 10 min in PBS-T). Blots were visualised by chemiluminescence and photographed. Actin immunoblots were used to confirm equal protein loading.

5.3 Results

Figure 5.1 shows the complexes synthesised and studied in this chapter. They were screened for cancer cell cytotoxicity and some analogues were found to be highly cytotoxic. Because the cytotoxicity of half sandwich Ru(II) arenes is thought to be due to hydrolysis of labile Ru – X bonds followed by binding to DNA (*vide supra*), hydrolysis studies were performed. In view of the unusual hydrolysis behaviour (*vide infra*) their redox chemistry was subsequently investigated electrochemically, inside cancer cells, with the biological reductant ascorbate and with the primary cellular antioxidant glutathione (GSH). Furthermore, cellular activation pathways were investigated for cancer cells after being exposed to one of the cytotoxic

complexes in order to gain some information about the 'downstream' effects of this class of complexes.

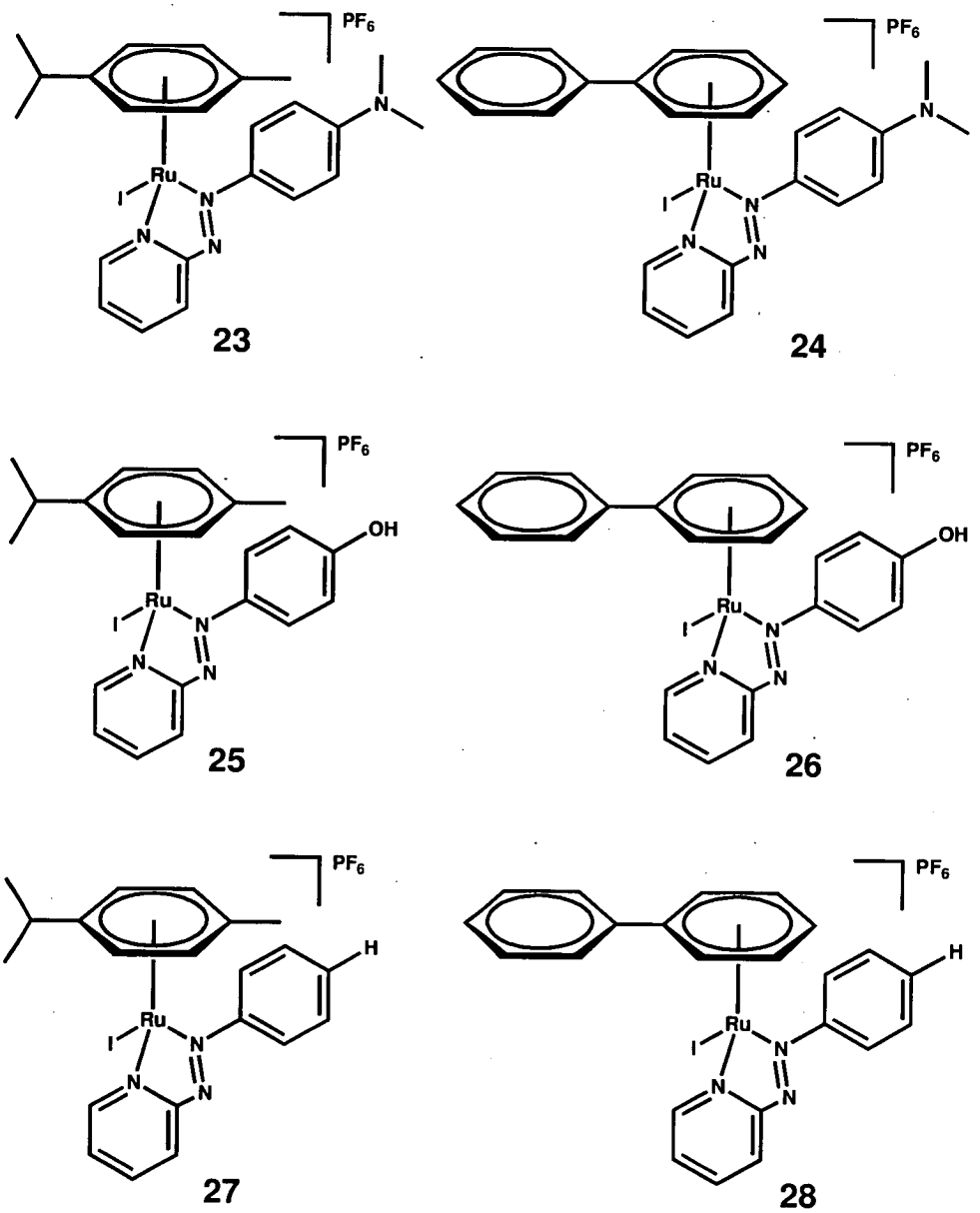

Figure 5.1. Molecular structure and numbering of ruthenium complexes studied in this Chapter.

5.3.1 Synthesis and Characterisation

The complexes were characterised by ^{1}H NMR, CHN and ESI-MS. In general the ^{1}H NMR spectra of the iodide complexes was similar to the corresponding chloride analogues.

5.3.2 Aqueous Solution Chemistry

5.3.2.1 Buffered Solutions

The aqueous solution chemistry was studied by ^{1}H NMR in 95% D_2O/5%MeOD at 100 μM ruthenium concentration in 10 mM phosphate buffer (pH 7.3) and at 310 K over 24 h. These conditions were chosen to mimic the concentration, pH, exposure time and temperature used for the biological cell tests.

For complexes **23**, **24**, **25** and **26** no new peaks / peak shifts occurred in the spectra over 24 h suggesting that no hydrolysis had occurred; this hypothesis was confirmed by performing ESI-MS on the NMR solutions where only one mass corresponding to the intact cation was observed (**23** found m/z 561.70 (M^+) calcd for **23** 561.99, **24** found m/z 588.75 (M^+) calcd for **24** 589.04, **25** found m/z 581.65 (M^+) calcd for **25** 581.98, **26** found m/z 608.71 (M^+) calcd for **26** 609.03).

For complexes **27** and **28**, however, changes in their ^{1}H NMR spectra occurred over the 24 h time period (**Figure 5.2** and **Figure 5.3** respectively). For compound **28**, after 24 h dissolution all peaks corresponding to the intact cation had disappeared and the only assignable peaks in the spectrum were due to free biphenyl in solution. For compound **27** the peaks corresponding to the intact cation were still present although at a reduced intensity and a new peak corresponding to free *p*-cymene in solution was observed.

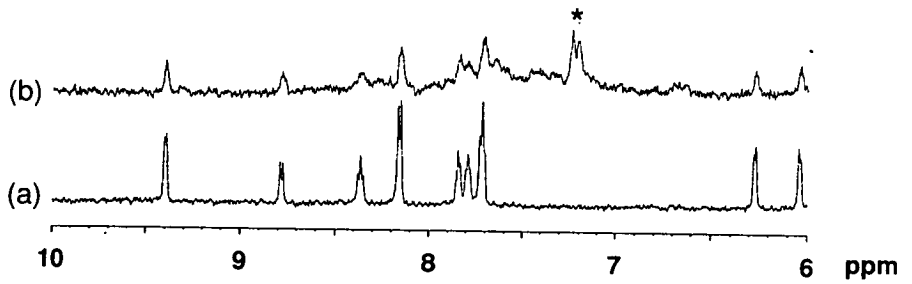

Figure 5.2. High frequency region ^{1}H NMR (100 μM **27**, 95% D_2O, 5% MeOD, 10 mM phosphate buffer, 310 K, internal reference dioxane (δ 3.75)) at (a) 10 min and (b) 24 h after dissolution. The peaks corresponding to the intact cation in (a) are reduced in intensity in (b) and a new peak assignable to free p-cymene in solution has appeared, marked *.

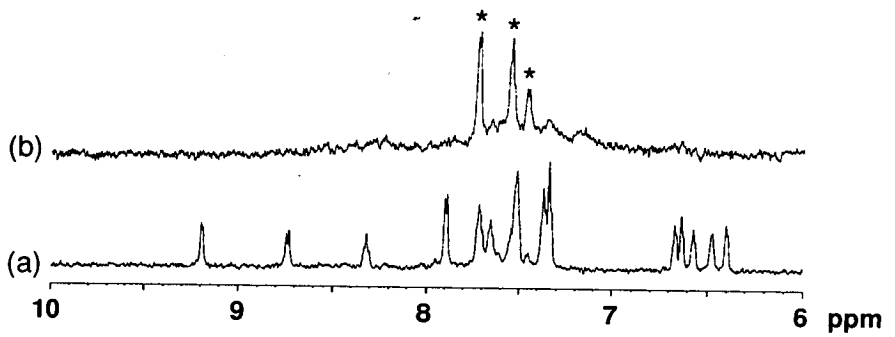

Figure 5.3. High frequency region ^{1}H NMR (100 μM **28**, 95% D_2O, 5% MeOD, 10 mM phosphate buffer, 310 K, internal reference dioxane (δ 3.75)) at (a) 11 min and (b) 24 h after dissolution. The peaks corresponding to the intact cation in (a) have disappeared in (b) and the only assignable peaks are due to free biphenyl in solution, marked *.

The reactions of complex **28** and **29** (50 μM complex, 10 mM phosphate buffer, 310 K, 24 h) were subsequently followed by UV-Vis spectroscopy where slow decompositions over the 24 h time period was observed (See **Figure 5.4**).

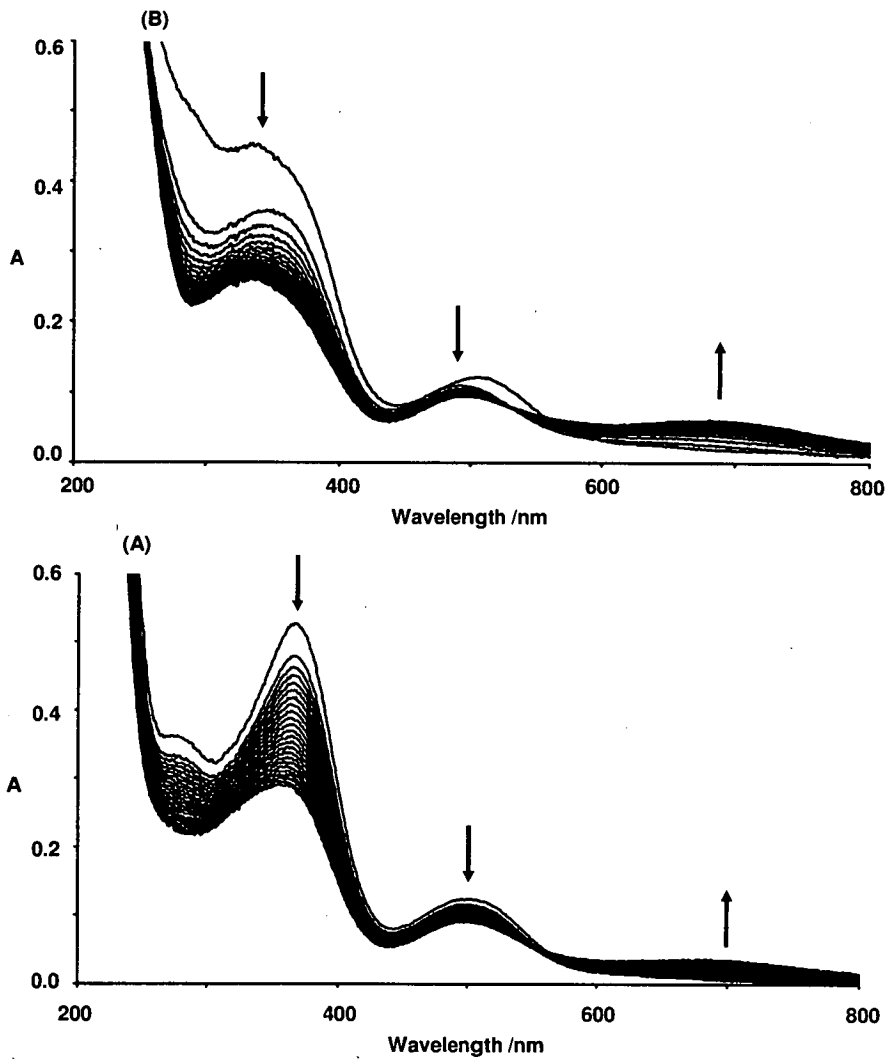

Figure 5.4. UV-Vis spectra recorded for (a) **27** and (b) **28** (50 μM Ruthenium, 10 mM phosphate buffer, pH 7.3, 95% H_2O, 5% MeOH) recorded every hour at 310 K over 24 h. In both cases there is a decrease in intensity of the UV-Vis bands over the time period and an increase in intensity between 600-800 nm.

5.3.2.2 Unbuffered Solutions

The solution chemistry was also studied in unbuffered aqueous solution. For complexes **23**, **24**, **25** and **26** again no new peaks / peak shifts occurred in the spectra over 24 h (data not shown) indicating that no hydrolysis had occurred. However, for complexes **27** and **28** after 24 h the intact cation accounted for ca. 95% of the species in solution and there was only a small amount of free p-cymene / biphenyl detected (accounting for no more than *ca.* 5% of the solution, determined by peak integration) suggesting that only a small amount of arene was lost from the complex (data not

shown) and that the complexes largely still existed as their intact cations. Thus the phosphate buffer appears to be accelerating the decomposition of these two complexes.

5.3.2.3 Reaction of complex 24 with excess NaCl

The reaction of **24** in 104 mM NaCl (to mimic extracellular [Cl^-]) was investigated by UV-Vis spectroscopy over 24 h at 310 K in order to investigate if chloride displaces iodide when present in a large excess. No changes in the spectrum occurred (data not shown) indicating no substitution of iodide by chloride had occurred.

5.3.2.4 pKa of Phenolic group in [(η^6-p-cym)Ru(azpy-OH)I]PF_6 (25)

A pK_a value of 6.50 was determined for deprotonation of the phenol group of azpy-OH in complex **25** (**Figure 5.5**), and so at physiological pH (7.2-7.4) the complex will be neutral.

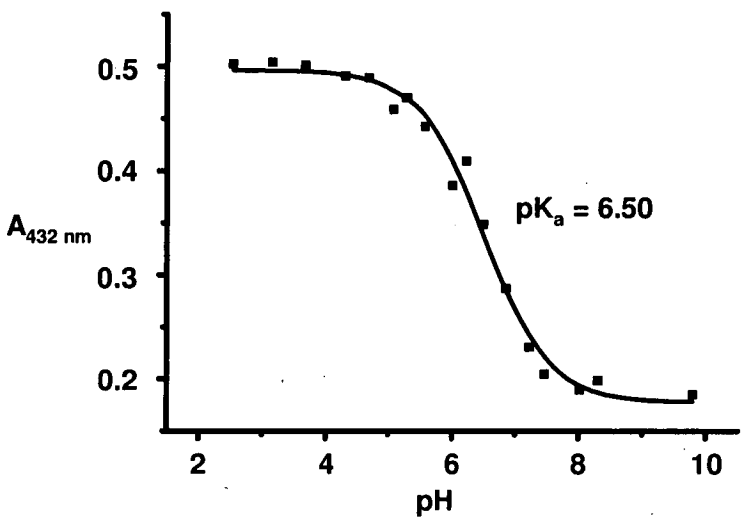

Figure 5.5. Plot of absorbance at 432 nm against pH for compound **25** and corresponding sigmoidial fit to give the pK_a of the deprotonation of the phenolic OH as 6.50.

5.3.3 Electrochemistry

The electrochemical reductions of all six ruthenium complexes were studied by cyclic voltammetry in DMF containing 0.1 M $TBABF_4$ as the supporting electrolyte.

Generally the complexes displayed two electrochemical reductions, the first reduction occurred at *ca.* -0.2 to -0.4V and a second at ca. – 0.7 to -1 V. There were further reductions observed near to the solvent cut off (ca. -2V) but these were not considered any further. The reduction potentials are summarised in **Table 5.1**.

Table 5.1. Irreversible electrochemical reduction potentials for ruthenium complexes **23-28** recorded in DMF with 0.1 M $TBABF_4$ at 0.1 Vs^{-1} referenced to the Ag/AgCl reference electrode.

Complex	First reduction (E_{Pc} / V)	Second Reduction (E_{Pc} / V)
23	-0.40	-1.0
24	-0.36	not observed
25	-0.33	-0.77
26	-0.26	-0.72
27	-0.22	-0.74
28	-0.18	-0.67[a]

[a] two subsequent reductions of reduced intensity were observed at ca. -0.90 V and -1.17 V, thought to be due to the instability and reduction of the di-anion decomposition products.

5.3.3.1.1 First Electrochemical Reduction

This reduction was confirmed as a one electron reduction for complex **27** using constant potential coulometry, see **Figure 5.6.** It was assumed, on the basis of this result that the first reduction for all six complexes was also a one electron reduction.

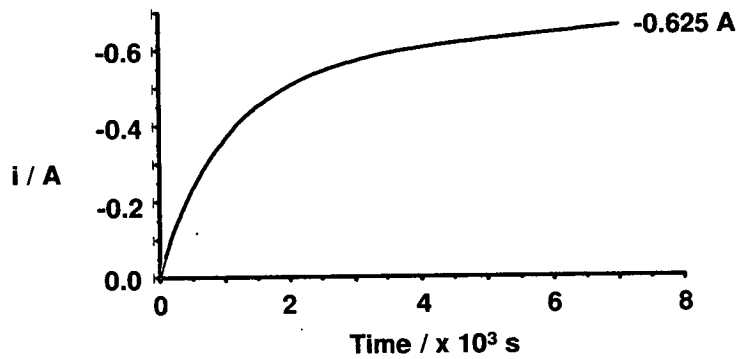

Figure 5.6. Constant potential (held at -0.40 V) coloumetry results showing current increasing with time for the reduction of 6.6 μmoles of complex [(η^6-*p*-cymene)Ru(azpy)I]PF_6, **27**. For n = 1, theoretically i = 0.636 therefore n = 0.98 (1).

The reduction potential becomes more positive as the arene is changed from p-cymene to biphenyl and also as the chelating azo ligand is changed from azpy-NMe_2, to azpy-OH to azpy (**Table 5.1**). Based on literature assignments of the reduction of ruthenium-phenylazopyridine complexes,[26-28] this reduction can be assigned to the addition of an electron into the phenylazopyridine ligands π* orbital centred on the azo group to form the azo anion radical, equation (**1**)

$$\text{-N=N- + e}^- \rightarrow \{\text{-N-N-}\}^{-\bullet} \qquad (1)$$

The relative order therefore reflects the decreasing π-acceptor capability of the substituted azpy ligands due to the addition of electron donating groups onto the phenyl ring.[29]

In all cases the reduction is essentially irreversible (no return peak observed, $0.1Vs^{-1}$, RT) and the complexes undergo an Electrochemical - Chemical type reduction; the electrochemically reduced product is not stable and so reduction is followed by a chemical reaction/transformation, where the major peak that appears on the return oxidative sweep (marked * on **Figure 5.7**) is the re-oxidation of the product formed after subsequent reaction of the reduced species, and not the reversible re-oxidation of the reduced species. Faster scan rates increased the reversibility of the reduction slightly with a corresponding decrease in the re-oxidised product.

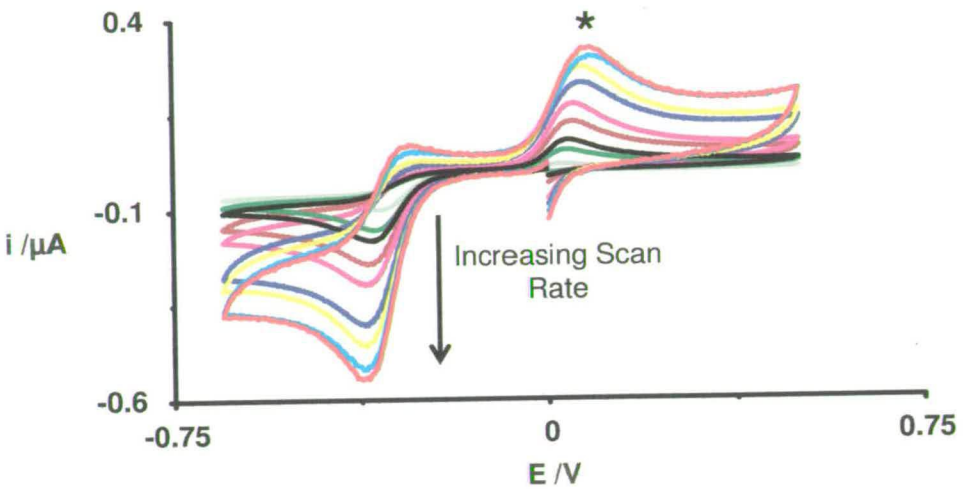

Figure 5.7. Cyclic voltammogram for complex **23** recorded in 0.1M $TBABF_4$ in DMF (sweep from 0 → -0.75 → +0.5 → 0 V) as the scan rate is varied from 0.01 – 1 Vs-1at ca. 298 K. The reaction becomes slightly more reversible at higher scan rates but in all cases the main product on the return sweep is marked *.

At lower temperatures the first reduction peak becomes more reversible, this re-oxidation peak either disappeared or was significantly reduced in intensity, see **Figure 5.8.**

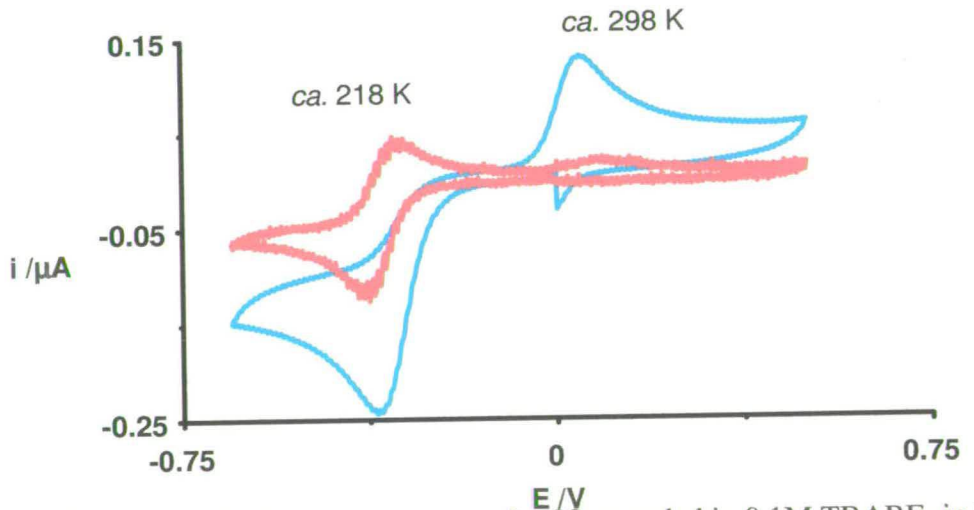

Figure 5.8. Cyclic voltammogram for **23** recorded in 0.1M $TBABF_4$ in DMF (sweep from 0 → -0.75 → +0.5 → 0 V, 0.1 Vs^{-1}) as the temperature is changed from ca. 298 K to 218 K. At the lower temperature scan the reduction becomes more reversible and the EC-product is significantly reduced in intensity.

5.3.3.1.2 Second Electrochemical Reduction.

This irreversible reduction step is assigned to the electrochemical reduction of the azo anion radical to the dianion species, equation (**2**)

$$\{\text{-N-N-}\}^{-\bullet} + e^- \rightarrow \{\text{-N-N-}\}^{2-} \qquad (2)$$

In polar aprotic solvents such as DMF, the two-electron reduction of the azo group is seen as two separate electrochemical reductions.[30] In cases where it was observable it appeared with a reduced intensity compared to the first reduction, presumably due to the instability of the mono-reduced species (hence not all is present to be able to be reduced to the dianion).

5.3.4 Reactions with Ascorbate

Ascorbic acid (pKa 4.2, ascorbate anion at physiological pH) is an important anti-oxidant and acts as a cell protector in nearly all aerobic organisms.[31] It is capable of donating two electrons and two protons sequentially to form the ascorbyl radical then dehydroxoascorbic acid.

5.3.4.1 Phenylazopyridine Ligands

The reaction of phenylazopyridine ligands Azpy-NMe_2 and Azpy-OH with ascorbate produced some changes in the UV-Vis spectrum with time (**Figure 5.9**) but on closer inspection it revealed that these changes were due to ascorbate decomposing in the solution and not due to reduction of the complex.

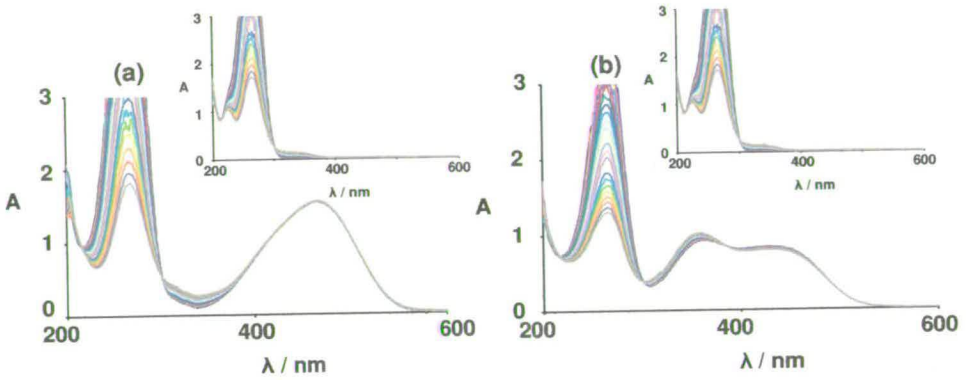

Figure 5.9. Reaction of (a) Azpy-NMe_2 and (b) Azpy-OH (50 μM, 95% H_2O, 5% MeOH) with Ascorbic Acid (250 μM) in 10 mM phosphate (pH 7.2). Readings were taken from 600-200 nm every hour over 24 h (310 K). Inset: The reaction of ascorbate alone under the same conditions.

5.3.4.2 Ruthenium Complexes

The reactions of **23-26** with ascorbic acid were followed over time using UV-Vis spectroscopy. Dramatic changes in the UV-Vis spectra of the ruthenium compounds occurred upon addition of ascorbate, notably a decrease in the intensity of the Metal-to-Ligand – Charge-Transfer (MLCT) band and the emergence of a new broad peak at ca. 350 nm (**25** and **26**) or at ca. 480 nm (**23** and **24**). Interestingly, on completion of the reaction, the UV-Vis spectra still showed the intense π-π* intraligand transitions of the phenylazopyridine[32] indicating that the azo moiety had not been reduced. Furthermore, isosbestic points at ca. 430 nm for complexes **25** and **26** suggested that the reaction was a single step transition from starting material to reduced product whereas for complexes **23** and **24** the absence of a true isosbestic point suggested that there may be intermediates involved in these cases. Representative spectra are shown in **Figure 5.10.**

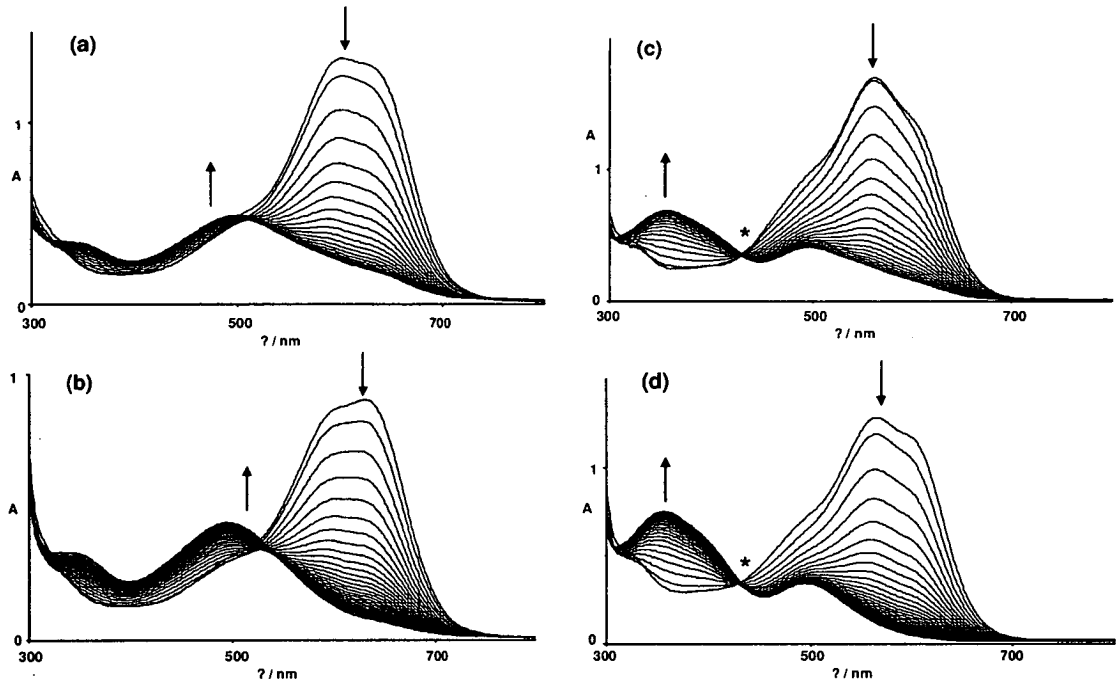

Figure 5.10. UV-Vis spectra recorded for the reactions of (a) **23**, (b) **24**, (c) **25** and (d) **26** (50 μM, 10 mM phosphate buffer, pH 7.3 95% H_2O, 5% MeOH, 310 K) with 10 equiv ascorbic acid. Readings were taken every 5 minutes over 3 h (**24** and **26**) or 15 minutes over 6 h (**23** and **25**). Isosbestic points are marked *.

Kinetic data were derived by following the change in absorbance at selected wavelengths with time. For the biphenyl complexes, the change in absorbance showed an initial plateau for compound **24** (for *ca.* 140 s independent of ascorbate concentration) and an initial quick slight increase in intensity for compound **26** (for ca. 200 s, independent of ascorbate concentration)[33] followed by a rate-determining-step (RDS) decrease in the intensity of the MLCT which gave good pseudo-first order kinetics with excess ascorbate to give the second order rate constants of 0.68 $M^{-1}s^{-1}$ (**24**) and 0.45 M^{-1} s^{-1} (**26**) and corresponding half lives of $t_{1/2}$ = 488 s (**24**) and 741 s (**26**) (**Figure 5.11**).

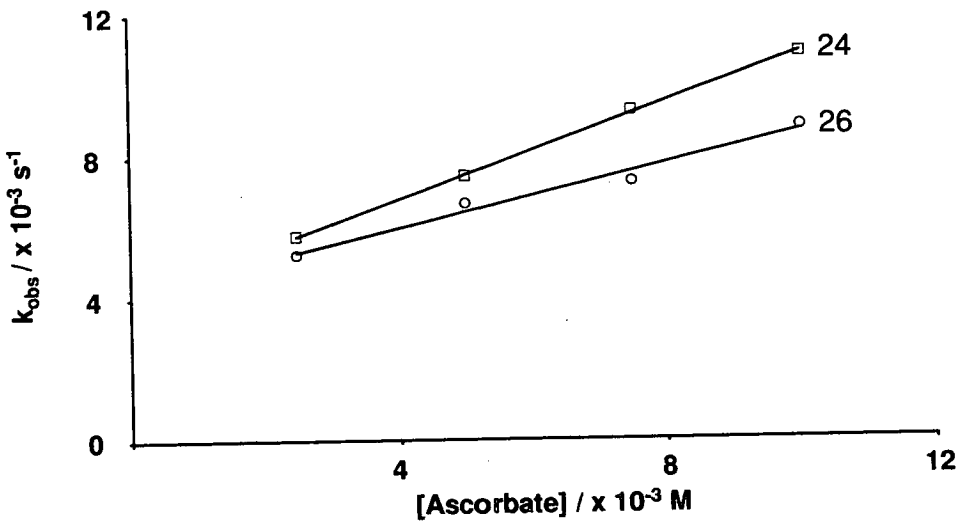

Figure 5.11. Plots of observed pseudo first order rate constants (k_{obs}) determined with differing concentrations of ascorbate and best fit straight lines for the reduction of **24** (50 μM, □) and **26** (50 μM, ○). The second order rate constants were determined from the gradients as 0.68 $M^{-1}s^{-1}$ (**24**) and 0.45 $M^{-1}s^{-1}$ (**26**) with corresponding half lives of 488 s (**24**) and 741 s (**26**).

The change in absorbance for the *p*-cymene complexes **23** and **25**, however was much slower and showed an initial increase in intensity which was found to follow pseudo-first order kinetics with differing ascorbate concentrations to give the second order rate constants of 3.4 M^{-1} s^{-1} (**23**) and 3.0 M^{-1} s^{-1} (**25**) and corresponding half lives of $t_{1/2}$ = 108 s (**23**) and 111 s (**25**), followed by a slow RDS decrease in absorbance which was independent of ascorbate concentration (**Figure 5.12**). The rate of reduction by ascorbate were determined to be *ca.* 1.4 x 10^{-4} s^{-1} for both complexes (half life $t_{1/2}$ = 1.4 h).

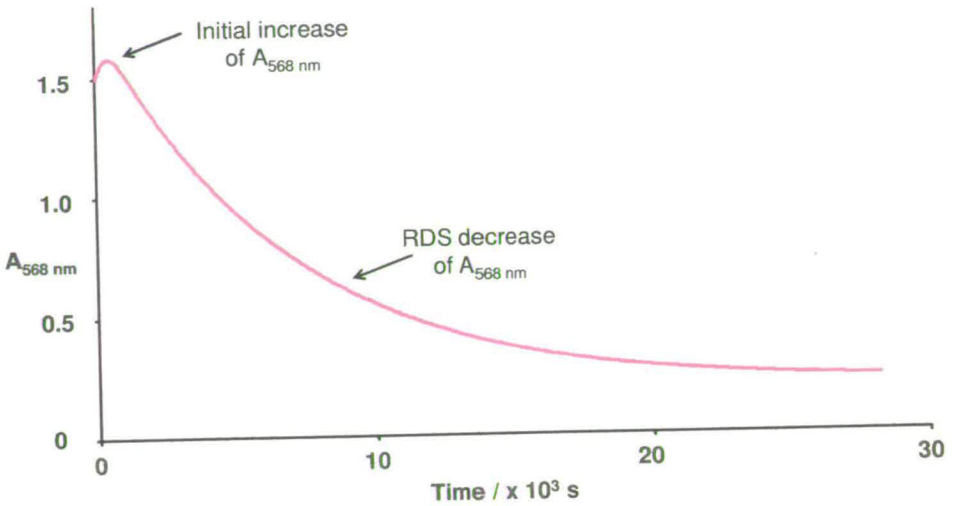

Figure 5.12. The change in absorbance at 568 nm for complex **25** (50 μM, 10 mM phosphate buffer, pH 7.35, 95% H_2O, 5% MeOD) with 10 equiv ascorbate. There is an initial increase in absorbance followed by a RDS decrease, independent of ascorbate concentration which gives rate for the reduction to be *ca.* 1.4 x 10^{-4} s^{-1} (half life $t_{1/2}$ = 1.4 h).

In order to identify the nature of the reduced species, the same reactions were followed by ^{1}H NMR. In all cases, the rate-determining step appeared to correlate with loss of bound η^6-arene from the complex as was evident from the appearance of new peaks in the aromatic region at δ 7.90, 7.70, 7.45 ppm assignable to free biphenyl, or at δ 7.23 ppm due to free *p*-cymene. The peaks for the starting complex decreased in intensity over time and eventually disappeared and several broad weak peaks appeared over the reaction course, suggesting that this reduced species was unstable and/or multiple products were forming. **Figure 5.13** shows representative ^{1}H NMR spectra for complexes **25** and **26**.

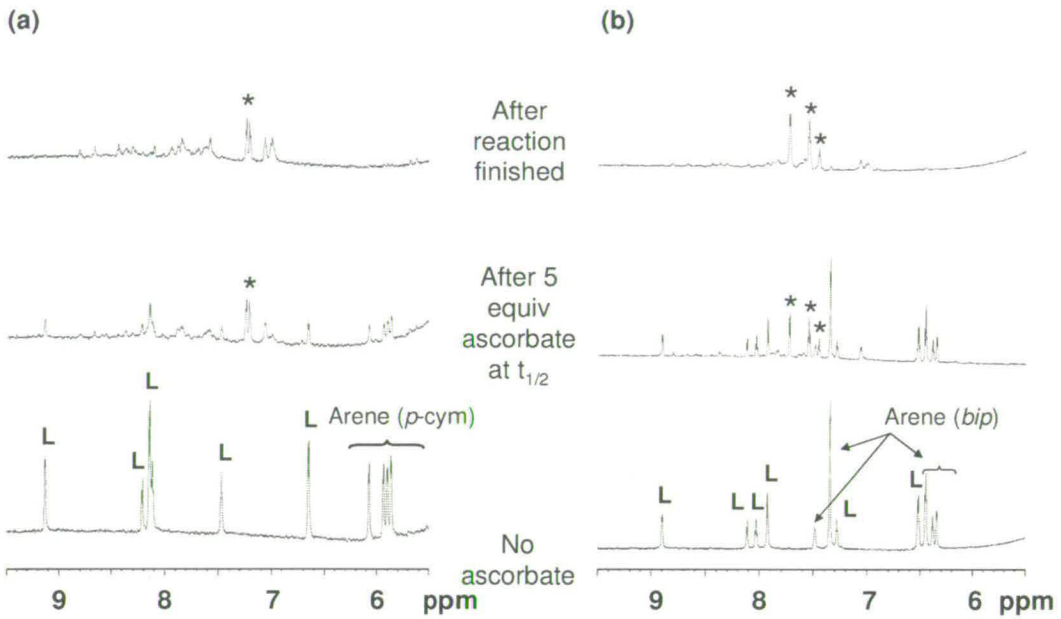

Figure 5.13. ^{1}H NMR spectra recorded for (a) complex **25** and (b) complex **26** (50 μM) in 95% D_2O, 5% MeOD, 10 mM phosphate buffer pH 7.2-7.4 during their reactions with ascorbate. Peaks marked * indicate free arene (p-cym/bip) in the solution. L = ligand 1H resonances.

5.3.5 Reactions with Glutathione (GSH)

Glutathione (GSH) is the primary cellular antioxidant and is present in mM concentrations inside cells (ca. 2-10 mM). For this reason reactions with glutathione were investigated.

5.3.5.1 Ru-X (X = Cl^-, I^-) Substitution

The reaction of complex **24** and the corresponding chloride complex [(η^6-biphenyl)Ru(Azpy-NMe_2)Cl]PF_6, **8** with GSH were studied by UV-Vis spectroscopy and HPLC.

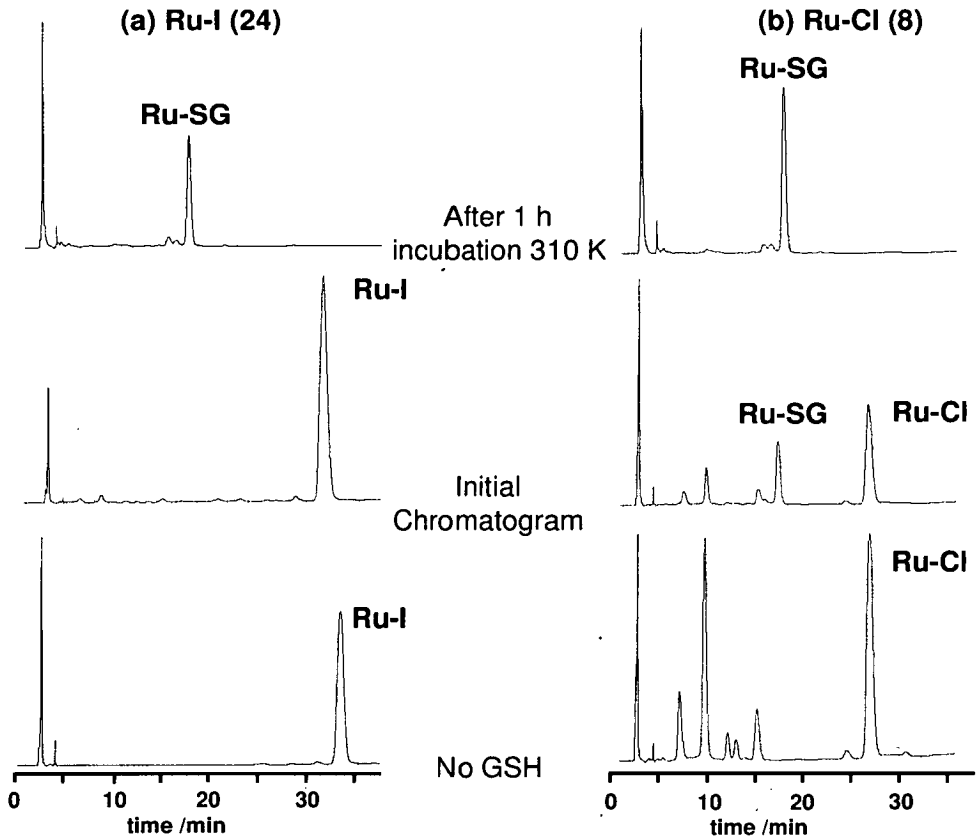

Figure 5.14. HPLC Chromatograms (λ = 286 nm) for the reaction of (a) complex 24 and (b) complex 8 (50 μM) with GSH (5 mM) at pH 7.9 (10 mM phosphate buffer, 95% H_2O, 5% MeOH). After 1 h incubation at 310 K the main peak corresponds to the GS-bound complex $[\eta^6$-(biphenyl)Ru(azpy-NMe_2)GS$]^+$ and the peaks corresponding to the starting material have disappeared.

Analysis of the reaction mixtures by HPLC (directly after addition of **8/24** to GSH, and after 1 h at 310 K, **Figure 5.14**), suggested that all the Ru-X was displaced to form Ru-SG, since no peaks for starting material were present, and one new peak formed at ca. 17 minutes. ESI-MS of this fraction confirmed that in both cases $[\eta^6$-(biphenyl)Ru(azpy-NMe_2)GS$]^+$ was present (m/z observed 788.0, calcd 789.2)).

For complex **24** the initial reaction mixture just contained one peak corresponding to the intact cation and after 1 h incubation at 310 K this peak completely disappeared and there was 100% conversion to the GS-adduct. For complex **8** initially several

peaks were present, thought to correspond to a mixture of hydrolysis products (phosphate, TFA, water coordinated to Ru) including the GS- adduct peak.

Isolation of this adduct, and subsequent ^{1}H NMR studies, showed that this species was relatively stable over 24 h with ca. 57% remaining intact after 24 h incubation at 310 K, and several breakdown peaks and arene loss was noted (data not shown).

The rate of displacement of Ru-X by GS^- in complexes **8** and **24** was determined by UV-Vis spectroscopy by following the change in absorbance at 597 nm (298 K). Substitution of the halide by GS^- substitution occurred with a half life of 1.3 min (kobs =8.73 x 10^{-3} s^{-1}) for Ru-Cl and 17.5 min for Ru-I (kobs = 6.58 x 10^{-4} s^{-1}), see **Figure 5.15**.

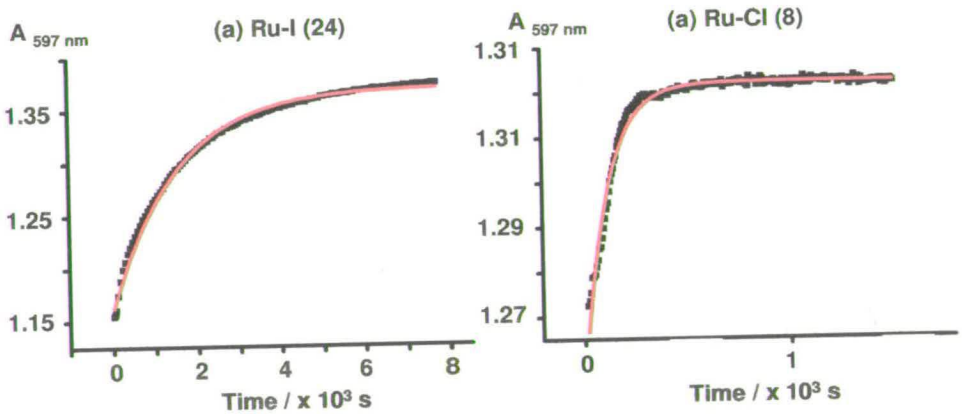

Figure 5.15. Change in the absorbance (black) at 597 nm with time for (a) [η^6-(biphenyl)Ru(azpy-NMe_2)I]PF_6 (**24**) and (b) [η^6-(biphenyl)Ru(azpy-NMe_2)Cl]PF_6 (**8**) (50 μM Ru, 95% H2O, 5% MeOH, 10 mM phosphate buffer pH 7) after the addition of GSH (5 mM). The change in absorbance was fitted to the appropriate equation foe pseudo-first order kinetics (red) to give rate constants and half lives of 8.76 x 10^{-3} s^{-1}, 1.3 minutes (**8**) and 6.58 x 10^{-4} s^{-1}, 17.5 minutes (**24**).

Thus the Ru-I bond is *ca.* 14 times more resistant to substitution by GS- than the Ru-Cl bond.

5.3.5.2 GSH oxidation

Interestingly, during the course of the reaction of the complexes [η^6-(biphenyl)Ru(azpy-NMe_2)I]PF_6, **24** and [η^6-(biphenyl)Ru(azpy-OH)I]PF_6, **26** with glutathione, it became apparent that GSH was being catalytically oxidised to GSSG

(as detected by ^{1}H NMR, *vide-supra*) over the course of the reaction. The overall redox process is shown in equation (**3**).

$$2GSH \rightarrow GSSH + 2H^+ + 2e^- \qquad (3)$$

Several experiments have been performed to try and ascertain the molecular basis of this oxidation, which must be facilitated by the ruthenium compound(s). The experiments were performed in the absence of dissolved oxygen since oxygen (dO_2) alone can oxidise GSH according to the following equation (**4**).

$$2GSH + ½O_2 \rightarrow GSSG + H_2O \qquad (4)$$

Thorough degassing of the solutions prior to following the oxidation allowed for the assessment of this catalytic oxidation to be made, without the competing effects of auto-oxidation of GSH by dO_2.

The reaction of [η^6-(biphenyl)Ru(azpy-NMe_2)I]PF_6, **24** and [η^6-(biphenyl)Ru(azpy-NMe_2)I]PF_6, **26** with GSH followed by ^{1}H NMR showed that incubation of GSH with **24** or **26** (10 mM GSH, 100 μM Ru, 10 mM phosphate pH 7.2, 85% H_2O, 10% D_2O, 5% acetone-d_6, 310 K, followed over 24 h) caused 3.7 mM and 4.6 mM GSH to be oxidised to GSSG steadily (**Figure 5.16**), as evidenced by the appearance of new peaks at δ 3.30 due to the β-CH_2 peaks of GSSG[34] (**Figure 5.16**, inset). The presence of GSSG was further confirmed by 'spiking' the NMR sample with GSSG, which resulted in an increase in the intensity of the peaks assigned to GSSG. Furthermore, ESI-MS of the solution after 24 h incubation showed two peaks corresponding to GS^- (found 305.2, calcd for GS^- 305.1) and GSSG (found 611.1, calcd for GSSG: 611.2).

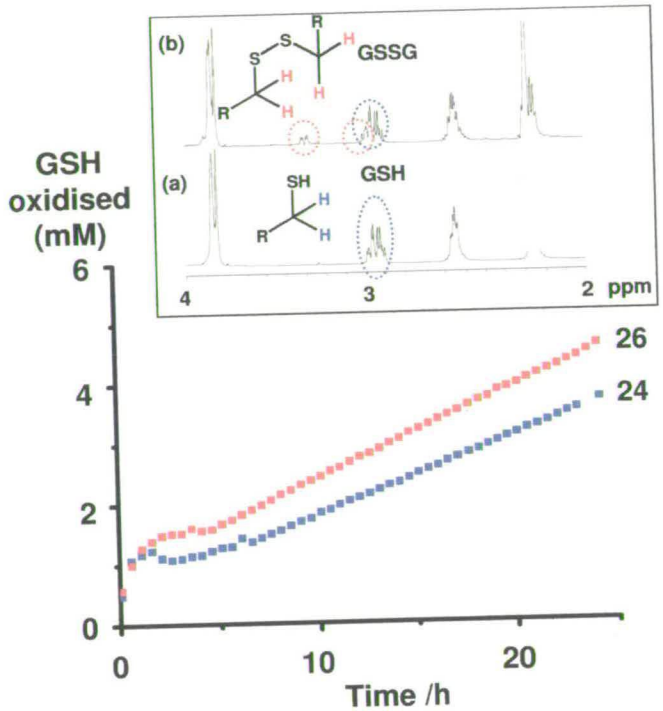

Figure 5.16. Amount of GSH (mM) oxidised to GSSG in the presence of 100 μM **24** (blue) or 100 μM **26** (red) over 24 h at 310 K. Inset (a) spectrum of GSH recorded after 30 min incubation with ruthenium compound and (b) the same sample after 24 h where peaks assignable to GSSG can be identified.

The results suggested that a catalytic oxidation of GSH to GSSG was being facilitated by the ruthenium compound in a mechanism not involving dO_2. Thus the ruthenium complex must be undergoing a redox cycle which must involve reduction of the complex (causing oxidation of GSH) followed by a subsequent re-oxidation of the ruthenium species to generate a catalytic cycle. In order to obtain information about the nature of this reduced intermediate species attempts were made to analyse the reaction mixture by LC-MS but this was unsuccessful and suggested that intermediates were transient. **Figure 5.17** shows the high frequency ^{1}H NMR spectrum of the reaction of **26** (100 μM) with GSH (10 mM) recorded initially and after 24 h at 310 K.

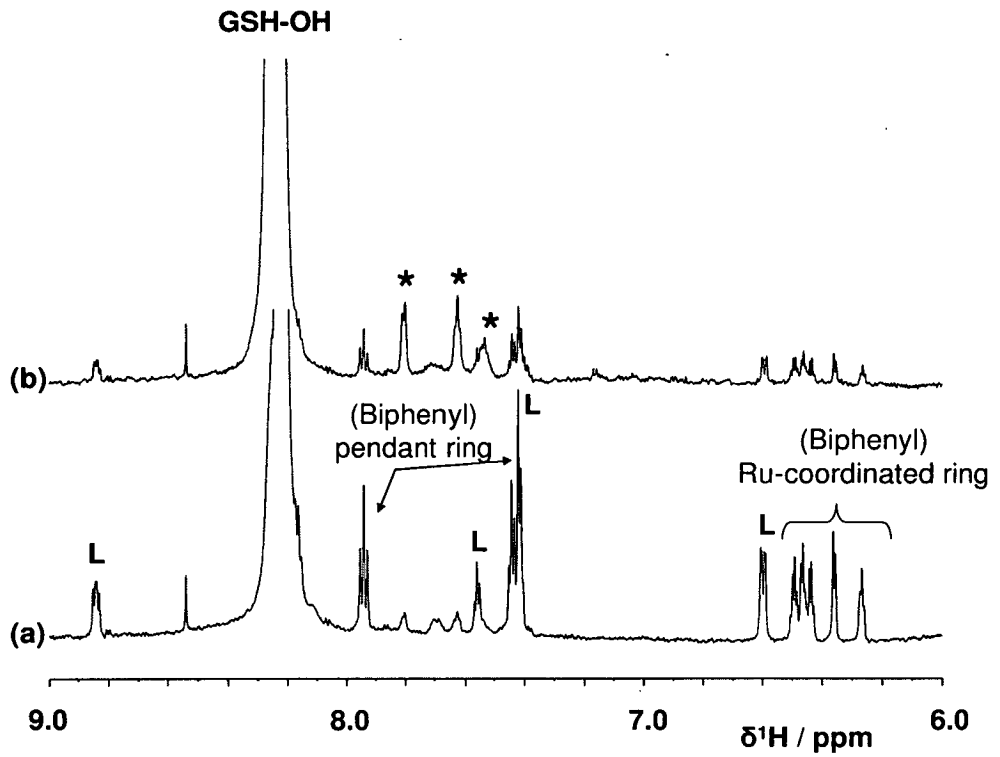

Figure 5.17. The high frequency region ^{1}H NMR spectrum of the reaction of complex **26** and GSH (10 mM GSH, 100 μM **26**, 10 mM phosphate buffer pH 7.2, 85% H_2O, 10% D_2O, 5% acetone-d_6, 310 K) recorded (a) ca. 15 mins after mixing and (b) after 24 h incubation. The peaks corresponding to complex **26** decrease in intensity over time and new peaks corresponding to free biphenyl in aqueous solution appear (marked *). L = ligand resonances (2 resonances appear underneath the GSH-OH peak).

The intensity of the peaks corresponding to the starting complex **26** drop to ca. 35% (as measured by ^{1}H integration) over the 24 h time period. Arene loss is occurring (as evidenced by peaks appearing due to biphenyl) but no new NMR active species are being formed. A similar speciation arises for complex **24**, with ca. 34% remaining after the 24 h time period, and arene loss occurs.

In order to ascertain the mechanism of GSH oxidation, several experiments were confirmed to exclude/try and prove a possible mechanism.

- The catalytic cycle occurred after degassing with either Ar or N_2. This proved that N_2 was not involved in the redox cycle.

- The catalytic cycle occurred when the buffer was phosphate, borate or even when no buffer was present (pH adjusted to ca. 7 with dilute NaOH/HCl). This suggested that the buffer was not playing a role in the redox cycle.
- The catalytic cycle occurred in the presence of 5% methanol-d_4 (instead of 5% acetone-d_6, added to help solubilise the ruthenium compound) which suggested that acetone was not involved in the redox cycle.
- The catalytic cycle also occurred for the corresponding chloride complex suggesting that released iodide (from **24** and **26**, when GS^- displaces I^-) was not involved in the redox cycle. This was further confirmed by adding 100 μM KI to a solution of GSH, where no oxidation of GSH occurred over a 24 h time period.

Under similar conditions neither the free ligands Azpy-NMe_2 nor Azpy-OH caused an oxidation of GSH to GSSG above the control/blank value.

5.3.6 Cytotoxicity

5.3.6.1 A2780, A549 and WI38 Cell Lines

Complexes **23-28** were tested for cytotoxicity towards the A2780 human ovarian cancer, A549 human lung cancer and WI38 human fibroblast (non-cancerous) cell lines (**Table 5.2**). The cytotoxicity data for complex $[(\eta^6\text{-bip})Ru(en)Cl]PF_6$ are also added for a comparison. The free phenylazopyridines were also tested for cytotoxicity towards the A2780 and A549 cancer cell lines only (**Table 5.2**).

Table 5.2. Cytotoxicity data (IC_{50} values) for ruthenium complexes **23-28** and [(η^6-bip)Ru(en)Cl]PF_6 towards the A2780, A549 and WI38 cell lines, phenylazopyridine ligands Azpy, Azpy-NMe2 and Azpy-OH towards the A2780 and A549 cell lines and cytotoxicity for the CDDP control. nd = not determined.

Complex / Ligand	IC_{50} A2870 / μM	IC_{50} A549 / μM	IC_{50} WI38 / μM
23	4	3	5
24	3	2	1
25	4	4	3
26	5	6	1
27	>100	>100	nd
28	39	51	nd
[(η^6-bip)Ru(en)Cl]PF_6	5[14]	2[35]	12
Azpy	>100	14	nd
Azpy-NMe_2	>100	>100	nd
Azpy-OH	>100	>100	nd
CDDP	5	5	6

Complexes **23-26**, containing phenyl rings substituted with electron donating groups on the phenylazopyridine ligand were highly cytotoxic to the A2780 human ovarian and the A549 human lung cancer cell lines with IC_{50} value of 2-6 μM, whereas complexes **27** and **28**, with an un-substituted phenyl ring on the phenylazopyridine ligand are much less cytotoxic (IC_{50} values ca. 40-50 μM (**28**) and >100 μM (**27**). Cytotoxicity data for the free azo ligands are also reported and, with the exception of Azpy-NMe_2 in the A549 cell line, these ligands were inactive.

The ruthenium phenlazopyridine iodido complexes were all slightly more cytotoxic towards the non-cancerous WI38 human lung fibroblast cell line than the cancerous A549 human lung, whilst the cisplatin control was comparably cytotoxic in both cell lines. The ruthenium complex [(η^6-bip)Ru(en)Cl]PF_6 was less toxic towards the non-cancerous cell line.

5.3.6.2 HCT-116 (Wild Type) and HCT116 (p53 Null) Cell Lines

The cytotoxicity of Complex **24** in the HCT-116 Human Colon Cancer cell line (wild type) and its p53 null analogue was evaluated. Cell survival was qualitatively assessed by fixing and staining the remaining (surviving) cells blue after a 24 h

exposure to the ruthenium complex. **Figure 5.18** shows the surviving cells for both cell lines

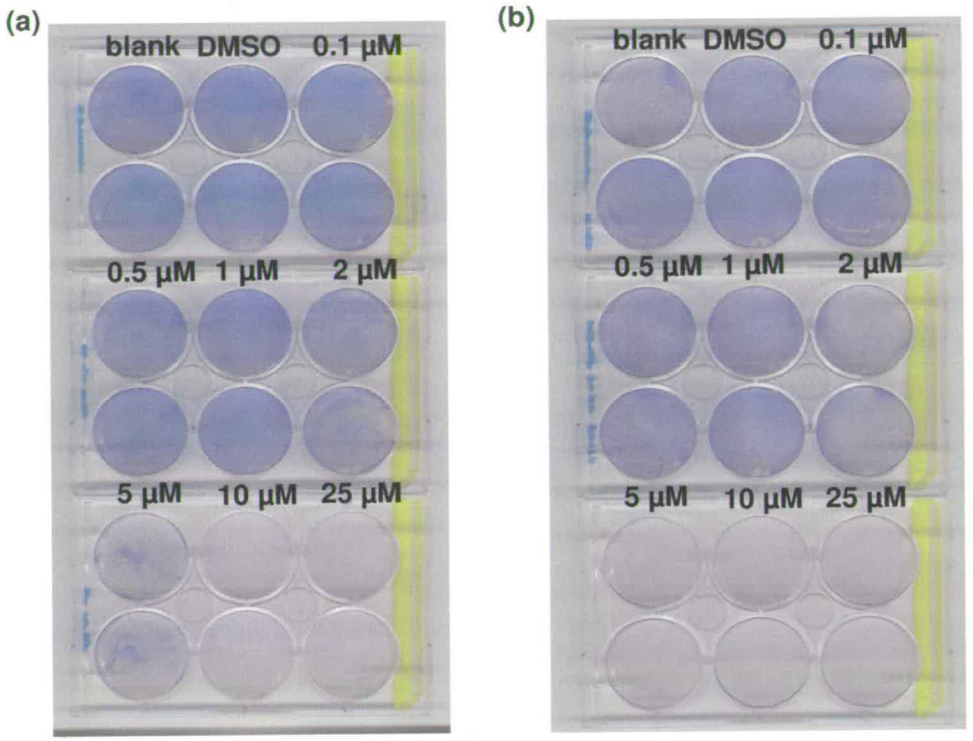

Figure 5.18. Cell survival (biomass stained blue) for (a) HCT-116 (WT) cells after 24 h exposure to ruthenium compound 24 and (b) HCT-116 (p53 null) cells after the same exposure. Concentrations were tested in duplicate.

The complex is very cytotoxic towards both cell lines, with no cells surviving after 25 and 10 µM exposure to the ruthenium compound. Furthermore the complex appears to be slightly more cytotoxic towards the HCT-116 (p53 null) cell line since no cells survived after 5 µM exposure and less cells after the 2 µM exposure whereas for the HCT-116 (WT) cells some cells still surviving after these concentration exposures.

5.3.7 Measurement of Oxidative Stress

5.3.7.1 Detection of Reactive Oxygen species (ROS)

The generation of ROS was detected inside A549 cancer cells over time using the molecular probe dichlorofluorescin-diacetate (DCFH-DA) which crosses the membrane of live cells, and is hydrolysed to dichlorofluorescin (DCFH). In the

presence of ROS it is oxidised to highly fluorescent dichlorofluorescein (DCF).[23] This probe measures general oxidative stress, rather than the detection of any particular ROS and different ROS have a different sensitivity for the probe. **Figure 5.19** shows the increase in fluorescence detected over time after A549 cancer cells were exposed to ruthenium compounds pre-loaded with DCFH-DA.

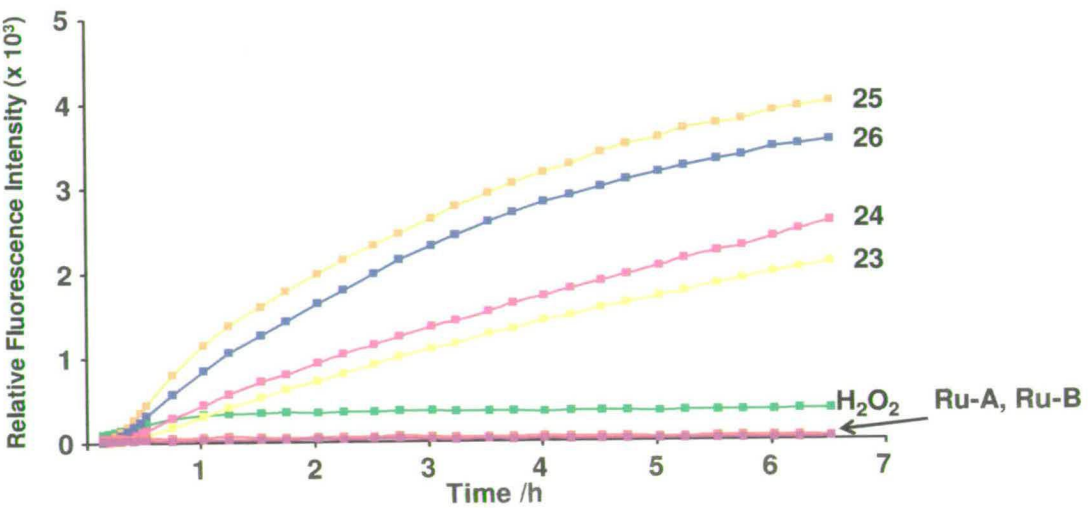

Figure 5.19. Relative increase in DCF fluorescence detected over time after exposure to 25 μM ruthenium compounds (**23-26**), Ru-A ([(η ^{6}-bip)Ru(en)Cl]PF_6), Ru-B ([(η ^{6}-tha)Ru(en)Cl]PF_6) and H_2O_2. For all compounds the fluorescence detected was averaged over 12 wells for each compound (n=12) and a 'blank' value was subtracted.

Compounds **23**, **24**, **25** and **26** all cause an increase in the DCF fluorescence detected with time, indicating that these compounds do generate ROS inside A549 cancer cells. In contrast, neither of the ethylenediamine chelates [(η ^{6}-bip)Ru(en)Cl]PF_6 nor [(η ^{6}-tha)Ru(en)Cl]PF_6 caused an increase in DCF fluorescence above the blank value showing that these two compounds do not generate ROS. The hydrogen peroxide control confirmed that hydrogen peroxide can oxidise the probe, where an increase in DCF fluorescence was observed over ca. 1 h before plateauing.

5.3.7.2 Effect of Increasing Intracellular Thiol Levels

Cell viability was determined in the A549 cancer cells after cells were pre-incubated with 5 mM N-acetly-L-cysteine (NAC) to increase intracellular thiol levels. **Figure**

5.20 shows the cell viability for the four ruthenium compounds (**23-26**) after 24 h incubation with the drug and 96 h recovery time at selected concentrations for both the untreated cells and cells pre-treated with NAC, as well as for the data for the cisplatin control (CDDP).

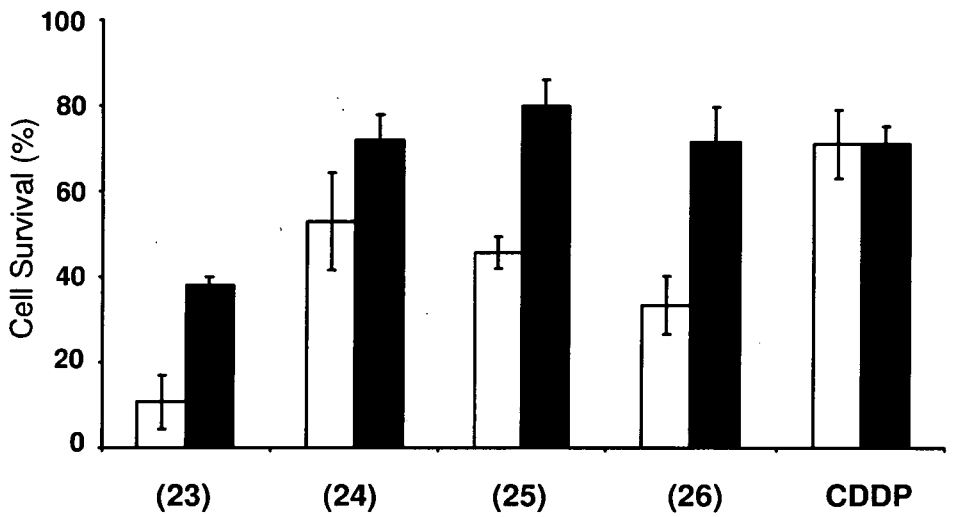

Figure 5.20. Percentage cell survival after 24 h exposure to ruthenium compounds and 96 h recovery at 1 μM (**24**), or 5 μM (**23**, **25**, **26**, CDDP) for untreated A549 cancer cells (lighter) and A549 cancer cells pre-treated with 5 mM NAC for 2 h prior to drug addition to increase intracellular thiol levels (darker). The error bars are the standard deviations from an average of three wells.

There is a greater cell survival for the cells that have increased thiol levels and have been exposed to ruthenium compounds whereas the cisplatin control remained unaffected by pre-supplementing the cells with NAC.

5.3.8 p53 and p21 Status

5.3.8.1 p53 levels and phosphorylation of p53 at Ser-15 and Ser-392

The activation of p53 protein by phosphorylation at sites serine-15 and serine-392 in HCT116 (WT) cells after exposure to different concentrations of complex **24** (0.1-5 μM) for 24 h was determined by immunoblotting. Total p53 levels were also determined, to confirm the presence of p53. **Figure 5.21** shows the immunoblots obtained.

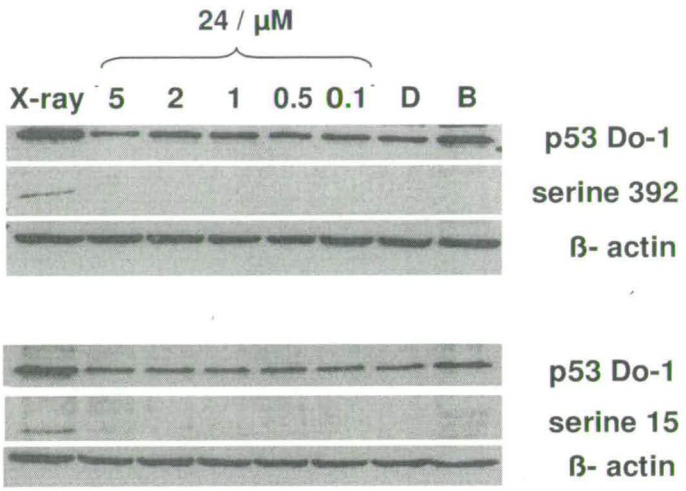

Figure 5.21. Western immunoblot analysis for p53 Do-1, p53 serineine-392 and p53 ser-15 after exposure to ruthenium compound 24 at different (μM) concentrations (5-0.1), a positive control (X-ray), DMSO (0.05% v/v) control (D) and a blank control (B). Equal protein loading was confirmed by blotting for β-actin.

The results show that no activation of p53 via phosphorylation at either serine-15 or serine-392 occurred after exposure to complex **24**. The p53 levels appeared constant (neither up nor down-regulated) irrespective of the concentration of ruthenium used.

5.3.8.2 p21 Levels

The levels of p21 protein was also determined, see **Figure 5.22**.

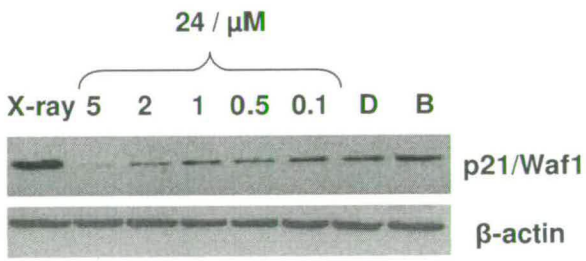

Figure 5.22. Western immunoblot analysis for p21/Waf1 after exposure to ruthenium compound 24 at different (μM) concentrations (5-0.1), a positive control (X-ray), DMSO (0.05% v/v) control (D) and a blank control (B). Equal protein loading was confirmed by blotting for β-actin.

Surprisingly increasing the concentration of complex **24** given to the HCT-116 cancer cell line decreased the level of p21 protein present.

5.4 Discussion

5.4.1 Complexes 23-26 are cytotoxic, despite the lack of hydrolysis

The cytotoxic compounds **23-26** are all resistant to hydrolysis over 24 h at 310 K and at micromolar (μM) concentrations and a physiological pH. Previous work has shown that the rate of hydrolysis of Ru-Cl in $[(\eta^6\text{-arene})Ru(XY)Cl]^n$ complexes can be controlled by changing the nature of the bonding of the chelate XY to the ruthenium centre[15, 36] and in particular slower hydrolysis can be achieved through incorporation of a π-acceptor ligand.[32, 37] In the design of metal-based anticancer drugs, however, a 'labile group' was often thought necessary for activity since it allowed the complex to be able to bind to DNA, the cellular target for most metal-based drugs. Examples of cytotoxic ruthenium complexes that do not hydrolyse are scarce in the literature and are mainly limited to complexes containing planar aromatic ligands that are cytotoxic by DNA intercalation.[38-40] Other examples of ruthenium(II) arene complexes containing carboxylate ligands such as $[(\eta^6\text{-p-cym})Ru(C_6H_6O_4)(PTA)]$ (PTA = 1,3,5-triaza-7-phosphatricyclo[3.3.1.1]-decane) are reportedly inert to hydrolysis in an aqueous solution yet still retain cytotoxicity comparable to the chlorido analogues ($[(\eta^6\text{-p-cym})Ru(Cl_2)(PTA)]$). The solution chemistry, however, was investigated at 293 K at mM concentrations and the time period over which the solution chemistry was followed was not specified, and so comparisons between the system and the complexes studied in this chapter cannot be drawn. Furthermore, upon reaction with ss 14mer (5'-ATACATGGTACATA-3') the ruthenium-arene carboxylate complex loses its carboxylate ligand to form similar adducts to the chloride analogues. The ruthenium(II) arene thiophenolate complex $[(\eta^6\text{-hmb})Ru(en)(SPh)]^+$ does not undergo hydrolysis in aqueous solution yet is cytotoxic towards A2780 cancer cells.[41] Current work into this anomaly suggests that the complex may initially be activated by oxidation (and then labilisation) of the thiol group.[42]

Thus this resistance to hydrolysis is interesting since current structure activity relationships would predict that, on the basis of inertness towards hydrolysis, these complexes would be inactive, and not exhibit good cytotoxicity towards both cell lines as the experimental results showed.

The ruthenium (II) arene complexes containing the un-substituted phenylazopyridine ligand azpy (complexes **27** and **28**) were not as cytotoxic towards the two cancer cell lines. In phosphate-buffered solutions, however, the complexes were unstable and formed a new species and so the instability of these two complexes is likely to account for the lack of observed cytotoxicity. Phosphate can act as a ligand for ruthenium complexes. For example, in the reaction of [(η^6-bip)Ru(en)Cl]+ with 5'-GMP (guanosine monophosphate) in phosphate buffer it was found that phosphate can act as a competitive ligand for binding to the ruthenium centre.[43]

5.4.2 Substitution of iodide for chloride dramatically increases the cytotoxicity of the [(η^6-arene)Ru(azpy-R)X]$^+$ complexes and this may be due to the extra stability of Ru-I vs. Ru-Cl

The iodide complexes are much more cytotoxic than the corresponding chloride complexes (Chapter 3) and this trend was initially thought to be unusual since it is not observed for the [(η^6-arene)Ru(en)X]$^+$ complexes. IC_{50} values are of a similar magnitude no matter whether the halide is Cl^- or I^- (e.g. [(η^6-benzene)Ru(en)Cl]PF_6, IC_{50} = 17 μM, [(η^6-benzene)Ru(en)I]PF_6, IC_{50} = 20 μM)[41] because in the presence of a large excess of NaCl (such as the cell medium), Ru-I bonds are substituted to Ru-Cl. The reaction of complex **24** with excess NaCl followed by UV-Vis spectroscopy showed, however, that exchange of iodide for chloride does not occur in the corresponding phenylazopyridine complexes. Furthermore the solution chemistry of the corresponding chloride complexes[32] shows that the complexes are less stable in water with slow hydrolysis of Ru-Cl and Ru-arene bonds ($t_{1/2}$ 9-21 h). The extra stability of the cation is obviously desirable for cytotoxicity.

The extra stability of the iodido complexes is due to iodide being a less electronegative ligand than chloride and behaving more like a simple two electron donor ligand to form a stronger bond to ruthenium, resulting in increased electron

density at the ruthenium centre available for back donation into the arene ring; hence a stronger ruthenium arene bond and no observable hydrolysis.

Reactions of complex $[(\eta^6\text{-biphenyl})Ru(azpy\text{-}NMe_2)I]PF_6$, (**24**) and the corresponding chloride complex $[(\eta^6\text{-biphenyl})Ru(azpy\text{-}NMe_2)Cl]PF_6$ (**8**) with GSH demonstrated that the chloride ligand is much more rapidly displaced by GS^- than the iodide ligand (rate of substitution ca. 14 times greater for **8** c.f. **24**). A major protective role of GSH is to act as a detoxifier of electrophilic substances such as metals via conjugation to form the thioether GS-X, X = electrophilic substance,[44, 45] and these conjugates can then be eliminated via an ATP-dependent GS-X pump.[46] GS-conjugation is the major deactivation mechanism for platinum complexes such as cisplatin.[47] The greater resistance of the Ru-I bond to conjugation to and possible detoxification by GSH compared with Ru-Cl in the complexes may be a further reason why the iodide complexes are much more cytotoxic since this would result in an overall greater uptake of ruthenium into the cells.

5.4.3 The coordination of the phenylazopyridine ligands to the arene-ruthenium iodido centre generates a redox active site biologically accessible to ascorbate

Phenylazopyridine ligands are well known potential electron transfer centres and each ligand can accept two electrons in one electrochemically accessible LUMO which is primarily azo in character.[48] Coordination of these ligands to the ruthenium's positive metal centre should allow for the ligand based reduction to occur at a much more positive potential; for example the first electrochemical reduction of azpy found it to occur at -1.31 V,[27][49] which is shifted significantly positive in the ruthenium phenylazopyridine complexes studied here (-0.22 V (27) and -0.18 V (28)). Reactions of Azpy-NMe_2 and Azpy-OH with ascorbate showed that ascorbate was not capable of reducing the ligands, however reduction of the ruthenium complexes by ascorbate occurred fairly rapidly.

^{1}H NMR studies of the reduction of the complexes by ascorbate showed that the rate-determining-step corresponded to loss of arene from the complex. Unfortunately, the absence of well defined product peaks in the NMR suggested that the reduced complex was unstable or paramagnetic, and as a result it could not be characterised

by this method. However, the UV-Vis spectrum after the reaction had gone into completion, still showed the presence of the intraligand $\pi \rightarrow \pi^*$ transitions indicating that the azo N=N moiety had not been reduced. Reduction to the hydrazo NH-NH would have resulted in loss of colour.

A reduction of arene hapticity from $\eta^6 \rightarrow \eta^4$ of the η^6-arene in ruthenium-arene sandwich complexes can occur upon electrochemical reduction at the metal centre due to ring slippage as a consequence of the metal re-attaining its 18 electron configuration.[50, 51] Thus addition of electron(s) into the LUMO centred on the azo π^* orbital, followed by the electron 'hopping' on to the ruthenium center causing loss of arene due to reduced hapticity coordination as a result of the extra electron(s) at the metal centre may be the reaction that is occurring but this needs further investigation.

5.4.4 Ruthenium Complexes 24 and 26 catalytically oxidise GSH to GSSG unlike the free ligands Azpy-NMe_2 and Azpy-OH

Glutathione (GSH) is the primary cellular antioxidant and is present in mM concentrations inside cells (ca. 2-10 mM).[44, 52] GSH can neutralise ROS via its oxidation to GSSG.[53] Here it is shown that under physiologically relevant conditions (100 μM Ru, 310 K, pH 7.5, 10 mM GSH) the ruthenium compounds can deplete GSH concentrations slowly over 24 h by catalytically oxidising it to the corresponding disulfide GSSG.

A proposed reaction scheme for this oxidation is shown in **Figure 5.23**.

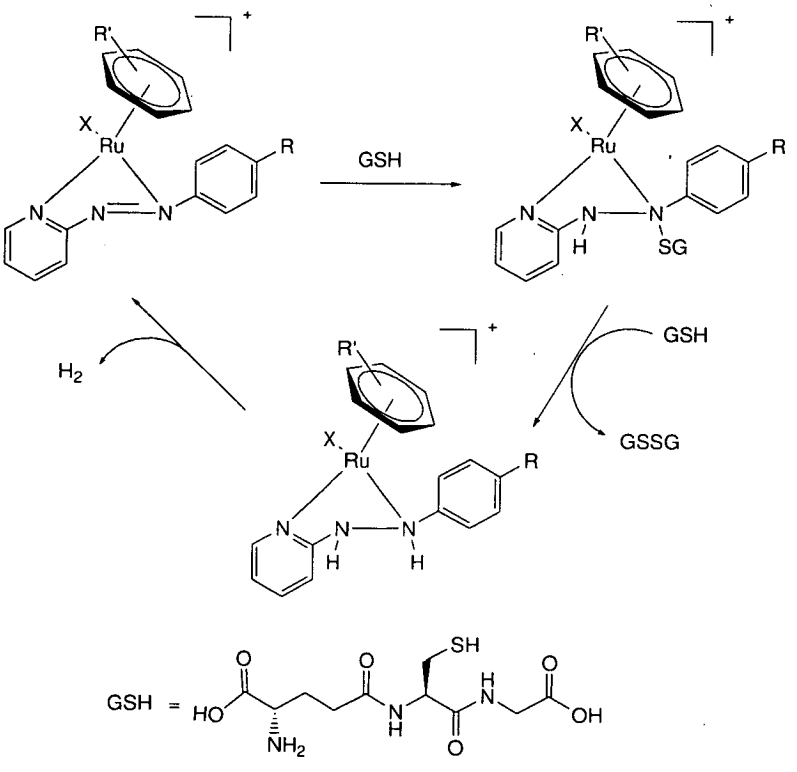

Figure 5.23. Proposed catalytic cycle for the catalytic oxidation of GSH to its corresponding disulfide GSSG by ruthenium(II) arene phenylazopyridine complexes.

This oxidation is proposed to proceed via conjugation across the azo double bond and subsequent reduction of the azo group to hydrazo, since this is reported to occur for azo ester ($C_6H_5N{=}NCOOCH_3$)[54] and diamide ($(CH_3)_2NCON{=}NCON(CH_3)_2$)[55] compounds. However for these reactions a stiochiometric amount of complex is required i.e. the compounds are not catalytic. Other examples in the literature of azo groups facilitating the oxidation of GSH include the hodgkins and non-hodgkins lymphoma drug procarbazine ($CH_3NH\text{-}NHCH_2C_6H_4CONHCH(CH_3)_2$), which contains a hydrazo (reduced form of azo group, NH-NH) which is easily oxidised to the corresponding azo compound and re-reduced to hydrazo via GSH oxidation to GSSG.[56] The re-oxidation of the hydrazo group is facilitated by the molecular oxygen present inside cells, and so this catalytic cycle would require O_2 (and upon re-oxidation of the hydrazo compound H_2O_2 is produced). Interestingly in this work oxidation of GSH to GSSG was not facilitated by molecular oxygen; the catalytic

oxidation took place in solutions that were thoroughly degassed with N_2/Ar to remove any dissolved oxygen.

In order for the reaction to be catalytic, a net H_2 (i.e. $2H^+ + 2e^-$) is lost from the system (from GSH→GSSG + $2H^+ + 2e^-$). The hydrogen could be lost as either H_2 or $2H^•$ (if it was lost as H^- and H^+, hydride (H^-) would react with water to generate H_2 and OH^- so this would be the same as H_2 loss). The reaction of hydrogen radicals with GSH is reported to produce H_2S as a product,[57] which would be observable by ^1H NMR (singlet at ca. 0.7 ppm). It is clear that nothing in the solution is being reduced since the reaction still proceeds in the absence of buffer and acetone-d_6, water is in its most reduced state, the GSH is only present as two species, GSH and GSSG. Attempts to detect H_2 production (or otherwise) from the system are ongoing.

This catalytic cycle is of potential therapeutic importance as a mechanism of cytotoxic action since it does not require molecular oxygen for activation, because tumours are hypoxic environments.[58]

BSO (Buthionine sulfoximine), is an anticancer drug which inhibits the rate limiting enzyme γ-glutamylcysteine synthetase in the synthesis of glutathione thus restoring the sensitivity to the oxidative cytotoxic effects of platinum compounds and alkylators.[59] The role of BSO as an anticancer agent is thought to relate to its modulation of cytotoxicity via GSH depletion.[60]

The oxidation of GSH to GSSG was not observed for the free ligands and this is not surprising since electron-donating groups (here NMe_2, OH) attached to the azo group decrease the ability for it to oxidise GSH;[30] coordination to the ruthenium centre must make the azo nitrogens positive enough for the redox reaction to occur.

5.4.5 A build up of Reactive Oxygen Species occurs inside A549 cancer cells

Reactive Oxygen Species derive and present a higher reactivity than molecular oxygen with redox activity.[61] The term not only encompasses free radicals such as the superoxide radical ($O_2^{•-}$), hydroperoxyl radical ($HO_2^•$) and the hydroxyl radical (HO•) but also non-radicals such at hydrogen peroxide (H_2O_2) and singlet oxygen ($^1O_2$). ROS are continuously generated in small quantities in normal cellular processes and are involved in several biological functions such as cell growth and

signalling.[61] Metal complexes that are redox active can generate ROS inside cells due to undergoing several possible redox reactions including Fenton type reactions, Haber-Weiss type reactions and also reactions with biological antioxidants.[62, 63] Excessive ROS generation inside cells is very harmful causing the oxidation of bio-molecules such as lipids, cell membranes, proteins and DNA, which results in a phenomenon called oxidative stress.[61]

The detection of DCF fluorescence in A549 cancer cells after exposure to complexes **23-26** confirmed that these compounds cause an increase in ROS production. Fluorescence was detected from the first reading and increased steadily for the 6.5 h acquisition period. The greater increase in fluorescence observed for **25** and **26** vs. **23** and **24** may be due to faster cellular uptake for the former; The pK_a of the phenolic OH in **25** was determined as 6.50 so that at physiological pH these complexes should be neutral in charge and this may facilitate faster uptake into the cells[64] compared with **23** and **24** which bear a positive charge. Importantly, no DCF fluorescence was detected for ruthenium arene complexes containing the ethylenediamine (en) chelating ligands and this result potentially illustrates a fundamental difference in the mechanisms of action of these two classes (azpy/en).

5.4.6 Oxidative Stress is an important factor contributing to cell death

Oxidative stress occurs due to a serious imbalance between the levels of ROS in a cell and its antioxidant defences in favour of the former.[65] In this work we have shown that the ruthenium complexes **23-26** cause a build up of ROS over time in A549 cancer cells. This could be due to (1) reduction of the complex *in vitro* which will generate ROS directly (*vide supra*) or (2) by depletion of the cells antioxidant capacity, which reduces the ability of the cell to neutralise ROS causing a build up. It is likely, on the basis that GSH is the primary cellular antioxidant, that the depletion of antioxidants is the primary mechanism by which oxidative stress occurs. Evidence for the direct effect of increased ROS levels on cell death is from the cell viability comparison of A549 cancer cells with / without pre-incubation with N-acetylcysteine (NAC). The antioxidant NAC is believed to act by raising intracellular concentrations of cysteine (and hence GSH) and also by interacting directly to neutralize ROS via its SH group.[66] Several reports thus show that NAC

can protect against ROS dependent cell death.[67-70] The results showed that the cells with increased thiol levels were more tolerant to exposure to the ruthenium-arene-phenylazopyridine compounds where an increase in cell survival was noted in all cases. So this result provides evidence that oxidative stress, by increasing ROS levels, is implicated in cell death.

The cisplatin control appeared un-affected by pre-incubation of the cells with NAC. Cisplatin exerts its cytotoxic action primarilly by binding to DNA to form covalent DNA adducts.[71] In addition it is also shown to generate ROS.[72] However, experiments studying the effects of cisplatin on GSH concentrations in A549 cancer cells have shown that increased thiol levels result due to cisplatin exposure anyway[73, 74] and separate in vitro experiments showed NAC only protected against cisplatin induced apoptosis when it was present in the cell medium with cisplatin, and chempoprotection was lost if it was removed from the cells prior to cisplatin treatment.[75] This result is in agreement with the results obtained in this Chapter.

5.4.7 Precedence for anticancer drugs that cause an increase in ROS

The relationship between the generation of ROS and the cause of cancer undoubtedly exists, thought to be due to the ability of ROS to damage DNA and alter intracellular signalling.[76] However, the involvement of excessive ROS production in the induction of senescence,[77] the fact that an increase in cell proliferation rate of normal cells due to elevated ROS pools was not sufficient to induce malignant transformation,[78] and that cancer cells (mainly multi-drug resistant cells) are more sensitive to the additional exposure to ROS than normal cells[78] has recently led to the suggestion of using ROS therapeutically to treat cancer.[56, 78] It is thus, perhaps not surprising that several established anticancer drugs have been shown to generate ROS or other radicals including adriamycin[79], cisplatin[72] and arsenic trioxide,[80] to name but a few.

Interestingly the Ru^{III} complex $[InH][RuCl_4(In)_2]$ (In = indazole) or KP-1019 which is active against primary tumours,[81] is 'activated by reduction' via a metal based reduction from Ru^{III} to Ru^{II} and the corresponding Ru^{II} species are supposed to coordinate more rapidly to biomolecules due to the labilisation of the Ru^{II}-Cl bond.[81] The cytotoxic action of KP1019 is put down to reaction with DNA to

various extents, but ROS were detected in colorectal tumour cells suggesting that the reduction to Ru^{II} generated ROS and that oxidative stress may be implicated in its mechanism of action.[82]

5.4.8 The role of p53 and p21/Waf1 proteins

The p53 protein is the major tumour suppressor protein in the body.[83] The importance of p53 for preventing cancer is highlighted by that fact that p53 is inactivated in almost 50% of all human tumours.[83] Wild-type (WT) p53 is of fundamental importance in cutaneous defence against genotoxic stress and becomes activated in cells damaged by exposure to a wide range of environmental agents, including ionising radiation.[84] In response to DNA damage, post-translational modifications and/or accumulation of p53 protein enable specific DNA binding to p53 and subsequent control of cell growth arrest, thereby reducing the risk of accumulation of genetically aberrant cells.[84] Post-translational modifications most commonly occur via phosphorylation (17 serine and three threonine residues) but can also occur by other mechanisms including acetylation and ubiquitination.[83]

In this work, activation of p53 via phosphorylation at the ATM kinase site at serine-15 and the CK2/FACT kinase site at serine-392[85] was investigated. The data showed that in the presence of increasing amounts of the highly cytotoxic compound $[(\eta^6\text{-biphenyl})Ru(azpy\text{-}NMe_2)I]PF_6$, (**24**) no evidence of p53 phosphorlyation (activation) at these two sites had occurred. Furthermore, total p53 levels were unaffected by exposure to increasing amounts of complex **24** suggesting no increase in p53 accumulation, and this result is in direct contrast to the dose-dependent accumulation of p53 detected in this cell line after exposure to increasing amounts of $[(\eta^6\text{-biphenyl})Ru(en)Cl]PF_6$.[21] The ruthenium complex **24** was found to be more cytotoxic towards the p53-null cell line than the WT and again, this is in contrast to $[(\eta^6\text{-biphenyl})Ru(en)Cl]PF_6$ where p53-null HCT116 cells were twofold more resistant to 24 h $[(\eta^6\text{-biphenyl})Ru(en)Cl]PF_6$ exposure (IC_{50} p53-WT 8 μM, p53-null 16 μM). These results together suggest that, unlike $[(\eta^6\text{-biphenyl})Ru(en)Cl]PF_6$, p53 is not required to be activated/accumulated for the mechanism of cell kill.

Interestingly, the action of p53 is reportedly intimately linked with RS (ROS).[76] ROS can increase p53 activity but if too many ROS are generated they can inhibit

p53 action. p53 has ten cysteine residues, some of which are involved in binding a zinc ion which is required for activity. Oxidation of these cysteine residues inhibits the action of p53 as a transcription factor.[76] Oxidative inactivation of p53 will in turn raise ROS levels since the normal low levels of active p53 are involved in maintaining the cellular antioxidant defence network.[76, 86] In this work the oxidation of glutathione cysteine residues to their corresponding disulfide was found to occur catalytically by ruthenium compound **24** and so it is possible that this compound could oxidise the p53 protein which would lead to its inactivation (and hence its non-activation by phosphorlyation).

The p21/Waf1 levels were down regulated with exposure to increasing amounts of 24 which, again is a different cellular response to $[(\eta^6\text{-biphenyl})Ru(en)Cl]PF_6$, which caused a dose-dependent increase in p21 levels.[21] p21/Waf1 belongs to the Cip/Kip family of cyclin kinase inhibitors (CKI). p21 expression is usually controlled by either the p53-dependent or the p53-independent pathway.[87] It is not easy to describe the exact function of p21 due to its vast array of regulatory pathways and interactions, however its main function is as a checkpoint in the cell cycle by inhibiting cyclin-dependent kinases at the G1/S and G2/M interfaces.[87] p21 is a modifier of apoptosis and it has been shown to both promote and inhibit apoptosis although it generally counteracts the apoptotic process.[87] An agent which down-regulates p53 will also down regulate p21[88] but in these experiments p53 levels remained unaffected.

Overall these results show that not only do the ruthenium-azo complexes have a different primary mechanism of cytotoxicity (i.e. not involving simple hydrolysis and DNA binding) but the further 'downstream' cellular signalling effects are also different. Furthermore, oxidation of p53 and its subsequent deactivation may occur since ROS are produced.

5.5 Summary

Ruthenium(II) arene complexes show a great scope for the design of potential anticancer drugs due to the many modifications that can be made to the structure of the complex and the corresponding changes in properties that occur as a result. Here we show that the attachment of redox-active (generally) non-cytotoxic

phenylazopyridine ligands to the {(η-^{6}arene)RuX}ruthenium-arene centre results in highly cytotoxic complexes when X = iodide. Oxidative stress (increase in production of ROS and/or depletion of antioxidants) is responsible for cell death since the complexes not only potentially generate ROS *in vitro* via ligand based reduction but also catalytically oxidise GSH to GSSG thus depleting antioxidant concentrations. These complexes are stable in aqueous solution and do not undergo hydrolysis, a feature quite unusual for metal based anticancer drugs. The corresponding chloride complexes, which are not as stable in aqueous solution (undergo slow reaction via hydrolysis of Ru-arene and Ru-Cl) are not as cytotoxic suggesting that increased stability of the Ru-I bond correlates with increased cytotoxicity. Overall these complexes have a different mechanism of action compared to the ethylenediamine analogues, evidenced from the lack of ROS produced for when the chelating ligand is en, and the different 'downstream' pathways that are (de)activated.

5.6 References

[1] J. Halpern, *Pure Appl. Chem.* **2001**, *73*, 209-220.

[2] A. Korfel, M. E. Scheulen, H.-J. Schmoll, O. Grundel, A. Harstrick, M. Knoche, L. M. Fels, M. Skorzec, F. Bach, J. Baumgart, G. Sass, S. Seeber, E. Thiel, W. E. Berdel, *Clin. Cancer Res.* **1998**, *4*, 2701-2708.

[3] N. Kröger, U. R. Kleeberg, K. Mross, L. Edler, D. K. Hossfeld, *Onkologie* **2000**, *23*, 60-62.

[4] P. W. Causey, M. C. Baird, S. P. C. Cole, *Organometallics* **2004**, *23*, 4486-4494.

[5] R. Meyer, S. Brink, C. E. J. van Rensburg, G. K. Joone, H. Goerls, S. Lotz, *J. Organomet. Chem.* **2005**, *690*, 117-125.

[6] G. D. Potter, M. C. Baird, M. Chan, S. P. C. Cole, *Inorg. Chem. Commun.* **2006**, *9*, 1114-1116.

[7] K. O'Connor, C. Gill, M. Tacke, F. J. K. Rehmann, K. Strohfeldt, N. Sweeney, J. M. Fitzpatrick, R. W. G. Watson, *Apoptosis* **2006**, *11*, 1205-1214.

[8] N. Sweeney, W. M. Gallagher, H. Mueller-Bunz, C. Pampillon, K. Strohfeldt, M. Tacke, *J. Inorg. Biochem.* **2006**, *100*, 1479-1486.

[9] C. Pampillon, N. J. Sweeney, K. Strohfeldt, M. Tacke, *Inorg. Chim. Acta* **2006**, *359*, 3969-3975.

[10] S. Top, A. Vessieres, G. Leclercq, J. Quivy, J. Tang, J. Vaissermann, M. Huche, G. Jaouen, *Chem. Eur. J.* **2003**, *9*, 5223-5236.

[11] A. Vessieres, S. Top, P. Pigeon, E. Hillard, L. Boubeker, D. Spera, G. Jaouen, *J. Med. Chem.* **2005**, *48*, 3937-3940.

[12] A. Vessieres, S. Top, W. Beck, E. Hillard, G. Jaouen, *Dalton Trans.* **2006**, 529-541.

[13] R. E. Morris, R. E. Aird, P. d. S. Murdoch, H. Chen, J. Cummings, N. D. Hughes, S. Parsons, A. Parkin, G. Boyd, D. I. Jodrell, P. J. Sadler, *J. Med. Chem.* **2001**, *44*, 3616-3621.

[14] R. E. Aird, J. Cummings, A. A. Ritchie, M. Muir, R. E. Morris, H. Chen, P. J. Sadler, D. I. Jodrell, *Br. J. Cancer* **2002**, *86*, 1652-1657.

[15] F. Wang, H. Chen, S. Parsons, I. D. H. Oswald, J. E. Davidson, P. J. Sadler, *Chem. Eur. J* **2003**, *9*, 5810-5820.

[16] H. Chen, J. A. Parkinson, O. Novakova, J. Bella, F. Wang, A. Dawson, R. Gould, S. Parsons, V. Brabec, P. J. Sadler, *Proc. Natl. Acad. Sci. U. S. A.* **2003**, *100*, 14623-14628.

[17] O. Novakova, H. Chen, O. Vrana, A. Rodger, P. J. Sadler, V. Brabec, *Biochemistry* **2003**, *42*, 11544-11554.

[18] O. Novakova, J. Kasparkova, V. Bursova, C. Hofr, M. Vojtiskova, H. Chen, P. J. Sadler, V. Brabec, *Chem. Biol.* **2005**, *12*, 121-129.

[19] H.-K. Liu, S. J. Berners-Price, F. Wang, J. A. Parkinson, J. Xu, J. Bella, P. J. Sadler, *Angew. Chem. Int. Ed.* **2006**, *45*, 8153-8156.

[20] L. H.-K. Liu, F. Wang, J. A. Parkinson, J. Bella, P. J. Sadler, *Chem. Eur. J* **2006**, *12*, 6151-6165.

[21] R. L. Hayward, Q. C. Schornagel, R. Tente, J. S. Macpherson, R. E. Aird, S. Guichard, A. Habtemariam, P. Sadler, D. I. Jodrell, *Cancer Chemother. Pharmacol.* **2005**, *55*, 577-583.

[22] H. Chen, J. A. Parkinson, S. Parsons, R. A. Coxall, R. O. Gould, P. J. Sadler, *J. Am. Chem. Soc.* **2002**, *124*, 3064-3082.

[23] H. Wang, J. A. Joseph, *Free Radic. Biol. Med.* **1999**, *27*, 612-616.

[24] F. M. Moodie, J. A. Marwick, C. S. Anderson, P. Szulakowski, S. K. Bioswas, M. R. Bauter, I. Kilty, I. Rahman, *FASEB J.* **2004**, *18*, 1897-1899, 1810 1096/fj 1804-1506fje.

[25] G. Cappelletti, M. G. Maggioni, R. Maci, *Cell Biol. Int.* **1998**, *22*, 671-678.

[26] S. Goswami, A. R. Chakravarty, A. Chakravorty, *Inorg. Chem.* **1981**, *20*, 2246-2250.

[27] S. Goswami, R. Mukherjee, A. Chakravorty, *Inorg. Chem.* **1983**, *22*, 2825-2832.

[28] G. K. Lahiri, S. Bhattacharya, S. Goswami, A. Chakravorty, *J.Chem.l Soc.; Dalton Trans.* **1990**, 561-565.

[29] R. A. Krause, K. Krause, *Inorg. Chem.* **1984**, *23*, 2195-2198.

[30] *The Chemistry of Hydrazo, Azo and Azoxy Groups, Vol. Part 1*, John Wiley & Sons, Bristol, UK, **1975**.

[31] P. Schluga, C. G. Hartinger, A. Egger, E. Reisner, M. Galanski, M. A. Jakupec, B. K. Keppler, *Dalton Trans.* **2006**, 1796-1802.

[32] S. J. Dougan, M. Melchart, A. Habtemariam, S. Parsons, P. J. Sadler, *Inorg. Chem.* **2006**, *45*, 10882-10894.

[33] The initial increase was too fast to measure to get accurate rate data. This initial increase in intensity was thus followed at a lower temperature (298 K) where the t1/2 values determined were independent of the excess of ascorbate concentration used.

[34] T. Nakayama, T. Isobe, K. Nakamiya, J. S. Edmonds, Y. Shibata, M. Morita, *Magn. Reson. Chem.* **2005**, *43*, 543-550.

[35] S. M. Guichard, R. Else, E. Reid, B. Zeitlin, R. Aird, M. Muir, M. Dodds, H. Fiebig, P. J. Sadler, D. I. Jodrell, *Biochem. Pharmacol.* **2006**, *71*, 408-415.

[36] R. Fernandez, M. Melchart, A. Habtemariam, S. Parsons, P. J. Sadler, *Chem. Eur. J* **2004**, *10*, 5173-5179.

[37] L. Dadci, H. Elias, U. Frey, A. Hoernig, U. Koelle, A. E. Merbach, H. Paulus, J. S. Schneider, *Inorg. Chem.* **1995**, *34*, 306-315.

[38] K. K. Patel, E. A. Plummer, M. Darwish, A. Rodger, M. J. Hannon, *J. Inorg. Biochem.* **2002**, *91*, 220-229.

[39] W. F. Schmid, S. Zorbas-Seifried, R. O. John, V. B. Arion, M. A. Jakupec, A. Roller, M. Galanski, I. Chiorescu, H. Zorbas, B. K. Keppler, *Inorg. Chem.* **2007**, *46*, 3645-3656.

[40] N. J. Wheate, C. R. Brodie, J. G. Collins, S. Kemp, J. R. Aldrich-Wright, *Mini-Rev. Med. Chem.* **2007**, *7*, 627-648.

[41] F. Wang, A. Habtemariam, E. P. L. van der Geer, R. Fernandez, M. Melchart, R. J. Deeth, R. Aird, S. Guichard, F. P. A. Fabbiani, P. Lozano-Casal, I. D. H. Oswald, D. I. Jodrell, S. Parsons, P. J. Sadler, *Proc. Natl. Acad. Sci. U. S. A.* **2005**, *102*, 18269-18274.

[42] Jingjing Xu, Fuyi Wang, Holm Petzhold, Peter J. Sadler, unpublished results

[43] H. Chen, J. A. Parkinson, R. E. Morris, P. J. Sadler, *J. Am. Chem. Soc.* **2003**, *125*, 173-186.

[44] A. Meister, M. E. Anderson, *Annu. Rev. Biochem.* **1983**, *52*, 711-760.

[45] G. J. Mulder, S. Ouwerkerk-Mahadevan, *Chem.-Biol. Interact.* **1997**, *105*, 17-34.

[46] K. Balendiran Ganesaratnam, R. Dabur, D. Fraser, *Cell Biochem Funct.* **2004**, *22*, 343-352.

[47] R. N. Bose, *Mini-Rev. Med. Chem.* **2002**, *2*, 103-111.

[48] B. K. Santra, G. K. Lahiri, *J. Chem. Soc., Dalton Trans.* **1997**, 129-135.

[49] Recorded vs Saturated Calomel electrode in MeCN from reference D. T. Pierce, W. E. Geiger, *J. Am. Chem. Soc.* **1992**, 114, 6063-6073. In order to convert to a potential relative to Ag/AgCl +0.045 V should be added.

[50] R. G. Finke, R. H. Voegeli, E. D. Laganis, V. Boekelheide, *Organometallics* **1983**, *2*, 347-350.

[51] D. T. Pierce, W. E. Geiger, *J. Am. Chem. Soc.* **1992**, *114*, 6063-6073.

[52] M. Valko, C. J. Rhodes, J. Moncol, M. Izakovic, M. Mazur, *Chem.-Biol. Interact.* **2006**, *160*, 1-40.

[53] R. Masella, R. Di Benedetto, R. Vari, C. Filesi, C. Giovannini, *Journal of Nutritional Biochemistry* **2005**, *16*, 577-586.

[54] E. M. Kosower, N. S. Kosower, *Nature* **1969**, *224*, 117-120.

[55] N. S. Kosower, E. M. Kosower, B. Wertheim, W. S. Correa, *Biochem. Biophys. Res. Commun.* **1969**, *37*, 593-596.

[56] M. F. Renschler, *Eur. J. Cancer* **2004**, *40*, 1934-1940.

[57] F. E. Littman, E. M. Carr, A. P. Brady, *Radiat Res.* **1957**, *7*, 107-119.

[58] M. J. Clarke, *Coord. Chem. Rev.* **2003**, *236*, 209-233.

[59] H. H. Bailey, *Chem.-Biol. Interact.* **1998**, *111-112*, 239-254.

[60] J. Rothbarth, A. L. Vahrmeijer, G. J. Mulder, *Chem.-Biol. Interact.* **2002**, *140*, 93-107.

[61] A. Gomes, E. Fernandes, L. F. C. Lima Jose, *J Biochem Biophys Methods.* **2005**, *65*, 45-80.

[62] M. Valko, D. Leibfritz, J. Moncol, M. T. D. Cronin, M. Mazur, J. Telser, *Int. J. Biochem. Cell Biol.* **2006**, *39*, 44-84.

[63] S. S. Leonard, G. K. Harris, X. Shi, *Free Radic. Biol. Med.* **2004**, *37*, 1921-1942.

[64] N. D. Hammer, S. Lee, B. J. Vesper, K. M. Elseth, B. M. Hoffman, A. G. M. Barrett, J. A. Radosevich, *J. Med. Chem.* **2005**, *48*, 8125-8133.

[65] B. Halliwell, M. Whiteman, *Br. J. Pharmacol.* **2004**, *142*, 231-255.

[66] O. I. Aruoma, B. Halliwell, B. M. Hoey, J. Butler, *Free Radic Biol Med.* **1989**, *6*, 593-597.

[67] M.-L. Aitio, *Br. J. Clin. Pharmacol.* **2006**, *61*, 5-15.

[68] D. J. Chang, G. M. Ringold, R. A. Heller, *Biochem. Biophys. Res. Commun.* **1992**, *188*, 538-546.

[69] M. Zafarullah, W. Q. Li, J. Sylvester, M. Ahmad, *Cell. Mol. Life Sci.* **2003**, *60*, 6-20.

[70] C. Montiel-Duarte, E. Ansorena, M. J. Lopez-Zabalza, E. Cenarruzabeitia, M. J. Iraburu, *Biochem. Pharmacol.* **2004**, *67*, 1025-1033.

[71] E. R. Jamieson, S. J. Lippard, *Chem. Rev.* **1999**, *99*, 2467-2498.

[72] A. Siomek, J. Tujakowski, D. Gackowski, R. Rozalski, M. Foksinski, T. Dziaman, K. Roszkowski, R. Olinski, *Int. J. Cancer* **2006**, *119*, 2228-2230.

[73] M. Skokrzadeh, F. H. Shirazi, M. Abdollahi, A. G. Ebadi, H. Asgarirad, *Pakistan J. Biol. Sci.* **2006**, *9*, 2734-2742.

[74] F. H. Shirazi, M. Skokrzadeh, M. Abdollahi, F. B. Rahimi, L. Hossinzadeh, *Int. J. Biol.Biotech.* **2005**, *2*, 397-402.

[75] Y. J. Wu, L. Muldoon Leslie, A. Neuwelt Edward, *J Pharmacol Exp Ther.* **2005**, *312*, 424-431.

[76] B. Halliwell, *Biochem. J.* **2007**, *401*, 1-11.

[77] M. R. Ramsey, N. E. Sharpless, *Nature Cell Biology* **2006**, *8*, 1213-1215.

[78] E. Agostinelli, N. Seiler, *Amino Acids* **2006**, *31*, 341-355.

[79] S. M. DeAtley, M. Y. Aksenov, M. V. Aksenova, B. Harris, R. Hadley, P. Cole Harper, J. M. Carneya, D. A. Butterfield, *Cancer Lett.* **1999**, *136*, 41-46.

[80] W.-C. Chou, C. Jie, A. A. Kenedy, R. J. Jones, M. A. Trush, C. V. Dang, *Proc. Natl. Acad. Sci. U. S. A.* **2004**, *101*, 4578-4583.

[81] C. G. Hartinger, S. Zorbas-Seifried, M. A. Jakupec, B. Kynast, H. Zorbas, B. K. Keppler, *J. Inorg. Biochem.* **2006**, *100*, 891-904.

[82] S. Kapitza, A. Jakupec Michael, M. Uhl, K. Keppler Bernhard, B. Marian, *Cancer Lett.* **2005**, *226*, 115-121.

[83] L. Romer, C. Klein, A. Dehner, H. Kessler, J. Buchner, *Angew. Chem. Int. Ed.* **2006**, *45*, 6440-6460.

[84] L. E. Finlan, N. M. Kernohan, G. Thomson, P. E. Beattie, T. R. Hupp, S. H. Ibbotson, *Br. J. Dermatol.* **2005**, *153*, 1001-1010.

[85] P. E. Beattie, L. E. Finlan, N. M. Kernohan, G. Thomson, T. R. Hupp, S. H. Ibbotson, *Br. J. Dermatol.* **2005**, *152*, 1001-1008.

[86] A. A. Sablina, A. V. Budanov, G. V. Ilyinskaya, L. S. Agapova, J. E. Kravchenko, P. M. Chumakov, *Nature Medicine* **2005**, *11*, 1306-1313.

[87] R. A. Blundell, *Am. J. Biochem. Biotech.* **2006**, *2*, 33-40.

[88] F. Tang, G. Liu, Z. He, W.-Y. Ma, A. M. Bode, Z. Dong, *Mol. Carcinog.* **2006**, *45*, 861-870.

Chapter 6

Targeting Ruthenium(II) Arene Iodido Azo Complexes to Cancer Cells

6.1 Introduction

Undoubtedly, the biggest drawback to using chemotherapy as a treatment for cancer is that the systematic drug administration likely results in an even distribution of the drug throughout the body leading to a reduced specificity for the desired target site, non-specific toxicity and other side effects resulting from the higher doses required. An attractive and emerging strategy to enhance the therapeutic index is to specifically deliver these cytotoxic agents to the target cancer cells thus keeping them away from the healthy cells, which are also sensitive to the toxic effects of the drug.[1] Currently there are several strategies including polymer-based, liposome-based and ligand-receptor mediated delivery systems.[2]

Another pathway recently been exploited to deliver complexes specifically to cancer cells involves making use of the naturally existing iron-binding protein transferrin (Tf) and the transferrin receptor (TfR)[3-6] since these proteins are biodegradable, non-toxic and nonimmunogenic.[7] Elliot et al. were the first to demonstrate that transferrin could carry cytotoxic agents to the cell, by showing that a cisplatin-transferrin complex (1-2 Pt bound to the Fe site) still inhibited growth towards feline lymphoma and human HeLa cells *in vitro* and also prevented metastatic spread and/or growth of tumors in the lungs of rats carrying the 13672NF mammary carcinoma in vivo.[8] Clinical trials of this platinum-conjugate were attempted.[9]

Transferrins are a family of iron binding proteins whose principal biological properties are thought to be iron binding and transport.[1] The human transferrin protein contains 679 amino acids residues and has a molecular weight of ca. 79 kDa.[10] The Tf molecule is divided into two lobes; the N-lobe (336 amino acids) and the C-lobe (343 amino acids), which are linked by a short space sequence. Each lobe has two domains connected by a hinge, and the domains interact to form a deep hydrophilic metal (Fe) ion-binding site. Both binding sites have four conserved amino acids (two tyrosines, one aspartic acid and one histidine). When the metal is bound it is further stabilised by two oxygen atoms donated from a carbonate anion (the synergistic anion) to stabilise the Fe^{3+} binding.

Iron is an essential metal for life and is involved in DNA synthesis, respiration and key metabolic reactions.[11] However, the levels of iron in the cell must be delicately

balanced as excess iron can lead to free radical damage through Fenton Reactions.[12, 13] Thus transferrin proteins bind circulating Fe and prevent it from travelling throughout the body in its toxic form. In human serum, the concentration of transferrin is about 2.5 mg/mL with 30% occupied by Fe[7] thus there are vacant sites available for coordination with other metals. Transferrins deliver iron into the cell by interaction with the transferrin receptor (TfR1) via a mechanism called endocytosis whereby the iron is internalised through binding to this receptor and a drop in pH to ca. 5 releases the iron from the transferrin and into the cell.

Interestingly the TfR1 appears to be over-expressed in cancer cells due to the cells increased requirement for iron; 10,000 to 100,000 TfR1 molecules per cell are commonly found on tumour cells or cell lines in culture whilst in non-proliferating cells, the expression of TfR1 is low or frequently undetectable.[1] Thus this over-expression thus provides a natural selectivity for cancer cells over healthy cells.

In this Chapter, attempts to attach the highly cytotoxic ruthenium arene complex [(η^6-*p*-cymene)Ru(azpy-OH)I]PF_6 (**25**) to transferrin by the following two different approaches is reported.

Strategy 1 Ester-Maleimide Linker. In the first approach the complex is derivatised at the azo ligand moiety to include an ester and a maleimide group (**Figure 6.1**). The maleimide group can react specifically with thiol (SH) groups on transferrin to allow for attachment to the protein. The ester group should hydrolyse upon endocytosis by acid-catalysed ester hydrolysis[14] liberating the free complex inside the cell.

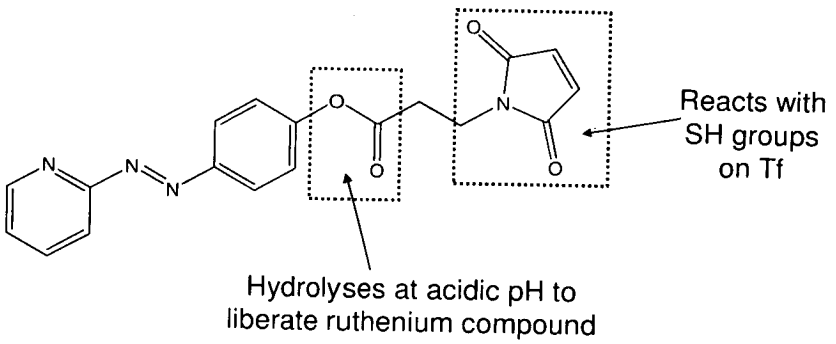

Figure 6.1. Derivatisation of ligand Azpy-OH to allow attachment to transferrin (via maleimide) and release from transferrin (via acid sensitive ester group).

A similar approach has previously been reported for conjugation of the anticancer drug chlorambucil to transferrin.[6] There are no accessible thiol groups on holo-transferrin and so the protein would have to be modified by the introduction of SH groups in order for the complex to bind. This can easily be achieved by using the reagent iminothiolane, which reacts with accessible NH_2 groups on the protein to introduce a thiol function.[15]

Strategy 2, Ru-Transferrin-Conjugate. In the second approach, the complex is bound directly to holo-transferrin in place of the synergistic anion bicarbonate via the phenolate group of complex **25**. Whilst bicarbonate is the synergistic anion *in vivo*, other anions (such as oxalate, malonate, glycolate) with similar physiochemical properties can substitute for carbonate *in-vitro*.[16] It should be noted that whilst these anions are all bidentate oxygen-donor ligands, the phenolate ligand is monodentate. Upon iron release (via endocytosis), the ruthenium complex would also be liberated from the binding site.

6.2 Experimental

6.2.1 Materials

The preparation of the starting materials is reported in previous chapters; [(η6-biphenyl)RuI_2]$_2$ (Chapter 2), Azpy-OH (Chapter 3) and [(η^6-*p*-cym)Ru(azpy-OH)I]PF_6 (Chapter 4). 3-maleimidopropionic acid, dimethylaminopyridine (DMAP),

dicyclohexylcarbodiimide (DCC) and Holo-Transferrin (98%) were purchased from Sigma Aldrich. All other reagents used were obtained from commercial suppliers and used as received. MeCN and DCM were dried over P_2O_5 or anhydrous quality was used.

6.2.2 Synthesis

6.2.2.1 Azpy-$O_2CCH_2CH_2$-maleimide

Azpy-OH (330 mg, 1.66 mmol) was dissolved in DCM (40 mL) and MeCN (ca. 10 mL) was added to fully solubilise the ligand. 3-Maleimidopropionic acid (93 mg, 0.55 mmol) and DMAP (53 mg, 0.60 mmol) dissolved in DCM (ca. 10 mL total) were sequentially added to the mixture and the mixture was cooled on ice. DCC (123 mg, 0.40 mmol) in DCM (10 mL) was added drop-wise and the mixture was allowed to warm to room temperature and stirred for ca. 7 h. The solvent was removed and the crude product was purified by column chromatography using silica and 98% DCM / 2% MeOH by collecting the first yellow fraction. This precipitate was re-dissolved in DCM and filtered through celite to remove dicyclohexylurea and repeated until no observable precipitate was present (x 5). The product was left to dry overnight in vacuo. Yield 130 mg (67.9 %) ^{1}H NMR ($CDCl_3$): δ 8.75 (d, 1H), 8.10 (d, 2H), 7.93 (t, 1H), 7.84 (d, 1H), 7.31 (d, 1H), 6.75 (s, 2H), 4.00 (t, 1H), 2.94 (t, 1H). ESI-MS: Calcd for $C_{18}H_{14}N_4O_4$ [M^+] m/z 351.11, found 350.91.

6.2.2.2 [(η^6-*p*-cym)Ru(azpy-$O_2CCH_2CH_2$-maleimide)I]PF_6 (29)

The dimer [(η^6-*p*-cymene)RuI_2]$_2$ (106 mg, 0.102 mmol) was dissolved in MeCN (40 mL. Azpy-$O_2CCH_2CH_2$-maleimide (72g, 0.204 mmol) dissolved in MeCN (20 ml) was added drop-wise to the red solution and no obvious colour change was noted. The solution was stirred at room temperature for 4 h. The mixture was filtered and volume of solvent was reduced to about 10 mL by removal of MeCN on a rotary evaporator. NH_4PF_6 (166 mg, 1.06 mmol) was then added and the solution was placed in the freezer overnight. No precipitation had occurred so the solvent was removed, the solid re-dissolved in DCM, filtered to remove excess NH_4PF_6, and the solvent removed to leave a sticky solid which was scratched with diethyl-ether to give a black crystalline product. Yield 105.3 mg (60.2 %) (Found: C, 39.09; H, 3.72

; N, 5.79. Calc for $RuC_{28}H_{29}N_4O_4IPF_6$: C, 39.19; H, 3.40; N, 6.53 %). ^1H NMR ($CDCl_3$): δ 9.39 (d, 1H), 8.63 (d, 1H), 8.21 (t, 1H), 8.17 (d, 2H), 7.78 (t, 1H), 7.41 (d, 2H), 6.79 (s, 2H), 6.29 (d, 1H), 5.95 (d, 1H), 5.84 (d, 1H), 5.75 (d, 1H), 4.04 (t, 2H), 2.98 (t, 1H), 2.72 (septet, 1H), 2.47 (s, 3H), 1.10 (dd, 6H). ESI MS: calcd for $RuC_{28}H_{29}N_4O_4I^+$ [M^+] m/z 713.02, found 712.73 [M^+].

6.2.2.3 [(η^6-p-cymene)Ru(azpy-OH)I]$^+$-Holo-Transferrin (HTf-25)

To a solution of holo-transferrin (110 mg, *ca.* 1.4 μmol) dissolved in 100 mM HEPES 4-(2-hydroxyethyl)-1-piperazineethanesulfonate) buffer (pH 8.48, *ca.* 8 mL), [(η^6-p-cymene)Ru(azpy-OH)I]PF_6 (10.5 mg, 15 μmol) dissolved in MeCN (1mL) was added and the mixture was incubated at 310 K for 45 min then left overnight at room temperature. The corresponding mixture was filtered through a molecular-weight-concentrator (Amicon-30 kDa) three times with HEPES buffer then passed down a Sephadex G25 PD10 Column using the HEPES buffer as the elutent. The resulting protein fraction was purified by FPLC using 100 mM tris-HCl (pH 7.5) as A and 100 mM Tris-HCl (pH 7.5), 800 mM NaCl as B. The purified mixure was concentrated to ca. 15 mL and kept stored in the fridge at 277 K.

6.2.2.4 [(η^6-p-cymene)Ru(azpy-OH)I]$^+$-Ferric-Binding-Protein (Fbp-25)

This Fbp conjugate was synthesised by Dr Arindam Muhkerjee (The University of Warwick) using a similar procedure as for the synthesis of the transferrin conjugate. Briefly holo-FbpA was expressed using a modified standard literature procedure[17] from a recombinant pTrc99A plasmid DNA transfected into TOP10 *E. coli* cells using the heat shock method. The overexpression was performed in Luria Broth overnight using 100 microgram/ml ampicillin. The medium was then centrifuged to obtain the cells as pellets and these were left overnight in 100 mM HEPES -2% CTAB (cetyltrimethylammonium bromide) solution (pH 8.0) on a rotor at 277 K to extract the periplasmic protein. The supernatant (obtained after centrifugation and decanting) was left in ice for 6 h to precipitate the CTAB and was then quickly filtered (0.2 μM filter) on to a FRACTOGEL-450 cation exchange resin which binds the protein and agitated gently for 3 min on a rotor. The resin was then washed to remove any neutral or loosely bound impurities using 100 mM NaCl solution. The

protein was then extracted from the supernatant with 300 mM NaCl. The crude protein was then extensively dialyzed overnight against 50 mM HEPES buffer (pH 8.0) at 277 K and subjected to cation exchange chromatography (FPLC) system as a final purification step. The column was washed with 10 volumes of 50 mM HEPES buffer (pH 8.0) to remove any unbound proteins and eluted with a gradient of 0 to 1M NaCl. The purified protein was concentrated to 10 mg/ml using a Centricon 10 micro concentrator and stored in 50 mM HEPES buffer pH8.0.

The holo-protein in 50 mM HEPES of pH 8.0 was loaded with the Ru-complex in 1:10 mole ratio in 50 mM HEPES buffer and incubated at 310 K for 2 h, then concentrated and passed through a PD-10 column pre equilibrated with ammonium acetate for efficient exchange with the same. The resulting solution was further concentrated in a molecular-weight-concentrator filter (Amicon-10k Da) and exchanged three times with 10 mM ammonium acetate. The resulting solution was kept stored in the fridge at 277 K.

6.2.3 Methods

6.2.3.1 FTICR-MS (Fourier Transform Ion Cyclotron Resonance-Mass Spectrometry

FTICR-MS was performed by Dr Arindam Muhkerjee (The University of Warwick) on a Bruker 12 Tesla FTICR mass spectrometer using Apex control (at The University of Edinburgh). The **FbP-25** sample was diluted to effective protein concentration of 20 μM (10 mM ammonium acetate-10% isopropanol). An electrospray mass spectrum was obtained by accumulating 200 scans and averaging the time-domain transient. A 1024 kb data set was used to store the transient. The applied capillary voltage was 240 V, the hexapole accumulation was 0.80 s, collision voltage was -20 V and the ions were excited with an attenuation of 5.0 dB.

6.2.3.2 ICP-MS (Inductively Coupled Plasma Mass Spectrometry)

ICP-MS data was acquired on an Agilent 7500ce ICP-MS machine by Dr Ana Pizarro and Dr Lorna Eades. Standards were made up as for ICP-OES.

6.3 Results

6.3.1 Ester-Maleimide Linker (29)

6.3.1.1 Synthesis and Characterisation of [(η^6-*p*-cym)Ru(azpy-$O_2CCH_2CH_2$-maleimide)I]PF_6 (29)

The synthesis of Azpy-$O_2CCH_2CH_2$-maleimide (**29**) (**Figure 6.2**) was based on literature syntheses for the esterification of carboxylic acids[18] with alcohols using DCC and DMAP activation of the carboxylic acid.[19] Briefly, two carboxylic acids add to the DCC to form the activated di-acetic anhydride and di-cicyclohexylurea as an insoluble by product. This acetic anhydride reacts with the DMAP's pyridine nitrogen to form an N-ketone, with regeneration of a molecule of the acid. The ketone carbon is sufficiently positive now (this acylpyridinium ion is stabilised by delocalisation onto the pyridine ring and NMe_2 substituent) for nucleophillic attack by the alcohol, and loss of this ester from DMAP regenerates the catalyst and forms the ester.

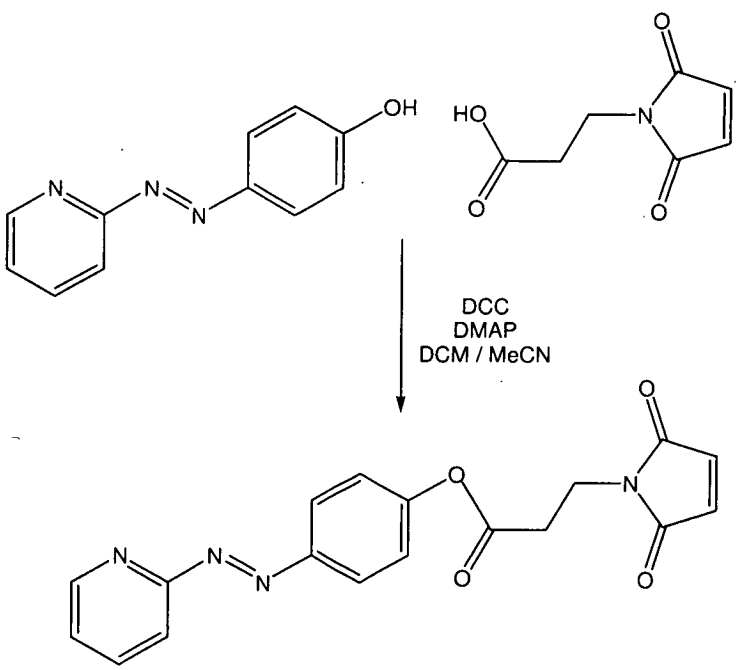

Figure 6.2. Reaction scheme for the synthesis of Azpy-$O_2CCH_2CH_2$-maleimide

The corresponding ruthenium complex was synthesised in a similar fashion to the other ruthenium complexes in this thesis. The complex was characterised by ^{1}H NMR, ESI-MS and CHN.

6.3.1.2 Stability in Water

The stability of the ester bond with respect to hydrolysis was investigated by ^{1}H NMR at pH* 6, 7 and 8 using the following conditions: 0.7 mM Ru, 2.1 % DMF-d_6, 97.9 % D_2O, 0.1 M borate buffer at 310 K. These conditions were chosen to mimic the conditions that would be used to couple this molecule to the SH groups on transferrin. Hydrolysis could be detected by the appearance of peaks corresponding to $[(\eta^6\text{-}p\text{-cym})Ru(azpy\text{-}OH)I]^+$ in aqueous solution and the disappearance of the starting material peaks. **Figure 6.3** shows the ^{1}H NMR spectra recorded for **29** at pH* 7 initially after dissolution (ca. 15 min) and after 2 h and 12 h incubation at 310 K.

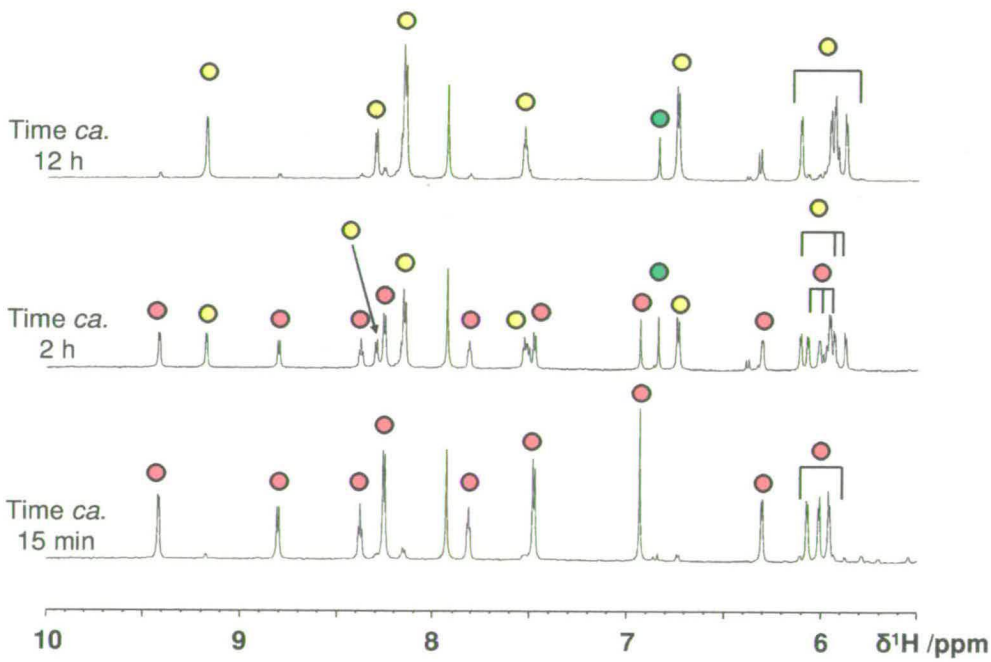

Figure 6.3. High frequency ^{1}H NMR spectra (0.1 M borate buffer (pH* 7.0), 0.7 mM Ru, 2.1 % DMF-d_6, 97.9 % D_2O, 310 K) recorded for complex $[(\eta^6\text{-}p\text{-cym})Ru(azpy\text{-}O_2CCH_2CH_2\text{-maleimide})I]PF_6$ (**29**) after certain time periods in solution. Key: dots are proton resonances for **29** (red), **25** (yellow) and for 3-maleimidopropionic acid (green).

Unfortunately at this pH the complex was rapidly hydrolysed with ca. 50 % hydrolysing after 2 h and full hydrolysis of the ester bond after 12 h. The complex was also found to be unstable at pH* 8 (50 % hydrolysis after 3 h) and at pH* 6 (50% hydrolysis after 13 h).

The stability of the ester linkage towards hydrolysis was also determined by UV-Vis spectroscopy under biologically relevant conditions (100 μM Ru, 0.5% DMSO, 310 K, 24 h) at pH 6.53, pH 7.03 and pH 7.53 (0.1 M borate buffer). Unfortunately, however, hydrolysis was also found to occur under these conditions. A Representative spectrum is shown in **Figure 6.4.**

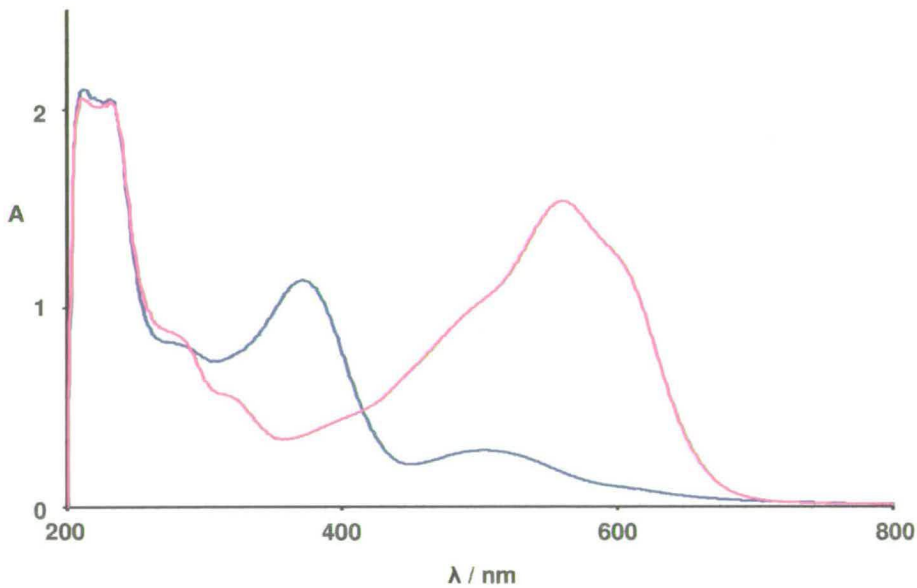

Figure 6.4. Time dependence UV-Vis spectrum of **29** (100 μM Ru, 0.5% DMSO, 310 K, pH 7.03, 0.1 M borate buffer) recorded initially (——, ca. 20 s after dissolution) and after 24 h incubation at 310 K (——).

Hydrolysis was readilly confirmed by the change in colour as $[(\eta^6\text{-}p\text{-cym})Ru(azpy\text{-}OH)I]^+$ is liberated (solution changed from pale orange to bright blue/purple). At all three pH values, the spectra after 24 h resembled the fully hydrolysed product suggesting that in biological tests, the ester bond would not be stable and would readily hydrolyse.

6.3.2 Ru-Transferrin-Conjugate (HTf-25)

6.3.2.1 Synthesis

The conjugate was synthesised by direct reaction of holo-transferrin and complex **25** at pH 8.5, since at this pH the azpy-OH ligand is in its fully deprotonated (O^-) form (pK_a phenolic OH determined as 6.50, Chapter 5), and will be more likely to bind as the synergistic anion. Furthermore, at this pH the iron will remain bound since iron is usually liberated from transferrin at lower pH values (ca. <5) only.

6.3.2.2 Purification by FPLC

The protein-ruthenium conjugate **HTf-25** was purified by FPLC using a Hi-Trap Capto Q column. **Figure 6.5** shows the FPLC trace obtained

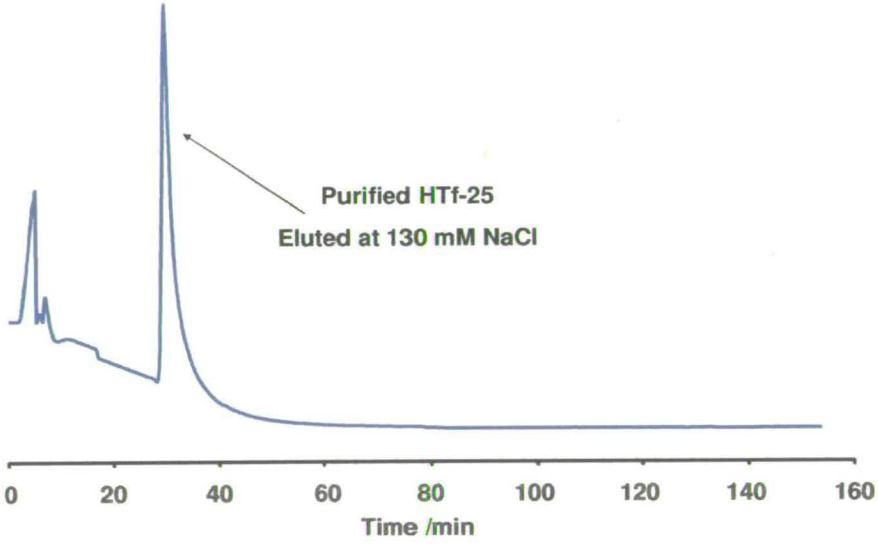

Figure 6.5. Chromatogram (λ = 280 nm) obtained for the purification of **HTf-25** by FPLC.

The complex was eluted at 130 mM NaCl concentration.

6.3.2.3 Characterisation by ICP-OES

ICP-OES and ICP-MS data for the crude product (filtered three times through a molecular weight concentrator to remove unbound **25** and passed through a

Sephadex G25 PD10 Column, prior to purification by FPLC) suggested that the composition of the protein was Fe:S:Ru:I, 2:39.4:3.7: 3.1.

The transferrin protein 38 sulfur atoms (from methionine and cysteine residues) and is iron saturated (two iron atoms per protein). This result thus confirmed that both ruthenium and iodide were present in the conjugate and that the Fe:S ratio (2:38) was essentially unaffected by the complex being present i.e. that ruthenium was not displacing iron in the metal ion binding site.

ICP-OES results on the purified complex, however, gave a Fe:S:Ru:I ratio of 2:43:1.8:0.11. Thus there are ca. two moles of ruthenium bound per mole of transferrin. Thus after extensive purification the iodide is not bound to the conjugate and the iron:ruthenium are present in approximately equal ratios. These results suggested that the iodide may have been present as a counter anion only and was exchanged for chloride during the FPLC purification process, in which a salt gradient is used to elute the protein. Furthermore the ruthenium: iron ratio decreased from ca. 3.7:2 to 1.8:2 suggesting that some of the ruthenium was initially present as a loosely bound species.

6.3.2.4 Characterisation by UV-Vis Spectroscopy

Figure 6.6 shows the UV-Vis spectrum recorded for holo-transferrin and that of the Ru-transferrin conjugate **HTf-25**.

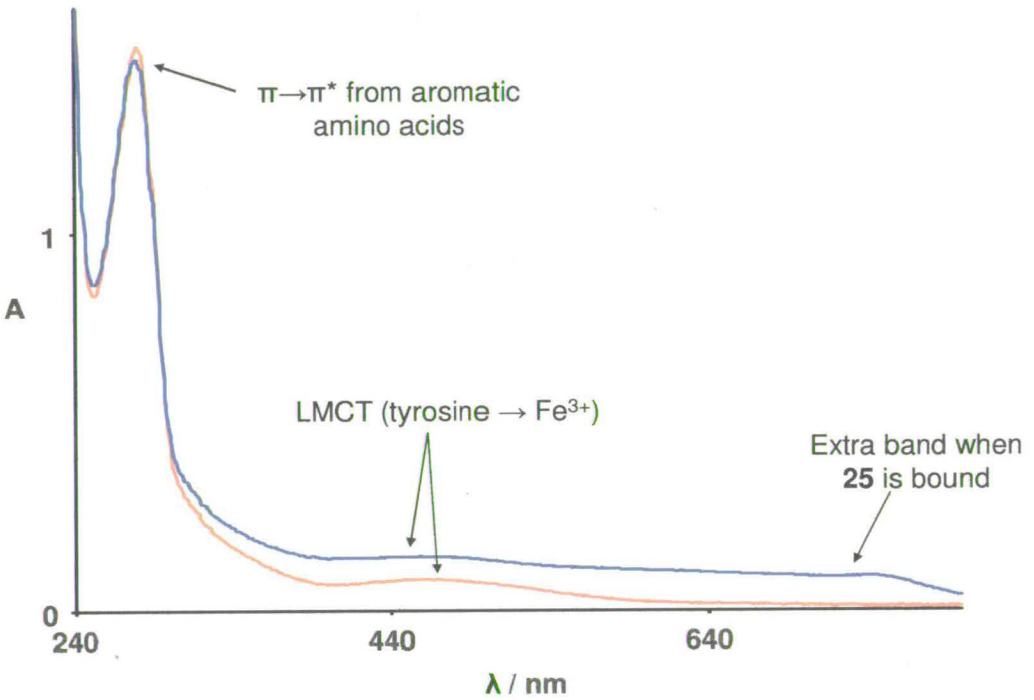

Figure 6.6. UV-Vis spectra recorded in 100 mM Tris-HCl (pH 7.5) for holo-Transferrin (hTf) (orange line) and **hTf-25** (blue line) at ca. 16 μM transferrin (as determined by ε_{278} nm = 93000 $M^{-1}cm^{-1}$).[20]

Both spectra contain an absorption band centred near 280 nm arising from π→π* transitions of the aromatic residues tyrosine, tryptophan and phenylalanine.[20] In both spectra there is also a band centred at ca. 465 nm which is characteristic for iron-containing transferrin[20] and is assignable to a LMCT between from the tyrosinate amino acid residue to the Fe^{3+}, although in the **HTf-25** spectra the intensity is slightly greater. There is also broad peak at longer wavelengths in the **HTf-25** spectrum and this could be due absorption from the ruthenium complex **25**, since at 30 μM it would have appreciable absorbance in this red region of the UV-Vis spectrum (blue/purple in colour).

6.3.2.5 Stability in Aqueous Solution

The stability of the conjugate was investigated over 24 h at 310 K. **Figure 6.7** shows the UV-Vis spectra recorded in Tris buffer (pH 7.5) and **Figure 6.8** shows a similar sample where 100 mM NaCl was added prior to aquisition.

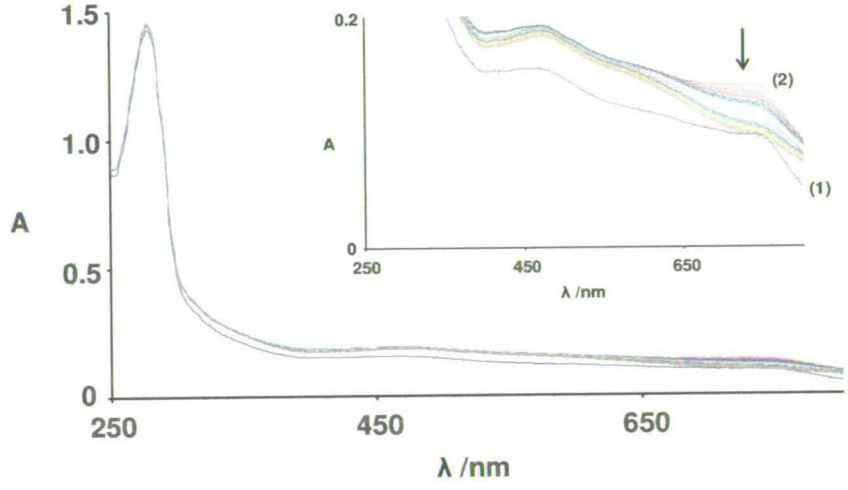

Figure 6.7. UV-Vis spectra recorded every hour over 24 h for the **25-HTf** conjugate over 24 h at 310 K in Tris buffer (pH 7.5). The inset shows the changes in the bands corresponding to the 25-HTf conjugate more clearly. There is an initial jump in the spectrum (from (1) to (2)) after 1 h incubation followed by a slow decrease in the intensity of the bands. No isosbestic points are present.

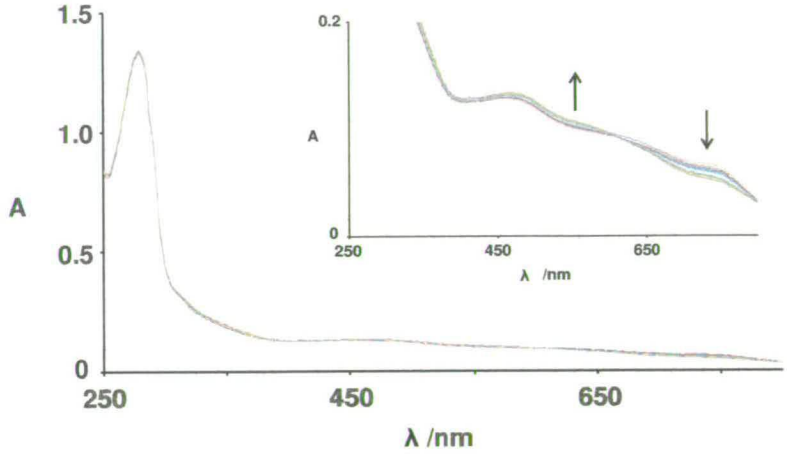

Figure 6.8. UV-Vis spectra recorded every hour over 24 h for the **25-HTf** conjugate over 24 h at 310 K in Tris buffer (pH 7.5) with 100 mM NaCl. The inset shows the changes in the bands corresponding to the 25-HTf conjugate more clearly. There is a slow decrease in the intensity of the band at ca. 740 nm and a corresponding increase in the intensity at ca. 540 nm. There appears to be an isosbestic point at 613 nm.

It can thus be seen that the addition of NaCl appears to stabilise the 25-HTf conjugate, a phenomenon that is well known for transferrin.[21] Since biological media usually contain ca. 100 mM NaCl, the latter stability result is more relevant.

6.3.2.6 Stability in the presence of Bicarbonate Anion

The stability in the presence of the natural synergistic anion bicarbonate was also investigated under physiologically-relevant conditions (Tris Buffer pH 7.5, 100 mM NaCl, 25 mM $NaHCO_3$). UV-Vis spectra were recorded every hour over 24 h but no change in the trace with time occurred (data not shown). This result either suggested that bicarbonate had not replaced the ruthenium complex as the synergistic anion, or that ruthenium is not bound to the Fe through the phenolate of the Azpy-OH ligand after all and is bound in some other fashion.

6.3.2.7 Characterisation of FbP-25 complex by FTICR-MS

The analysis of **HTf-25** by high resolution mass spectrometry cannot readily be achieved since the protein weight is ca. 79 kDa and this is outside the upper limit of detection of the machine. In order to gain information on whether the intact cation can bind to such an iron binding site, reaction of complex **25** with Fbp-A (ferric binding protein), **FbP-25**, was investigated. The molecular weight of this protein is only ca. 34 kDa. Fbp is found in the periplasm of several Gram negative bacteria.[22]

It is considered as a member of the transferrin family, although it is structurally homologous to only a single lobe of transferrin and binds only one iron per molecule in a similar binding site.[23] **Figure 6.9** shows the FTICR-mass spectrum obtained for **FpP-25**.

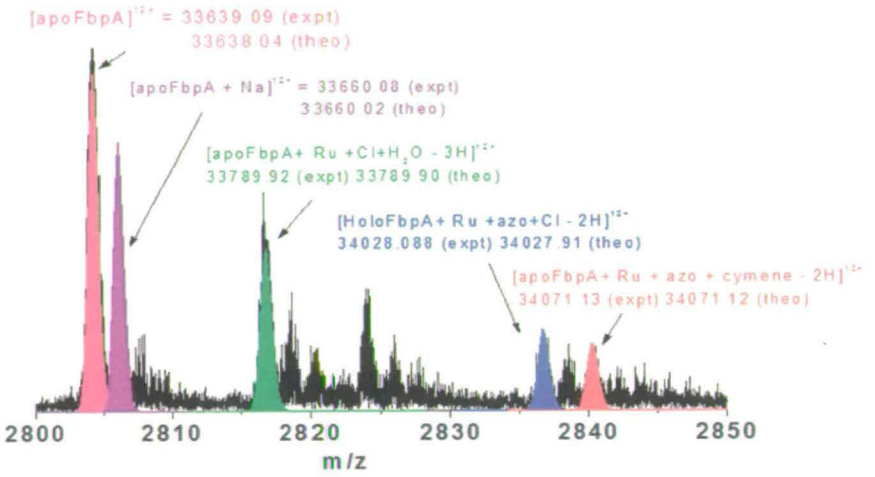

Figure 6.9. FTICR-MS obtained (12^+ charge state) for **FbP-25** (protein concentration 20 μM in 10 mM ammonium acetate-10% isopropanol). Key, azo = azpy-OH, cymene = *p*-cymene.

Peaks for several fragments were observed and many of these have been assigned. Interestingly there is a peak at m/z = 2839.26 which corresponds to the apo-FpP (i.e. iron loss had occurred) and complex **25**, without the iodide. This provided some evidence that the complex minus the iodide ligand was bound to the Fbp.

6.4 Discussion

6.4.1 Ester-Maleimide Linker (29)

The incorporation of an ester linkage attached to a maleimide linker (which could then be attached to transferrin) into the ruthenium complex [(η^6-*p*-cym)Ru(azpy-OH)I]PF_6 was synthetically possible. However this ester group was susceptible to hydrolysis at physiological pH values and was not stable enough for subsequent studies, since *in vitro* cell experiments are performed at pH values of between 7.2-

7.4. The concept of attaching cytotoxic compounds through acid-labile groups to transferrin is well documented. In general, more stability is observed when acid labile hydrazone groups ($R_2C{=}NNR_2$) are used as linkers instead of ester linkages.[24] These linkers, unlike ester groups, are stable at a basic pH and tend not to hydrolyse as readily.[6]

6.4.2 Ru-Transferrin (HTf-25)

The cytotoxic ruthenium complex $[(\eta^6\text{-}p\text{-cym})Ru(azpy\text{-}OH)I]PF_6$ has been successfully incorporated into holo-transferrin. The ICP-OES results show that the iron is not displaced by ruthenium (Fe:S ratio is consistent with two Fe atoms per transferrin) but that, upon reaction with the transferrin, iodide is lost from the complex. The purified conjugate appears stable over 24 h with physiologically relevant concentrations of NaCl to stabilise the protein. Furthermore, the complex is stable to physiological concentrations of bicarbonate (the 'natural' synergistic anion). This result is encouraging as it suggests that the ruthenium complex would remain bound to transferrin under the *in vitro* testing conditions. Initial FTICR-MS results for **FpB-25** suggest that the complex may bind as the intact complex minus the iodide since a peak appears corresponding to apo-FbP and the complex after iodide loss.

Initially it was hoped that the complex would bind to the Fe^{III} as the synergistic anion instead of bicarbonate. It should be noted, however, that the common features of synergistic anions are the presence of a carboxylate donor and, one or two carbon atoms away, a second (proximal) electron donor group that can act as a potential ligand for metal binding.[20] It is not known at this stage whether the complex is bound as the synergistic anion. However, since iodide is lost from the complex, this would generate a 'reactive site' for coordinative bonding. There are no accessible thiol (SH) groups on transferrin, but the complex may be binding to other amino-acid residues. For example, there are two highly exposed methionine sites on transferrin, Met 499 and Met 256 and these sites may be potential binding sites for complex **25**. Previous work has shown that the reaction of $[(\eta^6\text{-bip})Ru(en)Cl]^+$ with L-methionine (1:2 ratio) affords the S- bound $[(\eta^6\text{-biphenyl})Ru(S\text{-L-MetH})(en)]^{2+}$ adduct as a

product.[25] This reaction was, however, slow with a $t_{1/2}$ ca. 2.3 h, and after 48 h, only approximately 27% of the ruthenium complex had reacted with L-methionine. There are also several surface histidine residues present could be potential binding sites (His 16, 349, 350, 473, 598, 606 and 642 are exposed). The reaction of $[(\eta^6\text{-bip})Ru(en)Cl]^+$ and histidine (1:2 ratio) reached equilibrium after approximately 24 h, but only approximately 22% of the complex had reacted, with hydrolysis (59%) being the preferred reaction The ruthenium(III) complex indazolium trans-tetrachlorobis(1H-indazole)ruthenate(III) complex, or KP-1019, for example, has been shown to bind to transferrin via histidine residues.[26]

Further structural characterisation is, thus, required before *in vitro* cell tests could be performed.

6.5 Summary

The transferrin receptor TfR1 is over-expressed on the surface of cancer cells due to increased requirement for iron. For this reason there is currently much research aimed at targeting cytotoxic complexes specifically to the TfR1 via attachment to transferrin, to try and overcome some of the toxicity problems associated with chemotherapy. In this Chapter attempts were made to attach the cytotoxic ruthenium complex $[(\eta^6\text{-}p\text{-cym})Ru(azpy\text{-}OH)I]PF_6$ to holo-transferrin. The ruthenium complex has been successfully attached to transferrin to form a conjugate that is stable under physiologically-relevant conditions. Once further characterisation has been performed on the conjugate to confirm the binding site, this conjugate may be suitable for cellular studies including cellular uptake studies in a cancer cell line which forced to over-express the transferrin receptor as well as IC_{50} determination. Overexpression of this receptor can be achieved by adding an iron chelator to the cell medium to sequester iron so that less iron is available to the cells. As a consequence, more TfR1 receptors are expressed by cells to try and increase iron levels)[27]. These initial experiments would assess the suitability transferrin as a possible carrier of the complex.

6.6 References

[1] Z. M. Qian, H. Li, H. Sun, K. Ho, *Pharmacol. Rev.* **2002**, *54*, 561-587.

[2] M. A. Moses, H. Brem, R. Langer, *Cancer Cell* **2003**, *4*, 337-341.

[3] T. R. Daniels, T. Delgado, G. Helguera, M. L. Penichet, *Clin. Immunol.* **2006**, *121*, 159-176.

[4] K. Barabas, J. A. Sizensky, W. P. Faulk, *J. Biol. Chem.* **1992**, *267*, 9437-9442.

[5] T. Hoshino, M. Misaki, M. Yamamoto, H. Shimizu, Y. Ogawa, H. Toguchi, *J. Controlled Release* **1995**, *37*, 75-81.

[6] U. Beyer, T. Roth, P. Schumacher, G. Maier, A. Unold, A. W. Frahm, H. H. Fiebig, C. Unger, F. Kratz, *J. Med. Chem.* **1998**, *41*, 2701-2708.

[7] H. Li, Z. M. Qian, *Med. Res. Rev.* **2002**, *22*, 225-250.

[8] R. L. Elliott, R. Stjernholm, M. C. Elliott, *Cancer Detect Prev.* **1988**, *12*, 469-480.

[9] J. F. Head, F. Wang, R. L. Elliott, *Adv Enzyme Regul.* **1997**, *37*, 147-169.

[10] P. T. Gomme, K. B. McCann, J. Bertolini, *Drug Discovery Today* **2005**, *10*, 267-273.

[11] L. L. Dunn, Y. S. Rahmanto, D. R. Richardson, *Trends Cell Biol.* **2007**, *17*, 93-100.

[12] M. Valko, C. J. Rhodes, J. Moncol, M. Izakovic, M. Mazur, *Chem.-Biol. Interact.* **2006**, *160*, 1-40.

[13] S. S. Leonard, G. K. Harris, X. Shi, *Free Radic. Biol. Med.* **2004**, *37*, 1921-1942.

[14] J. Claydon, S. Warren, N. Greeves, P. Wothers, *Organic Chemistry*, Oxford University Press, **2001**.

[15] T. P. King, Y. Li, L. Kochoumian, *Biochemistry* **1978**, *17*, 1499-1506.

[16] P. J. Halbrooks, A. B. Mason, T. E. Adams, S. K. Briggs, S. J. Everse, *J. Mol. Biol.* **2004**, *339*, 217-226.

[17] M. Guo, I. Harvey, D. J. Campopiano, P. J. Sadler, *Angew. Chem. Int. Ed.* **2006**, *45*, 2758-2761.

[18] B. Neises, W. Steglich, *Org. Synth.* **1985**, *63*, 183-187.

[19] Anon, *Synlett* **2003**, 1568-1569.

[20] H. Sun, H. Li, P. J. Sadler, *Chem. Rev.* **1999**, *99*, 2817-2842.

[21] J. Williams, N. D. Chasteen, K. Moreton, *Biochem. J.* **1982**, *201*, 527-532.

[22] M. Guo, I. Harvey, W. Yang, L. Coghill, D. J. Campopiano, J. A. Parkinson, R. T. A. MacGillivray, W. R. Harris, P. J. Sadler, *J. Biol. Chem.* **2003**, *278*, 2490-2502.

[23] A. J. Nowalk, S. Burroughs Tencza, T. A. Mietzner, *Biochemistry* **1994**, *33*, 12769-12775.

[24] F. Kratz, U. Beyer, T. Roth, N. Tarasova, P. Collery, F. Lechenault, A. Cazabat, P. Schumacher, C. Unger, U. Falken, *J. Pharm. Sci.* **1998**, *87*, 338-346.

[25] F. Wang, H. Chen, J. A. Parkinson, P. d. S. Murdoch, P. J. Sadler, *Inorg. Chem.* **2002**, *41*, 4509-4523.

[26] C. G. Hartinger, S. Zorbas-Seifried, M. A. Jakupec, B. Kynast, H. Zorbas, B. K. Keppler, *J. Inorg. Biochem.* **2006**, *100*, 891-904.

[27] F. Louache, U. Testa, P. Pelicci, P. Thomopoulos, M. Titeux, H. Rochant, *J. Biol. Chem.* **1984**, *259*, 11576-11582.

Chapter 7

Conclusions and Future Work

7.1 Conclusions

This thesis is concerned with the synthesis and characterisation of potential ruthenium(II) arene complexes containing chelating azo ligands and determination of their cytotoxicity and the mechanism by which cytotoxicity occurs. Initial work on $[(\eta^6\text{-arene})Ru(\text{azo-ligand})Cl]^+$ (arene = p-cym, thn, bz, bip, azo-ligand = azpy, azpy-NMe_2, azpy-OH and azpyz-NMe_2) showed that these complexes were moderately cytotoxic towards both A2780 human ovarian and A549 human lung cancer cell lines (IC_{50} 18-88 μM) and that, compared to their en analogues, they were much more inert to hydrolysis in an aqueous solution and that arene loss could readily occur. Both phenomena can be attributed to due to the incorporation of this azo π-acceptor ligand.

The dinuclear analogues offered no improvement on the biological properties; these complexes were generally unstable in an aqueous solution and intriguingly decomposed in a reaction likely to involve radicals. Electrochemical and EPR measurements showed that the complexes can undergo a one electron reduction near to 0 V (-0.06 and -0.14 V in DMF, vs. Ag/AgCl) and that this forms the azo-anion radical, providing some evidence that the azo ligand is redox active when attached to ruthenium.

Replacement of the chloride 'leaving group' by iodide ($[(\eta^6\text{-arene})Ru(\text{azpy-R})I]^+$ (arene = p-cym, bip, R = NMe_2, OH)) led to complexes that were inert to hydrolysis over 24 h at 310 K. Iodide analogues containing the azpy ligand were unstable in an aqueous buffered solution and electrochemical studies showed that complexes containing this ligand were reduced at more positive potentials (by ca. 0.1-0.2 V, e.g. for $[(\eta^6\text{-bip})Ru(\text{azpy})I]^+$ E_{red} = -0.18 V, in DMF, whereas for $[(\eta^6\text{-bip})Ru(\text{azpy-}NMe_2)I]^+$ E_{red} = -0.36 V vs. Ag/AgCl) than the stable analogues suggesting that there is a balance between hydrolytic stability and electrochemical reduction in an aqueous solution.

Surprisingly, the complexes, which were stable in aqueous solution, were found to be highly cytotoxic towards both the A2780 and A549 cancer cell line (IC_{50} 1-6 μM) which implied that, unlike analogous en complexes, hydrolysis was not necessary to activate these complexes and suggested that these complexes may have a distinct

mechanism of action, thought to involve redox chemistry on the basis of the ease of electrochemical reduction. The complexes were found to steadily generate reactive oxygen species steadily in A549 cancer cells over *ca.* 6 h and it was thought that ROS may be implicated in their mechanism of action; this was confirmed by pre-incubating the cells with the anti-oxidant NAC before cell viability determination, where more cell survival was observed in this case. Reactions with ascorbate and GSH showed that the phenylazopyridine ligands alone were not redox-active under physiological conditions and that attachment to the positive $\{(\eta^6\text{-arene})RuI\}^+$ centre was necessary in order to achieve reductions biologically. Reactions with GSH (the most abundant non-protein thiol) showed that these complexes can catalyse the oxidation of GSH to GSSG, and this reaction is thought to be central to their cytotoxicity since GSH is the main cellular redox buffering system. The depletion of GSH levels will cause an increase in the production of ROS. The exact mechanism by which this catalytic oxidation occurs is still unknown although initial conjugation of GSH across the azo group, and subsequent reduction of the azo group to hydrazo with oxidation of GSH to GSSG seem plausible initial first and second steps based on similar reactions of azo groups and glutathione reported in the literature.

Initial investigations into possible "down-stream" mechanisms have shown that $[(\eta^6\text{-bip})Ru(azpy\text{-}NMe_2)I]^+$, unlike $[(\eta^6\text{-bip})Ru(en)Cl]^+$ does not activate the tumour suppressor protein p53 and that, unusually, it down-regulates p21. This suggests that the mechanism of action of these two types of complexes differs not only in their primary mechanisms, but probably more fundamentally in the later stages of cell death too.

These complexes were, unfortunately cytotoxic towards WI38 non-cancerous lung cells suggesting that these cancer cells would not be selective for cancer cells in vivo. However, cisplatin was also very cytotoxic towards this cell line. Thus work towards targeting complex $[(\eta^6\text{-p-cym})Ru(azpy\text{-}OH)I]^+$ specifically to cancer cells via the transferrin mediated endocytotsis uptake pathway was also attempted. The complex has been shown to bind to HTf and further work into determining the binding site is required before determining is this conjugate is cytotoxic at lower concentrations.

7.2 Future Work

Because the most promising potential anticancer complexes discovered in this thesis were the iodide complexes, much of the future work would involve additional investigation of this class. The following experiments would gain further insight into the cellular mechanism of action and allow for a better evaluation into the potential of the use of these complexes as anticancer agents.

7.2.1 Determination of mechanism of catalytic oxidation of GSH

This thesis has described the catalytic oxidation of GSH to GSSG by the ruthenium complexes $[(\eta^6\text{-bip})Ru(azpy\text{-}NMe_2)I]^+$ and $[(\eta^6\text{-bipRu}(azpy\text{-}NMe_2)I]^+$. The mechanism by which this catalytic cycle operates is unknown, although it seems probable that it is facilitated by the azo group attached to the ruthenium centre on the basis of literature for similar reactions, where the azo -N=N- group is reduced to hydrazo -HN-NH- with oxidation of 2GSH to GSSG. This mechanism by which this net loss of H_2 occurs which would regenerate the catalytic cycle is postulated to occur by direct loss of H_2. In order to prove this hypothesis, H_2 would have to be detected in the reaction medium. Unfortunately, H_2 is sparingly soluble in aqueous medium[1] and the ^1H NMR resonance of its protons appears at ca. 4.6 ppm[2] which would be obscured by the broad water resonance. Attempts to detect H_2 in aqueous solution by using linear sweep voltammetry at an ultramicro electrode[3] were unsuccessful. Gas Chromatography would be the most suitable method to detect dissolved H_2 since this technique is very sensitive.[4]

7.2.2 Measurement of intracellular thiol levels

Reactions of ruthenium(II) iodide (and chloride) complexes with glutathione in an NMR tube show that a catalytic oxidation of GSH to GSSG occurs. However, this result does not necessarily mean that this phenomenon will occur in the in-vitro cell tests; the cellular amount of GSSG is generally kept to very low levels (5-50 μM) by a highly efficient NADPH-dependent reduction of GSSG by glutathione reductase back to GSH.[5] The ratio of GSH/GSSG can be determined intracellularly by several methods and these have been thoroughly reviewed.[6, 7] For example, *o*-phthalaldehyde (opt) reacts specifically with reduced GSH to form a fluorescent

product and so GSH levels can be determined from standard curves by fluorescence emission at 420 nm after excitation at 350 nm.[8] Any changes to GSH levels (e.g. by oxidation to GSSG) could easily be shown by this method. Total thiol levels can also be determined by the 5,5'-dithiobis-(2-nitrobenzoic) acid DTNB assay.[9] DTNB binds to free SH groups and is reduced to form TNB which can be assayed colorimetrically at 412 nm. Addition of NADPH ensures all GSSG is first reduced to GSH.

7.2.3 Role of iodide in the cytotoxicity

Initial data demonstrated that the iodide complexes were much more inert in aqueous solution than the chloride complexes and this was thought to be the main reason why they were more cytotoxic. Studies with the biomolecule glutathione showed, however, that both I^- and Cl^- in Ru-I and Ru-Cl can be displaced by the sulfur nucleophile, essentially forming the same compound *in vitro*. Interestingly, however, in direct contrast to Ru-en analogues (where Ru-I was found to exchange for Ru-Cl in a high chloride concentration such as cell medium, e.g. for the complex $[(\eta^6\text{-hmb})Ru(en)I]^+$),[10] Ru-I in ruthenium(II) arene phenylazopyridine complexes is not substituted by chloride, implying that (more) iodide enters the cell. This may imply that iodide itself may have some role in the cytotoxicity.

There are several examples of biological reactions involving iodide; for example the oxidation of NADPH catalysed by horseradish peroxidase / H_2O_2 can be mediated by iodide and forms iodinated NADP as a product.[11] The iodide is first thought to be oxidised by H_2O_2 before interacting with the NADPH. Similarly, the oxidation of Fe^{II} cytochrome c by hypohalous acids (HOX, X = halide, generated from the reaction of HOCl and Br^-/I^-) (1:1 ratio) showed that the efficiency of the oxidation of the Fe^{II} centre to Fe^{III} decreases in the order HOI/I_2[12] ($\approx$ 98%) > HOCl ($\approx$ 60%) > HOBr ($\approx$30%).[13] The decreased ability of the HOCl and HOBr vs. HOI is thought to be due to their increased ability to halogenate amino groups (HOI is not reactive towards amino groups) and thus not interacting as specifically with the iron centre. The authors note that whilst this one electron oxidation to Fe^{III} would not be serious *per se* (the reduction is reversible), the one-electron transfer would lead to the generation of reactive radicals in the vicinity of the heme and these may conceivably

damage the protein.[13] The catalytic role of iodide on the oxidation of Fe^{II} cytochrome-c by N-halogenated compounds such as NH_2Cl was also observed and the catalytic effect of iodide was explained by redox cycling between I_2 and $2I^-$.[13] Bromide, on the other hand, was not found to be capable of catalysing this oxidation, probably because the oxidation of iodide is easier to achieve (the standard oxidation potentials at 298 K for the oxidation of $2X^- \rightarrow X_2 + 2e^-$ are -0.54 V (I^-), -1.09 V (Br^-) and -1.36 V (Cl^-)).[14] Other work in the same laboratory has shown that iodide can also increase the rate of oxidation of NADH by chloroamines and chloroamides.[15] These examples all show that iodide is capable of reacting with ROS such as HOCl or H_2O_2 and these reactive species produced can then undergo further reactions. Experimental data on the cytotoxicity of KI and KCl towards an immortalised thyroid cell line (TAD-2) showed that not only was KI cytotoxic with an IC_{50} of ca. 20 mM compared with KCl which had no effect up to 50 mM, but also that KI exposure generated ROS (as detected by the DCFH-DA assay) and caused extensive lipid peroxidation whereas KCl exposure did not.[16] Whilst this cell line contained thyroid peroxidase, which oxidises I^- to the very reactive I_2, and the cancer cell lines used in anticancer research presumably will not, this example nonetheless demonstrates that there is precedence in the literature for a possible biological redox role of iodide compared with chloride.

In future work the DCFH-DA assay should be repeated to include a chloride control (e.g. complex $[(\eta^6\text{-biphenyl})Ru(azpy\text{-}NMe_2)Cl]^+$, **8**), in order to assess if more ROS are detected in the iodide vs. chloride case. Cellular distribution of iodide could also provide some important information about possible mechanisms of action (*vide supra*).

7.2.4 Determination of cytotoxicity under hypoxic conditions

The work in this thesis has shown that ruthenium complexes of the type $(\eta^6\text{-biphenyl})Ru(azpy\text{-}R)X]^+$ (R = OH, NMe_2) can catalytically oxidise GSH to GSSG, a reaction that is thought to be a major factor contributing to their mechanism of cytotoxic action. Interestingly this mechanism of action does not necessarily require O_2, which is important since the tumour micro environment is considered hypoxic

(oxygen deficient),[17, 18] and so complexes that have a mechanism of action not requiring O_2 are of great importance.

In animals, most cells *in vivo* are exposed to low O_2 concentrations (1-10 mm Hg) whereas in the cell culture experimental conditions (95% air, 5% CO_2) the cells are exposed to *ca.* 150 mm Hg O_2 exposure.[19] This increased O_2 level (and many ingredients in the cell medium, e.g. Fe salts, absence of sufficient stable anti-oxidants such as ascorbate) causes the production of more ROS than is normal, and cells either enter senescence, die, or adapt.[20] For the cells that manage to survive (adapt), the oxidative stress they are under may affect their properties and cellular changes could include increasing antioxidant production, down-regulating levels of ROS-generating enzymes or altering cellular targets of oxidative damage to become more resistant to damage by ROS.[19] For cytotoxic complexes whose mechanism may involve ROS, these changes are potentially very important and may lead to a mechanism of cytotoxicity that is not mimicked *in vivo*.

For future work it would be interesting to determine IC_{50} values towards a cell line grown and maintained under both normal (ca. 20% O_2 (in 95% air), 5% CO_2) and under hypoxic conditions (e.g. 0.5% O_2, 5% CO_2, N_2 to balance)[21] to see if cytotoxicity is still observed. If better cytotoxicity towards the hypoxic cell line was observed, it would give a good indication that this complex may exhibit good *in vivo* cytotoxicity.

7.2.5 Ruthenium distribution in the cytoplasm / nucleus and on DNA / RNA / protein

Cellular distribution studies could provide some important information related to the mechanism of action of the complex as it could give an indication of the primary bimolecular target.

For example, the distribution of ruthenium on the DNA, RNA and protein can easily be determined. This is achieved by first using the reagent Trizol (Invitrogen), developed by Chomczynski and Sacchi,[22] which allows the isolation of total RNA from the cell. Following RNA isolation, DNA and protein can also be isolated by sequential precipitation.[23] By counting the number of cells, and by determining the concentration of isolated RNA (A_{260} nm), DNA (A_{260} nm) and protein (bicinchoninic

acid assay),[24] and determining the ruthenium concentration by ICP-OES, the amount of ruthenium per weight of DNA, RNA or protein can be determined. This experiment has previously been performed for $[(\eta^6\text{-biphenyl})Ru(en)Cl]^+$ and the distribution (A2780 cancer cells, 24 h exposure, 25.2 μM Ru) was determined to be ca. 350 ng Ru / mg RNA, 50 ng Ru / mg DNA and 50 ng Ru / mg protein.[25]

Other cellular distribution experiments include isolation of the cellular nuclei using the nuclei EZ prep nuclei isolation kit (Sigma Aldrich). Briefly cells are lysed and the nuclei are collected by centrifugation, counted and analysed for ruthenium analysis. The supernatant contains the cytoplasmic contents and can also be analysed for ruthenium. Again this experiment has been performed[25] for $[(\eta^6\text{-biphenyl})Ru(en)Cl]^+$ (A2785 cancer cells, 24 h exposure, 25 μM) and 65.3% of the ruthenium was found to be in the nucleus compared with 34.7% in the cytoplasm.

By performing these experiments, information on whether DNA/RNA/protein is the target and whether the complex is concentrated in the nucleus would be gained. This may help to elucidate the primary biomolecular target. Iodine analysis could also be performed in these experiments and this may give information on its cellular distribution snd whether iodide also has a biological target.

7.3 References

[1] M. W. Cook, D. N. Hanson, B. J. Alder, *J. Chem. Phys.* **1957**, *26*, 748-751.

[2] P. V. Grundler, O. V. Yazyev, N. Aebischer, L. Helm, G. Laurenczy, A. E. Merbach, *Inorg. Chim. Acta* **2006**, *359*, 1795-1806.

[3] J. V. Macpherson, P. R. Unwin, *Anal. Chem.* **1997**, *69*, 2063-2069.

[4] D. A. Skoog, J. J. Leary, *Principles of Instrumental Analysis*, Fourth ed., Saunders College Publishing, Florida, **1992**.

[5] K. Balendiran Ganesaratnam, R. Dabur, D. Fraser, *Cell Biochem Func,* **2004**, *22*, 343-352.

[6] T. P. M. Akerboom, H. Sies, *Methods Enzymol.* **1981**, *77*, 373-382.

[7] A. Meister, M. E. Anderson, *Annu. Rev. Biochem.* **1983**, *52*, 711-760.

[8] J. Treumer, G. Valet, *Exp. Cell Res.* **1986**, *163*, 518-524.

[9] D. Yildiz, C. I. Kuran, *Turkish J. Med. Sci.* **2004**, *34*, 233-238.

[10] F. Wang, A. Habtemariam, E. P. L. van der Geer, R. Fernandez, M. Melchart, R. J. Deeth, R. Aird, S. Guichard, F. P. A. Fabbiani, P. Lozano-Casal, I. D. H. Oswald, D. I. Jodrell, S. Parsons, P. J. Sadler, *Proc. Natl. Acad. Sci. U. S. A.* **2005**, *102*, 18269-18274.

[11] A. Virion, J. L. Michot, D. Deme, J. Pommier, *Eur. J. Biochem.* **1985**, *148*, 239-243.

[12] At pH 6-8, both HOI and I_2 are possible oxidants in this system.

[13] W. A. Prutz, R. Kissner, T. Nauser, W. H. Koppenol, *Arch. Biochem. Biophys.* **2001**, *389*, 110-122.

[14] P. W. Atkins, *Physical Chemistry*, Sixth ed., Oxford University Press, **2000**.

[15] W. A. Prutz, R. Kissner, W. H. Koppenol, *Arch Biochem Biophys,* **2001**, *393*, 297-307.

[16] M. Vitale, T. Di Matola, F. D'Ascoli, S. Salzano, F. Bogazzi, G. Fenzi, E. Martino, G. Rossi, *Endocrinology* **2000**, *141*, 598-605.

[17] M. J. Clarke, F. Zhu, D. R. Frasca, *Chem. Rev,* **1999**, *99*, 2511-2533.

[18] H. Nagasawa, Y. Uto, K. L. Kirk, H. Hori, *Biol. Pharm. Bull.* **2006**, *29*, 2335-2342.

[19] B. Halliwell, *FEBS Lett.* **2003**, *540*, 3-6.

[20] B. Halliwell, J. M. C. Gutteridge, *Free Radicals in Biology and Medicine*, 3rd Edition ., Oxford University Press, Oxford, UK, **1999**.

[21] G. Hotter, L. Palacios, A. Sola, *Lab Invest,* **2004**, *84*, 213-220.

[22] P. Chomczynski, N. Sacchi, *Anal Biochem,* **1987**, *162*, 156-159.

[23] P. Chomczynski, *BioTechniques* **1993**, *15*, 532-534, 536-537.

[24] P. K. Smith, R. I. Krohn, G. T. Hermanson, A. K. Mallia, F. H. Gartner, M. D. Provenzano, E. K. Fujimoto, N. M. Goeke, B. J. Olson, D. C. Klenk, *Anal. Biochem.* **1985**, *150*, 76-85.

[25] F. Wang, S. Guichard, R. Aird, B. Zeitlin, L. Eades, A. Habtemariam, H. Chen, D. Jodrell, P.J. Sadler, Unpublished results.

Conferences Attended

(1). Gordon Research Conference on Metals in Medicine, July 2006, (Oxford, UK), Poster Presentation.

(2). American Chemical Society 234th National Meeting, August 2007 (Boston, USA), Oral Presentation: Kinetically-inert organometallic ruthenium arene complexes: A new class of cancer cell cytotoxic agents. Dougan, S. J., Mukherjee, A., Habtemariam, A., Sadler, P.J. Abstracts of Papers, 234th ACS National Meeting, Boston, MA, United States, August 19-23, 2007 INOR-147.

Publications

(1). Phenylazo-pyridine and phenylazo-pyrazole chlorido ruthenium(II) arene complexes: Arene loss, aquation, and cancer cell cytotoxicity. Dougan, S. J.; Melchart, M., Habtemariam, A., Parsons, S., Sadler, P. J. *Inorg. Chem.* (**2006**), 45(26), 10882-10894.

(2). Ruthenium (ii) compounds. Dougan, S., Habtemariam, A., Melchart, M., Sadler, P. J., PCT Int. Appl. (**2007**)

(3). The design of organometallic ruthenium anticancer complexes. Dougan, S. J., Sadler, P. J., *Chimia*, in press.